



VLAKNA TEXTIL



Ročník 5.
1998



VÚTCH



CHEMITEX



Výzkumný ústav
Gumárenský
MATADOR

ISSN 1335-0617

Indexed in:

Chemical
Abstracts,
World Textile
Abstracts



**THE TECHNICAL UNIVERSITY OF LIBEREC,
DEPARTMENT OF TEXTILE MECHANIC TECHNOLOGIES**

and the

**RESEARCH INSTITUTE OF TEXTILE MACHINES,
LIBEREC**

take the liberty to invite you to the

IInd International Conference

on

“Novelties in Weaving Research and Technology”

organized in the scopes of the INCO-COPERNICUS Project ERBIC 15 CT 96-0711

“Network for Studying of Warp Related Weaving Problems”

Date of the conference: 16.–18. September 1998

**Place of the conference: Technical University of Liberec,
Liberec, Czech Republic**

Dear Friends!

We take the liberty to invite you to the II nd Conference on “Novelties in Weaving Research and Technology” organized by the members of the INCO-COPERNICUS Project ERBIC 15 CT 96-0711 “Network for Studying Warp Related Weaving Problems”. This second conference takes place on the Technical University in Liberec on 16 to 18th of September 1998.

The task of the conference is to exchange informations between the partners in the project as well as between other intertested visitors about present directions and results of research in the field of weaving technology, and about possibilities of influencing the weaving process and quality of produced fabrics by changing or improving the properties of textile materials on the loom and by new solutions of the dynamics of the loom and its individual mechanisms.

Up to now the organisers of the Conference obtained nearly 30 scientific papers dealing with problems in the following main areas of research of weaving and of properties of the resulting product:

- 1. Mechanical properties of textile materials processed on the weaving loom, and influencing or improving of these properties from the point of view of quality and stability of the weaving process.*
- 2. Chemical origin and properties of fibres from the point of their further processing on the loom*
- 3. Mechanical properties of produced goods – fabrics*
- 4. Dynamics of the weaving process and interaction between the weaving mechanisms and the textile material*
- 5. Measurements and new research methods applied in the weaving technology.*

The papers will be presented by authors in the order according to the programme which is the part of this invitation. The programme is divided into thematic groups, which may be accompanied in several cases by practical exhibitions. We wished that everybody who works or is interested in the weaving technics and technology could find some novelties and new ideas in the prepared performances.

*Thanks to the kindness of the publishers of the magazine *Fibres and Textiles*, the materials of the Conference will be handed to the participants in full texts in the form of the present special 3 rd issue 1998 of the Magazine instead of a conventional Book of Transactions. We are sure that this form of publication will guarantee a perfect quality of material presentation.*

The sessions are planned to take place mainly in the Conference Hall of the University Campus in Liberec. Two afternoon sessions nevertheless will take place off the University Campus: one in the weaving lab of the Technical University, with the possibility to watch measurements on the looms by using the High Speed TV Camera and other devices, and the other one in the premises of the Research Institute of Textile Machines in Liberec (VÚTS), with the possibility to see several research results of the institute.

Dr. Vangheluwe from the Department of Textiles of the Universiteit Gent, as the coordinator of the Project “Network for Studying Warp Related Weaving Problems”, as well as the organisers of the II nd Conference 1998 of this Project from the Technical University Liberec and from the Research Institute of Textile Machines in Liberec, invite you heartily to take part on the Conference programme.

In the name of all colleagues preparing the session looks forward to meet you in the town of Liberec

*Prof. Stanislav Nosek, DrSc.
President of the Conference*

PROGRAMME

of the II nd Conference on Novelties in Weaving Research and Technology,
16–18 th September 1998 in Liberec, Czech Republic.

Wednesday 16th of September (Conference hall)

7.30–9.00 Registration

Opening and introductory papers

Chairman: *Prof. S. Nosek*, DrSc. TF TUL

9.00–9.15 *S. Nosek*, Pres. of the Conference: Welcome to the conference. Session opening.

9.15–9.45 *D. Lukáš*, Rector of the TUL: Welcome to the Technical University in Liberec.
Introductory words about developing of modern science methods on the University.
Accompanying paper: *D. Lukáš, D. Halámek*: "Computer Simulation of Mechanical Properties of Two-Dimensional Fiber Nets".

9.45–10.15 *J. Militký*, Dean of the Text. Faculty of TUL: Welcome to the Textile Faculty.
Word on the connection between material research and research of mechanic technologies on the Faculty of Textiles.
Accompanying paper: *J. Militký, V. Bajžík*: "Air permeability and porosity of weaves".

10.15–10.45 *Vangheluwe L.*, Coordinator of the Project "Network for studying the weaving process":
Remarks to the Project.
Paper: *Vangheluwe L.*: "Determination of weft yarn breakage probability in air jet weft insertion via numerical simulation".

10.45–11.15 **Coffee break**

Phys. and chem. properties of text. materials and aux. means for weaving

Chairman:

11.15–11.45 *D. F. Turcu, D. Avram, A. Mihaescu*: POP technical yarns for weaving.

11.45–12.15 *D. F. Turcu, M. Neculaisa, A. Mihaescu, P. Heinisch*: The influence of some physicochemical and thermooxidative factors on the mechano-rheological characteristics of the POP technical yarns for weaving.

12.15–12.45 *R. H. Huizenga*: Development of Quicksolan SPR (for sizing).

12.45–14.00 Lunch

Wednesday 16th of September

The afternoon session takes place in the Laboratory of Weaving of the Textile Faculty, building E of the University.

Measuring and research methods in the weaving process I.

Chairman: *Doc.J.Mrázek*, CSc. TU Lib.

14.00–14.45 *A. Cvrkal, I. Brotz*: Practical demonstration of measuring and evaluation methods used in the weaving lab of TUL during research of the fabric forming process.

14.45–16.00 The representative of the firm Weinberger A.G, Dietikon, Switzerland:
New properties of the System High Speed-Cam 500 for studying the dynamics of processes.

16.00–16.30 **Coffee break**

16.30–17.00 *A. Cvrkal*: Observing of the cloth fell motion at the beat-up by means of a High-speed TV Camera.

17.00–17.30 *I. Jaksch*: Measurements of the weaving process and of fabric barriness.

17.30–18.00 *M. P. U. Bandara*: The measurement of the cloth fell drift during a loom stoppage.

Wednesday 16th of September. Evening event.

Social evening in a mountain restaurant off Liberec. Details see the invitation leaflet.

Thursday 17th of September. Morning session (Conference hall)

Mechanics of weaving and fabric forming, stability of the processes.

Chairman: Doc.J.Dvořák, CSc. Res. Inst.of Text. Mach. Lib.

- 8.00–8.30 *S. Nosek*: Logical connections between individual evolution steps in weaving technology and necessary directions of further research.
- 8.30–9.00 *P. Tumajer*: Numeric simulation of the start of a weaving loom.
- 9.00–9.30 *K. Adámek*: Conditions for high quality and reliable air jet weft insertion.
- 9.30–10.00 *J. Mrázek, M. Bílek*: Dynamic stress of heald shaft of weaving looms.
- 10.00–10.30 Coffe break
- 10.30–11.00 *F. Bamelis*: Contribution to higher productivity on Picanol's new rapier machine Gamma.
- 11.00–11.30 *L. Vangheluwe*: Theoretical aspects of back-rest roller rotation on weaving machines.
- 11.30–12.00 *G. Popov, G. Petrov*: Multifunctional system for controlling and analysis of processes and images in weaving.
- 12.00–13.00 Lunch

Thursday 17th of September. Afternoon session.

The afternoon session takes place in the Research Inst. of Textile Machines in Liberec. The transportation to the Res. Institute will be realized by bus from the Conf. Hall in the resident's area of TUL

Exposition of research and measuring methods and devices (VÚTS)

Guids: Coworkers of the Institute.

Measuring and research methods in the weaving process II.

Chairman: Doc. M. Václavík, CSc. general director of the Insitute.

- 13.00–13.30 *P. Šidlof, M. Svoboda, P. Škop*: The angular speed and angle measuring instrument.
- 13.30–14.00 *P. Škop, P. Šidlof*: Transducers for measuring of tensile forces of single yarn and warp.
- 14.00–14.30 *R. Kovář*: Influence of the yarn deformation on weaving process.
- 16.00–16.30 **Coffe break**
- 16.30–17.00 *G. Popov*: Determining of the bending rigidity of yarns using traditional dynamometer.
- 17.00–17.30 *Dang Vu Hung, L. Vangheluwe, P. Kiekens*: Frictional model of warp yarns running against objects.
- 17.30–18.00 *A. Müllen*: Forecasting the technical properties of woven fabrics with the aid of finite element analysis.
- 18.00–18.30 *Z. Stjepanović, M. Žiberna-Šujica, Z. Grobelšek, D. Voglar-Štic*: Methods of reduction of manufacturing costs in production of fine woolen fabrics.
- 18.30–20.00 **Evening session** – participants on the INCO-COPERNICUS project ERBIC 15 CT 96 0711 "Network for stud.warp related weaving problems"
Presiding: Dr.Ir.L.Vangheluwe, Coordinator of the Project.

Friday 18th of September. Morning session. (Conference hall of the TUL)

Mechanics of threads systems (warps, fabrics)

Chairman: Dr. ir. L. Vangheluwe, Univ. Ghent.

- 8.30–9.00 *B. Stříž*: Conception of the plain fabric elasticity
- 9.00–9.30 *J. Szosland, Z. Stempień*: The tension pulses generated in the textile linear products.
- 9.30–10.00 *J. Mevald*: Propagation of stress pulses through the warp (numerical method of solution).
- 10.00–10.30 *M. Ciocoiu, D. Avram, D. Mihaescu, N. Irimiciuc*: The behaviour of the warp yarns submitted to composed cyclic stresses.
- 10.30–11.00 **Coffee break**
- 11.00–11.30 *J. Słodowy*: Possibility of adjusting the optimum tensile properties of yarns to processing conditions thereof.
- 11.30–12.00 *M. Snyckerski*: New concept of formatting of properties of the weft package.
- 12.00–12.30 *S. Nosek*: Straining of warp and other linear textile bodies (LTB) during weaving or other technologies.
- 12.30 **Closing words about the IInd conference of the Project
“Network for studying weaving problems”**
Dr. ir. L. Vangheluwe, Coordinator of the project.
- 12.45 **End of the Conference, thanking for the visit.**
Prof. S. Nosek, DrSc., Pres. of the conference.
- 13.00–14.00 **Lunch**

Friday 18th of September. Afternoon event.

For those who are interested in a trip into the vicinity of Liberec (depends on the interest): a trip by bus to the castle Sychrov (20 km), visit to the castle, walk through the castle gardens.

Changes in the detailed programme are possible.

Presentation of other scientific contributions, which are not included into the sessions, is possible in the form of poster, placed in foyer of the Conference Hall.

CONTENTS

OPENING AND INTRODUCTORY PAPERS

<i>Lukáš, D., Halámek, D.</i>	69
Computer Simulation of the Mechanical Properties of a Two-Dimensional Fibre Nets	
<i>Militký, J., Trávníčková, M., Bajžík, V.</i>	72
Air Permeability and Porosity of Weaves	
<i>Vangheluwe, L.</i>	77
Determination of Weft Yarn Breakage Probability in Air-Jet Weft Insertion Via Numerical Simulation	

PHYSICAL AND CHEMICAL PROPERTIES OF TEXTILE MATERIALS AND AUX. MEANS OF WEAVING

<i>Ciocioiu, M., Avram, D., Mihaescu D., Irimiciuc N.</i>	83
Method and Equipment for the Study of the Warp Yarns Behaviour on the Weaving loom	
<i>Huizenga, R.H.</i>	87
Development and Practice Results of Quicksolan SPR	

MEASURING AND RESEARCH METHODS IN THE WEAVING PROCESS I.

<i>Cvrkal, A.</i>	91
Visualisation and Analysis of Fabric Forming Process	
<i>Jaksch, I.</i>	97
Measurements of Weaving Process of Fabric Barriness	
<i>Bandara, P.</i>	100
The Measurement of Cloth-Fell Drift during a Loom Stoppage	

MECHANICS OF WEAVING AND FABRICK FORMING, STABILITY OF THE PROCESS

<i>Nosek, S.</i>	105
Technical Perspectives of Weaving at the End of 20th Century	
<i>Tumajer, P.</i>	119
Numerical Simulation of the Start of Weaving Loom	
<i>Adámek, K.</i>	124
Conditions for High-Quality and Reliable Air Jet Weft Insertion	
<i>Mrázek, J., Bílek, M.</i>	131
Dynamic Stress of Heald Shaft of Weaving Looms	
<i>Bamelis, F.</i>	135
Contribution to Higher Productivity on Picanol's New Rapier Machine Gamma	

<i>Vangheluwe, L., Dewaele, D.</i>	143
Theoretical Aspects of Back Rest Roller Rotation on Weaving Machines	
<i>Popov, G., Petrov, G.</i>	147
Multifunctional System for Controlling and Analysis of Processes and Images in Weaving	
<i>Kovář, R., Drašarová, J.</i>	152
Influence of Yarn Deformation on Weaving Process	
<i>Popov, G.S., Gjoshkov, K.G., Peeva, V.G.</i>	155
Determining of Yarn Bending Deformation Module	
<i>Hung, D.V., Vangheluwe, L., Kiekens, P.</i>	157
Frictional Model of Yarns Running against Objects	
<i>Müllen, A., Wulfhorst, B.</i>	161
Forecasting the Technical Properties of Woven Fabrics with the Aid of Finite-Element-Analysis	
<i>Stjepanović, Z., Žiberna-Šujica, M., Grobelšek, Z., Voglar-Štic, D., Dubrovski, P.D.</i>	165
Methods for Reduction of Manufacturing Costs in Production of Fine Woollen Fabrics	

MECHANICS OF THREADS SYSTEMS (WARPS, FABRICS)

<i>Stráž, B.</i>	171
Conception of Plane Elasticity of Fabrics	
<i>Szosland, J., Stempień, Z.</i>	175
The Tension Pulse Generated in the Textile Linear Products	
<i>Mevald, J., Nosek, J.</i>	180
Tension Pulse Propagation through the Warp (numerical solution)	
<i>Avram, D., Ciocoiu, M., Mihaescu, D., Irimiciuc, N.</i>	184
Theoretical Aspects Regarding the Behaviour of the Warp Yarns Submitted to Dynamic Tensile Stresses	
<i>Śłodowy, J.</i>	188
Possibility of Adjusting the Optimum Tensile Properties of Yarns to Processing Conditions Thereof	
<i>Snycerski, M.</i>	193
New Concept of Forming of Properties of the Weft Package	
<i>Nosek, S.</i>	198
Straining of Various Linear Textile Bodies (LTBs) in Generalized Drawing Fields, Mainly in Warps on Looms	

Opening and Introductory Papers

COMPUTER SIMULATION OF THE MECHANICAL PROPERTIES OF TWO-DIMENSIONAL FIBRE NETS

David Lukáš, David Halámek

*Technical University of Liberec, KNT,
Hájkova 6, Liberec 1, 461 17, Czech Republic*

Abstract: We are developing a computer simulation method of predicting the mechanical properties of fibre net based on a microscopic description of it. The net is composed of fibres (bonds) connected one together by bond sites. The simulation starts with the known mechanical properties of a given fibre net components and with the known initial geometry of a fibre laid out. The restoring forces in elongated fibres are assumed elastic possibly nonlinear. The evolution of the system as it undergoes a selected distortion is computed using Davidon, Fletcher and Powell method of minimisation of a function of several variables. The function in question is the elastic energy of the net and the variables are co-ordinates of bond sites. The simulation method successfully describes the mechanical response of the net to the distortion.

I. INTRODUCTION

The objective of the contribution is to demonstrate that mechanical behaviour of textile materials predicted by computer simulation could be in reasonable agreement with experimental data.

The computer simulation of the mechanical behaviour of textiles was introduced by Baher and Petterson [1] for predicting the mechanical properties of area – bonded nonwovens. This work was later developed by Hearle and Stevenson [2]. In the beginning of eighties Britton et al. [3, 4, 5] demonstrated the feasibility of computer simulation of the mechanical behaviour of fibre nets under stress. These works were continued by computer simulation of stress – strain curves of point – bonded nonwoven fabric published by Grindstaff and Hansen [6]. Jirsak and Lukas made a study of fibre net

response to variations in net geometry, mechanical properties of bonds and bond sites [7, 8].

In general the computer models of mechanical behaviour of textiles are expected to provide us a faster, less expensive, and more consistent means for the development of new textile materials. In addition, modelling permits better understanding of local and microscopic phenomena occurring during textile materials testing and application.

II. A SIMPLE MODEL FABRIC

A model fabric is determined by specifying the position of all bond sites in the unstrained configuration of the fabric. The bond sites are connected by fibres which layout, density, orientation, connectivity, and curl

are estimated from microphotographs of the fabric being modelled. Our model implementation allows to connect at most four fibres in one bond site. The computer fabric sample occupies a rectangular area in a fixed plane.

The impute information to the main program involves the measured restoring forces in elongated fibres. These forces are presented in polynom form. We assume elastic forces in the system only.

The fibre net is strained in incremental steps by rigid displacing the bond sites at opposing edges of the sample. The remaining bond sites are left free to move and find new equilibrium positions in accordance with the laws of mechanics. With respect to the elastic nature of restoring forces the new equilibrium configuration of the net is determined by the total minimum of the elastic energy of the system. The elastic energy is given by positions of the free bond sites, witch co-ordinates are variables of the energy function. That is why we are facing the problem of minimisation the function of several variables.

III. MINIMISATION PROCEDURE

The initial equilibrium state of the fibre net is perturbed by a displacement along the chosen boundary. The task now is to restore the system to static equilibrium. During the restoration we are finding the new positions (co-ordinates) of free bond sites. For this procedure we have employed a method for minimisation of the system elastic energy, particularly a rapidly convergent descent method for minimisation a function of several variables introduced by Fletch and Powell [9]. This method supposes that the function of interest can be calculated at all points and that its gradient is defined at the same place.

The idea of Davidon, Fletcher, and Powell method is: near the sought minimum, the second-order terms in the function's Taylor series expansion dominate, that is why the method has to guarantee to find the minimum of a general quadratic form speedily.

The standard quadratic form in n dimension is

$$\mathbf{f} = \mathbf{f}_0 + \sum_{i=1}^n \mathbf{a}_i x_i + \frac{1}{2} \sum_{i=1}^n \sum_{j=1}^n \mathbf{G}_{ij} x_i x_j, \quad (1)$$

where the vector $\bar{\mathbf{x}} = (x_1, x_2, \dots, x_1, \dots, x_n)$ consists of all co-ordinates of bond sites, that belong to a perturbed net configuration. Let us denote $\bar{\mathbf{x}}_0$ the equilibrium vector for which the function \mathbf{f} has its minimum. We reserve $\bar{\mathbf{g}}$ to denote \mathbf{f} 's gradient

$$\mathbf{g} = \bar{\mathbf{a}} + \hat{\mathbf{G}} \bar{\mathbf{x}} \quad (2)$$

In the minimum $\bar{\mathbf{g}} = \mathbf{0}$ and (2) has the form

$$\bar{\mathbf{x}}_0 = -\hat{\mathbf{G}}^{-1} \bar{\mathbf{a}} \quad (3)$$

and the displacement $\bar{\mathbf{x}}_0 - \bar{\mathbf{x}}$ between the point $\bar{\mathbf{x}}$ and the equilibrium configuration $\bar{\mathbf{x}}_0$ is

$$\bar{\mathbf{x}}_0 - \bar{\mathbf{x}} = -\hat{\mathbf{G}}^{-1} \bar{\mathbf{a}} - \bar{\mathbf{x}} = -\hat{\mathbf{G}}^{-1} (\bar{\mathbf{a}} - \hat{\mathbf{G}} \bar{\mathbf{x}}) = -\hat{\mathbf{G}}^{-1} \bar{\mathbf{g}} \quad (4)$$

In Davidon, Fletcher, and Powell method the matrix $\hat{\mathbf{G}}^{-1}$ is evaluated using an iteration procedure.

IV. CALCULATION RESULTS

Numerical calculations were performed on a model of warpknitting fabric containing 143 bonds and 130 bond sites. A part of the unstrained configuration is shown in Fig. 1. The bond laid out was estimated from microphotographs of the fabric being modelled, see Fig. 2. The length of bonds were estimated using the intersection stereological method [10].

Bond stress-strain parameters were determined from stress-strain date for single bonds. The textile sample

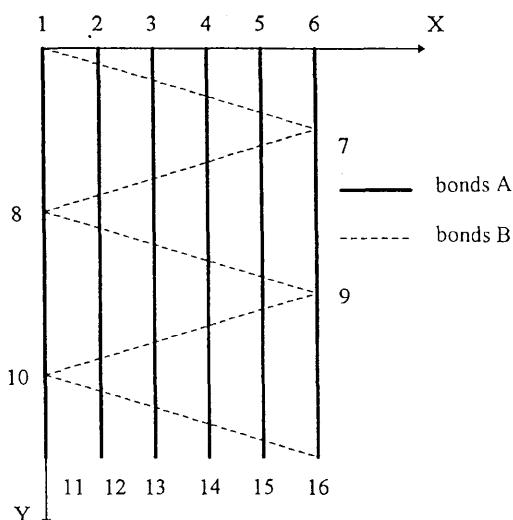


Fig. 1 A part of the initial configuration of the model fabric is shown. Solid and dashed lines (representing individual bonds A and B) are bonded at the chosen bond sites. The opposite edges of the fabric model are clamped at the mathematical jaws.

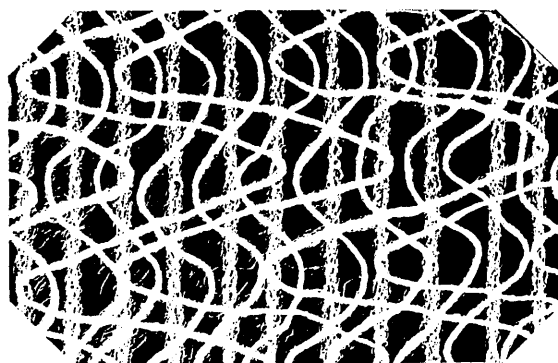


Fig.2 Microphotograph showing the inner structure of the modelled fabric at 70% strain.

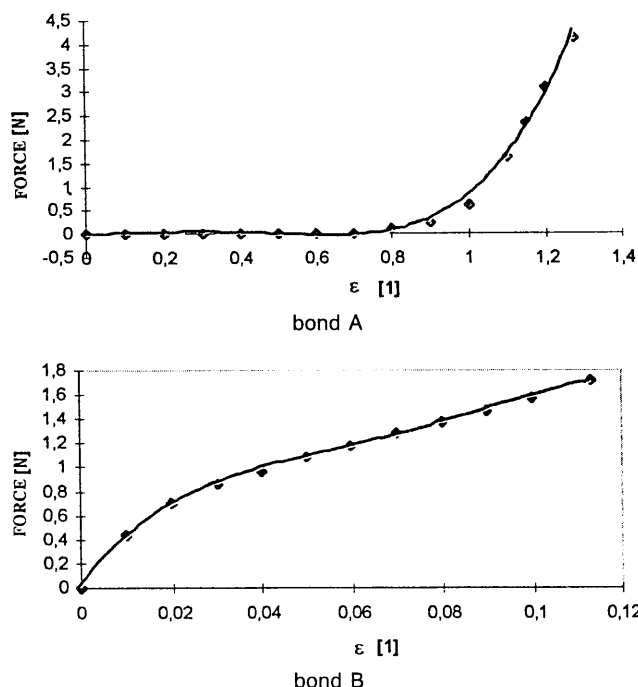


Fig. 3 Experimental stress-strain curves for the bonds A and B

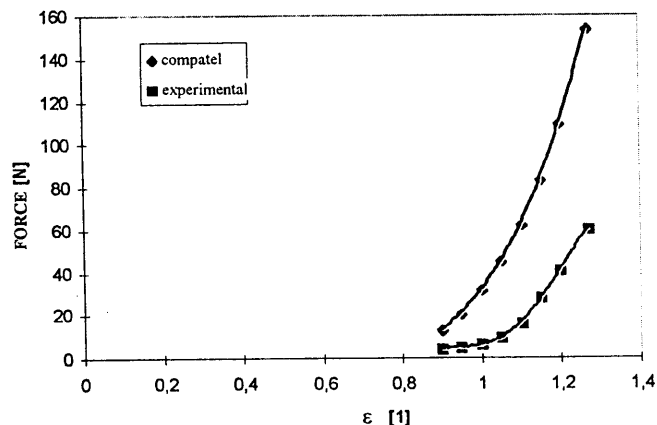


Fig. 5 Experimental stress-strain curve and that computed from the model

V. CONCLUSIONS

The calculations have demonstrated the feasibility of describing the important mechanical features of a textile material. Regarding practical implementation of the computer simulation methods for use in computer assisted design of new textile materials it will be neces-

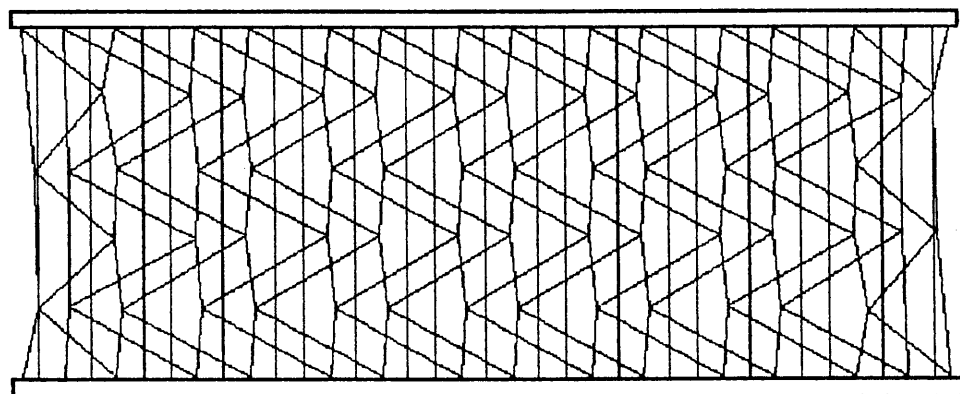


Fig. 4 The configuration of the model net at 120% strain.

is composed of two different bonds A and B which stress-strain curves are shown in Fig. 3. For the calculation restoring elastic forces of bonds A and B were taken to be in the form of polynoms

$$F_A = a_1 \varepsilon + a_2 \varepsilon^2 + a_3 \varepsilon^3 + a_4 \varepsilon^4 \quad (5a)$$

$$F_B = b_1 \varepsilon + b_2 \varepsilon^2 + b_3 \varepsilon^3 + b_4 \varepsilon^4 \quad (5b)$$

with $a_1 = -0,02784$, $a_2 = 1,8704$, $a_3 = -6,6757$, $a_4 = 5,6458$ and $b_1 = 50.548$, $b_2 = -976.01$, $b_3 = 9651.7$, $b_4 = -33504.0$.

The configuration of the model net at 120% strain is shown in Fig. 4. The stress-strain relations for the model as well as for the real fabric sample are shown in Fig. 5.

All calculations were performed on PC 486 computer. The output data for the model was generated using over 10 minutes of CPU time.

sary to co-operate between companies and research organisations.

LITERATURE

- [1] BACKER, S.: Textile Research Journal, **30**, 704, 1960.
- [2] HEARLE, J. W. S. - STEVENSON, P. J.: Textile Res. **33**, 877, 1963.
- [3] BRITTON, P. N. et. al.: Textile Res. **53**, 363, 1983.
- [4] BRITTON, P. N. et. al.: Textile Res. **54**, 1, 1984.
- [5] BRITTON, P. N. et. al.: Textile Res. **54**, 425, 1984.
- [6] GRINDSTAFF, T. H. - HANSEN, S. M.: Textile Res. **56**, 383, 1986.
- [7] JIRSÁK, O. - LUKÁŠ, D.: Geotextiles and Geomembranes, **10**, 115, 1991.
- [8] JIRSAK, O. - LUKÁŠ, D.: J. Text. Inst., **84**, 1, 1993.
- [9] FLETCHER, R. - POWELL, M. J. D.: The Computer Journal, **163**, 1963.
- [10] WEIBEL, E. R.: Stereological Methods, Vol.1, London 1979.

AIR PERMEABILITY AND POROSITY OF WEAVES

Jiří Militký, Marie Trávníčková and Vladimír Bajžík

Technical University of Liberec, Dept. of Textile Materials, Liberec, Czech Republic

ABSTRACT Main aim of this contribution is characterization of fabrics porosity by the light transmission and comparison of this characteristics with air permeability and idealized geometrical structure of selected weaves. For characterization of air permeability the classical apparatus has been used. The transmission of light through fabrics has been measured on the system LUCIA for image analysis. The porosity of textiles has been evaluated from corresponding construction parameters and idealized models of fabrics geometry. The dependencies between above mentioned characteristics were formalized by using of regression analysis.

1. INTRODUCTION

It is well known, that air permeability and light transmission through fabrics depend on many factors starting with geometrical structure. Both properties are apparently very closely connected and can be explained as so called **porosity**.

Porosity has decisive influence on utilization of fabric for some **technical application** (filters, sails, parachutes) and **clothing application** as well. Fabric porosity depends generally on the fabric and yarns constructions. Numerous methods have been proposed for porosity measurement. Classical one is based on the investigation of air permeability. Modern systems of image analysis enable to measure porosity as transmission of light through fabric.

It has been shown [1] that for tightly woven fabrics exists good agreement between air permeability and interfiber pore volume (porosity). For open weaved fabrics the correlation between air permeability and construction parameters of fabrics are not so strong.

Main aim of this contribution is the measurement of fabrics porosity by light transmission and comparison of this characteristics with air permeability and idealized geometrical structure of simple weaves. For characterization of air permeability the classical apparatus is selected. The transmission of light through fabrics is measured on the LUCIA system for image analysis.

The apparent porosity of textiles is evaluated from corresponding construction parameters and idealized fabrics models.

The dependencies between above mentioned characteristics are formalized by using of regression analysis.

2. EVALUATION OF FABRIC POROSITY

There exist a lot of models characterizing the idealized porosity P_i from some construction parameters of weaves. Classical parameters are sett (texture) of weft D_C [1/m], sett of warp D_M [1/m], fineness of weft yarn T_C [tex], fineness of warp yarn T_M [tex], planar weight of weave W_P [kg m⁻²], density of fibers ρ_F [kg m⁻³] and

thickness of fabric t_w [m]. For the idealized arrangement of yarns in fabric is

$$t_i = d_C + d_M \quad (1)$$

where d_C is diameter of weft yarn and d_M is diameter of warp yarn. When $t_w \approx t_i$ the yarns in fabric are roughly circular. This type of arrangements is assumed in sequel.

For idealized circular yarn with the same packing density is simple to compute diameters from the relation

$$d_C = \frac{2\sqrt{T_C}}{\sqrt{10^6 \pi \rho_C}} \quad (2)$$

$$d_M = \frac{2\sqrt{T_M}}{\sqrt{10^6 \pi \rho_M}} \quad (3)$$

Here ρ_C and ρ_M are unknown densities of weft and warp yarns. These densities are combinations of densities of fibers ρ_F and air $\rho_A = 1\,000$ [kg m⁻³] according to the packing of fibers in yarns. For known packing density μ_M is $\rho_M = \mu_M \rho_F$ and the same relation is valid for a weft yarn. The values ρ_C and ρ_M are therefore function of twist and method used for yarn creation. For the moderate level of twist it has been empirically found that

$$\rho_C/\rho_F = \mu_C \approx 0.525 \quad (4)$$

and this correction can be imposed to the relations (2) and (3) for computation of d_C or d_M .

For the noncircular yarns we can simply compute the area of yarn cross section

$$S_{YC} = T_C/(\rho_C \times 10^6) \quad (5)$$

or

$$S_{YM} = T_M/(\rho_M \times 10^6) \quad (6)$$

It is clear that ideal fibrous form (without pores) having the area S_Y has density equal to fiber density ρ_F . The yarn porosity is then defined as

$$P_{YC} = \rho_C/\rho_F \quad (7)$$

or

$$P_{YM} = \rho_M / \rho_F \quad (8)$$

By the same way we can evaluate the „density“ porosity of fabrics from relation

$$P_D = \rho_W / \rho_F \quad (9)$$

where ρ_W is defined by the relation

$$\rho_W = \frac{m_V}{v_V} = \frac{W_P}{t_W} \quad (10)$$

where m_V [kg] is weight and v_V [m³] is corresponding volume of fabrics having the surface of 1 m². From the measured planar weight W_P , fabric thickness t_W and known density of fibers is the simple to compute the „density“ porosity

$$P_D = \frac{W_P}{\rho_F \times t_W} \quad (11)$$

Second possibility of porosity evaluation is based on the definition of hydraulic pore for the filtration purposes [1]. The „volume“ porosity is defined as

$$P_D = 1 - \frac{\text{volume covered by yarns}}{\text{whole accessible volume}} = 1 - \frac{v_Y}{v_V} = 1 - \frac{v_Y}{t_W} \quad (12)$$

The v_Y is equal to the sums of volume of weft yarns SU_C and warp yarns SU_M

$$v_Y = SU_C + SU_D \quad (13)$$

where

$$SU_C = D_C v_{1C} \quad (14)$$

$$SU_D = D_M v_{1M} \quad (15)$$

Here the v_{1C} and v_{1M} are volumes of weft and warp yarn in the 1 m portion of fabrics

$$v_{1C} = \frac{l_C \pi d_C^2}{4} = l_C \frac{T_C}{10^3 \rho_C} \approx \frac{(1 + S_C / 100) T_C}{525 \times 10^3 \times \rho_C} \quad (16)$$

for v_{1M} the indexes C are replaced by the indexes M. Combination of eqn (13), (14), (15) and (16) and rearrangement leads to the equation

$$v_Y = \left[D_C \frac{(1 + S_C / 100) T_C}{525 \times 10^3 \times \rho_{FC}} + D_M \frac{(1 + S_M / 100) T_M}{525 \times 10^3 \times \rho_{FM}} \right] \quad (17)$$

For the case of negligible S_C and S_M and $\rho_{FC} = \rho_{FM} = \rho_F$ can be porosity P_V expressed by the relation

$$\begin{aligned} P_V &= 1 - \frac{525 \times 10^3}{t_W \times \rho_F} [D_C T_C + D_M T_M] = \\ &= 1 - \frac{1}{t_W} [D_C v_{1C} + D_M v_{1M}] \end{aligned} \quad (19)$$

More accurate determination of volume porosity is based on the idealized fabric surface structure projection shown on the Fig. 1.

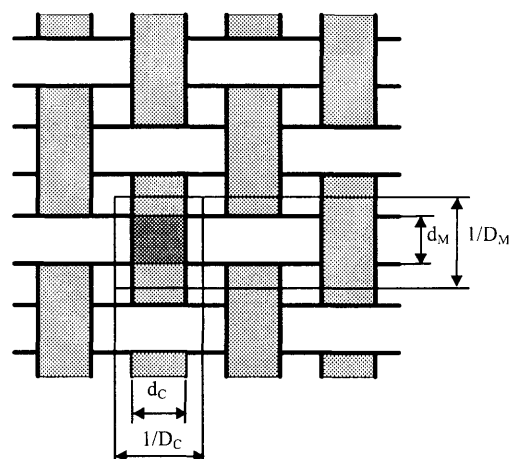


Fig. 1 Idealized surface of fabrics projection (solid lines bounds the unit cell)

The unit cell (element of structure) shown on solid line contains a part of curved weft and warp yarns portions. Volume of this cell is equal to

$$v_e = (d_C + d_M) / (D_C \times D_M) \approx t_W / (D_C \times D_M) \quad (20)$$

Length of crimped weft yarn portion is roughly equal to

$$l_{CC} = \sqrt{1.16 \times d_M^2 + (1/D_M)^2} \quad (21)$$

Here factor 1.16 is correction for approximation of weft yarn sine course by the line segment [5]. Length of crimped warp yarn is then

$$l_{CM} = \sqrt{1.16 \times d_C^2 + (1/D_C)^2} \quad (22)$$

The corrected volume of weft yarn is

$$v_C^* = \frac{\pi \times d_C^2}{4} \sqrt{1.16 \times d_M^2 + (1/D_M)^2} \quad (23)$$

and volume of warp yarn is

$$v_M^* = \frac{\pi \times d_M^2}{4} \sqrt{1.16 \times d_C^2 + (1/D_C)^2} \quad (24)$$

Corrected volume porosity is defined as

$$\begin{aligned} P_V^* &= 1 - \frac{v_C^* + v_M^*}{v_e} = 1 - \frac{\pi}{4(d_C + d_M)} \times \\ &\times \left(d_C^2 D_C \sqrt{1.16 d_C^2 D_C^2 + 1} + d_M^2 D_M \sqrt{1.16 d_M^2 D_M^2 + 1} \right) \end{aligned} \quad (25)$$

From pure geometrical point of view can be **surface porosity** evaluated from the cover factor CF of fabric. Classical Pierce definition of CF is based on the idealized projection of fabric (see. Fig. 1).

CF is defined as the area of yarn in the solid unit cell rectangle

$$A_Y = (d_C/D_M) + (d_M/D_C) - d_C d_M \quad (26)$$

divided by the area of dotted lines bounded rectangle
The CF has then form

$$CF = d_C D_C + d_M D_M - d_C d_M D_C D_M \quad (27)$$

The diameters of yarn can approximately computed from eqn. (2), (3) with corrections (4). More realistic are elliptical shapes of yarns (see[5]). "Surface" porosity based on CF is then

$$P_s = 1 - CF \quad (28)$$

This surface porosity is nearly the same as porosity P_o used in the evaluation of air porosity (see eqn. (29)).

3. AIR PERMEABILITY AND POROSITY

Let the fabric is modeled as the semi-porous sheet of thickness t_w . The overall pressure drop $\Delta p = p_{\text{ahead}} - p_{\text{behind}}$ of air flow passing through this semi-porous sheet is dependent on its porosity. This loss is suitably indicated by the loss of pressure coefficient LP [2]

$$LP = \Delta p / (0.5 \cdot \rho \cdot w^2) \quad (28)$$

ρ is air density (for dry air at standard atmosphere and 25° C is $\rho = 1.175 \text{ kg m}^{-3}$) and w is air velocity ahead material. The pressure loss depends upon the Reynolds number Re (ratio of the dynamic to the viscous forces of the flow). The Re can be expressed as [2]

$$Re = (w \cdot d) / (P_o \cdot \vartheta) \quad (29)$$

Here d is diameter of mean (cylindrical pore), P_o is the so called surface porosity (open area of fabric divided by the total area of fabrics) and ϑ is kinematic viscosity of air. In the standard tests is mean value $Re \cong 200$. The pressure loss can be divided to the dynamic losses and friction losses. Combining of these losses the LP can be expressed in the semi-empirical form [2].

$$LP = \frac{1 - P_o}{P_o^2} \left(\frac{40}{Re^{0.75}} + (1 - P_o) \right) \quad (30)$$

valid between $Re \cong 1$ (for all porosity ratio) and $Re \cong 10^3$ (for porosity ratio lower than 0.5). Gorbach [4] derived semi-empirical relation

$$LP = k_1 \frac{k_2 (1 - P_o)}{P_o^2 (P_o + \sqrt{P_o})} \quad (31)$$

where coefficients k_1 and k_2 are dependent on the Re and fabric structure.

If the pressure drop Δp is small the airflow through fabrics of surface area S_w follows D'Arcy law

$$(w/S_w) = (1/R_o) \times (\Delta p/t_w) \quad (32)$$

where R_o is air flow resistance. In the standard test is $S_w = 20 \text{ cm}^2$ and D_p (200 Pa) fixed. The air permeability AP is expressed in the form

$$AP = w/S_w = 50 \cdot w \text{ [m}^3 \text{s}^{-1} \text{m}^{-2}] \quad (33)$$

For standard test is the dry air permeability AP connected with coefficient of pressure loss LP through relation

$$LP = \frac{400}{1.175 w^2} = 8.5 \times 10^5 / AP^2 \quad (34)$$

The relation between air permeability and porosity can be obtained by combining of the relation (34) and (30) or (31).

In the contribution [3] the relation between AP and planar weight of fabric W_p has been derived

$$AP = K_1/W_p + K_2$$

Here constants K_1 and K_2 depend upon density of fibers and their resistance R.

4. EXPERIMENTAL PART.

The 40 various **weaves** from wool and blends of wool with polyester, polyamide and viscose fibers have been selected. Planar weights were in the range 0.15–0.38 kg m^{-2} .

The following construction parameters of fabrics are measured: sett (texture) of weft D_C [1/m], sett of warp D_M [1/m], fineness of weft yarn T_C [tex], fineness of warp yarn T_M [tex], planar weight of weave W_p [kg m^{-2}], density of fibers ρ_F [kg m^{-3}] and thickness of fabric t_w [m]. Three specimen were measured and the means used for calculations. From these parameters the following porosity characteristics P_D , P_V , P_V^* and P_s were computed.

The **air permeability** AP has been measured under standard conditions $\Delta p = 200 \text{ Pa}$ and $S_w = 200 \text{ cm}^2$ in the standard atmosphere. Ten repeating of measurements were realized and the mean value is used for calculations.

The **light transmission** was investigated by the image analysis system. The system consists of microscope, CCD camera and personal computer. The treatment of digital images were made by the software LUCIA-M. This software is designed for analysis of the high color (3 × 5 bits) images having resolution of 752 × 524 pixels. The original image of one fabric is shown on the Fig. 1.

The white objects (corresponding to the areas transmittable for light) were extracted from the original im-

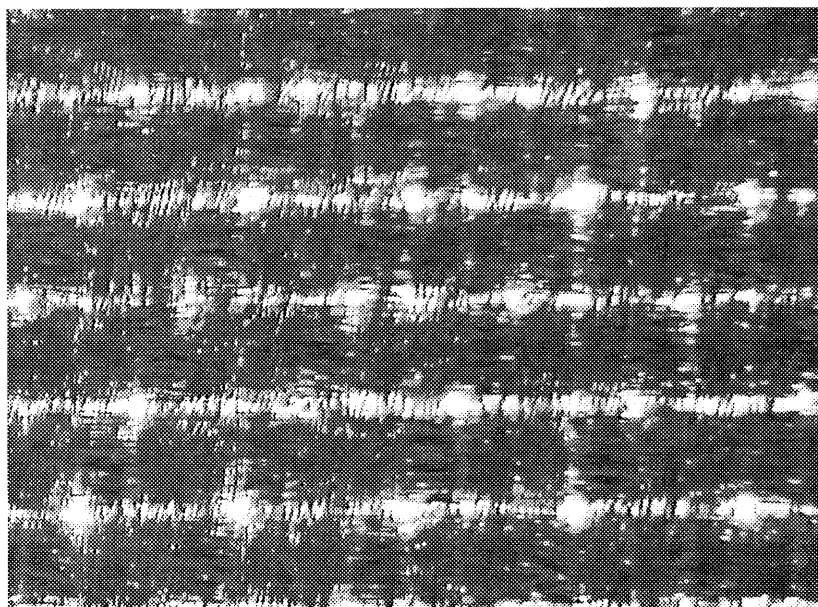


Fig 2 Original image for one fabric

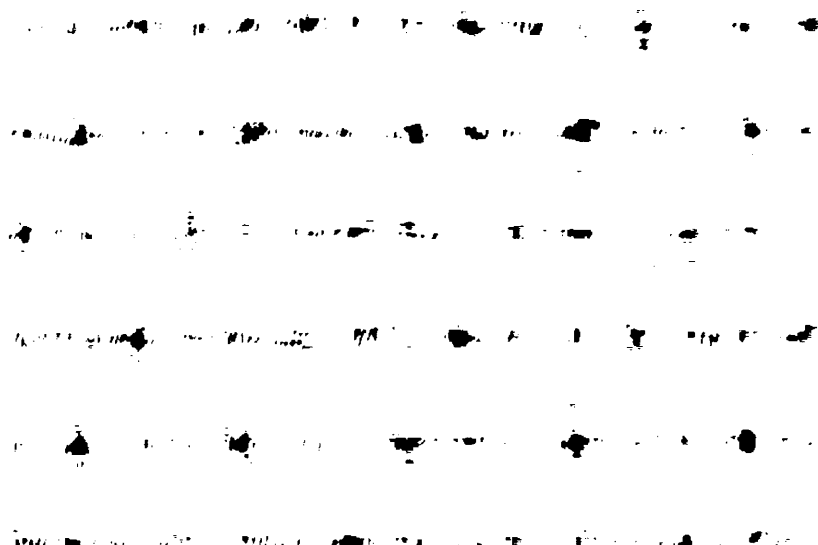


Fig. 3 Inverted image (white objects are black spots) for one fabrics

age. The threshold value 62 (all gray patterns are converted to the black ones) has been chosen. The relative **porosity for light** P_L was defined as the area of white objects divided by the whole area (see. Fig. 2)

5. RESULTS AND DISCUSSION

Comparison of porosity measures computed from fabric construction (P_D , P_V , P_V^* and P_S) and variables (AP or P_L) have been made by using of correlation analysis. The selected paired correlation coefficients were computed by using of ADSTAT package [6].

CORRELATION FOR POROSITY MEASURES

Paired correlation coefficients:

$$P_V, P_V^* = 0.982$$

$$P_S, P_V = 0.747$$

$$P_S, P_V = 0.546$$

$$P_D, P_V = 0.196$$

CORRELATION FOR VARIABLE P_L :

Paired correlation coefficients:

$$P_L, P_D = -0.3119$$

$$P_L, P_V = 0.1842$$

$$P_L, P_S = 0.5373$$

$$P_L, P_V^* = 0.2522$$

$$P_L, AP = 0.8486$$

CORRELATION FOR VARIABLE AP:

Paired correlation coefficients:

$$AP, P_D = -0.4162$$

$$AP, P_V = 0.1752$$

$$AP, P_S = 0.4479$$

$$AP, P_L = 0.2302$$

It is clear that the highest correlation exists between air permeability AP and light transmission P_L . From the point of view of the correlation of fabrics geometric characteristics of porosity with air permeability and light transmission is the best the surface porosity P_S . Generally, the porosity computed from geometrical characteristics of fabrics was far of reality.

In the second run the relation between air permeability and porosity P_L evaluated from the light transmission has been created. Based on the preliminary analysis the linear regression model has been selected. Parameters have been estimated by the least squares criterion by using of ADSTAT package[6].

Table 1 Results of regression of AP on P_L

Parameter	Estimate	Standard deviation	Test of $H_0: B[j] = 0$ vs. $H_A: B[j] \neq 0$		
			t-Criterion	H_0 hypothesis is	Sig. level
B[0]	1.8985E+03	2.8881E+02	6.5736E+00	Rejected	0.000
B[1]	3.5960E+04	3.6364E+03	9.8890E+00	Rejected	0.000
Correlation coefficient, R : 8.4862E-01					
Predicted correlation coefficient, R_p^2 : 8.3098E-01					
Regression line has the form AP = 2.8881E+02 + 3.6364E+03 × P_L					

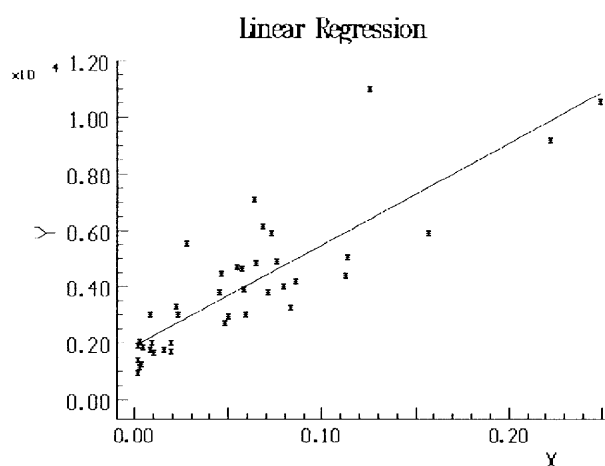


Fig. 4 The regression of AP on the P_L and experimental data

The regression line and experimental data are shown on the Fig. 3. From Fig. 3 and results of linear regression is clear that the dependence of air permeability on porosity evaluated from the light transmission is without marked nonlinearity.

The coefficients of pressure loss LP were computed from eqn. (34). The dependence between LP and P_o (porosity P_L was selected as good approximation) predicted by eqn. (31) has been evaluated by the nonlinear regression.

Nonlinear Regression

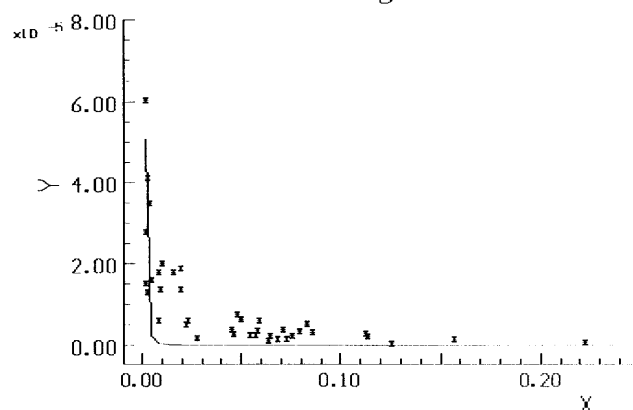


Fig. 5 The regression of LP on P_L

Estimate $K = k_1 \times k_2 = 3.874 \times 10^{-12}$ has been computed. Corresponding mean error of the prediction is $MEP = 2.33 \times 10^{-10}$. The data and regression curve are shown on the Fig. 4.

The only moderate degree of fit shows the limited validity of the prediction eqn. (31). Results obtained by using of eqn. (30) were worse.

6. CONCLUSION

The image analysis can be simply used for the prediction of the air permeability. Porosity computed from the fabric geometry is too idealized for close correlation with air permeability.

ACKNOWLEDGMENT: This work was supported by the Czech Ministry of Education Grant No. VS 97084.

7. REFERENCES

- [1] Robertson, A. F.: Text. Res. J. 19 838, (1950)
- [2] Hoerner, S. F.: Text. Res. J. 21 274, (1952)
- [3] Dent R. W.: J. Text. Inst. 67, 220, (1976)
- [4] Gorbach N. I.: IVUZ Technol. Text. Prom. 64, 8 (1968)
- [5] Hoffmann R. M.: Text. Res. J. 21 170, (1952)
- [6] Meloun M., Miličty J., Forina M.: Chemometrics for Analytical Chemistry, vol 2, Ellis Horwood, 1994
- [7] Miličty J., Trávníčková M.: Proc. Int. Conf. "Novelties in Weaving Research and Technology" Liberec, September 1998

DETERMINATION OF WEFT YARN BREAKAGE PROBABILITY IN AIR-JET WEFT INSERTION VIA NUMERICAL SIMULATION

Dr. ir. L. Vangheluwe

Department of Textiles (Universiteit Gent), Technologiepark 9, 9052 Zwijnaarde, Belgium

ABSTRACT The paper presents an approach to assess the risk of having a yarn break in pneumatic weaving. The equation of motion is solved via numerical integration. The statistical distribution of yarn load and its strength is obtained after Monte Carlo simulations of weft insertion behaviour for several yarn specifications. Using a statistical technique, the breakage rate can be calculated. The results show the influence of yarn strength, yarn modulus and their coefficient of variation and the variation of the air-drag coefficient of the yarn on the breakage rate. It is also demonstrated that the use of a controlled weft brake drastically reduces the risk of having a weft break.

1. INTRODUCTION

The paper will focus on the occurrence of weft yarn breakage in pneumatic weft insertion. Only breaks occurring between the weft accumulator and the receiving side of the loom due to the peak tension at stopper action will be studied. Although a number of other weft stop causes exist, this type of stop is relevant for air-jet weaving due to the high loading of the yarn at the end of weft insertion.

The influence of yarn parameters and loom settings can be studied experimentally via weaving trials. This approach is time consuming as a large number of weft insertions must be performed per yarn type or per loom setting. It is also almost impossible to find yarns that form a well designed sample set to study the effect of yarn parameters on breakage probability systematically. A theoretical approach is followed in the paper via the calculation of the flight of the yarn during insertion. The equation of motion (second law of Newton) is solved to this end.

It is obvious that a yarn will break when the load surpasses its strength. A statistical approach is needed as the breakage probability in weaving is rather low. The statistical distribution of yarn strength and of other relevant yarn properties must be taken into account. A Monte Carlo simulation in which random number generation is used allows to simulate weft insertion on air-jet looms for a large number of picks. The breakage probability can be obtained via evaluation of the risk of having a yarn break in using the statistical distribution of strength of a filling and yarn load at stopper action.

2. THEORY

2.1 Equation of motion of the weft yarn

The motion of the weft yarn in air-jet weaving can be

described via Newton's second law. Duxbury et. al. [1] were the first to publish a theoretical model for the calculation of weft insertion on air-jet looms. The law of motion that governs the motion of the weft yarn is represented in equation 1. After Duxbury et. al. [1] a number of other researchers [2-6] used the same approach to model yarn motion during pneumatic weft insertion.

$$m \cdot a = F_d - F_o \quad (1)$$

m – mass of the yarn being accelerated (kg); a – acceleration of the yarn (m/s^2).

The driving force F_d is given by equation 2 and the opposing force F_o originating from balloon forces and friction can be described in a form given in equation 3.

$$F_d = 0.5 \cdot c_d \cdot \pi \cdot d \cdot l \cdot \rho \cdot (v_a - v_y)^2 \quad (2)$$

c_d – air-drag (or air friction) coefficient of the yarn; l – length of the yarn on which the air stream acts; d – apparent yarn diameter; ρ – air density; v_a – velocity of the air; v_y – velocity of the yarn.

$$F_o = 0.5 \cdot T \cdot v_y^2 \cdot e^{\mu \alpha} \quad (3)$$

T – linear density of the yarn; v_y – yarn velocity; μ – coefficient of friction of the yarn against contact points; α – friction angle.

The first part of equation 3 expresses the theoretical balloon forces and the exponential factor represents friction being present in the yarn path.

When the complete length of yarn has been inserted, the yarn hits the stopper pin on drum of the weft accumulator and all kinetic energy of the yarn is converted into strain energy loading the yarn. A peak load in the yarn occurs as this force is superimposed on the force in the yarn being present just before stopper action.

Equation 4 gives the additional force due to stopper action under the assumption of a linear force extension curve of the yarn. This assumption can be considered valid for cotton yarns.

$$F_{stop} = v \cdot \sqrt{E \cdot T} \quad (4)$$

F_{stop} – additional force due to stopper action (N); v – speed of the yarn just before stopper action (m/s); E – yarn modulus of elasticity (N); T – linear density of the yarn (kg/m).

The part of equation 3 describing friction can be enhanced to take a controlled yarn brake into account. If a brake angle β and a coefficient of friction μ' of the yarn against the controlled brake are assumed, equation 3 takes the form of equation 5. The brake angle will depend on the time, being zero before the brake becomes active. The advantage of the brake is a reduction of the load of the yarn at the end of weft insertion through a reduction of the end velocity of the yarn.

$$F_o = 0.5 T \cdot v_y^2 \cdot e^{\mu \cdot \alpha} \cdot e^{\mu' \cdot \beta} \quad (5)$$

2.2 Results of the numerical solution of the differential equation

The differential equation 1 can be solved via numerical integration. A program has been written using standard C-code. The program runs on a personal computer and thanks to portability of the standard code used, also on workstations.

The parameters for the simulation model can be adapted so that a good match is obtained with experi-

Table 1 Windings times of the experiment and of the numerical simulation

Winding	Winding times (ms)	
	Experimental	Simulation
1	13.5	13.29
2	23.5	23.30
3	34.5	34.60
4	49.0	48.95

mental weaving results. A weaving trial was performed on a Picanol Omni loom. On modern looms, it is possible to measure the winding times. These are the times the yarn passes the sensor on the drum accumulator during weft insertion. The four winding times give the time at which each time one fourth of the filling length has been withdrawn from the accumulator drum. Table 1 shows the experimental times and the ones of the simulation after optimisation. During optimisation, the sum of the squares of the deviations between experimental and simulated winding times is minimised in changing the parameters of the numerical model.

Figure 1 gives an example of calculated position/time, speed/time and force/time curves. The simulation has been calculated with a controlled brake acting some milliseconds before arrival time of the weft yarn. The weft brake slows down the yarn before arrival. As a consequence, the additional peak force at stopper action (which can be calculated via equation 4) is lower. However, due to the brake action, an increase in tension occurs from the moment the brake is activated.

3 Breakage probability

Yarn mechanical properties and also the peak load

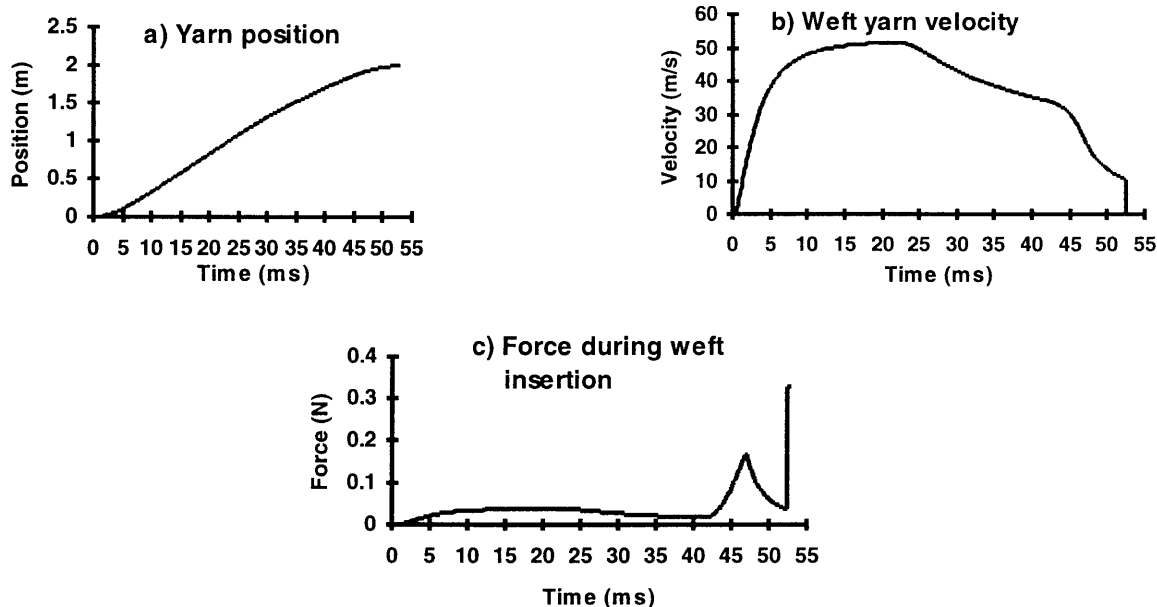


Fig. 1 Calculated curves characterising pneumatic weft insertion

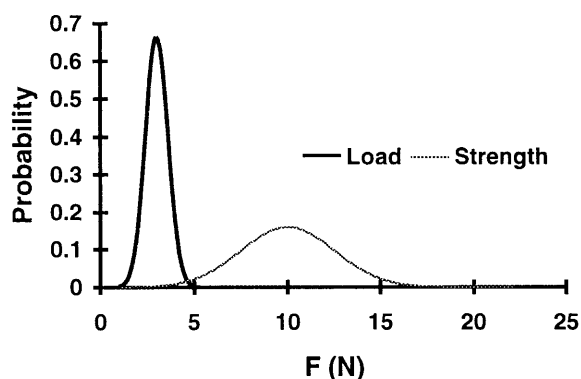


Fig. 2 Statistical distribution of yarn strength and of load of the yarn

are not constant for each pick but are subject to statistical deviations. The statistical distribution of strength as well as of yarn load should be taken into account for the calculation of the number of weft breaks in the shed. This was put forward by Krause [7–10] and by some author researchers [11–12]. Although the theory for the calculation of yarn breaks is general in nature, the best application is found in weft insertion.

The principle is illustrated in figure 2. Yarn strength and yarn load have a statistical distribution. A break will occur if the strength of a certain filling is lower than the load on it. The risk of break can be expressed under the form of equation number 6:

$$\varphi_b = \int_{x=0}^{\infty} \int_{y=x}^{\infty} \varphi_l(y) \cdot \varphi_s(x) \cdot dy \cdot dx \quad (6)$$

with φ_b – risk of having a yarn break; $\varphi_s(x)$ – statistical distribution of the yarn strength; $\varphi_l(y)$ – statistical distribution of the yarn load.

The breakage rate can also be calculated via formula 7 as the probability that the difference between yarn strength and load is negative. A condition to use the equation is that the distribution law of the difference between strength and load is known.

$$\varphi_b = \varphi(x - y < 0) \quad (7)$$

The breakage probability can be calculated using Monte Carlo simulation on the numerical simulation described in the previous section. Using random number generation and taking the statistical distribution of the different parameters of the model into account, a series of weft insertions can be simulated numerically. It is possible to evaluate at each weft insertion if the load of the yarn is higher than its strength. As the probability of weft break is very low, it would take a long calculation time especially if a large number of yarns or loom settings are to be compared. Therefore, another approach is followed. A range of insertions is calculated and the statistical distribution of yarn strength and yarn load is fitted afterwards. The breakage probability can be calculated using equation 6 or 7.

In order to perform the calculations, it has been assumed that yarn strength, yarn modulus and the drag coefficient of the yarn all follow a normal distribution. In first approximation, the parameters are supposed to be independent (this means that no significant correlation exists between the values). As tensile tests give mean values for a test length of 0.5 m, values for the simulations have to be calculated for the insertion length. This means e.g. for an insertion length of 2 m that the minimum strength of four tensile tests must be taken for the tensile strength whereas the modulus for one weft yarn is calculated as the mean for four tensile experiments.

Values are generated using the standard built-in random number generator of the C-language. As the generated values follow a uniform distribution, the Box-Muller formula is used to obtain values that follow the normal distribution with given mean value and standard deviation.

We assume here that the yarn influences on the drag force are concentrated in the drag coefficient. In practice, the drag coefficient of a yarn is affected by a large number of yarn constructional characteristics. As no direct measurement method exists to date for the drag coefficient, values are obtained via the selection of a value in order to fit experimental winding times during weaving.

Using the χ^2 – test it has been verified that yarn load as well as the yarn strength follow a normal distribution. Together with the fact that strength and load of the filling are not correlated, it means that the difference between strength and load may also be described using a normal distribution with mean and standard deviation given in equation 8:

$$\begin{aligned} \overline{\Delta F} &= \overline{F_s} - \overline{F_l} \\ s_{\Delta F} &= \sqrt{s_{F_s}^2 + s_{F_l}^2} \end{aligned} \quad (8)$$

F_s and F_l : yarn strength (N) and yarn load (N).

It follows that equation 7 can be used to calculate the breakage risk.

3. RESULTS OF BREAKAGE CALCULATIONS

At first, simulations have been calculated for weft insertion settings without use of a controlled weft brake. This is the worst situation as far as the risk of weft breaks concerns.

Simulations have been calculated for two different values for yarn strength (11.5 and 12.5 cN/tex), coefficient of variation of yarn strength (11 and 12 %), yarn modulus (50 and 55 N) and its coefficient of variation (6 and 8 %) and the standard deviation of the air-drag coefficient of the yarn (0.0004 and 0.005 for a mean value of 0.006076). Values for yarn strength have been chosen for a carded rotor spun yarn of 20 tex.

Table 2 Results table of the simulation of breaks in air-jet weft insertion

Mean strength (N)	Standard deviation strength (N)	Modulus (N)	Std deviation modulus (N)	Std dev. air-drag coeff.	Breaks per 100 000 picks
2.3	0.253	50	4.0	0.0005	0.0544
2.3	0.253	50	4.0	0.0004	0.0208
2.3	0.253	50	3.0	0.0005	0.0401
2.3	0.253	50	3.0	0.0004	0.0357
2.3	0.253	55	4.4	0.0005	0.2276
2.3	0.253	55	4.4	0.0004	0.2236
2.3	0.253	55	3.3	0.0005	0.2935
2.3	0.253	55	3.3	0.0004	0.2250
2.3	0.276	50	4.0	0.0005	0.5147
2.3	0.276	50	4.0	0.0004	0.4280
2.3	0.276	50	3.0	0.0005	0.5330
2.3	0.276	50	3.0	0.0004	0.1798
2.3	0.276	55	4.4	0.0005	2.1032
2.3	0.276	55	4.4	0.0004	1.0196
2.3	0.276	55	3.3	0.0005	2.1363
2.3	0.276	55	3.3	0.0004	0.9783
2.5	0.275	50	4.0	0.0005	0.0021
2.5	0.275	50	4.0	0.0004	0.0007
2.5	0.275	50	3.0	0.0005	0.0017
2.5	0.275	50	3.0	0.0004	0.0015
2.5	0.275	55	4.4	0.0005	0.0099
2.5	0.275	55	4.4	0.0004	0.0022
2.5	0.275	55	3.3	0.0005	0.0116
2.5	0.275	55	3.3	0.0004	0.0057
2.5	0.300	50	4.0	0.0005	0.0529
2.5	0.300	50	4.0	0.0004	0.0660
2.5	0.300	50	3.0	0.0005	0.0438
2.5	0.300	50	3.0	0.0004	0.0139
2.5	0.300	55	4.4	0.0005	0.2672
2.5	0.300	55	4.4	0.0004	0.1038
2.5	0.300	55	3.3	0.0005	0.1193
2.5	0.300	55	3.3	0.0004	0.1748

Table 3 Factor effects for break risk in air-jet weft insertion without use of a controlled brake

Strength				Modulus				Std deviation of air-drag coeff.	
Mean (cN/tex)		Coeff of var. (%)		Mean (N)		Coeff. of var. (%)			
12.5	11.5	12	11	55	50	8	6	0.0005	0.0004
0.055	0.563	0.564	0.072	0.494	0.124	0.319	0.300	0.401	0.217

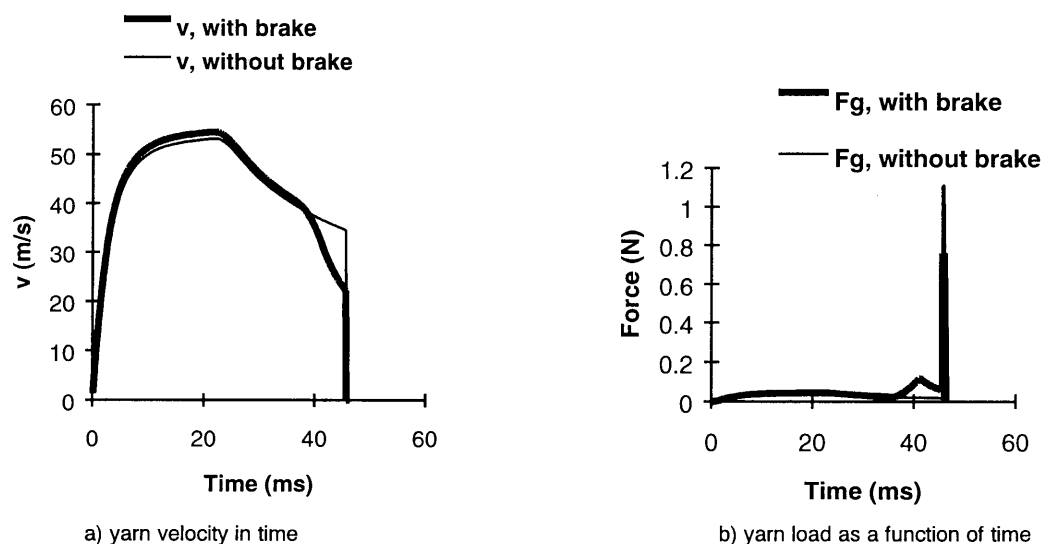
**Fig. 3** Comparison of weft insertion with and without a controlled weft brake

Table 4 Factor effects for break risk in air-jet weft insertion with use of a controlled brake

Strength				Modulus				Std deviation	
Mean (cN/tex)		Coeff of var. (%)		Mean (N)		Coeff. of var. (%)		of air-drag coeff.	
12.5	11.5	12	11	55	50	8	6	0.0005	0.0004
0.000005	0.000045	0.000049	0.000001	0.000039	0.000011	0.000026	0.000024	0.000039	0.000012

After 1000 simulated weft insertions, mean values and standard deviations for the yarn load and yarn strength have been calculated after which equation 7 is used to obtain the breakage rate. The results are expressed as breaks per 100 000 weft insertions and are given in table 2.

Table 3 gives an overview of the factor effects, this is the influence on the breakage risk for each of the parameters selected. The table gives the mean values for the break risk for each of the parameter levels selected and averaged over the other parameters.

The results of this factor analysis clearly show the effects of the different parameters used in the simulations. Changes in yarn strength or its coefficient of variation have the largest effect on the breakage rate. The influence of the coefficient of variation of the modulus is rather small.

Simulations have been calculated in which a controlled weft brake is used too. Using a control algorithm which takes the winding times into account, it is assured that the brake is activated some milliseconds before yarn arrival. In order to obtain the same arrival time as without a controlled brake, the air velocity should be increased. In the example given, an increase of the air speed from the main nozzle with three percent was required. Figure 3 shows velocity - time and force - time curves for the situations used in simulations with and without a controlled brake. The calculations have been made for a filling with average properties. The effect on the load on the yarn at stopper action can be clearly seen.

All simulations have been repeated with the use of a controlled brake. The factor effects are given in table 4 as the number of breaks to be expected per 100 000 insertions. The results clearly indicate the positive influence of the brake action on the breakage risk.

4. CONCLUSIONS

A model has been presented which allows to calculate the breakage rate of weft yarns in air-jet weaving. The law of motion of the weft yarn is solved numerically

and the statistical distributions of yarn load and yarn strength are calculated after Monte Carlo simulations of weft insertion. Using the distributions obtained, the risk of having a weft break can be calculated. The approach allows to assess the influence of yarn properties but also of insertion settings among which the use of a controlled weft brake has been demonstrated.

The results of the calculations clearly show the influences of yarn properties and the use of a controlled weft brake on the breakage rate in air-jet weaving.

REFERENCES

1. Duxbury, V., Lord, P., and Vaswami, T., A Study of Some Factors involved in Pneumatic Weft Propulsion, *J. Textile Inst.* **50**, 558-573 (1959).
2. Adanur, S., and Mohamed M.H., Analysis of Yarn Motion in Single-Nozzle Air-Jet Filling Insertion - Part I: Theoretical Models for Yarn Motion, *J. Textile Inst.* **83**, 45-56 (1992).
3. Salama, M., Adanur, S., and Mohamed, M.H., Mechanics of a Single Nozzle Air-Jet Filling Insertion System - Part III: Yarn Insertion through Tubes, *Textile Res. J.* **57**, 44-54 (1987).
4. Uno, M., A Study on an Air-Jet Loom with Substreams Added, Part I: Deriving the Equation of Motion for the Weft, *J. Textile Mach. Soc. Jpn* **18** (2), 37-44 (1972).
5. Uno, M., Shimomi, A., and Kise, H., A Study on an Air-Jet Loom with Substreams Added, Part II: Analysis of Various Weaving Factors by the Equation of Motion of Weft, *J. Textile Mach. Soc. Jpn* **18** (3), 86-92 (1972).
6. Wahhoud, A., Ein Beitrag zum Schusseintragsverhalten im Luftstrom, Ph.D.-thesis, RWTH-Aachen (1987).
7. Krause, H.W., Werden als Folge der höheren Tourenzahlen bei Webmaschinen bessere Garne benötigt ?, *Textil Praxis Int.* **32**, 263-272 (1977).
8. Krause, H.W., Über die Wahrscheinlichkeit von Fadenbrüchen, *Melliand Textilberichte* **60**, 551-553 (1979).
9. Krause, H.W., Nöbauer, H., and Shaheen, A., Erfassung und Prognose seltener Störeignisse an Webmaschinen, *Melliand Textilberichte* **71**, 585-589 (1990).
10. Krause, H. W., and Soliman, H. A., Technical evolution in weaving - do higher machine speeds require better yarns ?, *Int. symposium "West-European textiles tomorrow"*, Ghent-Belgium, 1990.
11. Zadlo, J., Fadenbruchzahlprognosen bei Webverfahren, *Textilbetrieb* **103** (6), 16-28 (1985).
12. Hahn, H., Vorausberechnung der Schussfadenbruch-Wahrscheinlichkeit, *Melliand Textilberichte* **72**, 612-615 (1991).

Physical and chemical properties of textile materials and aux. means of weaving

METHOD AND EQUIPMENT FOR THE STUDY OF THE WARP YARNS BEHAVIOUR ON THE WEAVING LOOM

Mihai CIOCOIU, Dorin AVRAM, Dumitru MIHAESCU, Nicolae IRIMICIUC

1. INTRODUCTION

The theoretical researches carried out in the mathematical model of the warp yarns' dynamic loading on the weaving loom, presented in the paper "Theoretical aspects regarding the behaviour of the warp yarns submitted to cyclic dynamic loading", led to the idea of conceiving and constructing an equipment for the simulation of such stresses.

The warp yarns are submitted on the loom to cyclic stresses as: tensile loading, friction against guiding and working devices, and also themselves, repeatedly bending, shocks, etc.

Warp's behaviour on the weaving loom has to be foreseen to be able to appreciate its performances, appreciation which is in most cases more or less subjective and it is based on the specialist's experience in comparing similar cases.

2. CONSTRUCTIVE PRINCIPLE OF THE EQUIPMENT

The equipment used for the current researches is presented in the Figure 1, and consists of the main working elements of the weaving loom taking part to the warp yarn stressing.

On the main frame (1) there are fitted the back rest (2) and the tensioning device (3) for the tested yarns, vertically operated by means of the rollers (4) and (5) driven by a group of cams (7); to easily obtain the desired warp density one of their end is fixed in a graduated front rest (6).

At the same time, the supporting frame of the front

rest, with an oscillating movement driven by the same group of cams (7), simulates the stress at the moment of beat-up. The elongation appeared during testing are taken over by the back rest's support (8), which slides in front of a rack (9) in which reaches a locking pawl mounted on the support (8) and doesn't permit the back rest to move forwards. These strains can be read on a graduated ruler (13). A loading cycle counter (10) controls the equipment's working; when the "0" value is reached, the counter stops automatically the device. The buttons (11) are used to select the stressing speed (rot/min) and on the LCD panel (12) are displayed the remaining number of stressing cycles.

In such conditions, the device will submit the yarns to some similar or quite identical stresses with those on the weaving loom.

The equipment is conceived in such a manner that it permits the testing function of the yarn type and of the weaving loom technological characteristics.

3. THE PRINCIPLE OF THE INTERPRETATION METHOD

A D_x length of the warp yarn is submitted to the test. The number of cycles, n , the yarns are going to be submitted to, is established function of the distance between the back-rest and the weft insertion zone and of the weft density of the fabric

$$n_c = D_b \cdot l \quad (1)$$

in which: n_c – number of the testing cycles; D_b – weft density (yarns/cm); l – sample yarn length (cm).

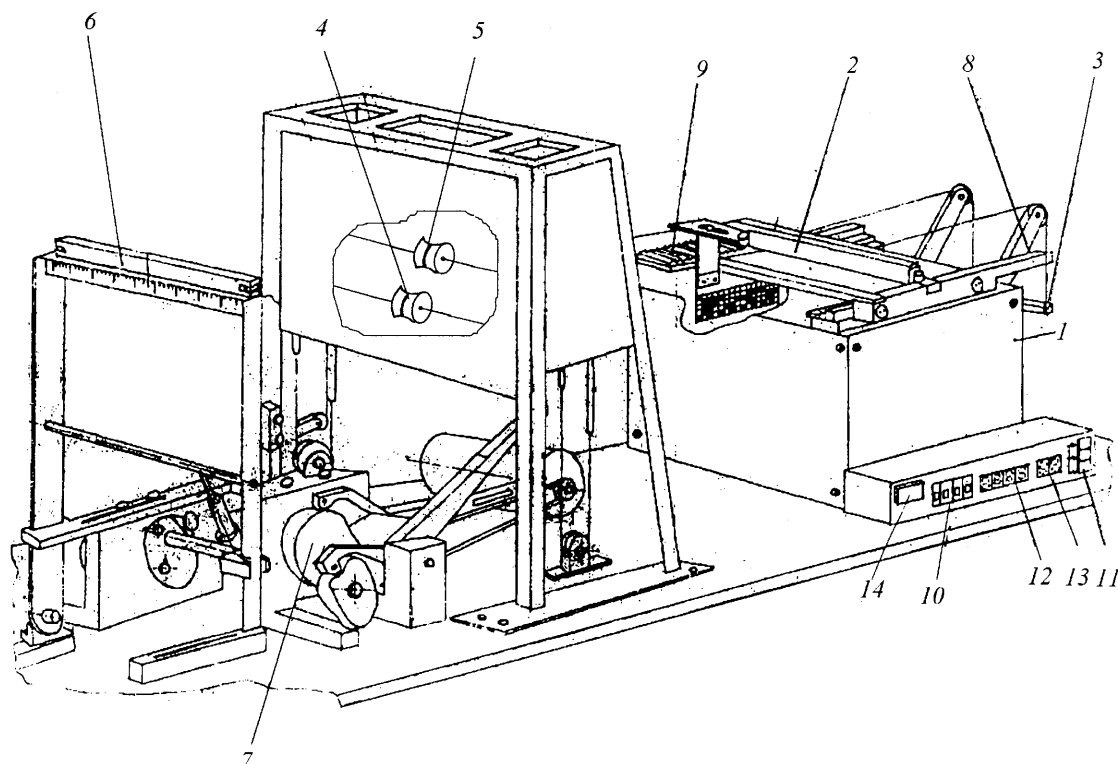


Fig. 1 Instalation layout

This value will be set on the programming counter. After the stressing, the yarns are tested for tensile strength and elongation on a dynamometer and there are evaluated the following indexes:

- the tensile strength at break

$$I_s = \frac{S_i - S_f}{S_i} \cdot 100 \quad (\%) \quad (2)$$

- the tensile elongation at break

$$I_s = \frac{a_i - a_f}{a_i} \cdot 100 \quad (\%) \quad (3)$$

in which: S_i , S_f – initial and final tensile breaking strength; a_i , a_f – initial and final tensile elongation.

The smaller these values are (towards zero) the better will behave the yarns on the weaving loom.

4. EXPERIMENTAL WORK

The testing conditions for our own researches:

- PP technical yarn, 150 dtex/64/40
- yarn's strength: 616 cN
- yarn's elongation: 21,24 %
- distance between the weft insertion zone and the shaft: 26 cm
- distance between the shaft and the back rest: 43 cm
- roller lifting distance: 3.5 cm.

The experiments have been made under the KONO factorial programming method.

Considering as independent variables the number of cycles and the tension during the warp yarn stressing, it has been obtained the experimental matrix presented in Table 1. As outcome variables there have been chosen the yarn's tensile strength and breaking elongation.

Data were computer aided processed by the use of the program REDOVAR (two variable egression) to find out the coefficients of the mathematical model, with the general form:

$$y = b_0 + b_1x_1 + b_2x_2 + b_{11}x_1^2 + b_{22}x_2^2 + b_{12}x_1x_2 \quad (4)$$

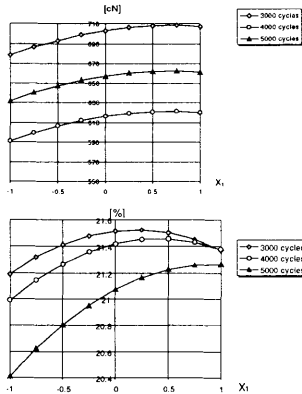
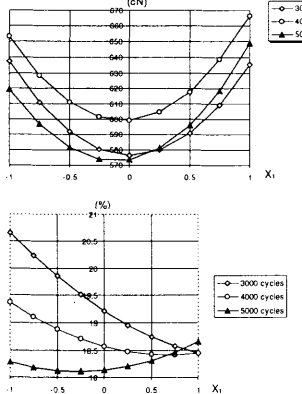
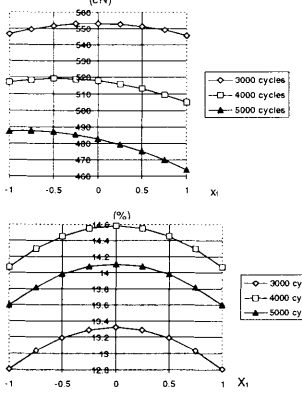
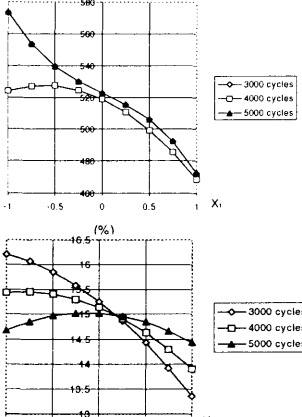
which puts in relation the resultant variable with the two considered independent variables.

The program checks the significance of the model's numeric coefficients by the Student test and the model's adequacy by the Fisher-Snedecor test.

Table 1

No. of experiment	Independent variables			
	Tension (cN/yarn), x_1		Number of cycles, x_2	
	real value	coded value	real value	coded value
1	4	0	4000	0
2	6	+1	5000	+1
3	2	-1	5000	+1
4	2	-1	3000	-1
5	6	+1	3000	-1
6	6	1	4000	0
7	4	0	5000	+1
8	2	-1	4000	0
9	4	0	3000	-1

Table 2

Variants	Equations	Graphics
V_{RI} V_I V_{AI}	$R_1 = 616.172 + 14.677x_1 - 23.058x_2 - 10.513x_1^2 + 63.986x_2^2$ $A_1 = 21.421 + 0.193x_1 - 0.445x_2 + 0.232x_1x_2 - 0.236x_1^2 + 0.095x_2^2$	
V_{R2} V_{II} V_{A2}	$R_2 = 599.488 + 6.764x_1 + 7.75x_1x_2 + 60.291x_1^2 - 25.708x_2^2$ $A_2 = 18.57 - 0.459x_1 + 0.647x_1x_2 + 0.337x_1^2 + 0.102x_2^2$	
V_{R3} V_{III} V_{A3}	$R_3 = 517.958 - 6.079x_1 + 4.707x_2 - 7.025x_1x_2 - 7.025x_1^2 - 40.025x_2^2$ $A_3 = 14.58 + 0.392x_2 - 0.51x_1^2 - 0.856x_2^2$	
V_{R4} V_{IV} V_{A4}	$R_4 = 519.064 - 27.828x_1 - 22.7x_1^2 + 3.799x_2^2$ $A_4 = 15.139 - 0.775x_1 - 0.116x_2 + 0.65x_1x_2 - 0.468x_1^2$	

The yarns have been stressed under the following conditions:

- a) cyclic tensile loading, for the simulation of the weft beat-up, with the amplitude of 10u/m at a frequency of 300 cycles/min;
- b) cyclic stress for the simulation of shedding and weft beat-up, at the frequencies of 100 and 200 cycles/min.

The results of the experimental data processing are presented in the Table 2, using the following notations:

- V_I – cyclic tensile loading with a frequency of 100 cycles/min
- V_{II} – cyclic tensile loading with a frequency of 300 cycles/min
- V_{III} – cyclic composed stress (beat-up + shedding) at a frequency of 100 cycles/min
- V_{IV} – cyclic composed stress (beat-up + shedding) at a frequency of 200 cycles/min
- R – tensile breaking strength
- A – tensile strain at break.

From the analysis of the equations and graphs presented in Table 2 it can be observed that the simple tensile stressing of the warp yarns, which simulates the beat-up, determines modifications of the properties of the tested yarns. Thus, the breaking tensile strength has variations up to 10% in the conditions of the variation of the stressing tensile force between 30 cN/yarn and 90 cN/yarn, the higher values corresponding to the working conditions of 300 cycles/min. In what concerns the elongation at break, their variations join the same intervals and variation direction as the breaking strength.

At higher stressing tensions (90cN) it has been found a rising tendency for the tensile strength and the diminishing of the elongation, behaviour which might be assumed on structural modifications of the filaments like macro-molecular chains re-orientation.

Under the conditions of composed stress there are comprised the effects of beat-up and shedding and it can be observed a diminishing tendency for the dynamometric characteristics of the tested yarns. There-

fore, the breaking strength, at low speed stressing, has a small variation (up to 4%) with the loading increase, while at higher stressing speeds this variation goes up to 18% for the same tension growth. The elongation at break follows the same tendency of variation, with values up to 10%, at the same level of loading.

In what concerns the testing duration, expressed by the number of cycles, there is no evident influence found. The differences between the dynamometric characteristics after 3000 cycles to 5000 cycles are at level of 5%; higher differences occur at lower stressing frequencies.

5. CONCLUSIONS

By the carrying out of the equipment described in the present paper, there have been brought the resources for the warp yarns testing in what concerns their weavability.

The equipment permits to test all types of yarns under similar conditions to those of any weaving loom and for any working speed.

After the tests, the 15 tex PP yarns showed a stronger influence of the tensile loading on the yarn's destruction process than that of the testing duration.

At the same time it is ascertained the amplification of the yarn's degradation phenomenon with the increase of the stressing frequency against the mark sample, without any significant variation corresponding to higher limits of the loading frequency.

The presented researches direct towards the necessity of carrying them on, with the testing of other yarn types and loading conditions.

REFERENCES

- [1] Tihomirov, V.B., Planirovanie i analiz experimenta, Moskva Iz. "Legkaia industria", 1972
- [2] Cochran, W. G., Cox, G. M., Experimental Design, N.Y.J. Wiley, 1957
- [3] Ciocoiu, M., Doctoral thesis, lito I.P. Iasi, 1980

DEVELOPMENT AND PRACTICE RESULTS OF QUICKSOLAN SPR

Dr. R.H. Huizenga

AVEBE b.a., Textile Laboratory

INTRODUCTION

AVEBE is a starch production company that is well known in the textile industry. For the textile industry AVEBE produces products for textile printing: adhesives and printing thickeners, and for warp sizing: sizing agents and waxes. Well known brand names are Solvitose, Solvitex, Kollotex and Quicksolan.

In this article the development and practice results of Quicksolan SPR are described. The sizing agent Quicksolan SPR is a relatively new name in the product mix of AVEBE's sizing agents. It is based on a new raw material: amylopectin potato starch.

CONSUMPTION OF SIZING AGENTS

For the sizing of spun warp yarn different polymers are being used. The main sizing agents used today are starch, polyvinyl alcohol (PVA), carboxymethylcellulose (CMC) and acrylics.

The ratio in which these compounds are used in a specific sizing recipe depends a.o. on the fibre material, the composition of the yarn, the yarn quality and cloth construction. The consumption is also influenced by local tradition and availability of the sizing agents.

As seen in table 1¹: The consumption of starch in Europe is more than 70 % of the total amount of sizing agent. In Asia and the USA it is over 60 %.

Table 1 Consumption of sizing agent per region in 1 000 tons

	Europe	USA	Far East
Starch	60	70	300
PVA	12	31	138
CMC	7	3	21
Acrylics	3	0	30

STARCH DERIVATIZATION

Starch is a polymer of glucose units. Starch can exist in two kind of polymers: linear called amylose, and branched called amylopectin.

The native, or pure starch is not suited for textile warp sizing. Solutions of native starch are too high viscous, difficult to process, and the solutions are unstable. Therefore the starch industry processes the raw

material. For the starch derivatives used for warp yarn sizing the main ways of derivatization are degradation and chemical substitution. Degradation is aimed to achieve the right viscosity. This can be done chemically (e.g. oxidation) or physically (e.g. extrusion). These processes break up the large polymer molecules. This results in a decrease in viscosity.

The viscosity of a sizing agent is important because it influences the pick up and the penetration of the sizing agent into the yarn (figure 1). A high viscous sizing solution will result in low penetration or surface sizing which is OK for coarse yarns. For fine yarn counts total penetration and high pick up is needed. Therefore low viscous sizing agents are favoured for fine yarn counts.

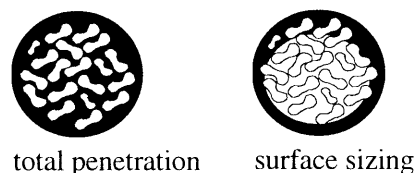


Fig. 1 Cross section sized yarn

The starch industry derivatizes starch also through chemical substitution to stabilise solutions of starch. The instability of starch solutions is caused by a process called retrogradation. It results in insoluble starch complexes that can clog conduct-pipes. The chemical derivatization through substitution not only improves the stability of solutions. It also has beneficial effects on film properties, like elasticity and solubility.

Starch is also chemically substituted to improve removability, which is important for desizing. Because of the good adhesion of starch to cellulosic fibres, enzymes are needed to desize cloth sized with most starch derivatives. To improve the removability a higher degree of substitution is necessary. If the degree of substitution is high enough the sizing agent can be removed from the woven cloth without the use of enzymes during the desizing process. To produce

Table 2 Derivatization of starch

degradation	chemical (oxidation) physical (extrusion) viscosity decrease
chemical substitution	stable solutions flexible films removability

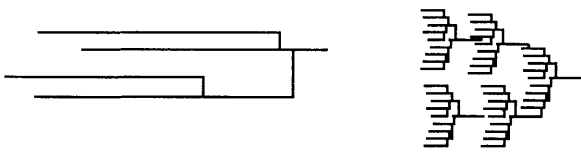
¹ SRI International: Specialty Chemicals, October 1992

these type of products the more sophisticated production method of extrusion is needed. The Quicksolan range is an example of the above. These are extruded carboxymethylated starch derivatives. They can be desized without enzymes.

STARCH COMPOSITION

Amylose and amylopectin are the main components of corn, tapioca and potato starch and the starch based sizing agents (table 3). These two types of molecules are present in different ratios in the starch granules. In

Table 3 Composition of potato starch



	20% amylose	80% amylopectin
chain length glucose units	200-500	15-25
degree of polymerisation	4000-6000	> 200,000
stability in solution	retrogradation	stable

general about 20 % of the weight of the starch is the linear amylose and about 80 % is the branched amylopectin. Not only the forms of the molecules differ, also the size of the molecules is significantly different. The amylopectin molecules are much bigger than the amylose molecules. The degree of polymerisation (= amount of glucose units per molecule) is higher than 200.000 for amylopectin. Whereas amylose has no more than 6.000 glucose unit per molecule. These figures are valid for potato starch. For tapioca and corn starch the molecule size of amylose and amylopectin is somewhat different than that from potato starch. The difference in size between amylopectin and amylose is the same.

Amylose starch solutions have a bad stability. This is caused by the ease of retrogradation of the amylose molecule. Retrogradation is the association of amylose with itself. In the practice of sizing this is seen as irreversible gel formation of the size solution upon cooling down to room temperature. The retrogradation of amylose is also responsible for the brittleness of films, made of starch. This brittleness of the film influences the performance of the sizing agent. It results in more dust during weaving and it will decrease efficiency.

The retrogradation of starch is a process that must be prevented in most starch applications. It has always been done by means of chemical derivatization of the starch. These chemical processes, however, are always a burden to the environment. Therefore AVEBE started 18 years ago a research project aimed at developing a potato that does not produce amylose. By us-

ing modern molecular biological techniques certain enzymes in the potato were blocked. This resulted in a potato that contains only amylopectin starch.

DEVELOPMENT OF QUICKSOLAN SPR

Based on this new raw material a new sizing agent was developed. Amylopectin starch still needs to be degraded to achieve viscosity's used for textile warp sizing and indeed it did not need derivatization to achieve stable solutions. The sizing agent had to fit in our Quicksolan range. This means that is desizable without enzymes. Therefore derivatization by carboxymethylation is still necessary for the desizing properties. Quicksolan SPR was developed. Quicksolan SPR is a carboxymethylated amylopectin potato starch derivative. It is made via the extrusion process.

On a laboratory scale different Quicksolan SPR's were prepared and compared with Quicksolan CMS as a sizing agent. Trials were done on a cotton Ne 36/1 yarn. On a laboratory sizing machine 25 yarns were sized. The sizing was done with different solutions at different concentration. The sized yarns were tested for 1. the amount of sizing agent present on the yarn (= pick up) and 2. abrasion resistance.

In figures 2 and 3 the relation between the pick up on the X-axis in a percentage and the abrasion resistance on the Y-axis is plotted. It is depicted as an interval. This is the 95% confidentiality interval of abrasion cycles in which all yarn samples break. If the interval is placed higher, then the abrasion resistance is better.

For the sizing trials different concentration of Quicksolan CMS were used. This resulted in the line that joins the different abrasion intervals. From the different Quicksolan SPR's only one concentration could be sized. In all cases the abrasion resistance interval is better than that of Quicksolan CMS. We see that at the same pick up a better abrasion resistance was found.

More trials were done including sizing wax as is common practice. 1% sizing wax (Glissofil Extra) was added to the sizing recipe. The percentage of 1% is

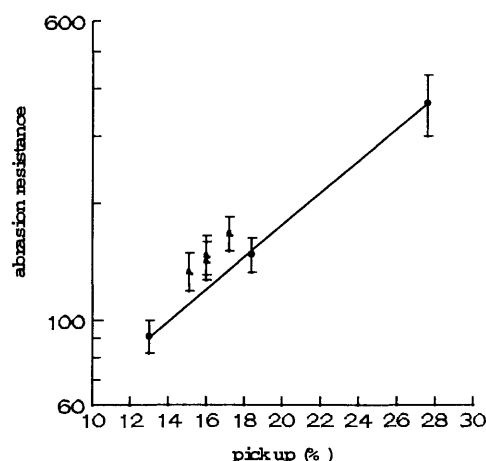


Fig. 2 Cotton Ne 36/1; ▲ Quicksolan SPR, ● Quicksolan CMS

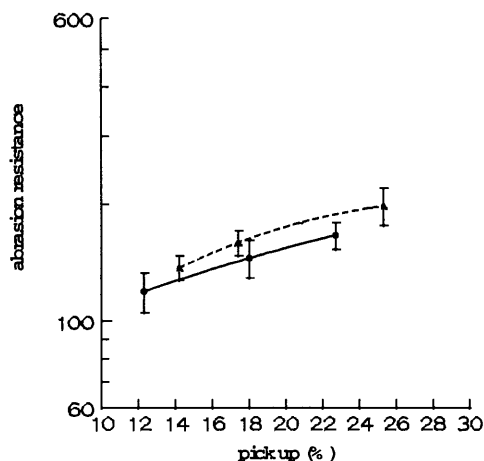


Fig. 3 Cotton Ne 40/1 + addition of 1% Glissofil Extra (size wax); ▲ Quicksolan SPR, ● Quicksolan CMS

based on the dry solids of the sizing agents. In figure 3 it is shown that Quicksolan SPR gives a better abrasion resistance than Quicksolan CMS.

In laboratory sizing trials on polyester/cotton 65/35 Ne 36/1 Quicksolan SPR performed better than Quicksolan CMS when the yarn was examined for pilling behaviour caused by abrasion.

Films of the sizing agents were also compared for tensile strength (table 4). The products were not only tested pure but also in combination with polyvinyl alcohol (PVA). A combination of sizing agents often used in practice.

The film of the pure Quicksolan SPR is stronger than that of Quicksolan CMS (37.2 vs. 35.0 N/mm²). Considering the combinations of Quicksolan with PVA there is the big drop in tensile strength upon addition of PVA to the starch derivatives. The tensile strength drops from 35 to 23 Newton per square metre for the Quicksolan CMS and from 37.2 to 31.1 for Quicksolan SPR. This decrease in tensile strength is normal. Interesting is, however, the fact that the combination of PVA with Quicksolan SPR gives a much stronger film than the combination with Quicksolan CMS: 31 Newton per square millimetre compared to 23. So films of the amylopectin starch based product are not only stronger themselves but they are also better compatible with PVA. In the 80/20 ratio the Quicksolan SPR/PVA film is over 30% stronger.

PRACTICE RESULTS OF QUICKSOLAN SPR

The laboratory results were put to the test in practice. In table 5 examples of results from practice are shown.

In the sizing recipe of example 1 for a multi-coloured dyed cotton yarn Ne 36, the polyvinyl alcohol (PVA) is replaced for 66% by Quicksolan SPR. This resulted in a

Table 4 Film strength (tested at 21 °C and 65% R.H.)

Product	Fmax (± 2.5) N/mm ²
Quicksolan CMS	35.0
Quicksolan SPR	37.2
Q.CMS/ PVA 80/20	23.0
Q. SPR/ PVA 80/20	31.1

decrease of breakage's from 1.5 per 100.000 to 1.25. The amount of defects in the cloth decreased with 70 %.

The second example shows a more drastic adaptation of a sizing recipe for Cotton Ne 40. The PVA could be banned from the recipe totally. The pick up increased from 14 to 18 %. But the weaving efficiency also increased significantly: from 69.9 to 74.4 %. The customer benefited with 1. lower sizing costs, 2. higher production output, 3. better quality in production (more A-grade cloth) and 4. more environmental friendly production process. Quicksolan SPR is a natural product based sizing agent and it is readily biodegradable.

In example 3, a dyed cotton yarn, the PVA in the sizing recipe is replaced by Quicksolan SPR. At a similar pick up 13.5 and 13.6 % the weaving efficiency increased with 4 %. Here we see a combination of decreasing the sizing costs while increasing the weaving efficiency.

In example 4 a combination recipe of starch and PVA. Deleting all synthetic polymer from the sizing recipe resulted in an increase in weaving efficiency.

Example 5 and 6 are about polyester/cotton yarn. In example 5 the replacement of an ordinary CMS-starch by Quicksolan SPR resulted in an increase of weaving efficiency of 10%. This problem quality could now be woven smoothly with a weaving efficiency of 92 %. In an other less problematic quality the weaving efficiency was increased by 3 %.

Quicksolan SPR can also be used for the sizing of spun polyester yarn. In combination with PVA very good results can be achieved. In the last example 7 the ratio PVA/Quicksolan SPR was brought to 6/6. The old recipe contained only synthetic sizing agents. The carboxymethylcellulose (CMC) could totally be replaced by Quicksolan SPR, as was a part of the polyvinyl alcohol (PVA).

The examples in table 5 show the versatility of Quicksolan SPR as a sizing agent. The examples show improvements and excellent results with: cotton yarn, raw and dyed; polyester/cotton yarn and with spun polyester yarn.

CONCLUSIONS

The new amylopectin potato starch gave AVEBE access to a totally new raw material. This resulted in Quicksolan SPR. Quicksolan SPR is a low viscous sizing agent that can be desized without enzymes. With this new product we give our customer the possibility to improve his weaving efficiency or to reduce his sizing costs.

That is why we called our product Quicksolan SPR. SPR is the abbreviation of Synthetic Polymer Replacer.

Properties of Quicksolan SPR:

- Based on amylopectin potato starch
- Low viscous sizing agent for all yarn types
- No enzymes needed for desizing
- Improving weaving efficiency/ reducing sizing costs
- Synthetic Polymer Replacer.

Table 5 Practice results with Quicksolan SPR

Example 1					
region Europe	yarn type Cotton dyed	yarn number Nm 60/1 Ne 35.4/1	number of ends 5400	loom type air jet	speed rpm 700
old recipe	(%)		new recipe	(%)	
PVA	13.6		Quicksolan SPR	9.1	
wax	0.54		PVA	4.54	
			wax	0.54	
breaks/100.000	1.5		breaks/100.000	1.25	
defects/100 m	2.7		defects/100 m	0.7	
Example 2					
region Asia	Yarn type Cotton	yarn number Nm 66/1 Ne 40/1	number of ends double width 12.500	loom type air jet	speed rpm 480
old recipe	(%)		new recipe	(%)	
PVA	10.4		Quicksolan SPR	10	
acid starch	4.4		starch ester	12	
Acrylic	0.75		acrylic	0.63	
Emulsified oil	1.2		wax	0.3	
pick up	14 %		18 %		
Weaving eff.	69.9 %		74.39 %		
Example 3					
region Asia	Yarn type Cotton Dyed	yarn number Nm 66/1 Ne 40/1	number of ends 7200	loom type rapier	speed rpm 400
Old recipe	(%)		ew recipe	(%)	
PVA	7		Quicksolan SPR	7.5	
Acid starch	8		acid starch	8	
Wax	0.4		wax	0.4	
Pick up	13.5 %		13.6 %		
Weaving eff.	68 %		72 %		
Example 4					
Region Europe	Yarn type Cotton	yarn number Nm 30/1 Ne 18/1	number of ends 6400	loom type rapier	speed rpm 450
Old recipe	(%)		new recipe	(%)	
PVA	1.39		Quicksolan SPR	5.55	
Quicksolan SPR	4.90				
Starch	5.55		starch	5.55	
Wax	0.21		wax	0.21	
Weaving eff	93 %		94–96 %		
Example 5					
Region Europe	Yarn type PE/C 65/53	Yarn number Nm 50 Ne 30/1	number of ends 7600	loom type air jet	speed rpm 600
old recipe	(%)		new recipe	(%)	
CMS-starch	8.4		Quicksolan SPR	8.4	
PVA	5		PVA	5	
Wax	0.2		wax	0.2	
Weaving eff	82 %		92 %		
Example 6					
region Europe	Yarn type PE/C 52/48	yarn number	number of ends	loom type	speed rpm ??
old recipe	(%)		new recipe	(%)	
CMS-starch	8.4		Quicksolan SPR	8.4	
PVA	5		PVA	5	
Wax	0.2		wax	0.2	
Weaving eff	89 %		92 %		
Example 7					
region Europe	Yarn type Polyester	yarn number Nm 34/1 Ne 20/1	number of ends	loom type	speed rpm ??
old recipe	(%)		new recipe	(%)	
PVA	9		PVA	6	
CMC	4		Quicksolan SPR	6	
Wax	0.2		wax	0.2	
Weaving eff	92 %		95 %		

Measuring and research methods in the weaving process I.

VISUALISATION AND ANALYSIS OF FABRIC FORMING PROCESS

Aleš Cvrkal

TU Liberec, Háfkova 6, 461 17 Liberec
e-mail: ales.cvrkal@vslib.cz

INTRODUCTION

The process of fabric creation is a difficult dynamic event affected by a chain of factors. They can be divided into certain groups firmly connected with the whole weaving process. A part of them depends mainly on the type and construction of the loom beat-up mechanism and on the method of weft inserting. All progress of new types of weft inserting and beat mechanisms was caused by demands for higher productivity of weaving machines. The modern weaving looms run at incredible high level of weaving frequency, but certain problems around accessibility of weft density or fabric weavability still remain.

This article deals with an optical searching method, which is based on recording fast object events. At the background of the beat-up process the operation of the High Speed Camera system and its possible application in the field of textile research is explained. A basic fast video laboratory, which is equipped for searching beat-up pulse events, is also introduced through its special superstructure software for the dynamic analysis of moving objects. The essential part of the paper (however, it could not be printed out here) also includes the replaying of slowed down recorded beat-up sequences in the suitable-enlarged macro-views.

1. FABRIC FORMING PROCESS

An important part of the weaving cycle is the phase of weft beating-up. During and after it the fabric is created up to its own woven structure. The fabric forming

process generally means the pushing of the inserted weft into the cloth fell and its fixing on the required weave by the warp thread. The zone of fabric forming also includes backward and forward weft slippages along the warp. During the weft sliding the weaving resistance R must be overcome by the beat-up force F_p . The background for the analysis of the weaving resistance and beat force are the deformation and movement events of the weft and warp round the cloth fell - it means the basic fabric forming process.

1.2 Beat – up event

Generally, there is a balance between the weaving resistance R and beat force F_p (see Fig.1). This balance includes many important processes, but the top process is the translating movement of the weft into the cloth fell. The weft is pushed by the help of reed close to the preceding-weft (*the weft woven during the last beat cycle*). The weft sliding path begins from the time point when the reed first hits the inserted weft towards to the cloth fell. At the contact moment of the pushed weft with the cloth fell the reed carries out a partial beat pulse y , which is consumed by a warp elongation x and weft indentation ζ . The condensing of the weft in the place A , by the given weft indentation z determines the weaving resistance R . For this still holds:

$$F_p - R = 0 \quad (1)$$

Where: value F_p can be the function of the beat stroke X . The value R is mainly the function of the weft density distance A and so of many other fabric creating

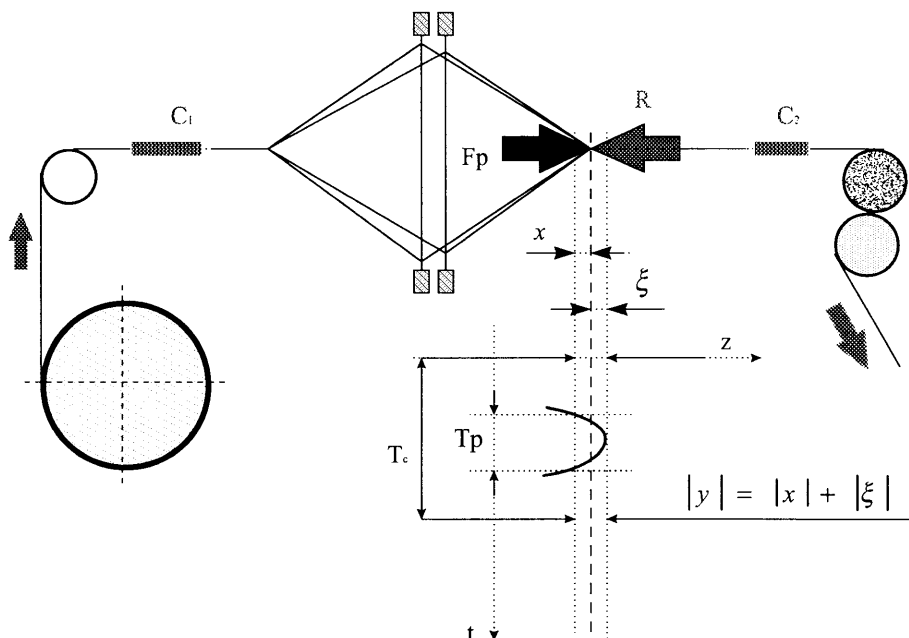


fig.1

factors. On the other hand, the value R should be expressed as a function of the weft sliding ζ to the cloth fell.

Note: This is the basic balance equation of beat-up process which is used here as a starting step to remind the problems of the fabric creation process. And also, from the point of use of the High Speed Camera System, this is the area where the fast recording system is applied.

Shortly, before the beat pulse the warp and fabric are loaded by the basic tension force Q , which is not changed progressively during the short time of beat-up pulse. The pulse contact between the cloth fell and

reed is increasing the warp tension and simultaneously, the fabric tension is decreasing. Substituting these warp and cloth changes by the elastic elements C_1 and C_2 , the tension forces Q_1 , Q_2 are put in equations:

$$\begin{aligned} Q_1 &= \bar{Q} + C_1 \cdot x \\ Q_2 &= \bar{Q} + C_2 \cdot x \end{aligned} \quad (2)$$

These static equations of tension forces are transformed into the beat-up force F_p equation, which is expressing the discussed common weaving process:

Standard weaving resistance situation

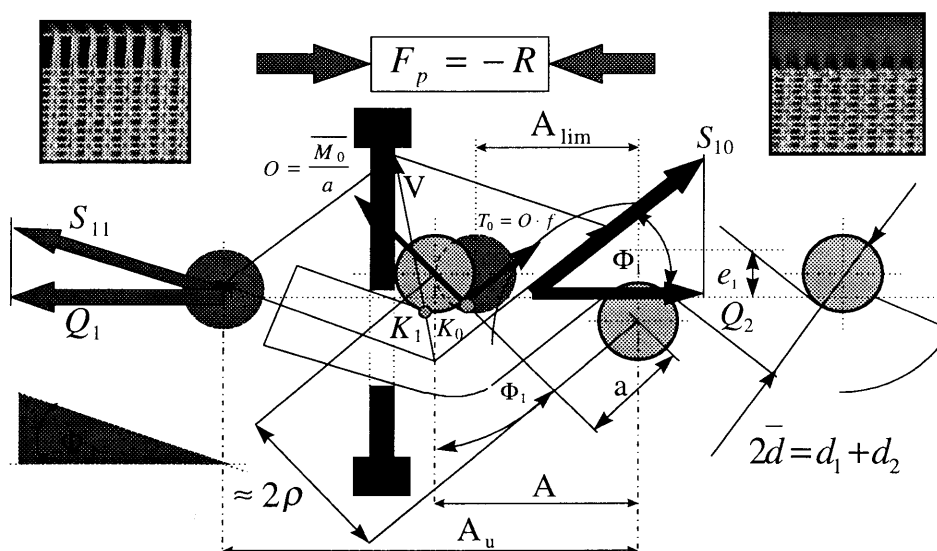


fig.2

$$F_p = Q_1 - Q_2 = (\bar{Q} + C_1 \cdot x) - (\bar{Q} - C_2 \cdot x)$$

$$F_p = (C_1 + C_2) \cdot x \quad (3)$$

(Note: we expected that the beat force F_p must be delivered for given weft density. Then, it is obvious that by improving the warp and cloth stiffness C_1 and C_2 the cloth fell stroke X could be shortened. No methods how to do that will be discussed in this article)

1.3 Weft beat-up acting forces

Pushing the weft in the open shed along the warp threads increases the beat resistance R . This resistance value is determined mainly by two basic influences – friction effect of weft along the warp threads and the forcing-out effect of the crossed warp threads. For better understanding of the situation, we deal with a **quasi-static example**, where the inertial forces of the weft mass and the time-kinetic-dependent friction are not considered.

The last beaten weft (*zero-weft*) is loaded by the resultant of warp stress forces S_{10} and S_{11} . The backward orientation of the resultant develops the weft pressing-out effect from the cloth fell. Other additional acting forces are caused by the fibre abrasion. The abrasion force arises at the warp-weft osculation point K_0 and is combined by two components T_L and T_0 . The first represents a force influencing fibre sticking and the second the adhesive force of sizing. The variable T_0 represents the sliding friction of loading point K_0 along the spreading warp threads. The sliding friction is determined by the friction coefficient f and pressure force of the warp O in the place of K_0 point. The pressure force O is a consequence of the spreading warp caused by the sliding weft. For that a limit bending moment \bar{M}_0 arises in the warp threads and creates the pressure force $O = \bar{M}_0 / a$ where a – is the distance between the contact points of the two neighbouring wefts: $a = (A - 2 \cdot \rho \cdot \sin \Phi_1) \cdot \cos \Phi_1$, ρ – radius of curvature

then the sliding friction force

$$T_0 = f \cdot \bar{O} = f \cdot \bar{M}_0 \cdot \frac{\cos \Phi_1}{A - 2\rho \cdot \sin \Phi_1} \quad (4)$$

If the tension in the warp outlasts and the force S_{10} will act together with forces T_L and T_0 on the entering side of the weft (it should be assessed that the tension in warp is to be arising exponentially according to the Euler fibre friction law).

The beat-up resistance R should be put in balance with the immediate tension force before and after the zero-weft $R = S_{11} \cos \Phi_0 - S_{10} \cos \Phi_1$. Using T_0 expression at entering K_0 point, the weft resistance R should be expressed in the universal form:

$$R = \left[(S_{10} + T_L + T_0) e^{f(\Phi_1 + \Phi_b)} - M_0 \frac{4}{\rho} (e^{f(\Phi_1 + \Phi_b)} - 1) \cos \Phi_b - S_{10} \cos \Phi_1 \right] \quad (5)$$

The tension loading of the warp is caused by the beat stroke X . Additionally, this stroke depends on weft-space distance A , or on the weft density $D_2 = 1/A$. Weaving resistance R should be rewritten into the linear combination of the influences of beat-up acting forces:

$$R = \bar{Q} \cdot r_Q(A) + T_L \cdot r_T(A) + \bar{M}_0 \cdot r_M(A) \quad (6)$$

where there are: r_Q – factor of warp tension, r_T – factor of weft-warp sticking, and r_M – factor of warp flexural rigidity.

2. OBSERVING CLOTH FELL EVENTS

This chapter deals with the possibilities of application of the optical analysis system in the beat – up process. This method is based on recording and analysing events within the desired area. The recorded objects are brought into the software environment analysed in motion. The slowed down scene begins to be analysed frame by frame and the basic dynamic values of the moving objects are immediately obtained on the PC screen. They are also stored in PC hard disc as a data file to plot by suitable plotting software program.

For our needs the beat-up pulse $Y(t)$ is substituted here by a one half of the sinusoid. The simplified pulse (see Fig. 3) is to be considered as the standard form of the beat-up pulse $Y(t) = |Y| \sin \omega_p(t)$, where: $|Y|$ – is the reed stroke in the contact with cloth fell

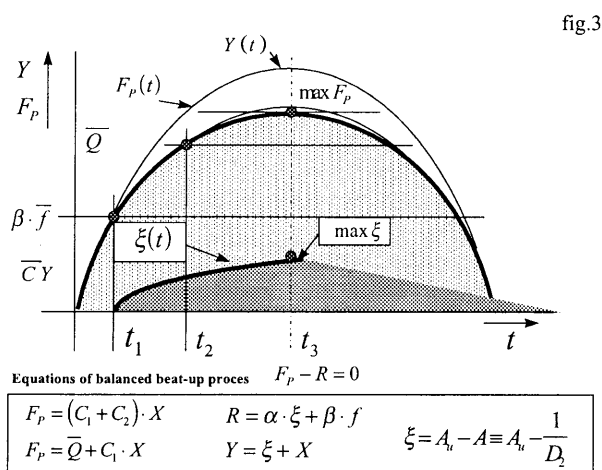
ω_p – is the weaving frequency, $\omega_p = 2\pi / T_p = 2\pi / \Psi T_C$

T_p – is the duration of beat-up

T_C – is the duration of weaving cycle, $T_C = 60/n$

2.1 Idea of beat-up pulse

During the beat-up process the weft is pressed into



the cloth fell on the sliding path ξ against the weaving resistance R . The beat-up mechanism must be able to develop the requested beat force F_p which is causing the warp elongation and cloth contraction. The tension in warp and cloth is changing progressively with F_p , so that: $F_p = Q_1 - Q_2 = (C_1 + C_2) \cdot X = \bar{C} \cdot X$

The beat process comes within two main phases:
1st phase: friction resistance remains insuperable for the weft. Warp is elongated until overcoming the friction: $X(t) = Y(t) = |Y| \sin \omega_p t$, $F_p(t) = \bar{C} \cdot X(t) \leq R_f \equiv \beta \cdot \bar{f}$.

2nd phase: friction resistance is exceeded at time t_1 and weft begins sliding:

$$\bar{C} \cdot X(t_1) = \beta \cdot \bar{f}, \quad X(t_1) = Y(t_1) = |Y| \sin \omega_p t_1$$

$$t_1 = (1/\omega_p) \cdot (\arcsin \bar{f}/\bar{C}|Y|)$$

This static solution shows that the sine course of the sliding weft $\xi(t)$ comes with the same phase of beat-up pulse, it means *without time delay*. The maximum weft slide into the cloth fell occurs at the moment when the reed is coming through the top of sine weave, however, beat force F_p still remains (*hatched difference in Fig.3*).

2.2 Cloth fell objects recording

The previous theory of beat-up process is giving the assumption that cloth fell is the area where an optical

recording system could be used. However, this very small space requires special optic facilities and, of course, a video system which is able to catch fast object events. Cloth fell is an important space where „beat-up objects are meeting,, (see Fig. 4). During the short time pulse the three objects are in close contact – *reed – weft – forming zone* – to create the desired weave and weft density. Under certain conditions the digital camera system is able to record interactions among the moving objects and replay them as a slowed down sequence or to print out each film frame as a photo. The quality of sequence or photo-print depends on many factors, but basically on the setting of speed of the recording camera (520Hz – 3,3 kHz).

The considered macro-space of cloth fell requires the mounting of a special extending tube and lens on the camera body and either stroboscopic light or high density illuminator directly spotted on the recording objects. The practical use of the digital camera also requires a special software for dynamic analysis of the moving object and, of course, a package of softwares for sequence processing and data plotting (see Fig. 5 to get general idea about optic laboratory). The software analysis makes that system advanced and applicable in the field of sciences where common measuring devices could not be applied. (*dynamics of object should be changed, etc.*).

Cloth-fell wiew

TIF. format converted film frames

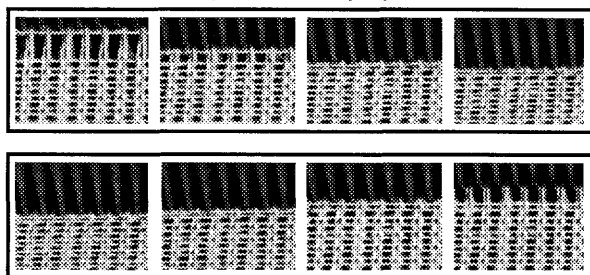


fig.4

2.3 Animation of beat-up pulse

Using the High speed camera system and software analysis the beat up pulse could be animated. The camera system is focused on objects – *reed – weft – cloth fell* – to visualise their time course around the top of beat pulse (see Graph 1). The recorded scene is cut by the PC software to create a short film of the beat pulse and to store it on the PC hard disc. Lay-out scene like that is processed through the motion software analysis. The beat pulse of desired objects is signed

directly on the PC screen by a colour point. When objects start moving, these points are tracked through the film scene in the last frame. The time course of their path appears on the screen immediately. The measured data are also stored on the PC hard disc together with the film scene in the corresponding file. (*The software analysis offers a variety of algorithms using a correlation or SSD, and also the automatic, semiautomatic or manual setting of object tracking can be set – all depends on the difficulty of the recorded scene*).

2.4 Fabric forming zone test

The theory of fabric forming process includes also events of moving wefts on the cloth fell (so-called: „travelling wefts,,) during the beat up

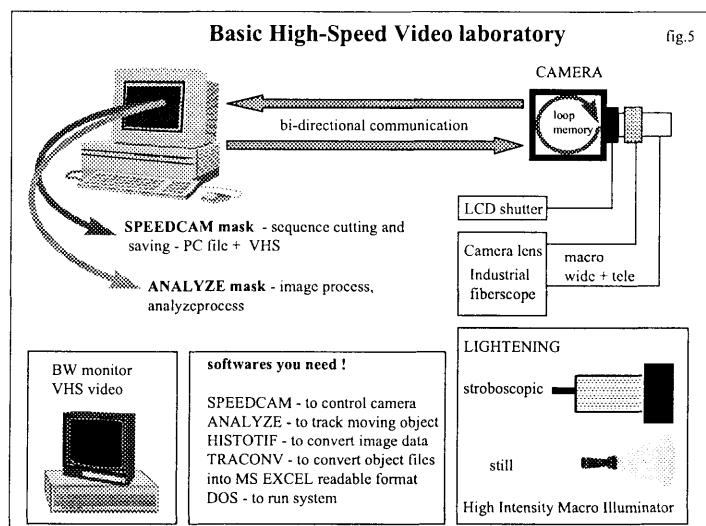


fig.5

pulses. On the top of beat pulse the first few wefts get close to each other. The „weft shifting,, is usually reduced on the first and second one (see Fig. 6). When

the reed releases the cloth fell these wefts get the backward shifting to find the balanced position at desired weft density. The conditions, weft shifting depends on, are mainly given by friction characteristics of both thread systems weft – warp (and on many others). Due to the weft condensing test the film recorded area was split up into three zones. The first one is a starting position of zero-weft (it is also a position of the first movie frame). The second zone is an area of supposed weft shifting, which includes two last beaten wefts. The third zone boundary depicts the area where the weft shifting is not expected. The sequence of weft condensing is recorded under given conditions (see Graph 2) on the top of beat up pulse, where the weft is getting as close as possible (depends on weaving conditions fabric weave e.t.a.). To verify if there is any change of weft space, the difference and between wefts 0 – 1st, 1st – 2nd and 2nd – 3rd is worked out (see Graph 3).

Test of weft condensing

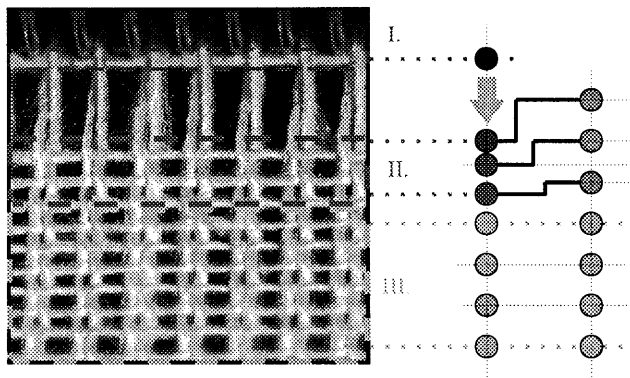
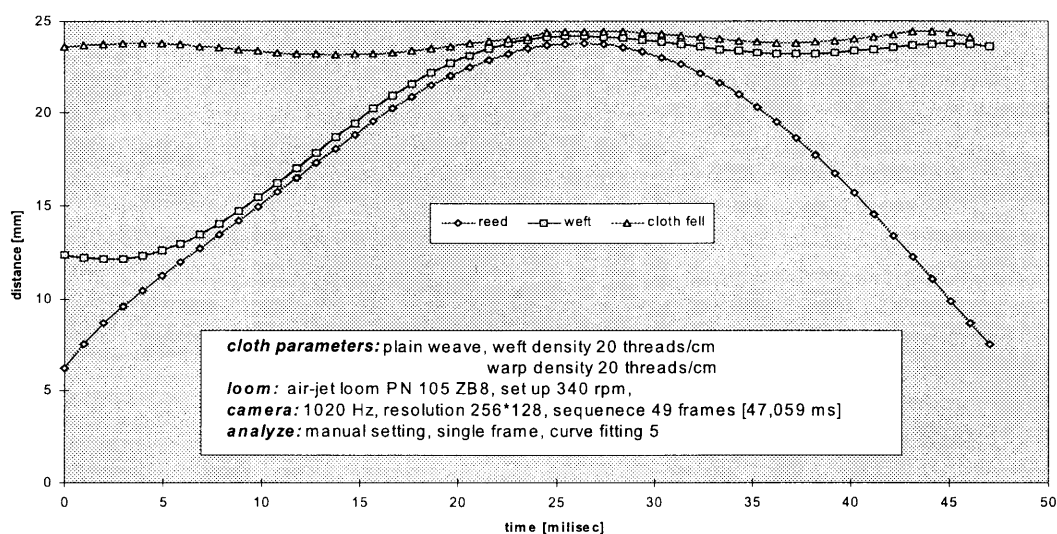


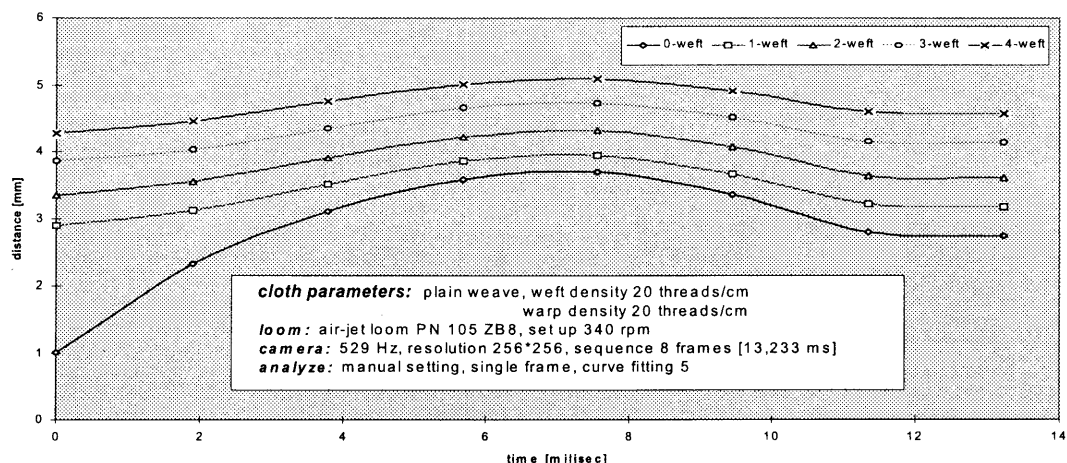
Fig. 6

Time course of reed stroke - top of beat pulse



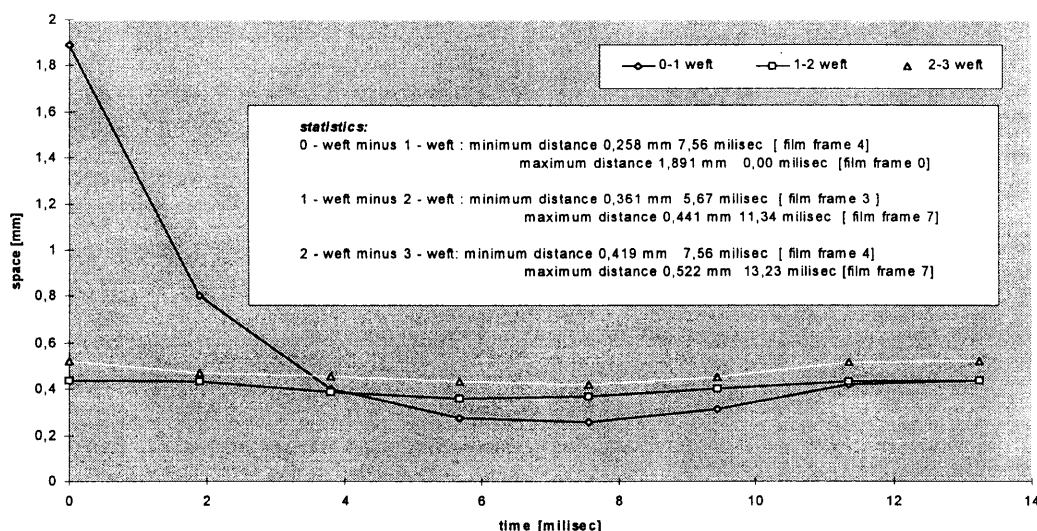
graph 1

Time course of weft condensing - top of beat pulse



graph 2

Time course of weft condensing - space difference



graph 3

3. CONCLUSION

The recorded sequences verified that the digital high speed video system is suitable to visualise events during the beat up process. A great progress has been made in recording the fast moving beat- up objects (reed, weft, cloth fell) and in adapting the film recording close to the problems of the weaving process. As far as the use of the motion analysis at the difficult motion of sliding weft the troubles still remain. The problem is caused by the recording speed of the camera system, which should be higher at the full camera resolution and the higher resolution makes the process of analysis more precise. However, some problems are also

caused by the special profiled reed which is covering the cloth fell on the top of the beat pulse and makes the cloth fell partly „invisible“ for recording. Resolving these problems will make the optic recording system very powerful for observing all the weaving cycle.

4. LITERATURE

- [1] Cvrkal A.: High Speed Video System – the Step to Overcome Rapid Motions, contribution, University of Lodž, 1997
- [2] Cvrkal A.: Vizualizace tkacího procesu, sborník CD, konference Vysoké Tatry, 1998
- [3] Nosek S.: Teorie tkacího procesu, díl I, II, Dům techniky ČSVTS, Pardubice 1988

MEASUREMENTS OF WEAVING PROCESS OF FABRIC BARRINESS

Ivan Jaksch

*Technical University of Liberec, Faculty of Mechatronics and Interdisciplinary Engineering Studies,
Department of Measurement*

1. INTRODUCTION

Fabric is a textile formation, which is created by means of interlacing warps and wefts distributed in regular distances. On the way of warp through the loom sometimes phenomena, which are very difficult to explain, occur. They appear in the fabric as periodical stripes, random stripes, sett changes, discomposed fabric and other phenomena connected with the quality of the fabric. Another problem is a fabric barriness after the loom stoppage.

The only way, how to find out the causes of these phenomena is the measurement and diagnosis of all the way of the warp. This paper deals with the measurement system and methods for the measurement of weaving process of fabric barriness (fabric regularity) directly on the loom. This paper does not deal with the influence of the processed textile material on fabric barriness and we assume that the textile material is faultless.

2. THE PROBLEM ANALYSIS

The analysis of the above mentioned problem shows that the loom systems (parts), which create the way of warp, have the decisive influence on its origin. They are:

- let-off motion
- beat-up mechanism
- take-up motion

Shed motion has no influence.

If the let-off motion feed in the loom cycle is irregular, sett changes, discomposed fabric or weft barriness can appear in the fabric. The same is valid for the take-

up motion. As a result of that we must measure the let-off and take-up feed per cycle.

By the cloth fell, the situation is complex and it is possible to find out the influence of both motions and also the influence of the beat-up mechanism. The cloth fell motion was measured at many looms to analyze its shape and to find out such quantities which are important for evaluation and can determine the influence of the take – up motion and the beat-up mechanism. The typical shape of cloth fell motion and quantities which are measured by cloth fell by this system are shown in Figure 1.

Summarizing this problem, we got the requirements for measured quantities.

- let-off motion feed per cycle [mm] – ORP
- take-up motion feed per cycle [mm] – ZRP
- cloth fell feed per cycle [mm] – CTKP
- beat-up angle in every cycle [°] – UP
- cloth fell beat-up shift in every cycle [mm] / 0 PP

The measured quantities must be taken simultaneously in every loom cycle and for a great number (ordinary hundreds) of weaving cycles.

3. MEASURING SYSTEM

The measuring system was designed as a distributed system consisting of the measuring unit JTS 2J connected to PC by the serial line RS 232. The PC in real time monitors and displays measuring quantities in physical (engineering) units and successively provides evaluation. The JTS 2J unit is equipped with its own single chip processor and program in EPROM. The JTS 2J activity is based on the absolute angle main shaft loom measurement.

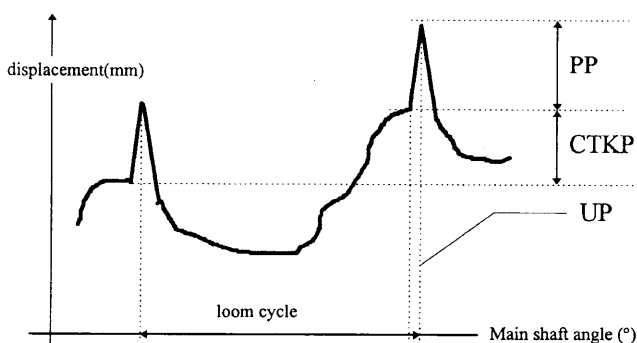


Fig.1 Cloth fell motion and measured quantities

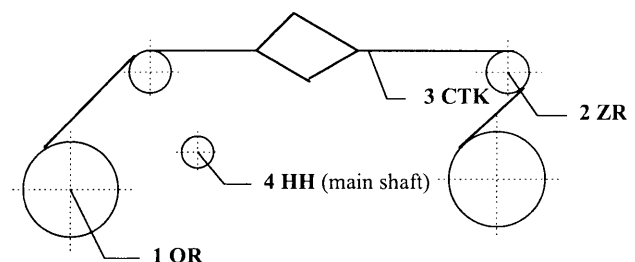


Fig.2 Sensors placing on the loom

The fixing of sensors in the loom is schematically shown in Figure 2. There are four sensors in the loom. The sensors for feed measurements are incremental encoders with division 20 000 P/R, the sensor for angle measurement is the incremental encoder with division 4096 P/R (12-bit converter for possibility to connect this system to the internal angle data bus of new looms). The sensors for the let-off feed -1OR, the take-up feed -2ZR, and the main shaft angle -4HH are mechanically fastened to these mechanisms, the cloth fell sensor -3CTK is needed wheel placed on a special mounting gripping about 1.5 cm from the cloth fell.

The first three above mentioned measured quantities (ORP, ZRP, CTKP) are measured directly by the incremental encoder counter reading, the last two are software evaluated from the cloth fell movement – see Fig.1. Prior to this software evaluation, many face cloth movements were measured and evaluated. Due to circular buffer memories placed in PC, it is possible to measure $N = 512, 1024$ or 2048 successive loom cycles or to measure and monitor for an arbitrary long time or cycles and to evaluate the last $512, 1024$ or 2048 measured quantities.

It is not necessary to measure all five quantities and it is possible to choose arbitrary ones. If we want only to analyze and diagnose the let-off motion, we will choose it in software and will use only -1OR and 4HH sensors, etc.

The main shaft angle reading takes $8 \mu\text{s}$ ($125\,000$ readings/s) which is quite good dynamics for this measurement. The system resolution is better than 0.01 mm and accuracy is better than 1% .

4. EVALUATION

The evaluation is performed after the measurement where PC works as an oscilloscope for the measured data. The measurement results are 5 (1–5) data arrays in engineering units (mm, °). The buffer is dimensioned for $256, 512, 1024$ or 2048 data points. The evaluation is provided both in time and frequency domain. The simple evaluation method is observing the time data, e.g. what happens with let-off and take-up motions, and cloth fell feed after the loom stoppage. For detailed evaluation in the time domain, the new evaluation method was developed. For the detection of the periodical barness and fault parts of mechanisms, the diagnostic based on statistical spectral analysis is used.

By the digital signal processing, the sampling frequency must be, at least, twice higher than the highest signal frequency in spectra. It should mean a great number of data in every loom cycle. If we choose the characteristic signal quantities as integrals (angles or shifts we can consider as integrals of angle velocities) or maximums (beat-up angle, cloth fell beat-up shift), we can take samples once per loom cycle without dis-

turbing the sampling theorem. The samples of measured signals are taken in so-called machine time. The sampling interval Δt is not expressed in seconds, but in dimensionless cycles (c). For further computation we can consider the sampling frequency as 1. Spectral frequency is not expressed in Hz but c^{-1} (cycles powered minus one) and the maximal frequency in the spectra equals $1/2 c^{-1}$. The reverse spectral frequency value is expressed in cycles - c - and it shows the number of loom cycles, after which the appropriate phenomenon (frequency) is repeated. This method has the following advantages:

- mean value and variance have important technological use,
- all statistic characteristics including spectra are independent on weaving frequency (for sampling in real time it is not true), so the influence on the take-up, let-off and beat-up mechanisms can be studied,
- high resolution spectra in frequency range of disturbances can be obtained from a relatively small number of data (for $N = 512$ loom cycles, the resolution in frequency range is $0.002 c^{-1}$).

We can simply say that the signals with frequencies lower than one half of the loom revolutions show certain mechanism irregularities in dependence on the constructional kinematic mechanism arrangement. If we find in the spectra the peak and the corresponding machine frequency, it is possible to find a machine part which works on this frequency. For easy evaluation, the normalized percentage power of spectral density function is computed. The normalization is performed by dividing power spectral density function by variance $-\sigma^2$. The values of the normalized power spectral density lie between 0 to 100, irrespective of the time series values.

From every measured quantity we can evaluate in the **time domain**:

- observing all measured quantities $X_i, i = \langle 1 - N \rangle, N = 512, 1024$ or 2048 and their edition,
- basic statistical values (mean value $-\mu$, variance $-\sigma^2$, standard deviation $-\sigma$, variance coefficient $-\sigma/\mu$). The variance and variance coefficient are important values for let-off and take-up quality assessment
 - textile parameters
 - machine sett,
- warp shortening percentage
- auto and cross correlation function $R_{xx}(r), R_{xy}(r), r = \langle 0, N - 1 \rangle$, useful for searching for the influence of one quantity to the other
- integral deviations (integral linearity) are defined

$$y_i = \sum_{k=1}^i x_k - i\mu_x = \sum_{k=1}^i (x_k - \mu_x) \quad i = \langle 1, 2048 \rangle$$

where: μ_x is the mean value of measured values x_i .

The integral deviations are the new evaluation method, which expressively contributes to the cloth fell position diagnostics in the range of hundreds or thousands of loom cycles and also to the let-off and take-up diagnostics. (It is possible to compare it to the integral non-linearity of A/D converter.) Integral deviations are the sums of differential divergences (deviations from the mean value) and show the deviations from the straight line under the condition that there are no deviations at the start and at the end of measurement (the deviations are zero). The integral deviations can be normalised by weft sett for easy evaluation.

And in the **frequency domain**:

- Spectral analysis
 - auto-spectra: centring, trend removing
 - power spectra: $G_{xx}(k)$, $g_{xx}(k) = G_{xx}(k)/\sigma_x^2 \times 100$,
 $k = \langle 0, N/2 - 1 \rangle$
 - where k represents the discrete machine frequency f_k (c^{-1})

$$f_k = k \Delta f, \Delta f = 1/(N \Delta t), \Delta t = 1 \text{ (c)}$$

Windows: Uniform, Barlett, Hanning, Hamming, Welsch, exponential

cross-spectra: $G_{xy}(k)$, $g_{xy}(k)$

5. CONCLUSION

This paper is a contribution to the methods for the measurement and evaluation of the weaving process of fabric barriness (fabric regularity) directly on the loom. The measuring system JTS 2J based on a single chip microcomputer, connected with PC through the serial line RS 232 was developed, together with evaluation methods and PC programs. The system serves for analysis and diagnostics for all variations and irregularities on the way of warp.

THE MEASUREMENT OF CLOTH-FELL DRIFT DURING A LOOM STOPPAGE

Palitha Bandara

School of Textile Industries, University of Leeds, Leeds LS2 9JT U.K.

Summary An experimental method of measuring the drift of cloth fell under laboratory conditions, based on a simple apparatus is described. An electro-optical sensor and an inductive sensor have been studied as for their suitability. Some results are presented to indicate the nature and magnitude of the drift that was observed.

INTRODUCTION

The drift of cloth fell during a loom stoppage has long been recognised as a principal cause of start up marks. The drift is the result of the viscoelastic creep behaviour of the warp yarn and the fabric under the influence of tension. The drift is time dependent, while being also determined by the previous tension cycling undergone by the warp and fabric. Its measurement has been of considerable interest, in connection with procedures to minimise the appearance of start up marks.

Greenwood [1] recognised the influence of cloth fell drift on start-up marks, and he presented a theory for explaining the nature of start-up marks. The amount and the direction of the drift would depend not only on yarn and fabric parameters but also on the machine settings as well as its position of stoppage. Waesterberg [2] presented a way of explaining this phenomenon based on the viscoelastic behaviour of the warp and cloth and the tension cycling undergone by them.

The incidence of start up marks seems to be more pronounced on the faster weaving machines of today, and is particularly a problem with certain types of synthetic filament yarns. In fact nearly all looms incorporate some means of combating start up marks [3]. The several solutions adopted by loom manufacturers suggest that no unique solution is yet available, and avoidance of start up marks remains an interesting topic of research in weaving technology.

It is well recognised that the cloth fell drift that takes place during a loom stoppage, while being primarily time dependent, may vary from one loom stoppage to another due to the loom parameters involved as well as the previous tension cycling that the warp and cloth have been subjected to. Due to this variation a particular cloth fell correction action may have a variable amount of effectiveness at each loom start up. The measurement of actual cloth fell drift during a loom stoppage would be helpful in enabling a more accurate cloth fell correction to be carried out during the start-up procedure [4].

This paper does not make an attempt to review various measures that have been proposed for measuring cloth fell drift. Such measurement is basically difficult due to a number of reasons, particularly that the amount of drift only amounts to a few micrometers. The availability of a variety of non-contacting proximity sensors nowadays seems to have made the task of measurement more tractable, as well as simpler and more accurate.

It was decided to evaluate the effectiveness of two such proximity sensors for this application on a wide loom. The paper is a report on the preliminary results available from this exercise.

The two sensors used are:

1. A laser based device with a maximum range of ± 1 mm, with a basic 'target' or working distance of 20 mm [5].

The device used makes use of a visible laser, and operates on the light triangulation principle.

2. An inductive proximity sensor working on the eddy current principle, having a basic working distance of 1 mm with a maximum range of ± 0.7 mm from the target [6].

Both devices employ electronic circuitry having high stability, good dynamic response, as well a good degree of linearity of output with the displacement of the target. The output signals of both devices are available as a voltage. Further amplification, after level shifting of the output signal, is necessary in both cases for measurement and recording purposes.

THE METHOD OF MEASUREMENT

Due to the small magnitude of the measurement involved, it is necessary that the mountings of the sensors be highly rigid. This ruled out floor-mounted vertical stands or a long bar mounted across the loom for carrying the sensors. Also for easy portability from loom to loom, to cover a variety of fabrics, a small sized apparatus is preferable, which can be mounted on a given loom quickly and with a minimum of adjustment.

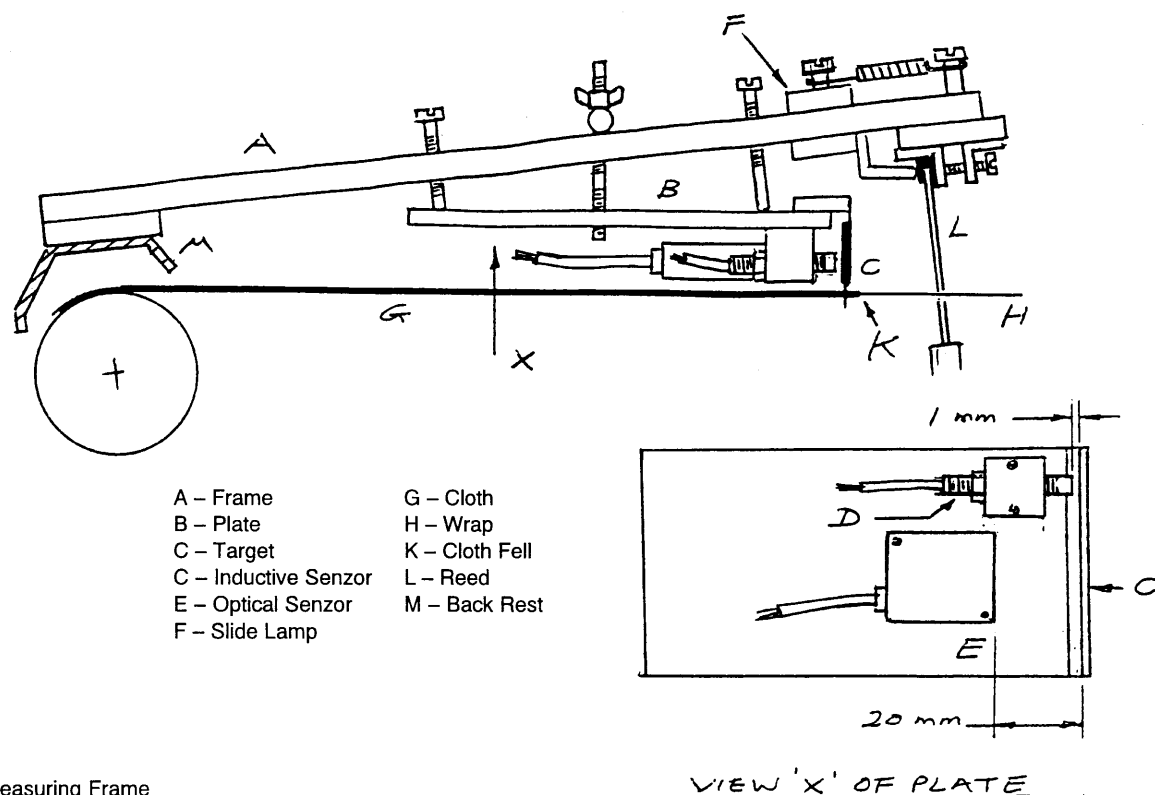


Fig. 1 Measuring Frame

After some consideration, it was possible to devise a light yet rigid frame that could be placed on the loom so that one end of it rested on the breast beam or the cover for the take up roller, and the other positively located on the reed. Most looms stop at closed shed, and at this position the reed is sufficiently away from the fell. The rigidity of the reed is utilised to prevent movement of the measuring frame, once the latter is positively restrained by the reed.

The two sensors were mounted on a rectangular plate, which was carried by the frame using bolts so that its height, inclination and position could all be flexibly adjusted and locked in any required position. The target was a rectangular steel plate, that was carried on the front edge of the plate, and attached by a leaf spring to allow movement at the bottom edge of the target. The lower edge of the target plate carries several fine short needle points for penetration into the fabric. Steel gives a higher sensitivity to the eddy current probe. A matt white paper was glued on the part of the target that faced the laser sensor.

Fig. 1 shows the arrangement used. To adjust the frame to suit a given loom, the loom is stopped, and inched to a suitable position where the reed is sufficiently back from the cloth fell. The front of the frame is placed on the reed as shown, with the back of the frame resting on the breast rail. The screws holding the plate are sufficiently loosened, and the plate adjusted in its inclination and height, so that the target plate is placed perpendicular to the fabric, and the needles penetrating the cloth about 4–5 mm behind the cloth

fell. When the plate is correctly adjusted and secured, the bottom edge of the target plate is parallel to the fabric and stands about 0.5 mm above the fabric. The front edge of the plate that bears on the reed can be finely adjusted using screws provided so that the position of the target with respect to the fell can be adjusted without disturbing the plate. A spring loaded slide was provided to hold the front edge of the frame securely on to the reed to prevent any relative movement.

In use the loom was allowed to run for the required number of picks and stopped. The frame, which had already been adjusted, was placed in the measuring position by first placing its back end on the breast rail, and lowering the front end gently till it rested securely on the reed. This ensured that the target is lowered vertically on to the fabric without applying any sideways force on the needles. An insert made from a 0.8 mm thick brass strip was placed between the target plate and the magnetic probe to ensure the correct level of gap between them so that the output signals can be displayed on an oscilloscope, with very little trace level adjustment. The insert was promptly withdrawn after the frame was placed on the loom.

Each sensor was provided with its own amplifier so that the output signal could be sufficiently amplified for display on the dual trace digital storage oscilloscope used. The amplifiers incorporate level shifting control so that the DC level of the output signals can be adjusted to suit the starting position of the target. The amplifier and the oscilloscope combination shows a negligible amount of signal drift over a period of 1000 s, the duration over

which the measurements were carried out. The instruments were switched on and allowed to warm up for a short period to ensure thermal stability before any measurements were carried out.

The measurement of cloth fell was carried out on two looms.

1. A Sulzer Ruti 5100 air-jet loom weaving a 50/50 polyester cotton warp and weft, both 30s Cotton Count. The fabric was a plain weave with 25 ends/cm and 23.6 picks/cm. The loom speed was 625 picks/min. The mean warp tension was measured at 52 g/end (2.6 g/tex).

The loom was allowed to weave for several minutes, giving more than 2000 weaving cycles, so that the warp and cloth reach steady load cycling conditions. The loom was then stopped, whereupon it automatically went to closed shed position at a shaft angle of 308 degrees. The frame was carefully positioned at the middle of the reed, the brass insert removed gently, and the oscilloscope traces started at 1000s/cm recording speed. At the end of 1000 s, the traces were stopped, and then copied on a dot matrix printer. The procedure was repeated several times.

2. A Sulzer TW11 projectile loom weaving a worsted fabric using R68/2 tex warp and 2/36 Worsted count weft, weaving a 2/2 twill with 21.3 ends/cm and 20.9 picks/cm. The loom speed was 270 picks/min. The mean warp tension was 90 g/end (1.5 g/tex).

This loom stops at open shed. This position was not changed for measurement, as at this setting the reed was at a distance suitable for the frame. Traces were recorded as described above and hard copies made.

RESULTS

Fig. 2 is a representative trace obtained on the air-jet loom. The traces from the two instruments show identical trends. It should be noted that the overall gain of the inductive sensor is several times higher, but still presented a relatively noise free signal. The direction of the signal movement here indicates the cloth fell drifting towards the back of the loom.

During calibration the inductive sensor showed a sensitivity of 16.7 mV/mm. Accordingly, the drift measured on the graph amounts to 27 mm. In fact this measurement has a small error due to the few seconds of delay involved in placing the frame on the loom. However it seems possible to make a correction for this by extrapolating the curve to time $t=0$ using the initial gradient of the curve. The optical sensor similarly showed a sensitivity of 1.7mV/mm. Accordingly the corresponding trace shows a cloth fell drift of approximately 29 mm. It will be possible to increase the gain of the corresponding amplifier, to enable a similar sensitivity to that of the inductive sensor.

A=0.5 V B=0.2 V TB= 100 s TD= 00

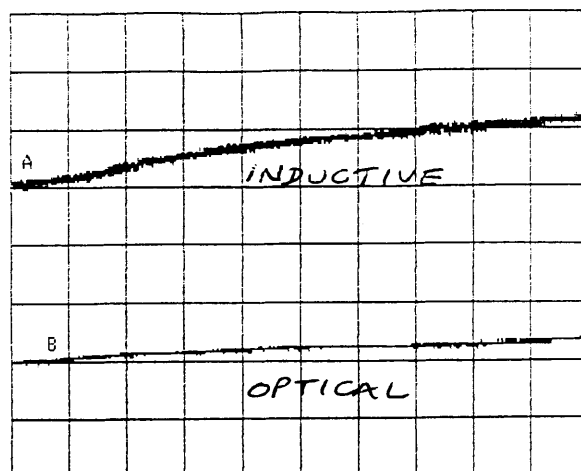


Fig. 2 Cloth Fell Drift on Air-Jet Loom

A=0.5 V B=0.2 V TB= 100 s TD= 00

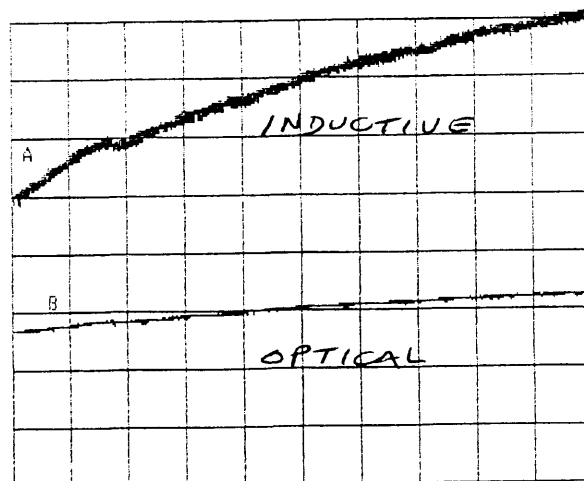


Fig. 3 Cloth Fell Drift on Projectile Loom

Fig. 3 similarly is a trace obtained on the projectile loom. The drift measured over a similar period is greater. However the loom was stopped at open shed, as well as the yarn involved was worsted. The curve is also not steady. This was observed a few times repeatedly, and may represent the influence of some slipping on the cloth support beam. The corresponding cloth fell drift indicated is approximately 90 mm.

CONCLUSION

The sensors employed and the simple apparatus used gave a useful method of observing cloth fell drift during a loom stoppage. Both sensors have a similar response, but the inductive device is more robust, smaller in size as well more economical than the other.

The method reported was more intended as a convenient way of measuring cloth fell drift, and not as one suitable for incorporation with a loom.

It should be observed that cloth fell movements are somewhat restricted on a wide loom due to the friction present at the temples. However, it is likely that the drift undergone by the fabric at the middle of the warp is relatively unaffected by this. It was also assumed that by attaching the target sufficiently close to the cloth fell, what is measured will be practically the same the actual cloth fell drift.

The measurement of cloth fell drift is not performed on any of the start up mark prevention methods currently incorporated on looms. This may be on account of certain inherent difficulties associated with applying this method. However the availability of suitable sensors may make this method a useful one, as it enables the measurement of the actual drift undergone by the cloth fell each time the loom stops. Furthermore the sensor could also be used in repositioning the cloth fell as necessary before the loom restarts. If this method works, an even simpler inductive sensor may be usable, as the actual determination of the cloth fell drift will become unimportant, so long as the sensor indicates which direction the cloth fell correction is to be

carried out and also give a signal when the cloth fell has been restored to its precise initial position.

ACKNOWLEDGEMENT *The author wishes to thank Mr. H. Rait for assistance with the apparatus, and Mr. J.C. Clarke, Mr. G. Brayshaw and Mr. Gungor Durur with performing the experiment and the preparation of the paper. The work was enabled by funding under the Inco-Copernicus project 'Network for Studying Warp Related Problems'.*

REFERENCES

- [1] Greenwood K., Vaughan G.N., The Beat-up Force and Pickspacing, *J.Text. Inst.*, 1957, 48, T39–T53
- [2] Waesterberg L., Nordhammer G., The Position of the cloth Fell on Power Looms, *J.Text. Inst.*, 1956, 47, T604–T607
- [3] Vangheluwe L., Puissant P., An Overview of Procedures to Avoid Set Marks in Weaving, *Fibres and Textiles in Eastern Europe*, 1997, 5, No.4, 56–58
- [4] Islam A.T.M.S., Bandara P., Cloth Fell Control to Prevent Start-up Marks in Weaving, *J.Text. Inst.* (Accepted for publication)
- [5] 'DISTEC' Non-contact Displacement Measuring System, Graham & White Instruments Ltd., St. Albans, Hertfordshire, AL1 4LZ, U.K.
- [6] Laser Analog Displacement Sensor, Model LAS- 2010V, Nippon Automation Co., 1-2-14, Shinmiyakoda Hamamatsu Shizuoka, 431–2103, Japan

Mechanics of weaving and fabric forming, stability of the process

TECHNICAL PERSPECTIVES OF WEAVING AT THE END OF 20th CENTURY

Stanislav Nosek

Technical University, Liberec.

1. INTRODUCTION

1.1. Arise and evolution of weaving technology

The production of fabrics – even if only of hand plaited ones – has existed for almost 30.000 years. In its history, *the evolution of fabric production was influenced by the economic state of the human society* at different time periods, with all attributes of economy including the increasing need of goods and abilities of the society to meet these needs, as well as the art of goods exchange (of the market), etc. *The evolution was of course influenced also by the „technical“ level of the society* – by „sophistication“ of the technology, i.e. by the level of knowledge or science, by the skill and creative phantasy of the producers, inventors and designers, and by the actual production potential of the society. Between the evolution of the economic state of the society and the evolution of the technical level of technology there is often a mutual connection.

Let us first watch the *evolution of weaving process*. In the past, the quality of the product was the main measure for appraising the technical niveau of the fabric production. The time spent on product manufacturing did not play any role. *At present the main parameter of production of a loom is the machine output per time unit*. The requested quality is regarded as being automatically granted. In weaving, the machine output is calculated as the amount of running meters of fabrics produced on the loom. Recently the production has been expressed more like *the number U of inserted meters of weft per time unit*, the parameter U being not dependent on the fabric width and density. The loom producers tend quite often to achieve the highest ma-

chine revolutions and they produce top-speed machines sometimes called „*The Formula I*“.

1.2. The laws of spontaneous development of weaving machine productivity

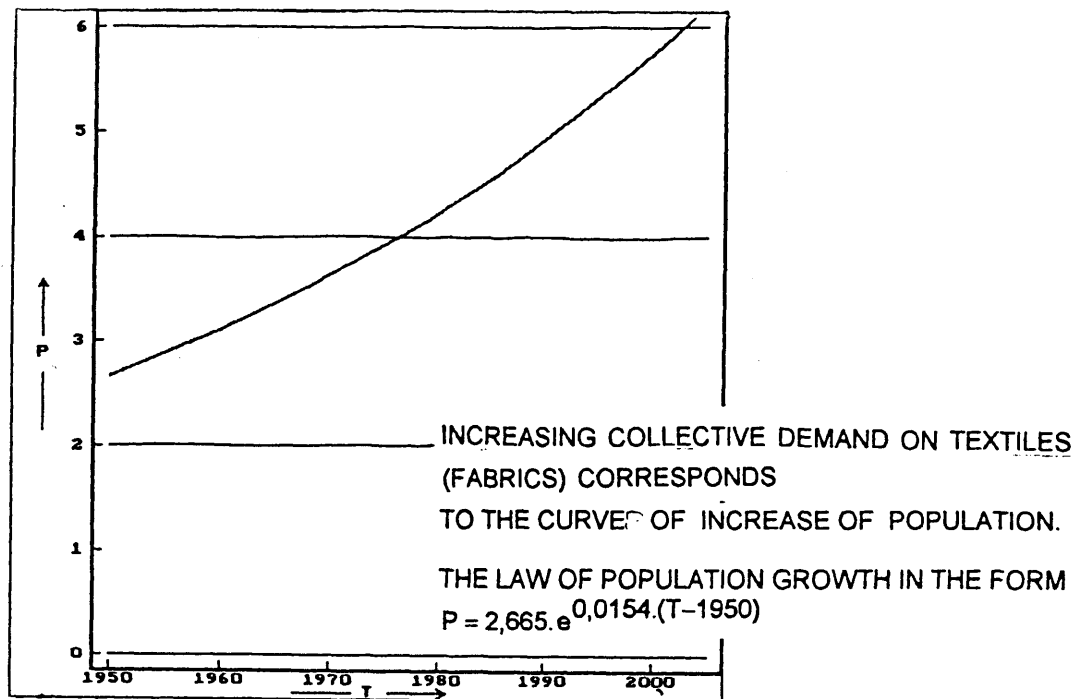
From experience we can state that the curve of increase of technical parameters of any producing system during a long time section has usually an approximate S-shape form.

The explanation of this S-shape form is relatively simple. Let be the main parameter of a developed weaving system e.g. *the loom productivity U(T) [m.min⁻¹ of inserted weft]*. The rate dU/dT of increase of the loom productivity corresponds to the *collective knowledge about the weaving system* gained at the given time by all (N) design ateliers working as usual simultaneously on similar problems. Their knowledge is proportional to the already *achieved technical level* of the system U(T). On the contrary, the rate of increase of the productivity during the development is inverse-proportional to the *difficulty of further design*. The difficulty of development grows with the „exhausting“ of the rest of the maximum available productivity of the system. From the relation

$$\frac{dU(T)}{dT} \approx \frac{\text{collective knowledge}}{\text{difficulty of solution}} \approx \frac{N \cdot U^a(T)}{1 / [U_{\text{lim}} - U(T)]^b}$$

yield the equations of productivity growth:

$$U(T) = \frac{U_{\text{lim}}}{1 + C \cdot e^{-k \cdot N \cdot (T - T_0)}}; \quad C = \frac{U_{\text{lim}} - U_0}{U_0} \quad (1)$$



THE LAW OF THE INCREASE OF LOOM PRODUCT.

SIMPLE RELATIONS :

TOTAL KNOWLEDGE $\sim N \cdot U^a(T)$.

RESTRICTIONS OF THE OUTPUT U_{lim} ,

REMAINING POSSIBILITIES $U_{lim} - U(T)$

DIFFICULTIES OF DEVELOPMENT $\sim 1/[U_{lim} - U(T)]$

THE RATE OF FURTHER PARAMETER INCREASE

$$\frac{dU(T)}{dT} \approx \frac{\text{total collective knowledge}}{\text{difficulty of development}} = k \cdot \frac{N \cdot U^a(T)}{1/[U_{lim} - U(T)]^b}$$

SOLUTION OF THE OUTPUT INCREASE

$$U(T) = U_{lim} \cdot \frac{1}{1 + C \cdot e^{-kN \cdot U_{lim}(T-T_0)}}; C = \frac{U_{lim} - U_0}{U_0}$$

FOR $a=b=1$

U_{lim}

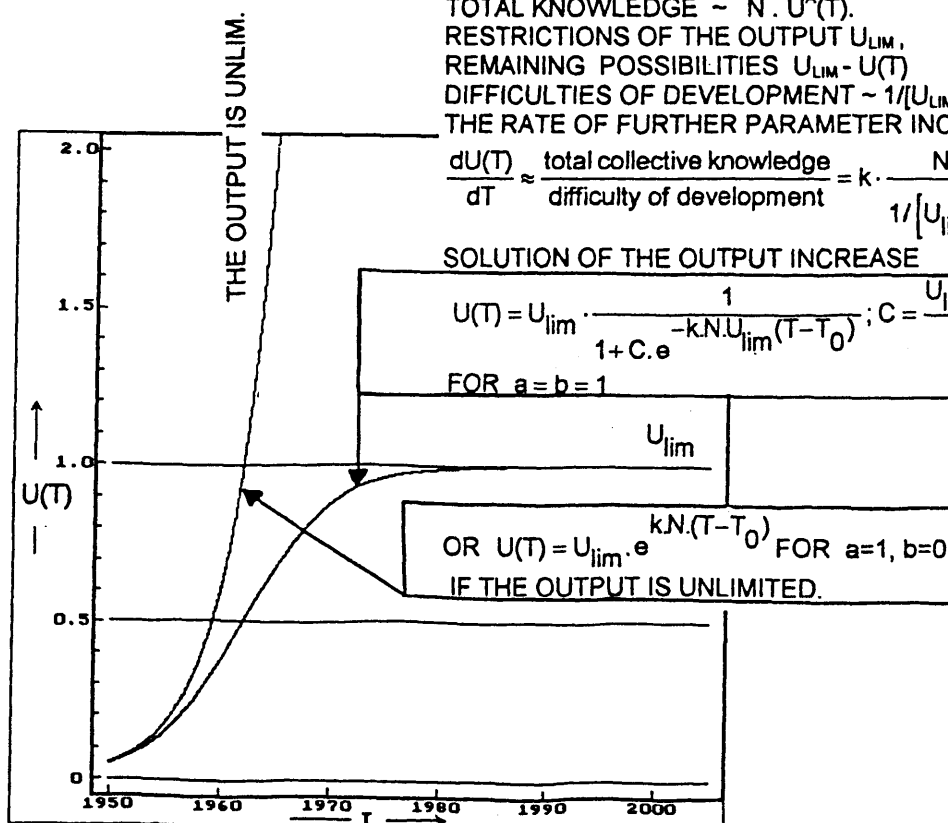


Fig. 1 The development of technical level of a machine (e.g. of the level of productivity of weaving machines) at the limited value of productivity U_{lim} (S-shaped curve) and at the unlimited productivity ($U_{lim} = \infty$) – the exponential growth. Above for comparison: the population curve of mankind.

for the exponents in the relations above e.g. $a = 1$, $b = 1$, or

$$U(T) = U_{\text{lim}} \cdot e^{+k \cdot N \cdot (T - T_0)} \quad (2)$$

for $a = 1$, $b = 0$ if $U_{\text{lim}} = \infty$ – the productivity of machine group is unlimited.

The first resulting equation (1) is the supposed S-shape „logistic“ curve for an individual weaving system, the productivity of which is technically limited. The second, exponential equation (2) represents the unlimited exponential growth of productivity of the group of all weaving systems together, including those which will be invented later in order to cover the needs of the human society for higher amount of fabrics (see Fig. 1).

In fact, when following the increase of machine outputs of separate weaving systems as they were presented at international exhibitions of textile machines ITMA, we find that the outputs of the systems (gripper, rapier, air jet and water jet looms, parallel- as well as series-type multiphase looms) coarsely follow S-shape curves with positive and negative random deviations from the theoretical line (see Fig. 2a). Yet if we put all these courses of development together in semi-logarithmic coordinates (Fig. 2b) we find that, on average, the „family“ of maximum outputs follows a linear,

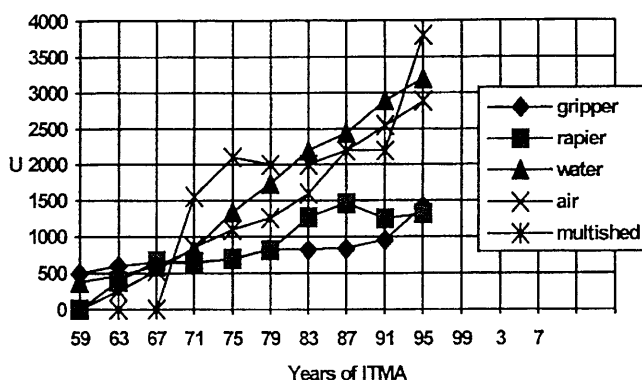


Fig. 2a Development of loom productivities (loom outputs U m.min⁻¹ of inserted weft) according to top parameters presented on ITMA exhibitions

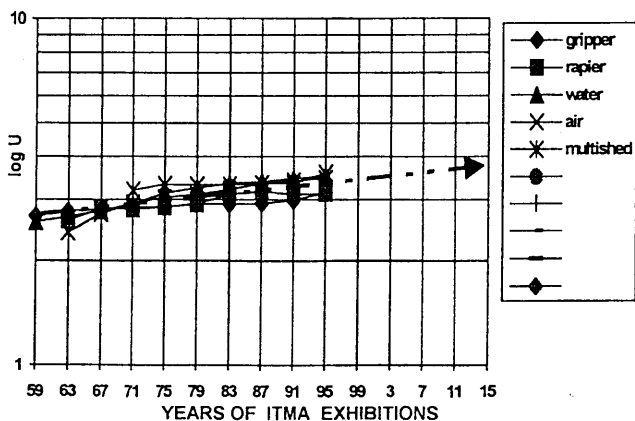


Fig. 2b Extrapolation of the development of loom productivities between 1959 and 2015

unlimited curve. After delogarithming we find that the general collective increase of productivity has the form given by the exponential equation (2). It holds:

The real collective output of looms follows an exponential, still unlimited growth

$$U_{\text{average}} = 277 \cdot e^{+0.048 \cdot (T - 1950)} \quad (3)$$

In the next years we can expect an average increase of collective productivity of all looms each 5 years $\Delta U_5 = 800\text{--}1000$ m.min⁻¹ of inserted weft, i.e. in

2000 it should be achieved round	$U_{2000} = 3110$ m.min ⁻¹ wft
2005	$U_{2005} = 3960$ m.min ⁻¹ wft
2010	$U_{2010} = 5050$ m.min ⁻¹ wft.

It is also interesting to notice that the collective looms output follows a similar exponential population curve of mankind, which is at present approximately

$$P_{\text{mlds inhab.}} = 2.665 \cdot e^{+0.0154 \cdot (T - 1950)} \quad (4)$$

(see the upper curve in Fig. 1). That points out that there may exist logic connection between the increase of population and the corresponding need of textiles, and the increase of weaving loom productivity accompanied with inventions of new weaving principles.

1.3. Stages of Development of Weaving Looms

The following data were the most important points in the prehistory of weaving technology:

- Plain „fabrics“ with warps interlaced by wefts came into being probably at least ... 30.000 y. ago,
- weft insertion into the warp parted into the sheds by hand 5-4 thous. y. ago,
- hand loom with a heald shaft originated 1.5 thous. y. ago,
- principle of mechanic dobby invented by Bouchon 1725,
- flying shuttle invented by Kay 1733,
- mechanical loom invented by Cartwright 1784.

The history of loom development following after that ran through three stages:

The 1st stage – the period of technical improvements of mechanical looms – lasted practically 150 years from the end of the 18 th century to the half of the 20 th century.

In this stage the mechanisation of main loom functions, mechanic automation of the weaving process, the patterning of fabrics, the control of the weaving process by means of various mechanic stop motions appeared. However the loom productivity didn't increase significantly; it reached some 200 revs. min⁻¹ only.

The 2nd stage of weaving machine development – the arise and implementation of new weaving principles with high production – started in the 2 nd half of our century.

This stage has had two lines: the line of making as light as possible the impulse-type inserting systems, and the line of application of harmonic or steady motions on the

continuously running inserting media. The first line brought the weft insertion with a light gripper in several variants (Sulzer, Nopas, Wüger) instead of insertion with relatively heavy shuttles. Then the line continued with ultralight water jet and air jet insertions, the second one comprising the confusor and/or relais-nozzles principles (systems Svatý, Maxbo, Te Strake and the followers) and with attempts for the s.c. „whip“ insertion of weft. The second line brought a whole group of rapier looms with one-side or both-side rapiers, with rigid, telescopic and flexible rapiers, all of them driven by a wide row of various mechanisms with more or less harmonic motion in the shed. Finally, the loom development continued with the multiphase weaving of the parallel as series types (the p-types with steady inserter motion were the Contis, Rütli, Russian-German type, ONA etc.; the s-types with rapier insertion were the systems Gentilini, Bentley, and in the last years with the air jet insertion – the M 8300 Sulzer-Rütli)

The 3rd stage of weaving loom development – the stage of heightening of lost weaving ability of looms due to high weaving speeds – arises, in fact, only at present.

The problem is that at very high tours the beat-up system does not have enough time to push the weft into the cloth fell against the time-dependent friction resistance of sliding weft on warp. Consequently, *the fabric density (the weaveability) tends to decrease* and can be kept on the necessary height only by *high warp tension and high beat-up forces*. The weaving process tends to *instability* after any stop of the machine, or at emptying the warp beam, or even quite spontaneously (randomly). Therefore, *the dynamics of beat-up and of fabric forming process have to be studied and respected in the present new machine designs*.

2. THE MAIN TASK OF THE 2ND STAGE OF LOOM DEVELOPMENT: THE REDUCTION OF NEGATIVE INFLUENCE ON THE LOOM PRODUCTIVITY BY THE INERTIA OF INSERTING MEDIA

2.1. Basic laws of loom speed

The main parameter affecting the weaving rate of a loom is the velocity of inserted weft. For studying the insertion and weaving speed let us recap some basic definitions:

The **loom output** (loom productivity) can be expressed as the *output of inserted weft*. For n being the machine revolutions and L the weaving width holds theoretically (in the case of full efficiency $\eta = 1$)

$$U[\text{m} \cdot \text{min}^{-1} \text{ of inserted weft}] = n[\text{min}^{-1}] \cdot L[\text{m}] \quad (5)$$

Machine revolutions are inverse-proportional to the time of all operations in a weaving cycle:

$$n = \frac{60}{T_c} = \frac{60}{T_p + T_i + T_{\text{reserv}}} \quad (= \frac{60}{T_i / \psi_i}) \quad (6)$$

(T_c – duration of the weaving cycle, T_p – time necessary for the shed exchange, T_i – time interval of weft inser-

tion, T_{reserv} – time reserve, ψ_i – coefficient of exploitation of the weaving cycle for weft insertion.)

The insertion time T_i dominates among other time intervals in today's looms. It takes more than 50 % (may be up to 70 %) of the time of the weaving cycle. Therefore, the machine output depends mainly on the duration of the weft insertion. The insertion time yields from the course of inserting velocity in the form of

$$v_i(x) = \frac{dx}{dt} \Rightarrow T_i = \int_0^L \frac{dx}{v_i(x)} \quad (7)$$

2.2. The courses of loom velocity in dependence on the inserter mass and on the existence of a driving force in the inserting path

The inserting velocity $v_i(x)$ may achieve different values and time courses in the inserting path for different inserting systems. There is a row of circumstances which can influence it. The velocity depends on:

- whether the weft is driven by a *steady force* acting throughout the whole inserting path;
- or whether the force acts only at the start of motion;
- what *the driving medium* is (a hard massive body or the inertia of weft or the air stream);
- what *kind of resistance* the weft produces against the flight, etc.

Let us examine the course of insertion speed by the analysis of a fictitious complex system of weft insertion containing *all possible means* affecting the weft in the inserting path. The fictitious inserting system is characterized: by using *an inserter with an inertia mass*, by presence of a *steady insertion force acting through the whole weaving width*, and by *the viscose resistance of the inserting channel against weft motion*.

This fictitious system will serve for the analysis of weft motion; as a real system it has been used in experimental devices only (see Fig. 3). The system consists e.g. of a gripper or inserter with the mass m which drags the *increasing length* x of weft (with the unit mass μ). The weft is taken from a feeder. A tensioner ensures the steady braking force T . While running through the shed the weft is exposed to ventilation resistance R of the air and of the friction. This resistance against the flight is proportional to the immediate length x of the moving weft and to the square of flight velocity $v_i^2(x)$. The gripper is driven by a steady force F along the whole weaving width. (In practice, such a force was experimentally carried out by the magnetic field of a linear electric motor situated along the inserting path and acting on the gripper containing a coil).

The insertion is a problem of energetic equivalence. The weft together with the gripper vary their total kinetic energy on each differential path dx by an amount δE_k due to the variation of velocity. Further, they dissipate some energy R . The energy losses are covered by the work of the driving force F . Such a situation can be described by the Lagrangian equation:

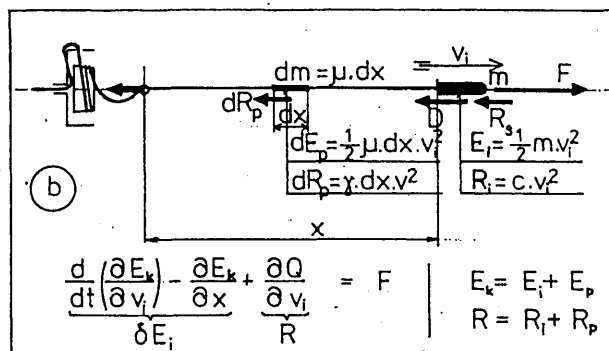
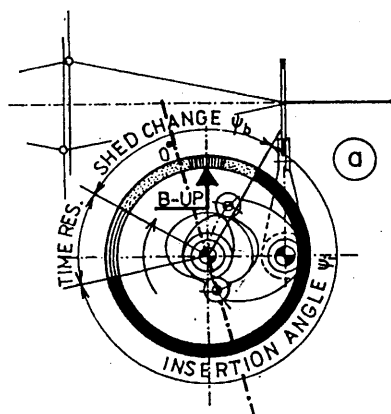
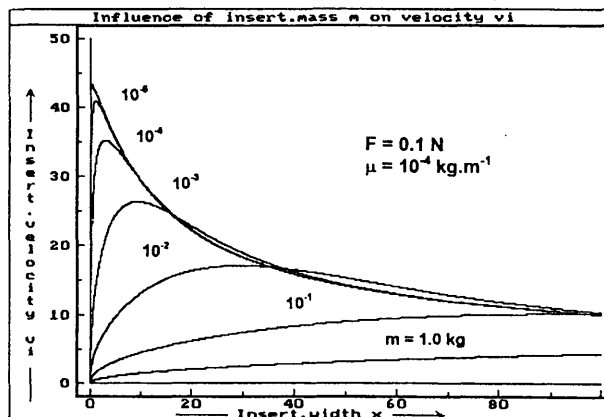


Fig. 3 The insertion of weft. Left: the exploitation of the weaving cycle (360°) for weft insertion (angle of weft insertion ψ_i). Right: the fictitious weft insertion system containing a complete set of possible attributes affecting the insertion: the existence of a gripper (gripper mass m); a driving system giving a steady driving force F ; the surroundings producing a certain resistance R against the weft+gripper flight. Below the sketch: graphs showing the course of inserting velocity $v_i(x)$ depending on the mass of the gripper, and (what concerns the height of curves) on the steady driving force F .



$$\left[\frac{d}{dt} \left(\frac{\partial E_k}{\partial v_i} \right) - \frac{\partial E_k}{\partial x} \right] + \frac{\partial Q}{\partial v} = F \quad (8a)$$

($E_k = 1/2(m + m \cdot x) \cdot v_i^2$ is the kinetic energy of the inserter and weft, $\frac{d}{dt} \left(\frac{\partial E_k}{\partial v_i} \right) - \frac{\partial E_k}{\partial x} = \partial E_k$ is the energy variation, $\frac{\partial Q}{\partial v_i} = R = (c + \gamma \cdot x) \cdot v_i^2 \equiv \gamma \cdot x \cdot v_i^2$ is the resistance against weft motion caused by energy dissipation, and $F = k \cdot m$ is the steady driving force, e.g. of a linear el. motor). The resulting motion equation is

$$\frac{d(v_i^2)}{dx} + \frac{\mu + 2\gamma \cdot x}{m + \mu \cdot x} \cdot v_i^2 = \frac{2 \cdot F}{m + \mu \cdot x} \quad (8b)$$

The solution of this differential equation in general has the form of

$$v_i^2(x) = \frac{2F}{m} \cdot \frac{1}{1 + \frac{\mu}{m} \cdot x} \cdot \frac{\int_0^x e^{\frac{2\gamma \cdot x}{\mu}} \cdot \left(1 + \frac{\mu}{m} \cdot x\right)^{-\frac{2\gamma \cdot m}{\mu^2}} \cdot dx}{e^{\frac{2\gamma \cdot x}{\mu}} \cdot \left(1 + \frac{\mu}{m} \cdot x\right)^{-\frac{2\gamma \cdot m}{\mu^2}}} \quad (9)$$

$$\left(\cong \frac{2F}{m} \cdot \frac{1 - e^{-\frac{2\gamma \cdot x}{\mu}}}{1 + \frac{\mu}{m} \cdot x} \text{ for heavier inserters} \right)$$

The course of inserting velocity $v_i(x)$ increases with the increasing width x from zero to a maximum and then descends asymptotically back to zero (Fig. 3b). The height and steepness of the curve depend on the driving force F and on the mass m of the inserting medium. From the curves it is evident that *lighter inserters move with significantly higher velocities* even if the driving force has not been increased (see Fig. 4).

Therefore, newly designed inserting systems still use less massive inserting media.

2.3. The concrete reductions of inserter masses and their consequences.

The reduction of inserter masses ran through several development steps:

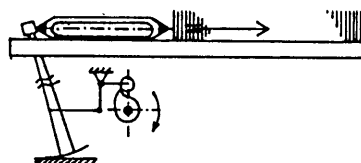
a) Massive inserters – with accelerating force acting only on the entry of the shed.

Massive inserters, like *shuttles* or (*lighter*) *grippers*, are heavy enough to fly only on account of their inertia through the whole shed length. They obtain only the initial momentum $m \cdot v_{i0}$ by an inserting mechanism on the entry into the shed and then they continue to move autonomously without any driving force F . The accelerating (inserting) forces are high.

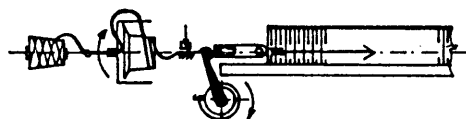
b) Very light inserters accelerated also before entering the inserting path.

With further mass reductions of inserters or inserting media new problems arose with the ability of the system to carry the weft to a satisfying insertion distance. Very light inserters suddenly possessed not enough kinetic energy $mv_{i0}^2/2$ to hold the necessary course of

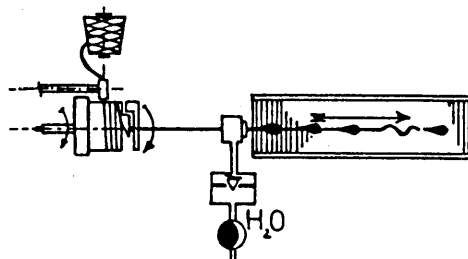
MECHANIC SHUTTLE LOOM
 * INVENTED 1784
 OUTPUT $U=600 \text{ m.min}^{-1}$ OF INSERTED WEFT
 ENERGY CONSUM. $e=150 \text{ J.m}^{-1}$ OF INS.WEFT



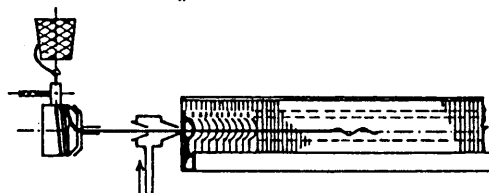
GRIPPER LOOM
 * PATENTS 1911,1925
 REALISATION 1942-1950
 OUTPUT $U=1200 \text{ m.min}^{-1}$ OF INSERTED WEFT
 ENERGY CONSUM. $e=210 \text{ J.m}^{-1}$ OF INS.WEFT.



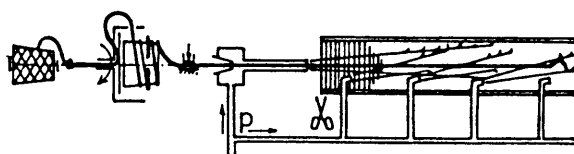
WATER JET LOOM
 * REALISATION 1945-1950
 OUTPUT $U=1600-2800 \text{ m.min}^{-1}$ OF INS. WEFT
 ENERGY CONSUM. $e=240 \text{ J.m}^{-1}$ OF INS.WEFT.



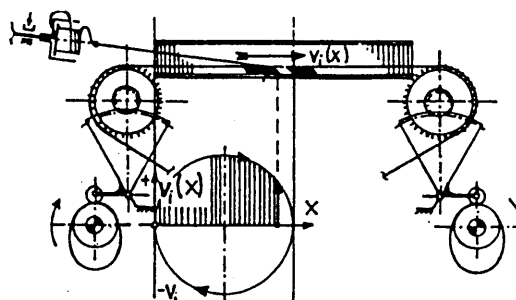
AIR JET LOOM - MONOJET (CONFUSOR TYPE)
 * REALISATION 1945-1950
 OUTPUT $U=1200 \text{ m.min}^{-1}$ OF INSERTED WEFT
 ENERGY CONSUM. $e=280 \text{ J.m}^{-1}$ OF INS.WEFT.



AIR JET LOOM - RELAY JETS
 * PATENT 1932
 REALISATION 1965-1970
 OUTPUT $U=1600-2600 \text{ m.min}^{-1}$ OF INSER. WEFT
 ENERGY CONSUM. $e>400 \text{ J.m}^{-1}$ OF INS.WEFT.



RAPIER LOOM (THE TYPE WITH FLEXIB. RAPIERS)
 * PATENTS 1925-30
 REALISATION 1940-1950
 OUTPUT $U=800-1400 \text{ m.min}^{-1}$ OF INSERTED WEFT
 ENERGY CONSUM. $e=180 \text{ J.m}^{-1}$ OF INS.WEFT.



MULTIPHASE LOOM (ON FIG: PARALLEL TYPE)
 * PATENTS 1901-1942
 REALISATION 1960-1980 (PARAL.TYPE),
 1995 (SERIES TYPE - NEWLY)
 OUTPUT $U=2400-3800$ (EXHIB. 5800) m.min^{-1} OF INS.WFT.
 ENERGY CONSUM. $e=120 \text{ J.m}^{-1}$ INS.WEFT - PARAL.TYPE
 $e=?$ SERIES TYPE WITH AIR WFT.INS.

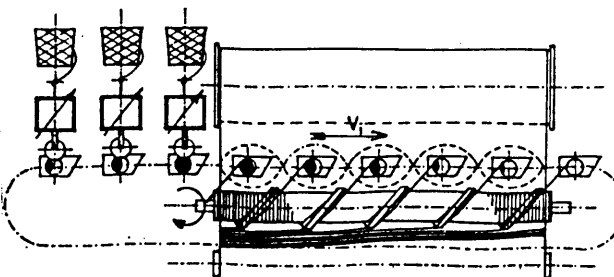


Fig. 4 Evolution of shuttleless weaving systems

inserting velocity $v_i(x)$ for flight to longer distances (so it was, e.g. with the attempt to use a very light plastic gripper inserted into the shed by a sort of an air-gun).

Similar problems arose with the air insertion of weft on the „mono-jet“ looms, even when using the inserting channel with the s.c. confusor lamellae.

2.4. The influence of simple reducing the inserter masses on the loom productivity

Due to narrow weaving width resulting from excessive reduction of the inserter mass and from the loss of its kinetic energy in the preceeding case of very light inserters, the loom productivity does not increase any more with further diminishing of the inserters.

The influences on the loom productivity by variation of inserter mass m and weaving width L are evident from this consideration: The machine output is $U = n \cdot L = (60 \cdot L) / T_C = (60 \cdot L) / (T_i + T_p + T_{\text{reserv}})$. Suppose that the time reserve $T_{\text{reserv}} = 0$. The duration T_p of the shed exchange is in constant relation to the duration of the weaving cycle, $T_p = \psi_p \cdot T_C$. The inserting time T_i is the integral of inverse inserting velocity

$$T_i = \frac{1}{v_{i0}} \int_0^L \left(1 + \frac{\mu X}{m} \right)^{\frac{1}{2} \frac{\gamma m}{\mu^2}} \frac{\gamma X}{e^{\mu X}} dX =$$

$$\equiv \frac{\mu / \gamma}{v_{i0}} \left\{ \left[\frac{\gamma_L}{(e^{\mu} - 1)} - \frac{\gamma}{\mu} L e^{\mu} \right] + \frac{\mu^2}{2 \gamma m} \left[\frac{\gamma_L}{\mu} L e^{\mu} - (e^{\mu} - 1) \right] \right\} \quad (10)$$

$$= \frac{1}{v_{i0}} \left\{ g_1(L) + \frac{\mu^2}{2 \gamma m} g_2(L) \right\}$$

Then we obtain for the loom productivity an expression containing m , L , v_{i0} :

$$U = \frac{60 \cdot (1 - \psi_i) \cdot L \cdot v_{i0} \cdot m}{m \cdot g_1(L) + \frac{\mu^2}{2 \gamma} \cdot g_2(L)} \quad (11)$$

Here, the functions $g_1(L)$, $g_2(L)$ in the denominator are exponentially increasing functions of weaving width L .

The machine output $U(L, v_{i0}, m)$ grows only in a certain part of increased weaving width L until the curve reaches a maximum (which lies practically in most looms at $L = 3-3,5$ m) and then it slows down.

The effect of reduction of inserter masses m as low as almost zero can be of small importance or even negative for the machine output. With excessive decreasing of inserter masses the machine productivity starts to decrease at last. It is evident from the eq. (11), where for a very low value of m the first member of the denominator gets negligible. Therefore, with further decrease of inserter mass the loom productivity evidently decreases.

The dependences of machine revolutions n and machine productivity U on the machine width L and on the initial inserting velocity v_{i0} are shown in Fig. 5 a, b.

2.5. Further arrangements for achieving higher loom productivity

c) Ultralight inserting medium with the driving force acting along the full loom width (air jet with relay nozzles).

The loss of flight range with very light inserting elements, and consequently the loss of loom productivity were the reasons for searching new ultralight inserting systems, yet with the weft being driven by a steady force through the whole shed length. As a result, **the air insertion systems with relay jets** had been invented.

The system consists of a main nozzle which gives the weft the initial velocity v_{i0} , and of a row of auxiliary nozzles, the air of which has to tract the weft inside the inserting path. The weft velocity has approximately a course similar to the curves in Fig. 3b, but starting from the initial velocity v_{i0} at the point x_0 .

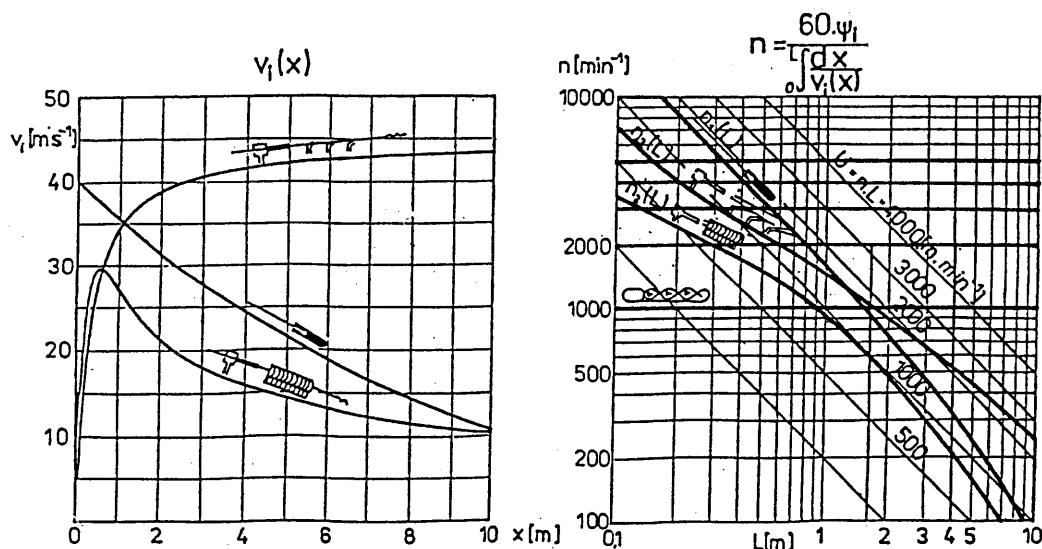


Fig. 5a,b: a) The courses of insertion velocities of main weaving systems (From above: Air jet with relais nozzles; gripper loom; single air with the confusor.); b) The dependence of machine revolutions n on weaving width L . From above: gripper loom; air jet with relais nozzles; single jet with confusor; multiphase (parallel type). Oblique lines – levels of constant loom productivities $U = n \cdot L$.

From the solution of the eq. (8a,b) for the inserting mass $m \rightarrow 0$ yields that the inserting velocity again follows a curve increasing at the beginning, but reaching a maximum considerably later (if ever) than with a monojet loom and then slowly descending.

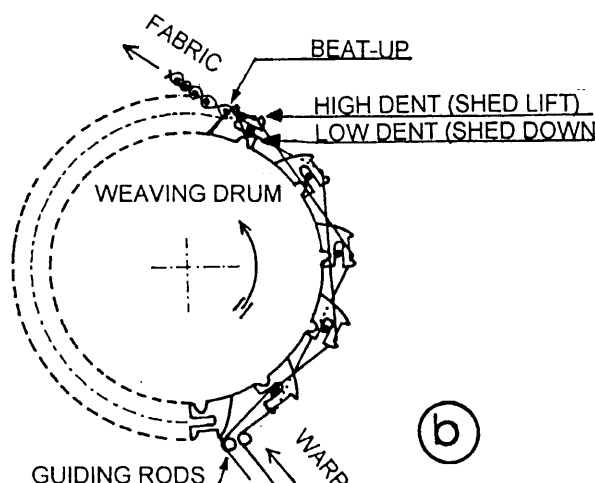
Nevertheless, this system brings a serious problem with high consumption of energy for preparation of pressure air for the insertion. The limited action radius and energetic requirements were reasons (among others) for the arise of systems with controlled inserter motion.

d) Inserting systems with kinematically driven inserters – rapier looms and parallel-type of multiphase looms.

There is another way how to increase the average inserting velocity by not increasing the energy consumption. It is the way of using kinematically controlled inserters instead of leaving the weft fly autonomously owing to its inertia or to other tracting forces.

In the *rapier loom* the aim of designers was not mainly to heighten the machine output. The main reason for developing the rapier inserting systems was the struggle for building looms with completely controlled weft insertion. In such systems it is possible to design the course of insertion so that the weft as well as the inserting mechanism are optimally strained during weaving.

The last weaving system is the system with continuous weft insertion – the s.c. multi-phase weaving loom [5] – see Fig. 6. „Continuous“ means that in every moment several picks are inserted simultaneously into a row of also simultaneously opened waveform sheds. The sheds move one by one either in the longitudinal direction of the loom (that is the *series type (S-type)* of the multiphase loom), or they run in harmonic waves across the loom (the *parallel type (P-type)* of the multiphase loom where the sheds are opened beside each other).



In the s-type of the multiphase loom the weft insertion is carried out by the same systems as in the single-phase looms: by grippers, by air, by rapiers. The shed opening and the beat-ups are provided by thin rotational lamellae of the s.c. weaving drum (rotating reed).

In the p-type of the multiphase loom the weft insertion is provided by a number of inserters – small shuttles carrying the weft necessary for one weaving width. The inserters move inside of the waveform sheds running across the loom. The inserting and transporting speeds are steady and very low ($2-4 \text{ m.s}^{-1}$). The beat-up is provided by various types of lamellae, either swinging in waves, or rotational ones with their s.c. beat-up noses arranged in a helix on the reed surface and rotating with some phase delay of the noses against the inserters.

High output of the p-type multiphase loom is achieved by the large (theoretically unlimited) weaving width and by the high number N of inserters working at the same time in 1 m of the weaving width:

$$\begin{aligned} U &= 60 \cdot N \cdot L \cdot v_i \text{ (e.g. } U = \\ &= 60 \cdot 5 [\text{inserters/m}] \cdot 4 [\text{m}] \cdot 2 [\text{m/s}] = \\ &= 4800 [\text{m/min}]) \end{aligned} \quad (12)$$

3. NEW PROBLEM: THE DECREASE OF WEAVEABILITY IN HIGHLY PRODUCTIVE LOOMS

3.1. Weaveability from the point of view of fabric forming at high weaving speeds

The struggle for achieving the maximum inserting velocity is not the only textile-technological problem of increasing the loom productivity. It is probably not the most difficult one. The main problem of further increasing of weaving speed seems now to be *the ability of the loom, at high weaving frequencies to weave the fabrics with high densities, good quality, and also with good*

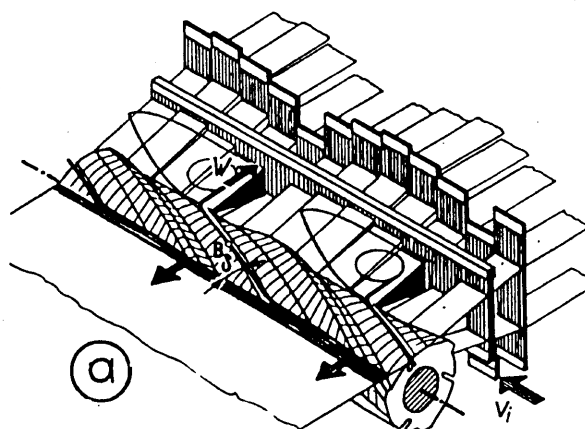


Fig. 6 Multiphase weaving principles: a) parallel type with parallelly opened row of waveform sheds; in each of the waves runs an inserter (shuttle). b) series type of multiphase loom with sheds opened in waves running in longitudinal direction of the loom; here the weft is inserted by air stream.

efficiency. It turns up in newly designed looms that the *weaveability decreases for many reasons with the increase of the speed*.

Let us shortly analyse the *dynamics of fabric forming*, i.e. the question of sufficient reaction fastness of picks on still faster beat-up pulses. The picks have to manage the slipping between the warp ends in time sections gradually shortening with the progress in weaving speed. The beat-up process proceeds as follows (see Fig. 7):

- owing to the beat-up force $F_p(t)$ produced by the beat-up pulse $y(t)$ of the reed,
- the weft slips along the warp ends into the fabric by the path $\xi(t)$;
- simultaneously the frictional reaction between weft and crossed warp threads elongates the warp (and loosens the fabric) by some elongation $x(t)$;
- both paths x and ξ must be met by the reed lift y .

With higher weaving rates the weaving cycle duration T_c shortens inverse-proportionally to the weaving frequency n . Consequently, there is still less time for the reed to push the wefts inbetween the warp ends in the cloth. Now a physical phenomenon comes in effect that *the weft sliding velocity as well as the warp and fabric deformations depend not only on the acting forces, but also on the time course of these forces*. At higher weaving speeds the sliding resistance of weft

and the deformation forces in warp become higher. Therefore, *the weft resists the rapid beat-up pulses more intensively*. With increasing weaving frequencies *the weft slides into the fabric only by the successively decreasing paths ξ* .

For a certain transition period after any change of weaving parameters a bar with lower or higher weft density arises in the fabric before the cloth fell „grows“ successively closer to the reed and the warp elongation x at the beat-up becomes bigger enough and yields again a higher (or lower) beat-up force. Then, *the beat-up process steadies on a new level of parameters*. Yet the increase of beat-up force can bring along higher amount of end downs and/or the production of *faulty fabric (with irregular density, bariness)*.

3.2. The equilibrium of beat-up parameters during fabric forming at slow weaving speed

From experience, at low weaving frequency the quantities of beat-up process (forces, deformations, translations) remain steady and practically do not vary with the speed. Then, we can find a steady relation between the beat-up pulse y and resulting pickspacing A or weft density D_2 .

During the beat-up lift of the reed (i.e. during its contact with the last weft) the reed provides parallelly two actions (see Fig. 7):

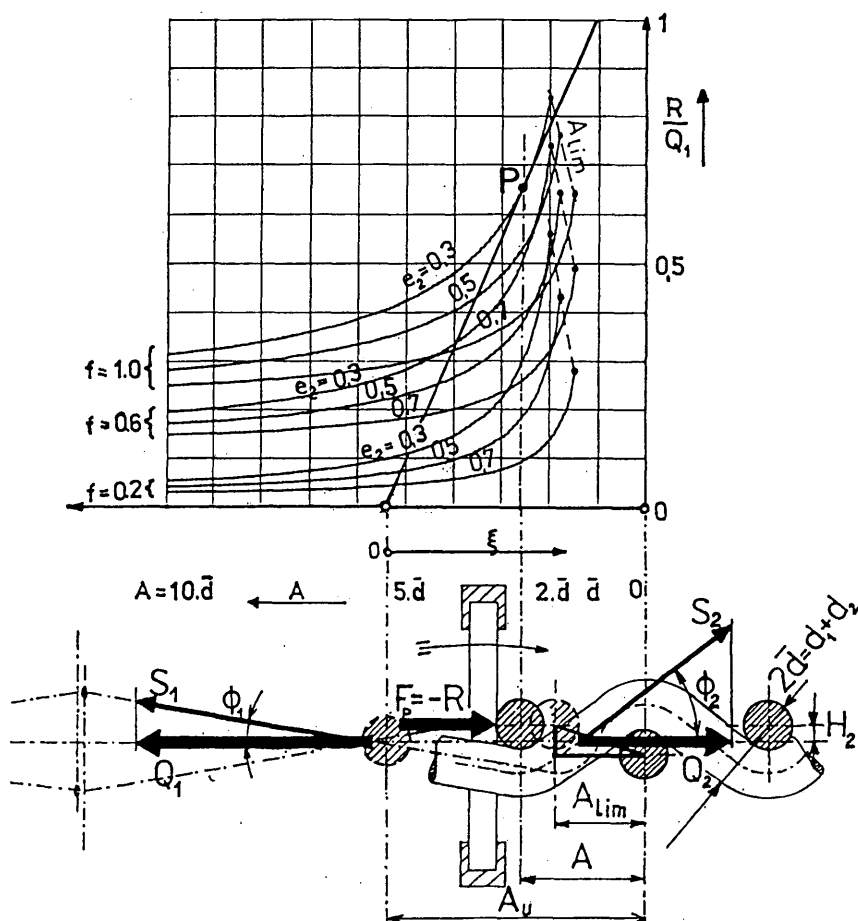


Fig. 7 The process of weft beat-up. Below: the sliding of weft inbetween the warp ends by a path $x = A_u - A$; $A = 1/D_2$. Here F_p is the beat-up force, R the weaving resistance caused by work of friction and of threads crimping. Above: dependence of weaving resistance on the achieved pickspacing A and on coefficient of friction f .

- First, the reed pushes the weft into the fabric by a path $\xi = A_u - A$ from the insertion position A_u to the given pick-spacing $A = 1/D_2$ which represents the definitive weft position.
- Second, due to the reaction R of weft sliding between the warp threads, the elastic warp and fabric elongate or contract themselves by a length ξ so that the beat-up force arises

$$F_p = Q_1 - Q_2 = (\bar{Q} + C_1 x) - (\bar{Q} - C_2 x) = (C_1 + C_2)x \quad (13)$$

It holds a steady equilibrium between the sliding (= weaving) resistance R and the beat-up force F_p

$$F_p - R = 0 \quad (14)$$

Note: The first clear explanation of fabric forming – i.e. of the process of achieving a certain pickspacing A as a result of reaching the equilibrium between the weaving resistance R and the beat-up force F_p which is equal to the above mentioned reaction $F_p = Q_1 - Q_2$ of warp and fabric – published by Greenwood *et al.* [6] in the 50ties. The authors supposed that the weaving resistance R followed the s.c. law of inverse distance $R(\xi) = \text{const}/A$. The weaving resistance R was expressed later by other authors in various forms, e.g. in the form of exponential law of weft density [7] or on the basis of dynamic friction of warp threads belted round the picks [8].

The two motions arising in the fabric during the beat-up, namely the slide of weft ξ into the fabric as well as the cloth fell motion (warp elongation) x , must be met by the beat-up lift y of the reed:

$$y = x + \xi \quad (15)$$

The beat-up lift then yields from the equation (13) when substituting for the forces

$$F_p = (C_1 + C_2) \cdot (y - \xi) = R(A) = \frac{\text{const}}{A} \Rightarrow y = (A_u - A) + \frac{\text{const}}{C_1 + C_2} \cdot \frac{1}{A} \quad (16)$$

Using the approximate Greenwood formulation of weaving resistance, we obtained the necessary height of the beat-up pulse of the reed y which depends only on the pickspacing A .

3.3. The measure of weaveability of fabric densities

The path ξ , by which the loom pushes the weft into the fabric under the given conditions, namely at the given weaving speed, can be used as a measure of weaveability of the loom. It corresponds with the weft density almost linearly, the higher members of the following expansion converging rapidly:

$$D_2 = \frac{1}{A} = \frac{1}{A_u - \xi} \cong \frac{1}{A} + \frac{1}{A^2} \cdot \xi + \dots \quad (17)$$

At slow weaving speeds the weaveability ξ remains constant. We shall see in the following analysis that with the increasing weaving frequency the weaveability ξ decreases.

3.4. Dynamic fabric forming process at higher weaving speeds

Similarly as the static, also the dynamic beat-up is a matter of dividing the beat-up pulse $y(t)$ into two motions: into warp elongation $x(t)$, and weft slip on warp ends $\xi(t)$.

During the dynamic beat-up the beat-up force $F_p = (C_1 + C_2) \cdot x$ arises, which at today's weaving speeds can be still regarded approximately as being steady. Let us take the expression for it still approximately true also for higher weaving frequencies.

(Note: Nevertheless, very soon it will be necessary to calculate with dynamic (i.e. varying) elasticity of warp and fabric by taking in account their „hardening“ due to deformation resistance caused by energy dispersions in the threads at higher straining frequencies on the loom. We will be also urged to take in account the distributed masses in yarns and calculate with finite velocity of propagation of deformation waves in warp.

The weaving resistance $R(\xi) = R(y - x)$ is not steady any more. Its value yields mainly from energy losses caused by speed dependent friction of weft on warp. The weaving resistance is a dynamic quantity and varies practically with all weaving frequencies. We cannot therefore use any more the weaving resistance in the simple Greenwood's form of an inverse distance law, but we must derive it from the friction between the threads in the cloth fell. Weaving resistance $R(A, f)$ depends first on immediate pickspacing A , and on immediate value of friction coefficient f . It can be derived on the basis of Fig. 7. From here yields the weaving resistance R :

$$R = Q_1 - \left[1 - \frac{\cos \Phi_2}{\cos \Phi_1} e^{-f(\Phi_1 + \Phi_2)} \right];$$

$$\cos \Phi_2 = \frac{2 \cdot \left(\frac{d}{A} \right)^2 \frac{H_2}{d} + \sqrt{1 + 4 \left(\frac{d}{A} \right)^2 \left[1 - \left(\frac{H_2}{d} \right)^2 \right]}}{1 + 4 \cdot \left(\frac{d}{A} \right)^2 \left(\frac{H_2}{d} \right)^2} =$$

$$= \frac{2\kappa_2^2 e_2 + \sqrt{1 + 4\kappa_2^2 (1 - e_2^2)}}{1 + 4\kappa_2^2 e_2^2} \quad (18)$$

Φ_1 is the given angle of shed opening. The angle Φ_2 of warp waviness is derived from binding geometry of warp threads – here from the Peirce's geometry. $\bar{d}/A = \kappa_2$ is the s.c. linear covering of fabric by weft and $H_2/\bar{d} = e_2$ is the relative height of weft waviness. The re-

sulting dependences of weaving resistance R on the immediate pickspacing A , on warp tension \bar{Q} and on the varying coefficient of Coulomb friction f are plotted in Fig. 7. above. For further applications, it is more convenient to use a linearized form of weaving resistance which is true in the vicinity of the „working point“ P of resistance curves of studied weave. By differentiation we obtain

$$R(A, f) = R_0 + \frac{\partial R}{\partial A} (A_0 - A) + \frac{\partial R}{\partial f} f_{dyn} = \alpha (A_u - A) + \beta f_{dyn} \quad (19)$$

The weaving resistance obtains thus the form of a linear combination of the influence of weft slip into the fabric $\alpha \cdot (A_u - A) = \alpha \cdot \xi$, and of the influence of dynamic friction $\beta \cdot f_{dyn}$. Here, the dynamic coefficient of friction f_{dyn} is a part of total friction varying considerably at least with the speed v_p of weft slip on warp. For our tasks we shall work with the form of the coefficient of friction:

$$f = f_0 + f_{dyn} = f_0 + \varphi_k \cdot v_p(t). \quad (20)$$

The dynamic beat-up process can be then described by a set of equations:

- of force equilibrium on the last weft,
- of values of the beat-up force and dynamic weaving resistance,
- of dividing of the beat-up pulse into the warp elongation and weft sliding, and
- of the form of the beat-up pulse.

The beat-up pulse $y(t)$ may have different forms according to the beating system. Suppose that the beat-up pulse has a half-sinus form with duration $T_p = \psi_p T_c$, the angle of beat-up duration being some $\psi_p^0 = 10^\circ$, the exploitation of weaving cycle for beat-up being small, $\psi_p = 10/360^\circ = 0.03...$

The equations of the dynamic beat-up process are the following ones:

$$F_p(t) - R(t) = 0$$

$$F_p(t) = (C_1 + C_2) \cdot x(t)$$

$$R(t) = \alpha \cdot \xi(t) + \beta \cdot \varphi_k \cdot \frac{d\xi(t)}{dt}$$

$$y(t) = x(t) + \xi(t)$$

$$y(t) = |y| \cdot \sin \omega_p t; \quad \omega_p = \frac{\pi}{T_p} = \frac{\pi}{\psi_p \cdot T_c} = \frac{\pi \cdot n}{60 \cdot T_c} \quad (21)$$

The solutions of these basic beat-up equations give the time course of weft slip into the fabric $\xi(t)$ and the course of the beat up force $F_p(t)$ respectively of the weaving resistance $R(t)$:

$$\xi(t) = K_\xi |y| \left[\frac{1}{\sqrt{1 + \omega_p^2 T_1^2}} \sin(\omega_p t - \psi_\xi) + \frac{\omega_p \cdot T_1}{\sqrt{1 + \omega_p^2 T_1^2}} e^{-t/T_1} \right] \quad (22)$$

$$F_p(t) = K_\xi |y| \left[\frac{\sqrt{1 + \omega_p^2 T_2^2}}{\sqrt{1 + \omega_p^2 T_1^2}} \cdot \sin(\omega_p t + \psi_R) - \frac{\omega_p T_1}{\sqrt{1 + \omega_p^2 T_1^2}} \cdot e^{-t/T_1} \right] = R(t) \quad (23)$$

where $K_\xi = (C_1 + C_2)/(C_1 + C_2 + \alpha)$; $T_1 = (\beta \cdot \varphi_k)/(C_1 + C_2 + \alpha)$; $T_2 = (\beta \cdot \varphi_k)/\alpha$ are the constants of proportionality and the time constants of the weft motion in response on the exciting signal of the half-sinus beat-up pulse.

The course of weft motion $\xi(t)$ (i.e. of the weft response on a half-sinus beat-up pulse $y(t)$), as well as the course of beat-up force $F_p(t)$, are also harmonic curves, yet in practice, they are damped by friction so intensively that they perform only one swing during the whole beat-up. The weft moves only ahead and halts in its front position. The courses of beat-up pulses $y(t)$ in dependence on increasing beat-up frequency ω_p as well as the responses of weft slips $\xi(t)$, and of beat-up forces $F_p(t)$ (weaving resistances $R(t)$) on these pulses are plotted in Fig. 8. We can notice that *with increasing beat-up frequencies the slips $|\xi|$ are getting successively lower whereas the resistances $|R|$ increase. The weaveability worsens.*

3.5. Frequency characteristics of weaveability

The maximum values of weft slips $|\xi|$ and of beat-up forces $|F_p|$ can be expressed separately from the time courses (22), (23) and plotted in graphs showing the weaveability or the difficulty to weave higher fabric densities in dependence on the increasing beat-up frequency ω_p . These graphs are called **frequency characteristics of weaveability**.

In the above mentioned equations the transition processes (i.e. the second members of the right sides of these equations comprising the expressions $\exp(-t/T_1)$) are usually damped so intensively that they almost fade to zero before the first (harmonic) members on the right sides of equations reach their maxima. Further, in common cases, instead of the beat-up lift $|y|$ the given parameters are the fabric density D_2 or the weft slip into the fabric $|\xi| = A_u - A = A_u - (1/D_2)$. Then, the „absolute values“ of ξ and F_p or R are from (22), (23).

$$|y(\omega_p)| = |\xi| \frac{1}{K_\xi} \sqrt{1 + \omega_p^2 T_1^2}; \quad |F_p(\omega_p)| = |\xi| \alpha \sqrt{1 + \omega_p^2 T_2^2}$$

The graphical representations of the functions are shown on the characteristics (a)–(c) in Fig. 9. It is evident that the weaveability $|\xi|$, the beat-up pulse $|y|$ or the beat-up force $|F_p| = |R|$ stay constant at low weaving frequencies, before the critical frequency $\omega_{pcrit} = 1/T_1$ or $1/T_2$ of the half-sinus course of beat-up has been reached.

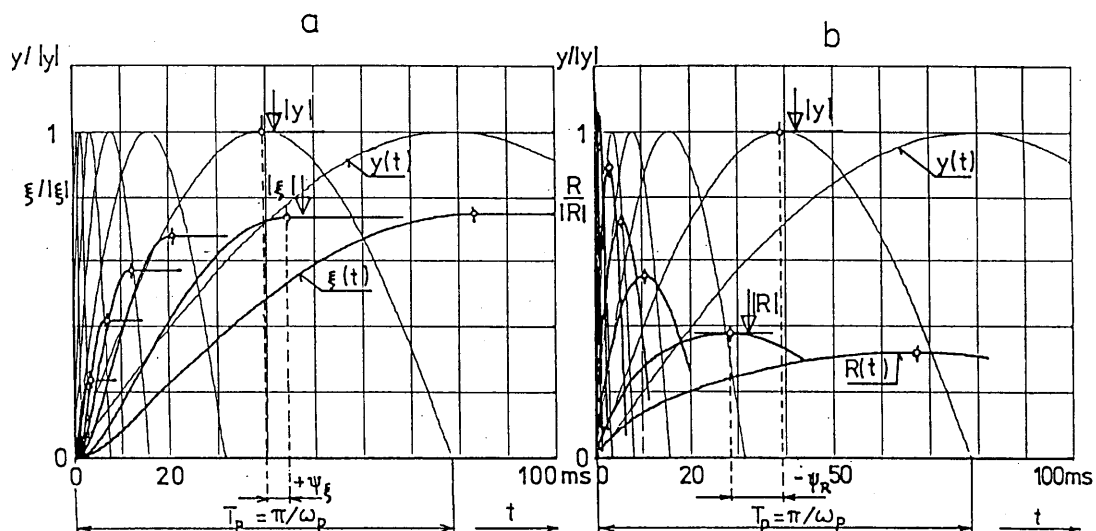


Fig. 8 The courses of beat-up pulses $y(t)$ in dependence on decreasing duration of the beat-up pulse $T_p = \pi/\omega_p$ resp. on increasing beat-up frequency $\omega_p = \pi \cdot n / (60 \cdot \psi_p)$, and the responses of weft slips $\xi(t)$ and of weaving resistances $R(t)$ or beat-up forces $F_p(t)$ on these pulses. Notice that with increasing beat-up frequencies (with narrowing y -curves) the slips $|\xi|$ get successively shorter whereas the resistance $|R|$ increases. The weavability worsens!

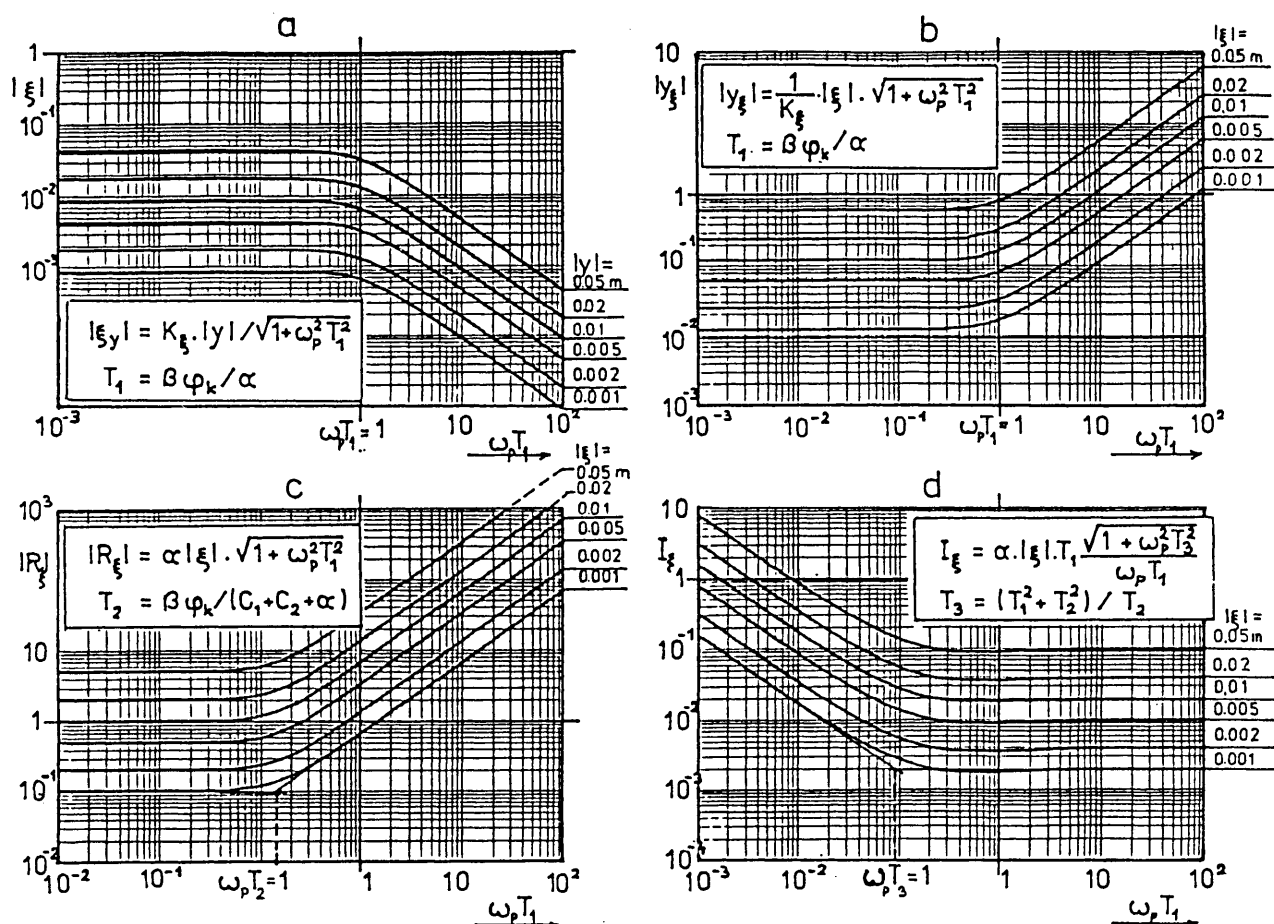


Fig. 9 Graphical representations of dependencies on beat-up freq. ω_p of the quantities: a) of weft slip $|\xi|$ into the fabric (weavability of the weft density $D_2 = 1/A = 1/(A_0 - \xi)$) at the given height of the beat-up pulse $|y|$; b) of the height of beat-up pulse $|y_\xi|$ necessary for the requested slip $|\xi|$ of weft in the fabric; c) of maximum values of weaving resistances $|R_\xi| = |F_p|$ at the given weft slips $|\xi|$;

d) of beat-up force impulses $I_\xi(\omega_p) = \int_0^{T_p} F_p(t) \cdot dt$ needed for achieving the weft density D_2

At higher beat-up frequencies the weaveability $|\xi|$ successively decreases whereas the weaving resistance $|R|$ or the necessary height of the beat-up pulses $|y|$ increase. At present it is the result of trends of heightening of weaving machine productivity. Therefore, it is necessary to search for solutions of this new difficult situation.

4. WAYS HOW TO IMPROVE (HOW TO ELIMINATE) THE DECREASE OF WEAVEABILITY IN HIGHLY PRODUCTIVE LOOMS.

4.1. The impulse $\int F_p dt$ of the beat-up force „consumed“ by the fabric

To find a new basis for possible elimination of weaveability decrease in high productive looms, it seems to be necessary to take in consideration a new view on the beat-up process – that the beat-up process represents reaching of equilibrium between the s.c. impulse of the beat-up force imparted by the loom to the fabric, and the necessary impulse consumed by the fabric in order to achieve the requested fabric density.

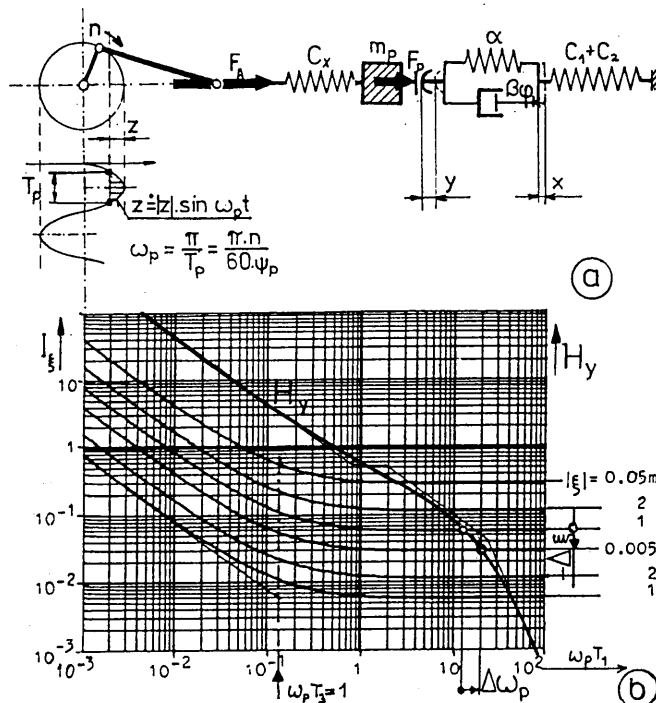


Fig. 10 a) A simplified model of the beat-up (crank, mass m_p , and compliance C_x) with a model of acting beat-up resistance (proportional resistance $[\alpha + \beta \cdot \phi_x \cdot (d/dt)] \cdot x(t)$) and with elasticities ($C_1 + C_2$) of warp and fabric; b) The equilibrium point between the impulse of beat-up force requested by the fabric for achieving the given density $D_2 = 1/(A_u - \xi)$, and the change of momentum $H_y(\omega_p)$ of the loom beat-up system (representing the imparted impulse of beat-up force at the given height of the approximately half-sin formed beat-up pulse).

During fast beat-ups the reed acts upon the last weft by increased beat-up forces $F_p(t)$ for certain, gradually still shorter time sections T_p . That means that the weft in the fabric always consumes at each beat-up an impulse I_ξ of force \times time. More exactly: the weft always consumes the quantity resulting from time-integration of the equation (23) over the time T_p :

$$I_\xi = \int_0^{T_p} F_p(t) dt \equiv \int_0^{T_p} R(t) dt = |\xi| \alpha T_1 \frac{\sqrt{1 + \omega_p^2 T_3^2}}{\omega_p T_1} \quad (24)$$

where $T_3 = (T_1^2 + T_2^2)/T_2$ is a new time constant arisen by integration.

Plotting this quantity as a graph (d) in the frequency characteristics in Fig. 8, we can see that the consumed beat-up impulses $I_\xi(\omega_p)$ of force $F_p(t)$, in the contrast to other characteristics, decrease with increasing beat-up frequency until they reach a critical value $\omega_{p \text{ crit}} = 1/T_3$. Since that the frequency of the impulses of beat-force has become practically steady. Therefore, the consumed impulse of the beat-up force is invariant from the beat-up frequency at high weaving speeds.

The „amount“ of the imparted and consumed impulse of the beat-up force can be called the *intensity of beat-up*. The intensity of beat-up is the decisive factor for achieving the requested fabric densities on highly productive looms. Now, the question is how to produce the necessary beat-up intensities to ensure the correct weaving process.

4.2. Impulse of the beat-up force imparted to the fabric on a classical weaving loom

The impulse $I(\xi)$ needed for achieving the requested fabric density D_2 or the corresponding slip $|\xi|$ of weft must be met by the same amount of the force impulse H produced by the loom. The impulse produced by the loom goes

1. on account of the change of momentum $\Delta H_1 = m_{\text{red(b.up)}} \cdot \Delta v_p$ of the beat-up mechanisms during the beat-up pulse, mainly of the slay. Then, the mechanism acts as a hammer.

2. on account of the time integral

$$H_2(T_p) = \int_0^{T_p} C_A \cdot [z(t) - y(t)] \cdot dt \quad (\text{where } T_p = \frac{\pi}{\omega_p})$$

of elastic forces $C_A \cdot (z - y)$ in the driving mechanism of the reed – see the chain of links, masses elasticities and compliances in the complex beat-up system in Fig. 10 a,b. From this point of view the beat-up mechanism works as a press.

The impulse of beat-up force produced by the loom in the Figure represents the beat-up intensity

$$H(\omega_p) = \int_0^{T_p} F_p(t) \cdot dt \approx 2 \cdot m_{\text{red.b.up}} |y| \cdot \frac{\alpha}{\alpha(C_A + C_1 + C_2) + C_A \cdot (C_1 + C_2)} \cdot \frac{1}{\omega_p} \cdot \frac{\sqrt{1 + \omega_p^2 T_1^2}}{\sum_k \sqrt{1 + \omega_p^2 \tau_k^2}} \cdot \cos \psi \quad (25)$$

This intensity of beat-up (the impulse of beat-up force) is a decreasing function of the circular frequency $\omega_p = \pi \cdot n / (60 \cdot \psi_p)$ of the half-sinus-formed beat-up pulse. Plotting the consumed and imparted impulses $I_x(\omega_p)$ and $H(\omega_p)$ together in Figure 10b, we find that a point of equilibrium (working point) always arises at a certain beat-up frequency $\bar{\omega}_p$. If the loom works with the revs n , we see that automatically the beat-up course settles on an angle of duration $\psi_p^0 \approx T_p$. If now the machine revs would be increased, first the beat-up frequency $\bar{\omega}_p$ would increase, too. The curve of the imparted beat-up impulse $H(\omega_p)$ at that frequency $\bar{\omega}_p$ would cross another curve belonging to a lower weavability $\xi = A_u - 1/D_2$. Owing to the inner autocontrol process, after a while – due to not deeply enough beaten-up picks – the cloth fell would increase against the reed and the beat-up duration $\psi_p \approx T_p$ would increase, too. A new beat-up frequency ω_p would be settled with a correct fabric density, but with higher straining of the warp.

4.3. Ways how to increase the impulse of beat-up force

There are, at least, two ways how to reach the necessary „amount“ of the impulse of beat-up force:

- to repeat the beat-up pulses or to transform the time course of the beat-up pulse to a rectangular or triangle etc. form,
- to heighten the force (and the duration of the beat-up) by the rigid slay construction.

The repeated or even vibration beat-up is theoretically as well as experimentally based on the established fact that it is practically equal whether the impulse of force has been imparted to the fabric by one high beat-up or by several lower strokes, provided that the total areas of both beat-up pulses are equal.

Each new repeated pulse $y_n = y - \sum_n \Delta \xi_{n-1}$ is, in fact, lower by the total achieved shift of weft into the fabric. Nevertheless, the weft slide into the fabric theoretically aims at the absolute utilisation of the original height of the first beat-up pulse, $\lim_{n \rightarrow \infty} \sum_n \Delta \xi_n = y_1$.

The beat-up can be repeated also by using an active back rest [11, 12], i.e. a swinging back rest roller driven by a cam on the main shaft of the loom. The secondary beat-up pulses produced by the swinging back rest are

positioned inside the weaving cycle next to the neighbourhood of the main beat-up pulse. Attempts have been also done to use a resonance back rest which provides several high swings following the main beat-up.

The main contemporary method for increasing the intensity of beat-up is the use of rigid but light slays which allow the autoregulation process in the weaving system to heighten the beat-up force as needed without destroying the mechanism. The slay arms have very short lengths and the slay beam is supported on several places of the weaving width.

Similar possibilities as the rigid slay brings today the rotational reed assembled of several hundreds of rotational lamellae on a shaft with a row of beat-up „noses“ on their perimeter – the s.c. weaving drum.

LITERATURE

- [1] Adovasio J.M., Soffer O., Hyland C., Klíma B., Svoboda J.: Textiles, Basketry, and Nets in Upper Paleolithic Moravia – Perishable Technology in the Pavlov Culture. In: 1957–58 Excavations in Dolní Věstonice, Brno 1997
- [2] Talavášek O. Shuttleless Weaving Machines, SNTL Praha, and Elsevier Amsterdam 1981, Talavášek O. Tkací stroje (in Czech), SNTL Praha 1988.
- [3] Nosek S. Teorie tkání I–III. (Theory of Weaving I–III, in Czech). Dům techniky Pardubice 1988.
- [4] Patent literature Sulzer Ruti of the weaving drum as well as the patents on the parallel-type multiphase weaving system 1960–1998.
- [5] Nosek S. Víceprošlupní tkací stroj roku 2000 – sériový nebo paralelní? (The multiphase loom in 2000 – a series or parallel type? In Czech). A study TULiberec 1998, not yet published.
- [6] Greenwood K., Cowling W.T., Vaughan G.M. The position of the cloth fell in power loom. J.Text.Inst 47 (1956), 241, 254, 274.
- [7] Horn V. Über die Kettspannung beim Anschlag in Abhäng. von der Gewebedichte. Textilpraxis 7 (1966)
- [8] Nosek S. Cloth Forming Process. English in: Věda a výzkum v průmyslu textilním, (Science and Res.in Textile Industry) 5 (1966), 70
- [9] Nosek S. Factors controlling weavability with regard to beat-up motions in modern looms. Engl. in: Věda a výzkum v průmyslu textilním (Science and Research in Textile Industry), 15 (1976), Brno.
- [10] Nosek S. Dynamics of fabric forming on the loom at high weaving rates. Ind. Journ. of Fibre and Textile Research, 19 (1994), 125–138
- [11] Nosek S. On peculiar behaviour of the back-rest roller on the weaving loom. Internat. Conference „Novelties in textile research and technology“, Tech. Un. Lodz 1997. Also in: Fibres and Textiles in Eastern Europe 22.(1997)
- [12] Hanzl J., Brotz I. Measurements on the resonance back-rest. Internat. Conference „Novelties in textile res. and technology“, Tech.Un. Lodz 1997. Also in Fibres and Textiles in Eastern Europe 22.(1997).
- [13] Nosek S. Mechanics of arising of stop-marks and structural periodic bars in the fabric. Imtex 95, Tech. University Lodz. 1996. Also in Fibres and Textiles in Eastern Europe 20 (1996).
- [14] Nosek S. Autocontrol of cloth structure in the weft. English in: Věda a výzkum v průmyslu textilním. (Science and Research in Textile Industry) 8 (1967), 93–140, Brno. Dito.... in the warp, I. et II., see in dtdo, 9 (1968), 135–166, and 12 (1971) Brno.
- [15] Wulffhorst B., Obolenski B. Beurteilung von Massnahmen zur Vermeidung von Anlaufstellen in Geweben. Melliand Textilber. 1 (1990), 24–43.

NUMERICAL SIMULATION OF THE START OF WEAVING LOOM

TUMAJER Petr, Ing

Technical University of Liberec

1. INTRODUCTION

The increase of the productivity of one shed weaving looms is mainly achieved by increasing the revolutions of the machine. Due to this, it is necessary to optimise each mechanism of the weaving loom from the point of view of its dynamic behaviour so that the function and maximum life of individual machine parts could be assured. But this is not the only factor which must be taken into consideration when designing a weaving machine. It is also necessary to pay attention to textile-technological problems which occur when increasing the revolutions of weaving machines.

One of the problems is the formation of the so-called set-bars in the fabric. This set-bar appears at the start of the weaving loom and it is formed by unequal spacing of several wefts. This article deals with the use of the numerical simulation to clear up the problem. The simulation will be carried out mainly with regards to the dynamic behaviour of the loom at its start and stop.

2. DYNAMIC MODEL OF WEAVING LOOM

This part describes by means of non-linear differential equations the behaviour of the weaving loom at its start, at stabilised running, and at the stop. These equations will be formed on the basis of the model which includes the main mechanisms of the weaving loom: the drive, the beat-up and the shedding mechanism. (see Fig.1)

A three-phase asynchronous electric motor drives the driving part of the friction clutch. The propelled part of this friction clutch is fixed on the main shaft. The transfer between the main shaft and the bottom shaft is carried out by means of gears. The beat-up device is here indicated by the kinematic scheme of a four-member hinged mechanism and the shedding device is substituted by a three-member hinged mechanism.

Fig. 2 shows the model which will be used for setting up the equations of motion

The driving moment M_h is given by the moment characteristic of the electric motor. In the following calculations we will use the substitute linearised dependence of this moment characteristic according to Fig. 2a. The moment M_r and force F_o characterise the influence of the textile material.

The start of weaving loom is carried out in two phases:

Before starting the machine the electric motor and driving part of the clutch (freely hung on the main shaft) are rotating. If at the time $t=0$ the machine is started by clutch connecting, then at that moment the angular speeds of the propelling and of the propelled parts of the clutch are different, i. e. the speed of propelled part is zero and the speed of the propelling part is other than zero. Under the influence of different speeds between the propelling part and the propelled part of the clutch the frictional moment M_t originates. In the first phase of the start the frictional moment M_t gradually reduces the angular speed of the propelling part of the

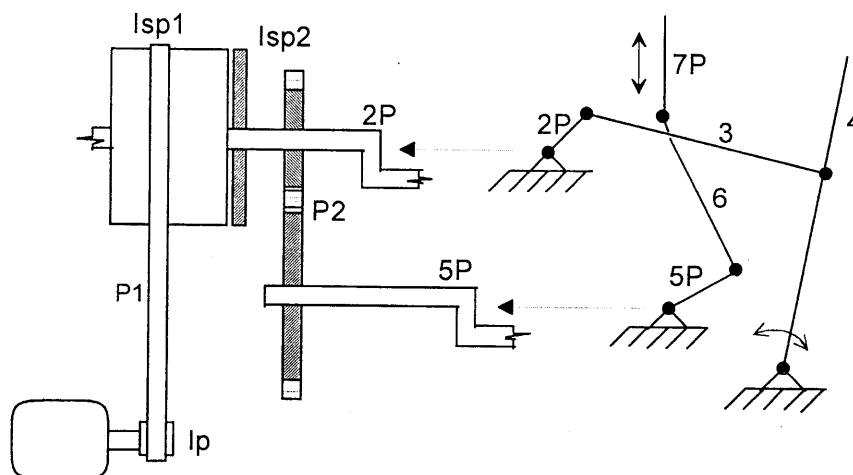
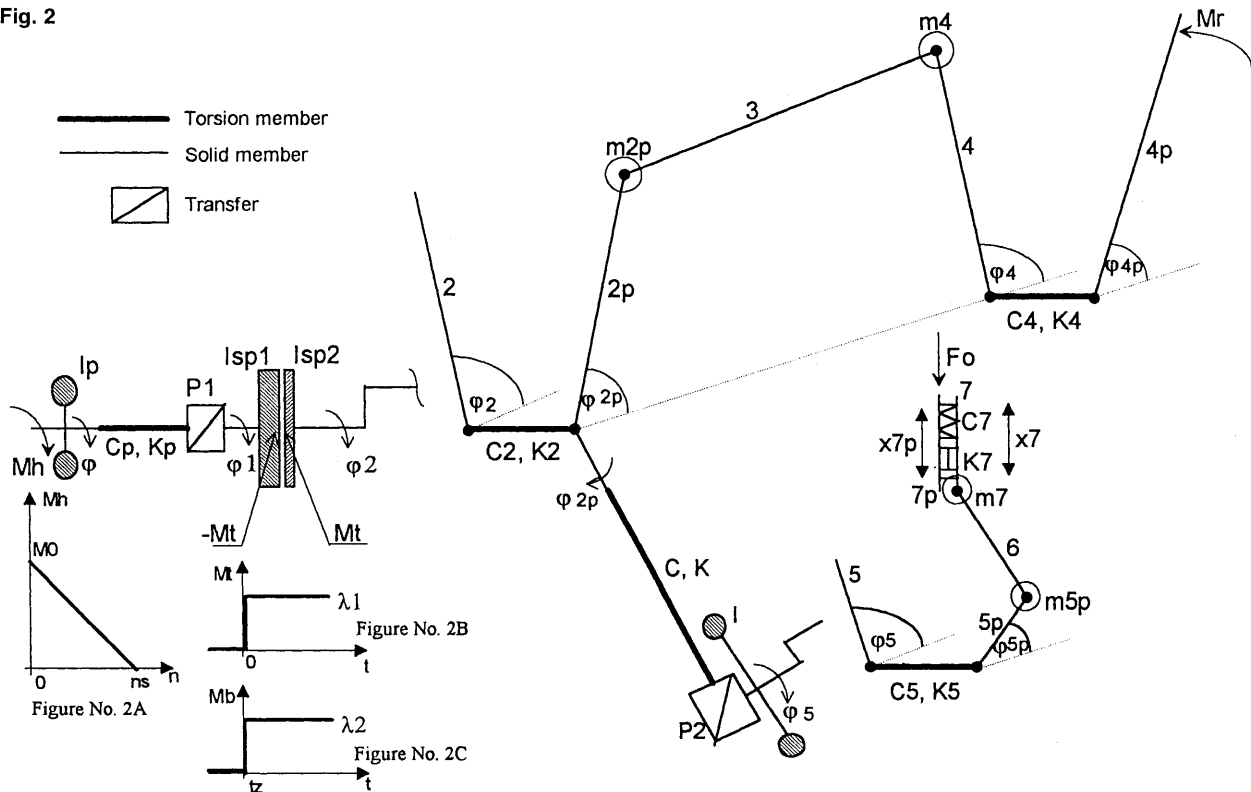


Fig. 1

Fig. 2



clutch and increases the angular speed of the propelled part of the clutch with the main shaft. At this phase the driving moment of the machine is the frictional moment M_t .

At the moment, when the speeds of both parts of the clutch equalise and the frictional moment M_t is then zero, the second phase of the starting process begins. In this phase the driving moment of the machine is the moment of the electric motor M_h . The angular speed, in this phase, gradually stabilises at the standard working value.

At stopping the machine in the time $t = t_z$ the clutch is disconnected and the brake is put into action. The brake is acting on the main shaft by the braking moment M_b and is reducing the angular speed as far as to zero value.

If the angular speeds of the propelling part and of the propelled part are different, then in our calculations we will consider the frictional moment M_t as, part by part, a constant function with the value of λ_1 (see Fig. 2b). The braking torque M_b will be also considered as, part by part, a constant function with the value of λ_2 (see Fig. 2c).

The equations of motion of the weaving loom model are set up here by using the Lagrangian equation of the second kind:

$$\frac{d}{dt} \left(\frac{\partial K}{\partial \dot{q}} \right) - \frac{\partial K}{\partial q} = - \frac{\partial U}{\partial q} - \frac{\partial R}{\partial \dot{q}}$$

where: K is the kinetic energy, U is the potential energy, R is the dissipate function, q is a general co-ordinate and the symbol $\dot{}$ is the derivation according to the time.

In the first phase of the start we express the kinetic and potential energy and also the dissipate function for the drive and all the remaining part of the machine. In the second phase these relations are expressed for the complex weaving loom model and, in the case of stopping, for a part of the weaving loom model which does not include the drive. By the derivative of these relations and by the substitution into the Lagrangian equation we will set up systems of second-order differential equations which describe the behaviour of the weaving loom in both phases of the start, at the stabilised running and stopping.

• The first phase of the start of the machine

– system of equations describing the behaviour of the drive:

$$I_p \cdot \ddot{\varphi} - M_h = -C_p \cdot P_1(P_1 \cdot \varphi - \varphi_1) - K_p \cdot P_1(\dot{\varphi} - \dot{\varphi}_1) \quad [2.1]$$

$$I_{sp1} \cdot \ddot{\varphi}_1 = -C_p \cdot (\varphi_1 - P_1 \cdot \varphi) - M_t - K_p \cdot (\dot{\varphi}_1 - P_1 \cdot \dot{\varphi}) \quad [2.2]$$

– system of equations describing the behaviour of the remaining part of the machine:

$$I_{sp2} \cdot \ddot{\varphi}_2 - M_t = -C_2 \cdot (\varphi_2 - \varphi_{2p}) - K_2 \cdot (\dot{\varphi}_2 - \dot{\varphi}_{2p}) \quad [2.3]$$

$$\begin{aligned} I_2 p \cdot \ddot{\varphi}_{2p} + I_4 \cdot (\mu_{2,4} \ddot{\varphi}_{2,4} \varphi_{2p}^2 + \mu_{2,4}^2 \ddot{\varphi}_{2p}^2) = \\ = -C_2 \cdot (\varphi_{2p} - \varphi_2) - C_4 [\dot{f}_{2,4}(\varphi_{2p}) - \varphi_{4p}] \mu_{2,4} - \\ - C \cdot P_2(P_2 \varphi_{2p} - \varphi_5) - K_2 (\dot{\varphi}_{2p} - \dot{\varphi}_2) - \\ - K_4 (\mu_{2,4} \cdot \dot{\varphi}_{2p} - \dot{\varphi}_{4p}) \cdot \mu_{2,4} - K \cdot P_2 \cdot (P_2 \cdot \dot{\varphi}_{2p} - \dot{\varphi}_5^*) \end{aligned} \quad [2.4]$$

$$I4p.\varphi_{4p}'' = -C4[\varphi_{4p} - f_{2,4}(\varphi_{2p})] - Mr - K4(\dot{\varphi}_{4p} - \mu_{2,4}\dot{\varphi}_{2p}) \quad [2.5]$$

$$I.\varphi_5'' = -C(\varphi_5 - P2.\varphi_{2p}) - C5(\varphi_5 - \varphi_{5p}) - K(\dot{\varphi}_5 - P2.\dot{\varphi}_{2p}) - K5(\dot{\varphi}_5 - \dot{\varphi}_{5p}) \quad [2.6]$$

$$I5p.\varphi_{5p}'' + m7(\mu_{5,7}\vartheta_{5,7}\varphi_{5p}^2 + \mu_{5,7}^2\varphi_{5p}'') = -C5(\varphi_{5p} - \varphi_5) - C7[f_{5,7}(\varphi_{5p}) - x_{7p}]\mu_{5,7} - K5(\dot{\varphi}_{5p} - \dot{\varphi}_5) - K7(\mu_{5,7}\dot{\varphi}_{5p} - \dot{x}_{7p})\mu_{5,7} \quad [2.7]$$

$$m7p.x_{7p}'' = -C7[x_{7p} - f_{5,7}(\varphi_{5p})] - F0 - K7(\dot{x}_{7p} - \mu_{5,7}\dot{\varphi}_{5p}) \quad [2.8]$$

• The second phase of the start and the stabilised running of the machine

– system of equations for the complex model of the weaving loom:

$$Ip.\varphi'' - Mh = -Cp.P1(P1\varphi - \varphi_2) - Kp.P1(\dot{P1\varphi} - \dot{\varphi}_2) \quad [2.9]$$

$$Isp.\varphi_2'' = -Cp(\varphi_2 - P1\varphi) - C2(\varphi_2 - \varphi_{2p}) - Kp(\dot{\varphi}_2 - P1.\dot{\varphi}) - K2(\dot{\varphi}_2 - \dot{\varphi}_{2p}) \quad [2.10]$$

The equations [2.9] and [2.10] will be completed by the equations [2.4], [2.5], [2.6], [2.7] and [2.8], which are identical for the first and the second phases of the start.

• The stopping of the machine

– system of equations for the part of the weaving loom model does not include the drive:

$$Isp2.\varphi_2'' = -Mb - C2(\varphi_2 - \varphi_{2p}) - K2(\dot{\varphi}_2 - \dot{\varphi}_{2p}) \quad [2.11]$$

The equation [2.11] will be completed by the equations [2.4], [2.5], [2.6], [2.7] and [2.8] which are again identical for the first phase of starting and also for stopping.

The behaviour of the drive of the weaving loom is not substantial from the point of view of fabric forming and that is why it will not be solved here.

In the equations we have used the usual marking for the gear functions of hinged mechanisms: The gear functions of the beat-up mechanism (four-member hinged mechanism):

- the zero gear function: $f_{2,4}(\varphi_{2p})$
- the first gear function: $\mu_{2,4}(\varphi_{2p})$
- the second gear function: $\vartheta_{2,4}(\varphi_{2p})$

The gear functions of the shedding mechanism (three-member hinged mechanism):

- the zero gear function: $f_{5,7}(\varphi_{5p})$
- the first gear function: $\mu_{5,7}(\varphi_{5p})$
- the second gear function: $\vartheta_{5,7}(\varphi_{5p})$

These functions can be expressed in analytical form by means of hinged mechanism geometry.

Further, we will express force F_0 which originates by the warp extension at opening the shed. This force will be expressed as a function of the shaft lift (see Fig. 3).

Further, it is necessary to express the moment M_r acting on the slay during the beat-up event. For expressing this moment we use the equations of the beat-up process. These equations were derived in [1].

The equations of the beat-up process:

- balance between the beat-up force F_p and the weaving resistance R : $F_p - R = 0$
- expression of the beat-up force by means of the elasticity constant of the warp C_1 , the elasticity constant of the fabric C_2 and the absolute warp extension, exactly fabric compression in the course of the beat-up event X : $F_p = (C_1 + C_2)X$
- expression of the weaving resistance by means of the coefficient of the geometrical component α , weft sliding ξ , the coefficient of frictional component β and the coefficient of friction f , which depends on the speed of the sliding and on the time: $R = \alpha.\xi + \beta.\varphi_K.\xi'$. We have used one of the simplest models of dependence of the friction coefficient on the weft sliding speed: $f = \varphi_K.\xi'$
- expression of the beat-up pulse by means of the warp extension and the sliding of the weft: $Y = X + \xi$

If we introduce the marking: $\underline{C} = C_1 + C_2$, $K_1 = \underline{C}/(\underline{C} + \alpha)$ and $K_2 = \beta/(\underline{C} + \alpha)$, and from the equations of the beat-up process we will express the weft sliding and we will obtain the equality: $\xi = K_1.Y - K_2.\varphi_K.\xi'$. We will differentiate this equation with respect to time and we will calculate the weft acceleration at the beat-up process:

$$\xi'' = (K_1.Y' - \xi')/(K_2.\varphi_K)$$

where $Y' = I.\varphi_{4p}'$ and I is the length of the slay.

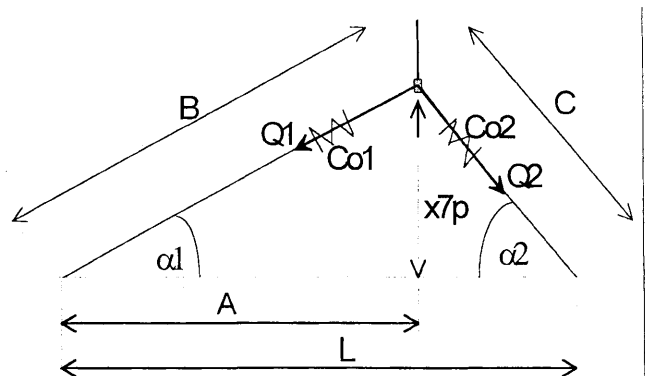


Fig. 3

$$F_0 = N(Q1.\sin\alpha1 + Q2.\sin\alpha2)$$

N total number of warp threads

We will complete the systems of equations of motion of the weaving loom model by this equation and we will solve it. The solution is performed numerically by the Euler method.

Note: *Self-regulation in the weaving process.*

The change of the amplitude of the beat-up pulse, which is caused by the change of the position of the fabric face in individual weaving cycles, is considered as the self-regulation process. Briefly, this process can be described in this way: For example: If in a certain weaving cycle a weft bar occurs, then the position of the fabric face changes with respect to the standard position, corresponding exactly to the value, by which the weft was pressed into the fabric. In the following cycle the reed will meet the fabric face earlier and the amplitude of the beat-up pulse will increase. (see Fig. 4). If we express the deviation of the sliding weft into the fabric in the k -th weaving cycle by $\Delta\xi_k = |\xi_{k-1}| - |\xi_k|$, the amplitude of the beat-up pulse in the $(k+1)$ st weaving cycle is given by the equation: $|Y_{k+1}| = |Y_k| + \Delta\xi_k$.

If a certain "defect" event enters the weaving process (for example at the start of the weaving loom), which causes a deviation of the pressing of the weft from the standard value, then, at the calculations in the following weaving cycles, it will be necessary to correct the amplitude of the beat-up pulse by these deviations.

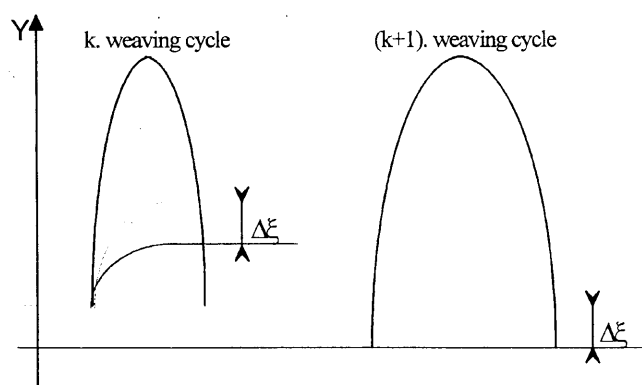


Fig. 4

3. NUMERICAL SIMULATION OF THE START OF THE WEAVING LOOM AT VARIOUS REVOLUTIONS

As mentioned above, the improvement of productivity of weaving looms is mainly achieved by increasing the revolutions. To be able to assess the influence of increasing weaving frequency on the origin of set-bars, in this part we will simulate the start of the weaving loom at various revolutions. In practice, the change of the weaving frequency is mostly carried out by the replacement of pulley on the shaft of the electric motor, i. e. by the change of the transfer between the shaft of the electric motor and the main shaft of the weaving

loom. We will also use a similar approach at the numerical simulation and the solution of the equations will be performed gradually for three different transfer values: $P1$: $P1=1/3, 1/2, 1$. The values of the other constants will remain unchanged. The results of the solution, represented graphically, are in the supplements. In each supplement [A], [B] and [C] three graphs are depicted. The first graph represents the dependence of the angular speed of the main shaft on the time, the second graph represents the dependence of the weaving resistance on the time and the third graph shows maximal values of the weft sliding for individual wefts.

The results will be used for the evaluation of the distribution of wefts in the fabric at the start of the loom. This evaluation will be performed by means of maximal values of the weft sliding for individual wefts which will be deducted from the relevant graph. We will always observe the first five wefts woven-in after the start of the machine. First, we will state the mean value of the achieved sliding for these five wefts:

$$\xi_{\max}^S = \frac{1}{5} \sum_{i=1}^5 \xi_{\max,i}$$

and then, we will define the deviation of the sliding by the relation:

$$\Delta_i = \frac{|\xi_{\max,i} - \xi_{\max}^S|}{\xi_{\max}^S} \cdot 100$$

These values, given for individual wefts, and for the different value of the transfer $P1$, are depicted in the graph (see Fig. 5).

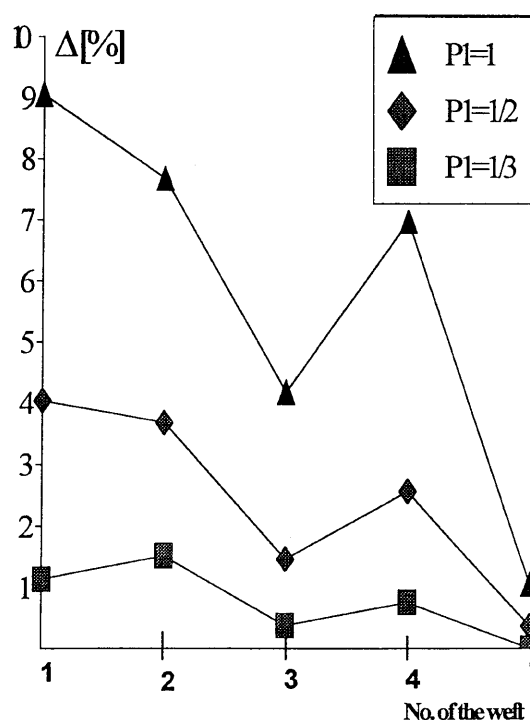
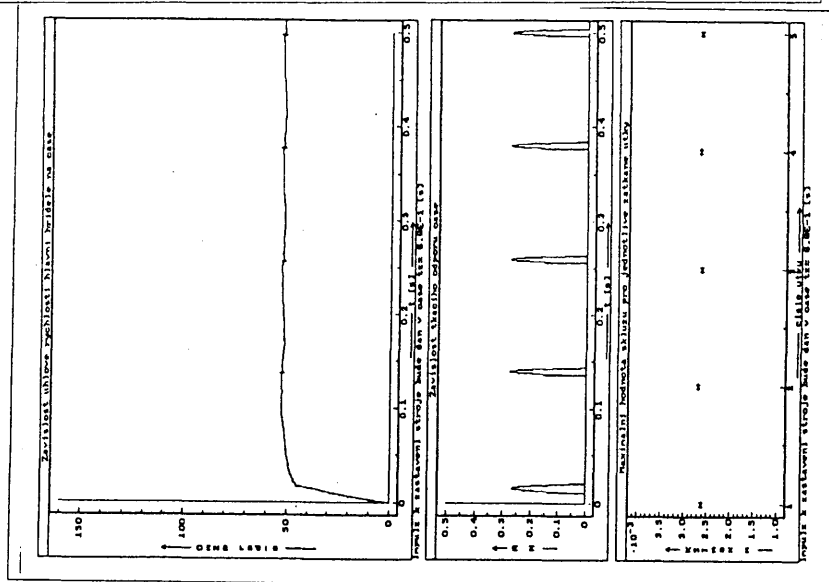
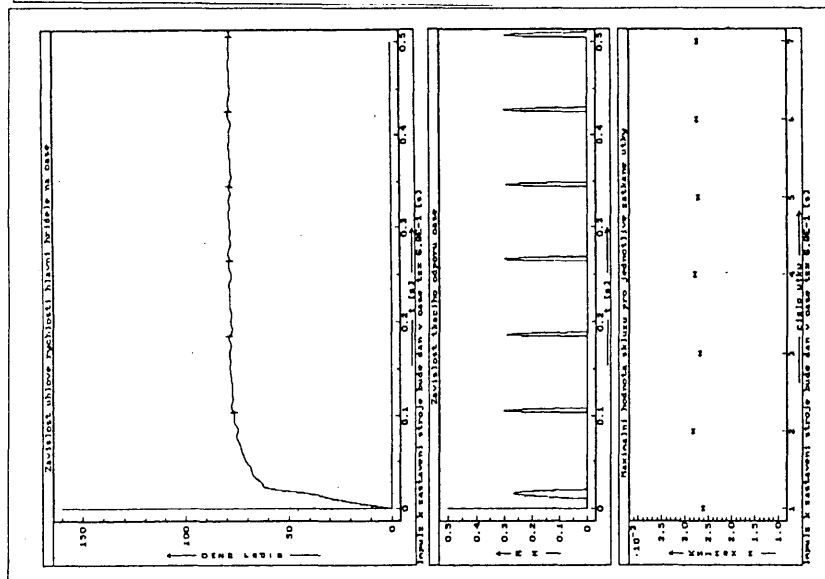


Fig. 5

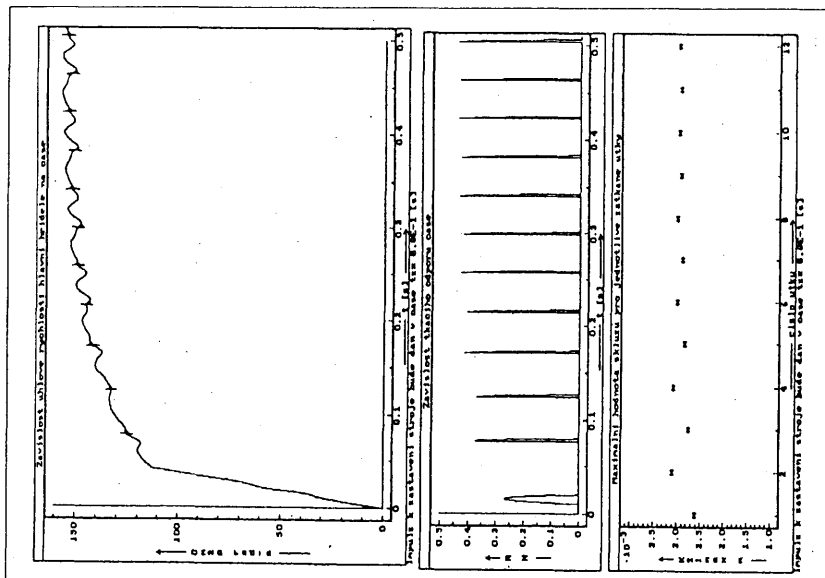
SUPPLEMENT A
 $Pf=1/3$



SUPPLEMENT B
 $Pf=1/2$



SUPPLEMENT C
 $Pf=1$



4. CONCLUSION

It is evident from the graph that the deviation values of the weft sliding will increase with the increasing weaving frequency and the number of wefts with a deviation of the sliding will increase, too. When increasing weaving frequencies, the origin of more considerable set-bars can be expected at the start of the weaving loom. Any further increase of revolutions of the looms must be taken into consideration. When designing the looms, it is necessary to optimise their individual machine parts and minimise their weight. Further, it is necessary to pay more attention to the construction of the clutch and the brake of the weaving loom. These factors highly influence the duration of the first and second phases of the start and the stop. However, in the case of further increase of revolutions, it will be necessary to use some "artificial" elements reducing the origin of the set-bar (for example: the controlled shift of the fabric face before starting the machine and the like).

Additional remark: The numerical simulation is here related to the problems of the origin of the set-bar at the start of the loom after a very short stop. In addition to the above mentioned dynamic phenomena, the origin of the set-bar, after a longer stopping of the machine, is also influenced by the reological properties of textile materials.

5. LITERATURE

- [1] S. Nosek: Teorie jednoproskupní a víceprosкупní tvorby tkaniny, 2. část, Dům techniky Pardubice 1988.
- [2] J. Mrázek: Dynamické vlastnosti tkacího stroje, výzkumná zpráva 1986

CONDITIONS FOR HIGH-QUALITY AND RELIABLE AIR JET WEFT INSERTION

Karel Adámek

Research Institute of Textile Machines Liberec

INTRODUCTION

By contemporary development of main parts of air picking system there are studied the inner flow and expansion of compressed air in weaving nozzles – both the main and auxiliary ones – and the free stream propagation in the atmosphere after leaving the nozzle outlet, as well as the interaction between the stream and profiled reed wall – partial reflection and penetration of the flow. Obtained velocity (dynamic pressure) field transports the textile yarn – the linear body with small and badly defined cross dimensions and small bend stiffness – to create the cloth. For the highest number of loom operating revolutions it is necessary to observe dynamic response of air supply system, too.

Aerodynamic forces influencing on acceleration and transport of weft yarn are limited with dissipation of free stream going out from nozzle outlet. For increase of the weaving performance and reliability it is necessary to eliminate that dissipation by several means. Analysis of essential parts of air picking system is closed with numerical 3-dimensional model of viscous turbulent flow

of expanding air in weaving channel of complicated shape with partially "porous" walls.

MAIN NOZZLE

The main nozzle designed as an ejector accelerates the weft yarn and transports this through the reed channel. Experiments with a lot of real designs of ejector show the dependence of relative air drag (F/F_{\max}) on the ejector opening, it means at the entry gap of incoming compressed air, see Fig. 1. Opening the air inlet, the air drag increases from zero to maximum and then decreases a little, so the value of drag with greatest nozzle opening is of about 50% to 75% of maximum drag. It is clear that the same value can be obtained with smaller ejector opening, it means with smaller air consumption, too.

The air drag is proportional to the square of relative velocity ($w-u$), where w is flow velocity and u is weft velocity. The transfer of mechanical output from the flow to the weft depends on the third potential of relative velocity ($w-u$) after Fig 2. The maximum efficiency of the process is reached when $u/w = 1/3$. Real weaving process applies an usual picking velocity of about 85 m/s and measured flow velocity in channel reaches the value of about 100 m/s. So the real relation $u/w = 0,9$ means the efficiency is not optimum.

Numerical modelling can explain some complicated processes in flow of expanding compressed air along the mixing tube of an ejector. Influence of the mixing tube shape of an ejector and intensity of shock waves in the flow shows following serial on the Fig. 3. All dimensions of ejectors are identical, the output diameter is changed, only (with mixing tube a – cylindrical, b – stepped, c – divergent). Thermodynamic condition are identical, too, the used pressure ratio is above critical of $p/p_0 = 1/7$.

On the Fig. 3a with cylindrical mixing tube there is observable a considerable shock wave area with non-homogenous velocity field. Intensity and position of visualized shock wave is here given first of all with inner shape of the mixing tube beginning. On the Fig. 3b there arises only one strong shock on the step. This design is better for the stable weft position in flow and for its more reliable picking – the maximum flow velocity operates on the weft tip, the very flexible weft yarn is

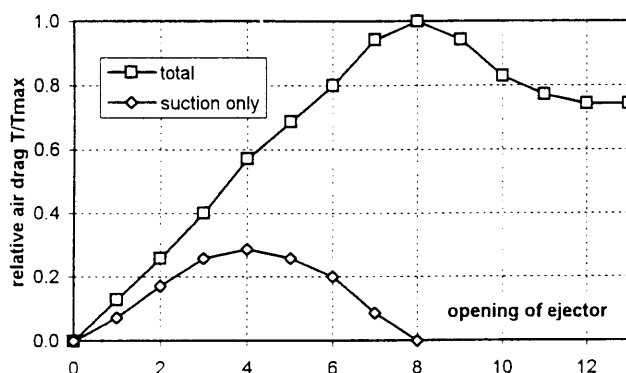


Fig. 1 Air drag as function of ejector opening

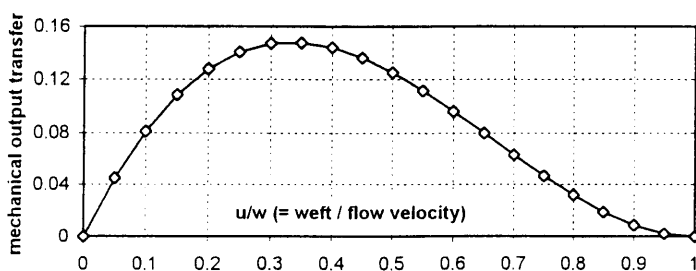


Fig. 2 Efficiency of mechanical output transfer from air flow to transported body

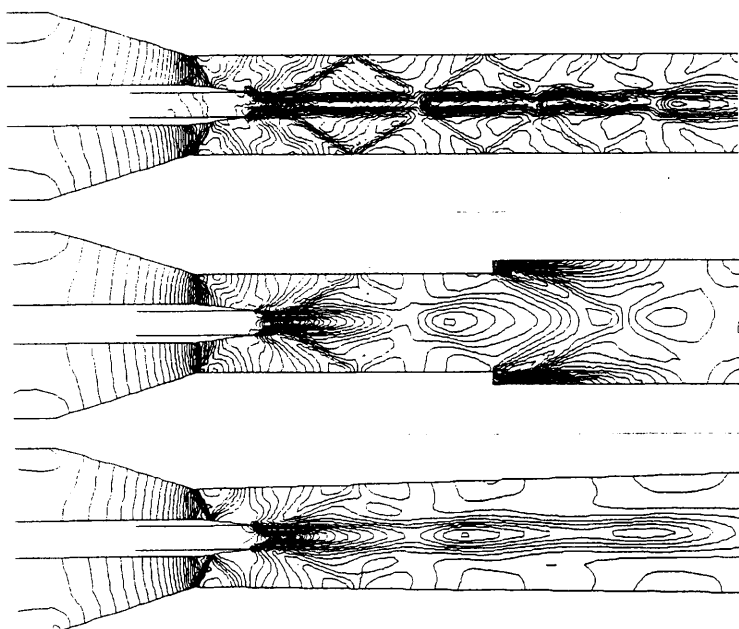


Fig. 3 Velocity field of an ejector ($p/p_0 = 1/7$) with mixing tube: a) cylindrical, b) stepped, c) divergent

pulled out, not pushed like in the Fig. 3a. The idea has been verified with actual weaving tests. The Fig. 3c shows the divergent shape of the mixing tube, which

complies better with conditions for the used above critical expansion. The flow field with higher velocity values and feeble shock waves was reached, only. Corresponding longitudinal velocity profiles along the axis of the mixing tube shows Fig. 4.

Next Fig. 5 shows a possible evaluation of results from Fig. 3a – in different scales there are values of u – velocity, ρ_0 – density, $(\rho/2 \cdot w^2 \cdot \Delta x)$ – expression proportional to the elementary air drag and summary drag from the beginning.

Fig. 6 shows detail of the central tube outlet for another design of ejector (for example with convergent mixing tube or with central tube shifted more to the left side of the design or with increased entry of compressed air etc.). The mixing tube is here “overfilled” by the flow, some part of expanding air is flowing back and the necessary suction of broken weft yarn is none. Such kind of ejector is not suitable for practical weaving.

So-called “classical” design of main jet is presented on following Fig. 7. In comparison with previous modern design the expansion is “divided” here into two parts. The first part of expansion is realized through

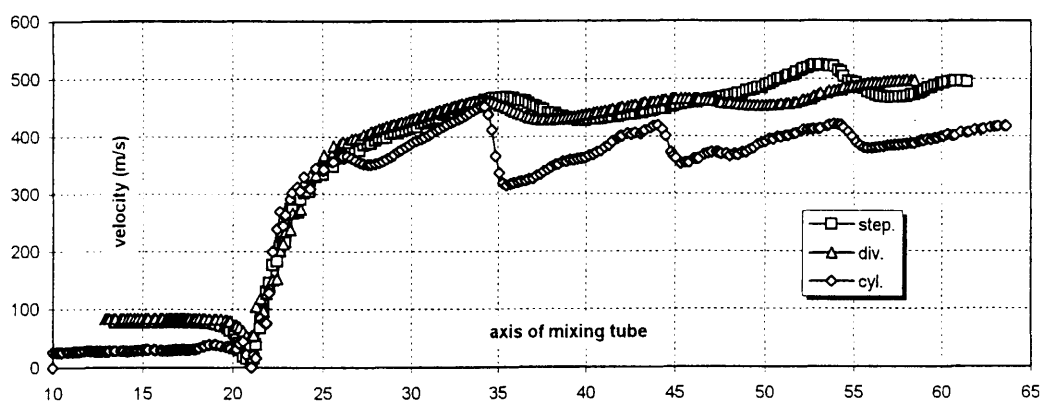


Fig. 4 Velocity profiles of ejectors from Fig. 3

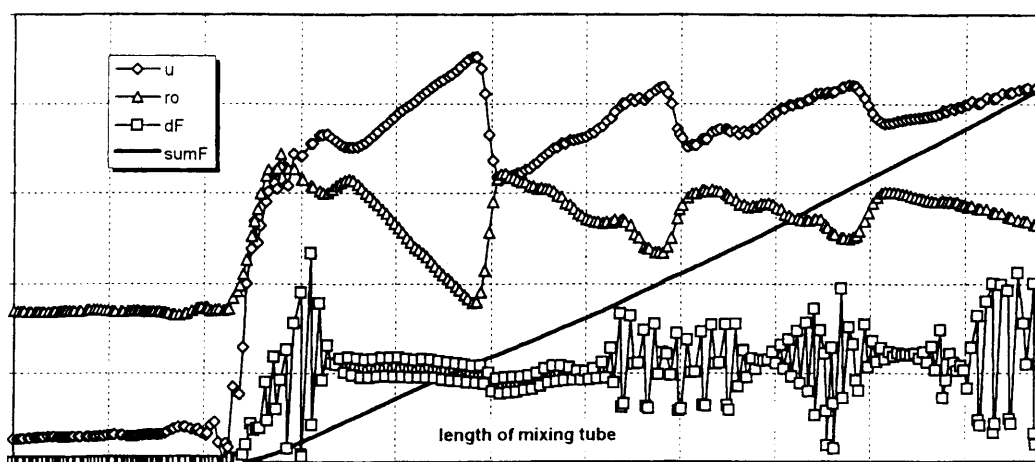


Fig. 5 Profiles of several flow quantities (for ejector from Fig. 3a)

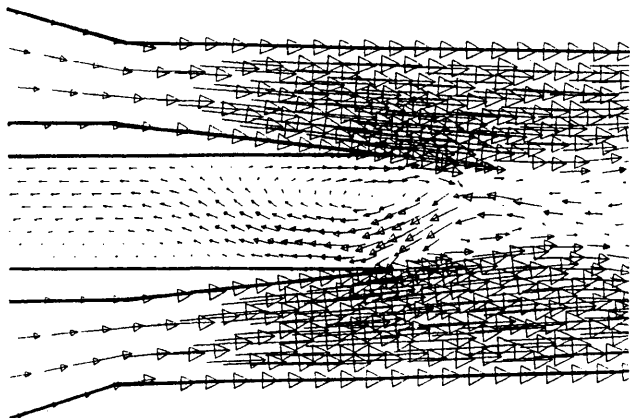


Fig. 6 Backflow in the middle tube of an ejector

cross wall at the entry, without contact to accelerated and transported weft, located in the middle tube. Only the second part of the expansion has an important influence on the weft. In comparison with previous type of main nozzle this type does not reach the highest weaving performance but at the same time it gently handles the weft. It is important for weaving materials with small firmness, as for example spun yarns. On the other side, with previous type of main nozzle we can reach the highest weaving performance but extreme tensile strength needs special materials, as for example polyester rayon.

AUXILIARY NOZZLES

System of auxiliary nozzles situated along the reed channel covers the flow losses given by free flows dissipation. The flow inside auxiliary nozzle is characterized with its sharp bend directly before the outlet. The expressive stream separation and contraction in classical auxiliary nozzle after Fig. 8a affects the unstable free stream direction when air pressure in the supply is reset.

In the double wall thickness after Fig. 8b the flow is guided better, the free stream direction is more stable. The same positive effect has the "shower" nozzle with several small orifices, see Fig. 8c. The elementary flows create quickly one common flow, practically independent on the outlet shape. A special case is the "channel" nozzle with inner channel after Fig. 8d. Its fluent bend before the nozzle outlet is designed in such a way that there is no flow separation and the value of velocity in the outlet cross-section is approximately constant. It is the ideal case, the flow is well guided and the free stream direction is independent on the air pressure in the supply. The theoretical presumptions were verified with measuring of serial of ceramic nozzles with inner channel.

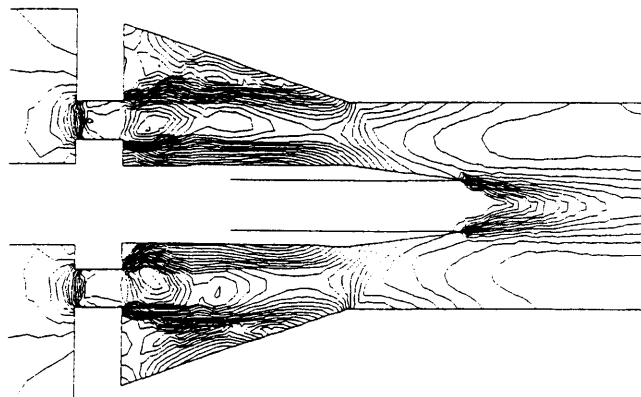


Fig. 7 Detail of double expansion in the entry part of classical ejector

Note: The pressure ratio of $p/p_0 = 0,7$ was assigned here, only, so the flow keeps subsonic. For the really used above critical pressure ratios (from $1/4$ to $1/7$ approx.), the vorticity of flow increases, the convergence of the numerical solution is bad or none and a correct solution cannot be obtained. Software used here is not destined for swirled flows.

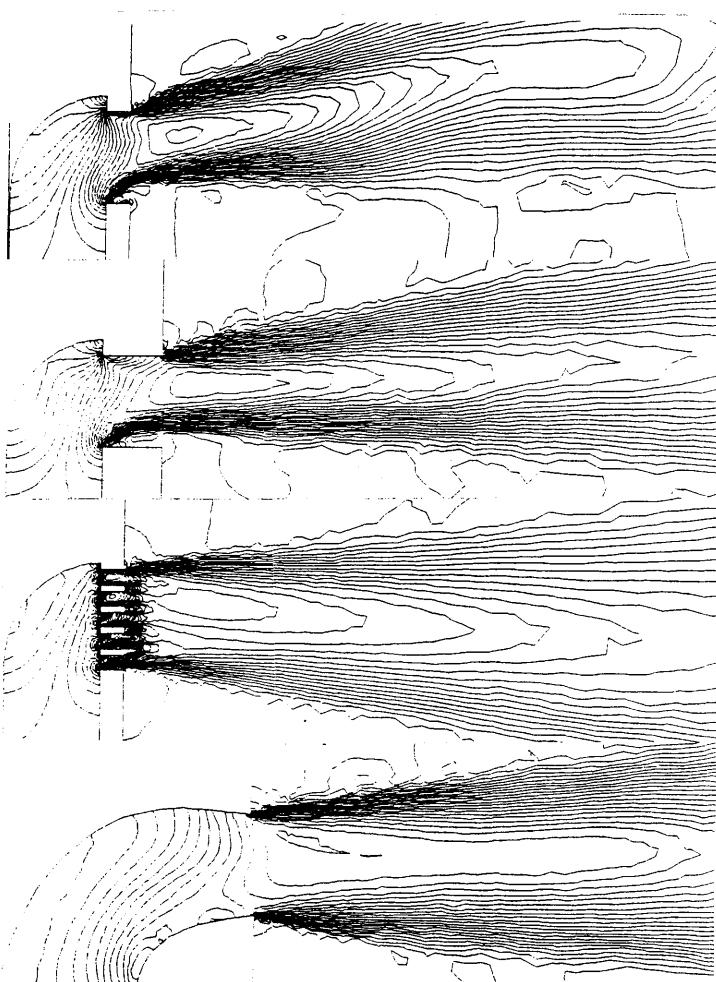


Fig. 8 Flow in outlet of several auxiliary nozzles: a) simple wall thickness, b) double wall thickness, c) multi-orifice nozzle, d) with inner chan-

Using correct production technology we can state that the quality of serial production of standard nozzles is very good. Changing the inlet air pressure in usual range of 400–600 kPa the free flow direction changes no more than $1,5^\circ$ and standard deviation of the free flow direction in a set of tested nozzles is not greater than 1° .

NOZZLES SETTING AND ADJUSTING

Theoretical dissipation of free flow from nozzle outlet, given by the hyperbolic law, was verified through experiments with diverse types of auxiliary nozzles, see

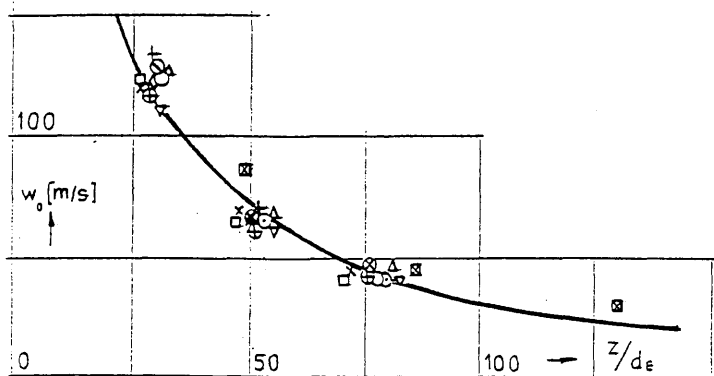


Fig. 9 Axis velocity dissipation from nozzle outlet

Fig. 9. An ideal velocity profile along the reed channel should have a constant value. In consequence of the free flow dissipation of the velocity field created by series of auxiliary nozzles, measured lengthways along the reed channel axis, has the form of a wave. Extreme values of the wave depend on setting and adjusting individual auxiliary nozzles, on the reed density, on the nozzle flow etc.

To get the highest weaving performance it is necessary to make some checking procedures. Though nozzles and reed are made with high quality, the velocity profile measured at checking the nozzles adjusting is not good – see Fig. 10 lower case. It seems that it is necessary to adjust all nozzles in the same position to the reed channel using a stencil. After this procedure the average value of velocity profile is twice higher and its standard deviation decreases to 1/4 approx. (see Fig. 10 upper case). Higher weaving performance with higher reliability are achieved as well.

The first step of setting the nozzles is setting of maximum dynamic pressure in a definite distance from nozzle outlet. The second step is checking of followed minimum dynamic pressure in each nozzle pitch. Extreme

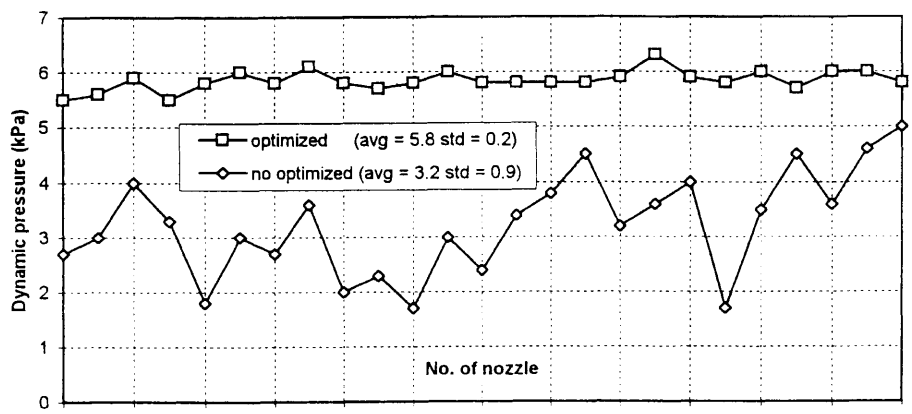


Fig. 10 Influence of nozzles setting and adjusting on dynamic pressure values in weaving channel

values should be prevented to obtain equalized velocity profile.

VELOCITY FIELD IN REED CHANNEL

Using theoretical description of free stream propagation for geometric penetration of conical free flow with U-shaped weaving channel, we can state that no more than approx. 30% of kinetic energy of conical flow is situated in weaving channel in individual common cross sections, see Fig. 11. In the practice, some reflection of conical flow from channel walls increases the value a little but in general, efficiency of the process is small.

The U-shaped weaving channel designed in profile reed prevents the dissipation of free air flows from auxiliary nozzles. Fig. 12 shows the influence of profile reed wall on values of dynamic pressure in weaving channel. Using Laser-Doppler-Anemometer (LDA), it was measured along the axis situated in the middle of the reed channel. The coefficient of amplification evaluated directly in the main conical flow from the nozzle outlet, is slightly greater than 1 but out of this area, the coefficient is greater, about 2 and more.

FLOW INTERACTION WITH REED WALL

The shape of reed dent edges influences on the reflection of the free stream from the reed wall and on the penetration through reed gaps, too. Three angular shapes of reed dents were modelled (rectangular, convergent and divergent) and three rounded shapes (on the left, right and both edges of each dent). The real shape of reed dents, depending on production technology, is usually convergent and both-sides-rounded. Complicated spacial reality was modelled in two dimensions, only. Typical interaction of a large constant flow (velocity of 100 m/s) with a reed wall (inclined of 5 degrees to the flow) show Fig. 13 for a) rectangular and b) double rounded edge shapes. The flowfield is simi-

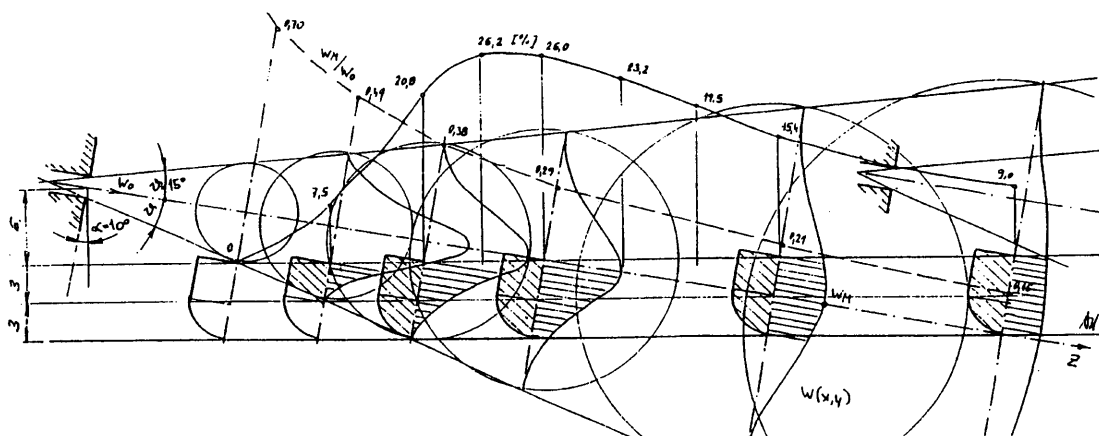


Fig. 11 Theoretical part of total air flow movement from auxiliary nozzle in area of weaving channel

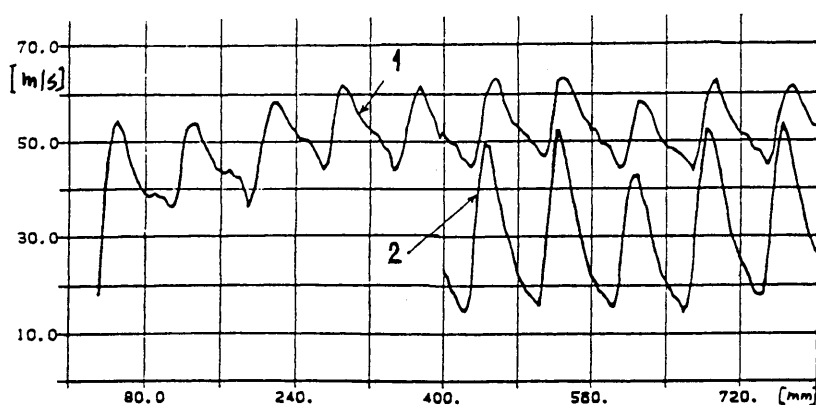


Fig. 12 Velocity profile along axis of weaving channel: 1) with reed, 2) without reed

The very interesting situation, when one of reed dents is modelled in wrong position, shows Fig. 14:

- in the first gap there arises a standard flow
- in the second gap a greater flow (next reed dent is pushed out from the line of the reed wall) occurs
- in the third gap arises a small backflow
- in the fourth gap there is a small flow in the right direction
- in the fifth and next gaps a standard flow again arises

lar for all tested dent shapes. The large main flow is disturbed a little, approx. as far as the depth corresponding to the dent thickness. In each gap is the flow separation accompanied with a vortex. The vortex length is of about 25% of the whole gap length for all right-angled shapes and of about 75% for all rounded shapes of reed dents. The share of the flow penetration of the whole incoming flow reaches 5% for convergent reed dent shape and 9% to 11% for all other reed dent shapes.

COMPLEX VIEW

Previous analysis of several elementary parts of air jet picking system were made as numerical models verified with experiments. The following step of the research is synthesis.

For solving of real spatial viscous turbulent flow of expanding air it is necessary to use more powerful hardware and software, too. Fig. 15 shows the first model of

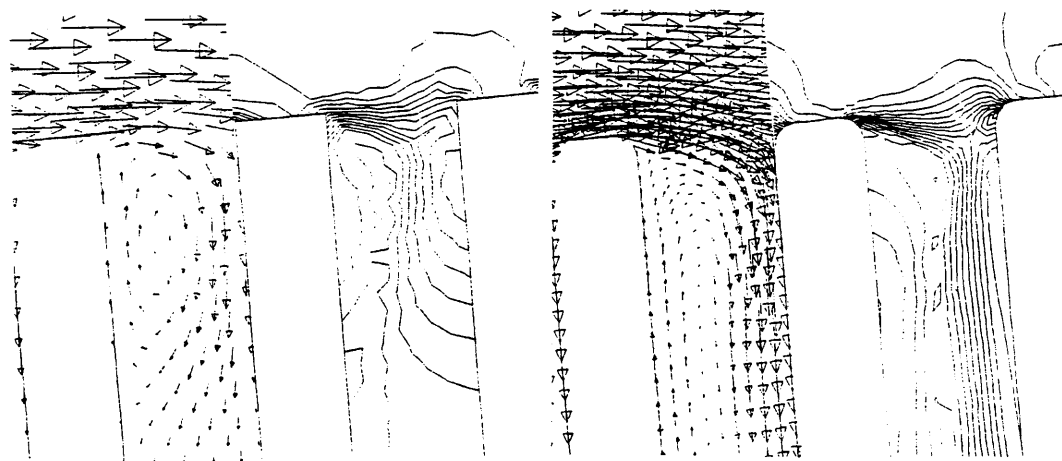


Fig. 13 Flow reflection and penetration – a) rectangular reed dents edge, b) rounded reed dents edge

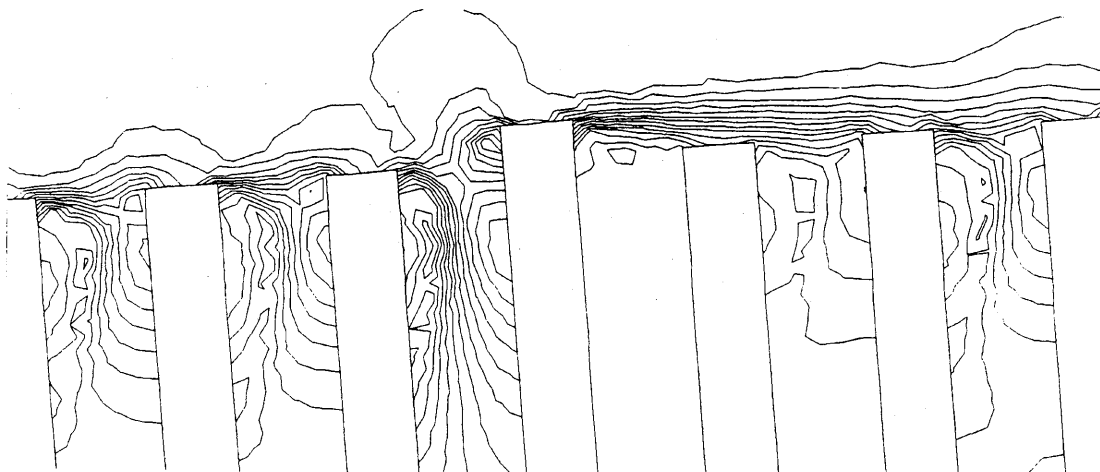


Fig. 14 Influence of wrong position of one reed dent on velocity field along reed wall

reed channel with auxiliary nozzle – the surroundings of one pitch, only with so-called “periodical” boundary condition at inlet and outlet sides (considering to the weft movement). Next Fig. 16 shows several horizontal cross sections through the space of reed channel made in distances of 1 – 2 – 3 – 5 – 7 mm from channel bottom. Visualized area of free flow from the nozzle outlet presents area of maximum velocity and its partial reflection and penetration, too. Comparison of several similar solution, when can express the influence as follows:

- setting or adjusting auxiliary nozzle,
- shape of the profile reed dents
- filling (density) of profile reed wall etc.

After images of velocity field we can judge about system configuration advisable for quick, reliable and economic weft insertion. Of course, the best verification of those theoretical conclusion are given with real weaving test, only, as yarn qualities can not be numerically modelled up to this time.

Measured real spacial velocity profile between two neighbouring nozzles shows Fig. 17.

there is the observable ceasing of the flow from the previous nozzle and then the rising of the flow from the new nozzle – gradually from the outer to the inner channel side till the maximum and then the ceasing again... Velocity profile along each measured axis can be expressed simply using first terms of Fourier analyse, as a goniometric function, characterized by mean value, amplitude and phase shift. The frequency keeps the same, it is given by nozzle pitch.

REFERENCES

[1] Kopecký V., Adámek K.: Using of LDA and Hydraulic Analogy in Air Jet Weaving. Proc. of the 5th Symp. on Flow Visualization, Prague, 1989. In: Flow Visualization V, Hemisphere Publishing. Co., New York, 1990, p. 703–710

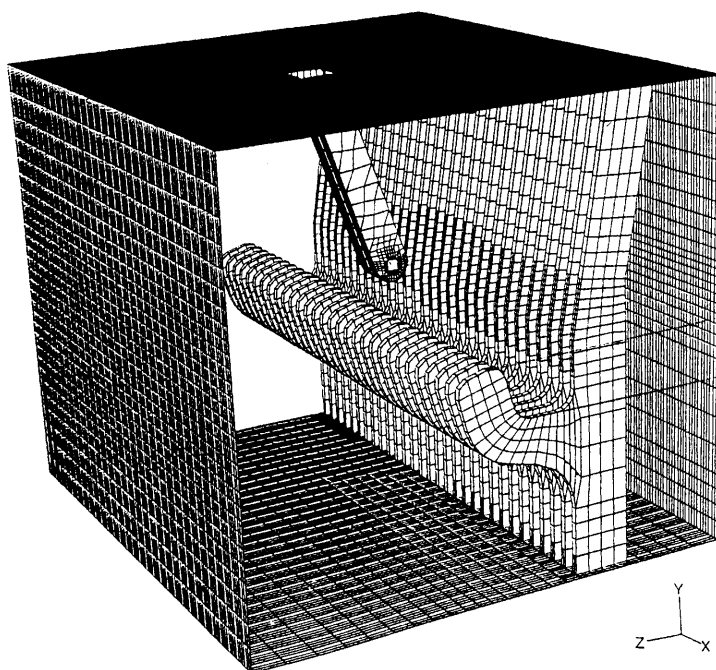


Fig. 15 Spacial model of reed channel with auxiliary nozzle

- 2 Adámek K.: Influence of Nozzle Position on Air Jet Weaving. In: Textil technics, 2 (1990), VÚTS Liberec, p. 15–22 (in Czech)
- 3 Adámek K.: Stafettendüsen hergestellt im Feingussverfahren. In: 6. Weberei Kolloquium, Inst. für Textil- und Verfahrenstechnik, ITV Denkendorf, 1990,
- 4 Adámek K.: Channel Relay Jets. In: Proc. of the 6th Int. Conf. on the Theory of Machines and Mechanism, Vol. B, p. 5–10, TU Liberec, 1992 (in Czech)
- 5 Adámek K.: Ceramic Relay Nozzles. Habilitation lecture, TU Liberec, 1992 (in Czech)
- 6 Adámek K.: Channel Relay Jets. In: Textile Technol. Int., Hong Kong, 1993, p. 140–14
- 7 Adámek K.: Shock Waves as a Tool ? In: Proc. of 2nd Int. Symp. on Exp. and Comput. Aerodynamics of Internal Flows, Czech Academy of Sciences, Prague, 1993, vol. 1, p. 109–114
- 8 Adámek K.: Problèmes aérodynamiques de jet d'air dans les machines à tisser, Séminaire pour Inst. de Mécanique Statistique de la Turbulence, Université Aix-Marseille, 1994
- 9 Adámek K.: Air jet weaving of flat tapes. In: 20th Int. Weaving

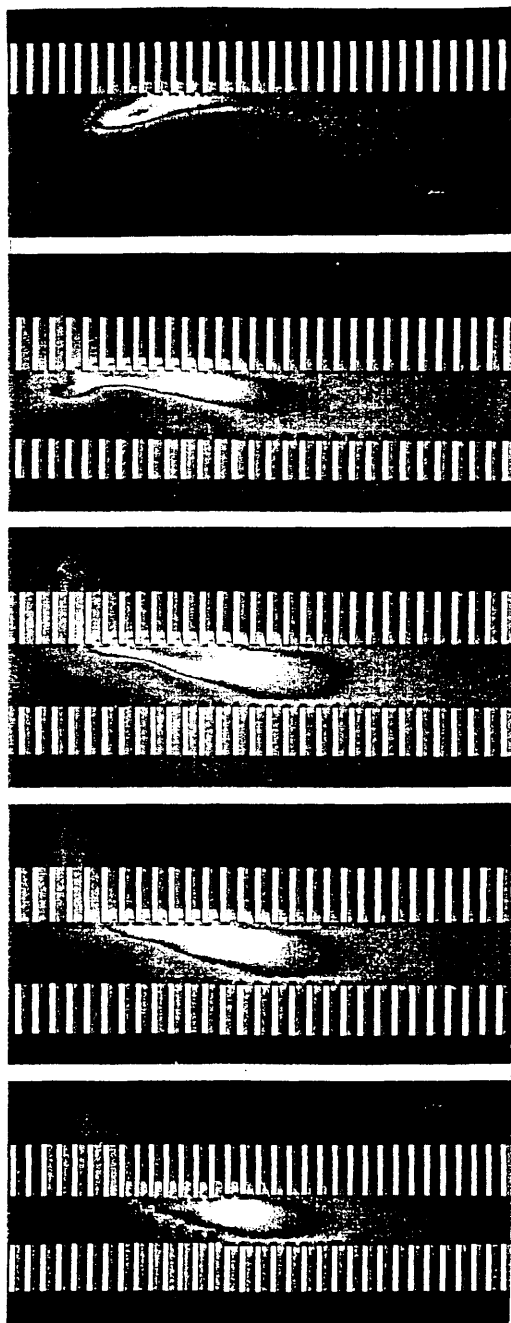


Fig. 16 Serial of horizontal cross section in velocity field from Fig. 15 (numerical model)

- Conf., High Tatras, 1994, 12 p. (in Czech)
- 10 Adámek K.: Description of Flows in Ejector using FVM. In: Proc. of Int. Conf. Applic. of Exp. and Numer. Methods in Fluid Dynamics. High Tatras, 1995, p. 109–114 (in Czech)
 - 11 Adámek K.: Design of Parts for Air Jet Weft Insertion by F.V.M. In: Young Textile Science, TU Liberec, 1995, 8 p.
 - 12 Adámek K.: Beschreibung der Webdüsenströmung mit FVM. In: 5. Chemnitzer Textilmaschinen- tagung, TU Chemnitz-Zwickau, 1995, p. 85–93
 - 13 Adámek K.: Experience with FVM in Research of Air Jet Weaving System. In: Computer Modelling and Simulation in Engineering, Sage Science Press, 1996, 12 p.
 - 14 Adámek K.: Description of Flows in Air Jet Weaving System. In: Proc. of 21st Int. Weaving Conf., High Tatras, 1996, 7 p. (in Czech)

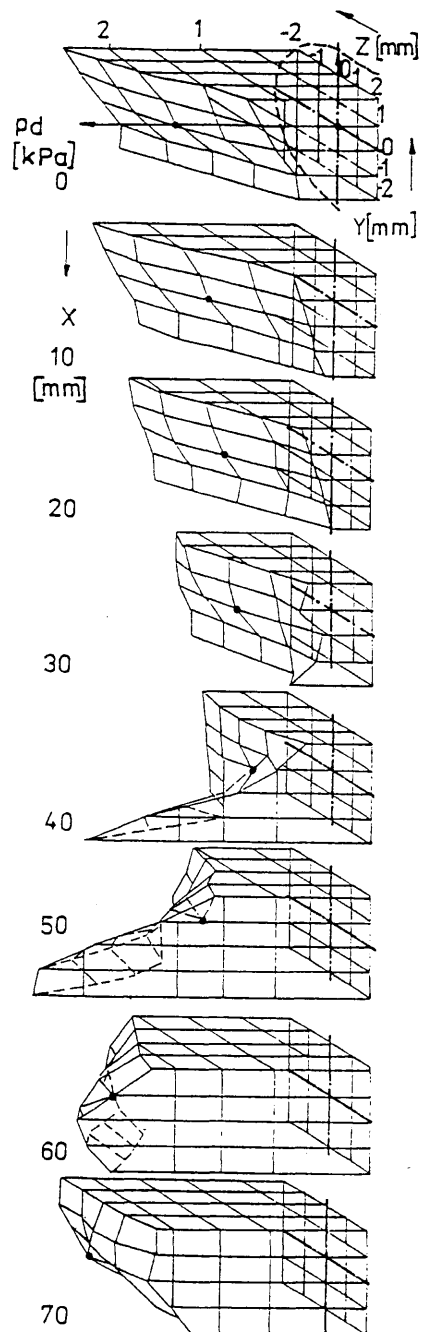


Fig. 17 Measured spacial velocity in reed channel (nozzle at 0 mm, pitch of 80)

- 15 Adámek K.: Interaktion zwischen Luftstrom und Schussfaden. In: Wissenschaftliche Jahrestagung GAMM, Prag, 1996
- 16 Adámek K.: Numerical Modelling of Air Flow Effect by Air Jet Weaving. In: Proc. of 7th Int. Conf for the Theory of Machines and Mechanisms, TU Liberec, 1996, p. 11–16 (in Czech)
- 17 Adámek K.: Experience with Numerical Modelling in Air Jet Weaving. Lecture for Fac. of Math. and Phys. of Charles' University, Prague, 1997
- 18 Adámek K.: Numerische Modellierung der Strömung im Webkanal. In: 6th Chemnitzer Textil maschinentagung, TU Chemnitz-Zwickau, 1997, poster
- 19 Air Jet Loom IC 966, Ih-Ching Machinery, Tchaiwan, 1992
- 20 Air Jet Weft Insertion for Terry Looms, Nuovo Pignone, Italy, 1994
- 21 Air Jet Loom ALPHA – Trustfin Vsetín, 1995
- 22 Air Jet Loom BETA – Amoco Fibres and Fabrics, USA, 1996

DYNAMIC STRESS OF HEALD SHAFT OF WEAVING LOOMS

MRÁZEK JIŘÍ, BÍLEK MARTIN

Department of Textile Machine Design
Technical University of Liberec, Hálkova 6, 46117 Liberec, Czech Republic

INTRODUCTION

The shedding motion together with a beat-up mechanism represent basic mechanisms of a loom, which ultimately determine the running speed and the quality of the produced fabric. These mechanisms jointly influence the dynamic behaviour of the machine as whole.

The main problem of presently used shedding motion and heald shafts is the provision of the higher reliability and of longer working life of different parts of shedding mechanism, like working life of heald shaft frames and namely of healds.

This contribution deals with modelling of the mechanical system of shedding mechanism – heald shaft – heald – warp and with attempts to analyse the dynamic behaviour of one of the many possible structures of shedding motion, frames of heald shafts with healds. The paper analyses new principle of shedding mechanism with straight line displacement and without side guides of heald shafts.

In the model the motion of healds with considering of clearances between healds and heald rod, in the heald eye between heald and warp thread during one turn of loom main shaft is analyzed.

The results are represented by graphs of kinematic quantities on individual elements of mechanism in dependence on mass parameters (rigidity, moment of inertia, mass), on clearances in kinematic pairs of the mechanism, between heald and heald rod on warp thread.

MATHEMATICAL MODEL OF THE SYSTEM

This system is a bit complex due to the number of elements and kinematic chains concerned. Mathematical model of the shedding mechanism has been formulated with the following assumptions, where two heald shafts M and L are driven by a single mechanism 2, 3, 4:

- masses of heald shafts M and L and elements 7, 8, 9 are reduced to the joints of the elements 4 and 6
- masses of elements 3, 5 are replaced by two mass concentrated points and are considered as rigid
- rocking levers of elements 2, 4, 6 are rigid and are mutually joined by torsion rods
- clearances in kinematic chains are considered in elements 2 and 4
- viscous damping in individual elements is also considered in the model.

Equations of motion of the system are formulated using Lagrange's equation of the type II in the form

$$\frac{d}{dt} \left(\frac{dK}{d\dot{q}_i} \right) - \frac{\partial K}{\partial q_i} = - \frac{\partial U}{\partial q_i} - \frac{\partial R}{\partial \dot{q}_i} \quad (1)$$

where $i = 2, 4, 6$. (K – kinetic energy, U – potential energy, R – dissipative function)

Substituting different parameters K , U and R in equation (1), we obtain the following equations of motion:

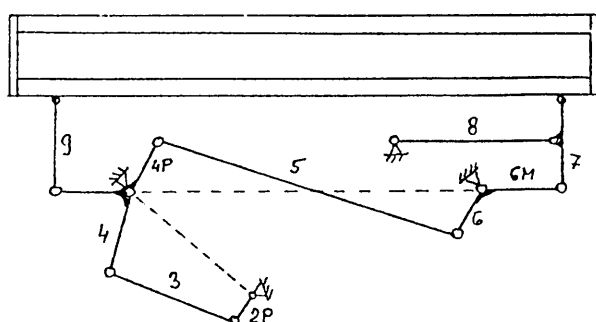


Fig. 1 Scheme of system

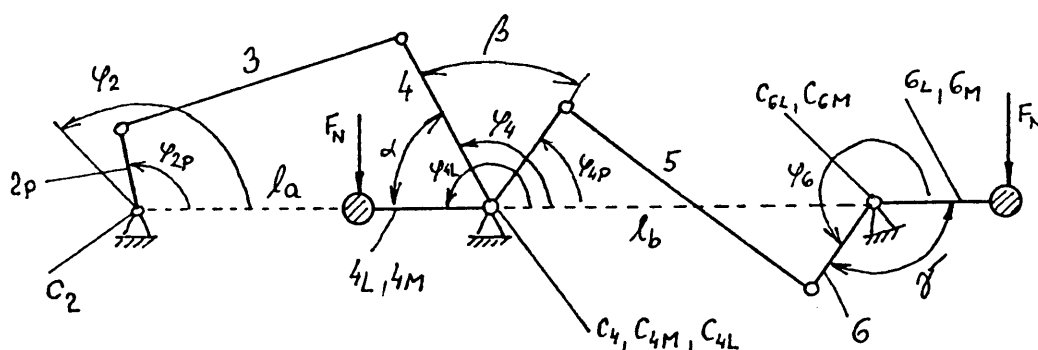


Fig. 2 Schematic diagram for calculation

$$\ddot{\varphi}_{2P}(I_{2P}+I_4\mu_{24}^2)=-I_4\mu_{24}V_{24}\dot{\varphi}_{2P}^2-C_2(\varphi_{2P}-\varphi_2)+C_4\mu_{24}(\varphi_{4P}-\varphi_4+\beta)+k_2(\dot{\varphi}_{2P}-\dot{\varphi}_2)+k_4\mu_{24}(\dot{\varphi}_{4P}-\dot{\varphi}_4) \quad (2)$$

$$\ddot{\varphi}_{4P}(I_{4P}+I_6\mu_{46}^2)=I_6\mu_{46}V_{46}\dot{\varphi}_{4P}^2-C_4(\varphi_{4P}-\varphi_4+\beta)+C_6\mu_{46}(\varphi_{6L}-\varphi_6-\gamma)+C_6\mu_{46}(\varphi_{6M}-\varphi_6-\gamma)-k_4(\dot{\varphi}_{4P}-\dot{\varphi}_4)+k_6\mu_{46}(\dot{\varphi}_{6L}-\dot{\varphi}_6)+k_6\mu_{46}(\dot{\varphi}_{6M}-\dot{\varphi}_6) \quad (3)$$

$$\ddot{\varphi}_{4L}I_{4L}=-C_{4L}(\varphi_{4L}-\varphi_4-\alpha)-k_{4L}(\dot{\varphi}_{4P}-\dot{\varphi}_4)-M_{4L}+F_N R_{4L} \cos \varphi_{4L} \quad (4)$$

$$\ddot{\varphi}_{4M}I_{4M}=-C_{4M}(\varphi_{4M}-\varphi_4-\alpha)-k_{4M}(\dot{\varphi}_{4P}-\dot{\varphi}_4)-M_{4M} \quad (5)$$

$$\ddot{\varphi}_{6L}I_{6L}=-C_{6L}(\varphi_{6L}-\varphi_6-\gamma)-k_{6L}(\dot{\varphi}_{6L}-\dot{\varphi}_6)-M_{6L}+F_N R_{6L} \cos \varphi_{6L} \quad (6)$$

$$\ddot{\varphi}_{6M}I_{6M}=-C_{6M}(\varphi_{6M}-\varphi_6-\gamma)-k_{6M}(\varphi_{6M}-\varphi_6)-M_{6M} \quad (7)$$

In equations of motion the following transmission functions μ_j , v_j are used

$$\varphi_4 = f_{24}(\varphi_{2P}); \dot{\varphi}_4 = \mu_{24} \cdot \dot{\varphi}_{2P}; \ddot{\varphi}_4 = v_{24} \dot{\varphi}_{2P}^2 + \mu_{24} \cdot \ddot{\varphi}_{2P} \quad (8)$$

$$\varphi_6 = f_{46}(\varphi_{4P}); \dot{\varphi}_6 = \mu_{46} \cdot \dot{\varphi}_{4P}; \ddot{\varphi}_6 = v_{46} \dot{\varphi}_{4P}^2 + \mu_{46} \cdot \ddot{\varphi}_{4P} \quad (9)$$

Clearances occurring in the kinematic pairs of the chains are replaced by angular differences of the elements 2 and 4 and they are incorporated into the model under following conditions:

$$\begin{aligned} |\varphi_{iP} - \varphi_i| &\leq \Phi_i \Rightarrow \varphi_{iP} - \varphi_i = 0 \\ \varphi_{iP} - \varphi_i &> \Phi_i \Rightarrow \varphi_{iP} - \varphi_i = \varphi_{iP} - \varphi_i - \Phi_i \\ \varphi_{iP} - \varphi_i &< -\Phi_i \Rightarrow \varphi_{iP} - \varphi_i = \varphi_{iP} - \varphi_i + \Phi_i \end{aligned} \quad (10)$$

where $i = 2, 4$.

We analysed the heald motion with help of equation of motion in the form

$$m_n \cdot a_n = F_O(t) - m_n \cdot g \quad (11)$$

where m_n – heald mass, a_n – heald acceleration, g – gravity acceleration, $F_O(t)$ – warp tension

In the calculation we consider clearance in heald eye (the warp thread is led through the heald eye). The design clearance between heald and heald rod is considered, too. The heald is running by free motion and

Table 1 Entrance parameters for calculation

Clearances			
heald shaft – ψ	1.8 mm	kinematic pairs link 2 – Φ_4	0.02 mm
heald eye – v_{eye}	5 mm	kinematic pairs link 4 – Φ_4	0.26 mm
heald mass – m_n	1.8 g	angular velocity of crank	62,87 rad.s ⁻¹

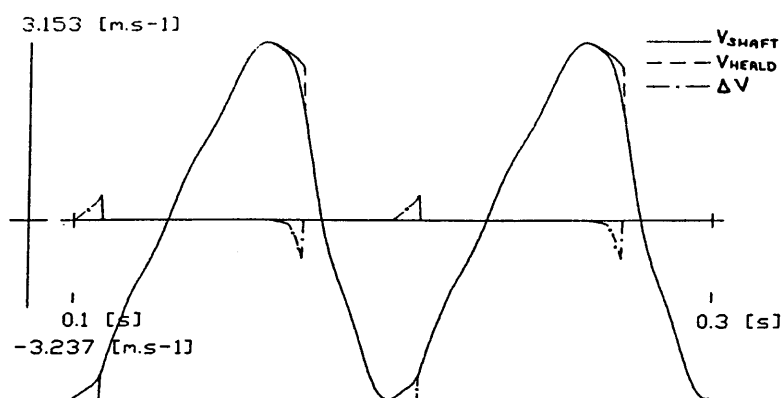


Fig. 3 Heald shaft and heald velocities

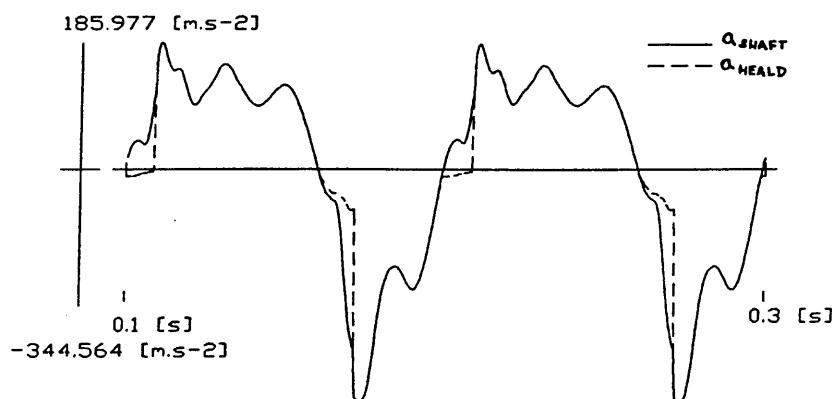


Fig. 4 Heald shaft and heald accelerations

when clearance is taken up, it is running with the heald shaft together.

The clearances of heald eye are incorporated into the model under the following conditions:

$$\begin{aligned} |x_{\text{heald}}| \leq v_{\text{eye}} &\Rightarrow x_{\text{warp}} = 0 \\ x_{\text{heald}} > v_{\text{eye}} &\Rightarrow x_{\text{warp}} = x_{\text{heald}} - v_{\text{eye}} \\ x_{\text{heald}} < -v_{\text{eye}} &\Rightarrow x_{\text{warp}} = x_{\text{heald}} + v_{\text{eye}} \end{aligned} \quad (12)$$

For calculation the dimensions and masses of shedding mechanism, heald shaft and healds are given as well as the dependence of the warp tension on the main shaft angle.

Equations were solved using Runge-Kutt method for input parameters of the given lifting mechanism with heald shaft. The position of the mechanism with zero acceleration of element 4 and zero deformation of all elastic elements were taken as the starting point during calculations. Coefficient of viscous damping were calculated from logarithmic decrements on the basis of measurements in the lifting mechanisms.

RESULTS

The problems were solved by means of a personal computer. The diagrams of kinematic values of different elements were evaluated giving importance to motion of heald shaft and heald.

For example we can show the diagram of velocities (Fig. 3) and diagrams of accelerations (Fig. 4) of heald shaft and healds and their difference. On Fig. 5 we can see diagrams of the heald shaft and heald displacement and their difference. There are also diagrams of warp thread tension in direction of heald shaft motion and reaction between heald shaft and heald. We calculated all diagrams for angular velocity $w = 62,87 \text{ s}^{-1}$. From this diagram we can get the period of contact and of free motion of heald. The period between 300 and 400 rpm represents the unstable motion of the calculated system. On the Fig. 6 we can see differences of velocities dependant on heald shaft clearances during one turn of the main shaft. When revolutions and clearances between healds and heald rod get higher,

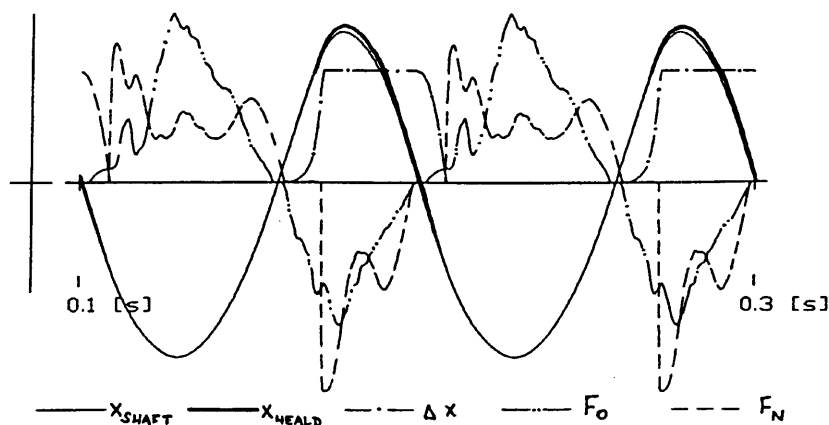


Fig. 5 Heald shaft and heald displacement, reaction and wrap forces

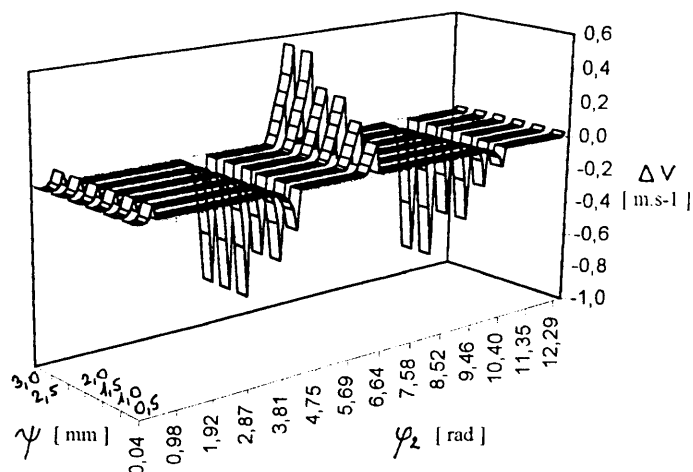


Fig. 6 Difference of heald shaft and heald velocities

Table 2 Heald velocities and acceleration dependent on n

n [min ⁻¹]	v_{HEALD} [m.s ⁻¹]		Δv [m.s ⁻¹]		a_{HEALD} [m.s ⁻²]		Δa [m.s ⁻²]	
200	-1.043	0.9994	-0.273	0.1898	-50.98	32.558	-27.96	27.39
300	-1.57	1.5012	-0.314	0.2605	-84.98	64.305	-17.08	34.76
400	-2.106	2.0356	-0.406	0.3201	-145.5	104.97	-49.54	58.61
500	-2.58	2.5685	-0.651	0.356	-245.4	154.63	-101.6	83.40
600	-3.23	3.17	-0.523	0.3714	-342.2	190.64	-152.7	101.5
700	-3.814	3.7868	-0.744	0.558	-485.4	303.37	-230.5	159.47

Table 3 Heald velocities and acceleration dependent on clearances heald and heald shaft

ψ [mm]	v_{HEALD} [m.s ⁻¹]		Δv_{HEALD} [m.s ⁻¹]		a_{HEALD} [m.s ⁻²]		Δa_{HEALD} [m.s ⁻²]	
0.5	-3.165	3.168	-0.219	0.1642	-305.61	190.69	-134.87	98.64
1	-3.196	3.168	-0.432	0.274	-323.37	190.96	-143.7	98.63
1.5	-3.220	3.168	-0.504	0.352	-336.11	190.69	-149.8	98.92
2	-3.238	3.168	-0.714	0.374	-347.41	190.69	-154.5	103.06
2.5	-3.255	3.168	-0.803	0.551	-356.758	195.57	-157.6	106.8
3	-3.267	3.168	-0.805	0.556	-362.302	199.34	-158.6	98.63

Table 4 Heald velocities and acceleration dependent on m_n and Φ_4

m_n [g]	v_{HEALD} [m.s ⁻¹]		a_{HEALD} [m.s ⁻²]		Φ_4 [mm]	v_{HEALD} [m.s ⁻¹]		a_{HEALD} [m.s ⁻²]	
1	-3.234	3.21	-324.99	197.65	0	-3.164	3.146	312.05	169.65
1.5	-3.234	3.19	-331.75	191.58	0.26	-3.23	3.152	-354.51	192.63
2	-3.23	3.152	-354.51	192.63	0.5	-3.28	3.177	-389.5	218.9
2.5	-3.217	3.117	-392.18	200.67	1.3	-3.35	3.235	-512.34	314.58

velocity and acceleration differences increase (Tab. 2 and 3) and so does even the healds and heald rod impact load. Higher clearance values in kinematic pairs of shedding mechanism increase significantly the acceleration peaks of the healds. The increase of acceleration is obvious from higher values of heald masses (Tab. 4).

REFERENCES

- [1] Mrázek, J.: Theoretical analysis of dynamics four-bar beat up mechanisms of a loom. In.: Mechanism and machine theory, Pergamon Press, 1992, USA
- [2] Mrázek, J.: Contribution to the dynamics of dobby mechanism of a loom. Proceedings Eight World Congress on the Theory of Machines and Mechanisms. Vol. 4, pp. 1053–1056, Prague, 1991, Czech Republic.

CONTRIBUTION TO HIGHER PRODUCTIVITY ON PICANOL'S NEW RAPIER MACHINE GAMMA

Speaker: F. Bamelis

Marketing Manager, PICANOL N.V., Belgium

Rapier weaving machines represent an impressive share of the worldmarket in weaving machines (fig. 1).

Picanol has conquered a comfortable place in the rapier machine market since almost 25 years. The development of the GTM rapier in 1981 did partially include the speed increases which people did expect for the next 15 years. When we today write the history of the GTM rapier, then there are different milestones alongside its lifespan. These marks are mainly based on speed or productivity increase (fig. 2).

In 1983 when the machine was introduced on the market, 360 RPM was a top speed for rapiers, it gradually increased to 450 RPM in 1989 and landed in 1994 at its ultimate speed of 520 RPM. To realize higher speeds with the existing machine was no more possible.

From different market investigations and customer contacts it was clear for us that another rapier machine was needed with some remarkable features:

- a higher speed potential
- a lower energy level
- easier and faster handlings
- greater flexibility in widths, colours
- pronounced versatility with regard to yarns and fabrics
- acceptable noise level
- faster style changes.

The GAMMA rapier machine (fig. 3)

Picanol's GAMMA machine is proving to be a technological breakthrough in the rapier world, breaking all

previous records and bringing the 600 RPM boundary within grasp. After one and a half years of operation all over the world and in most textile applications, the GAMMA has already earned itself a place in the rapier "Hall of Fame". Its rise has been meteoric:

- first delivery: September 1996
- first 1000 machines installed: September 1997
- total number of machines supplied to date: 2800 (June 98).

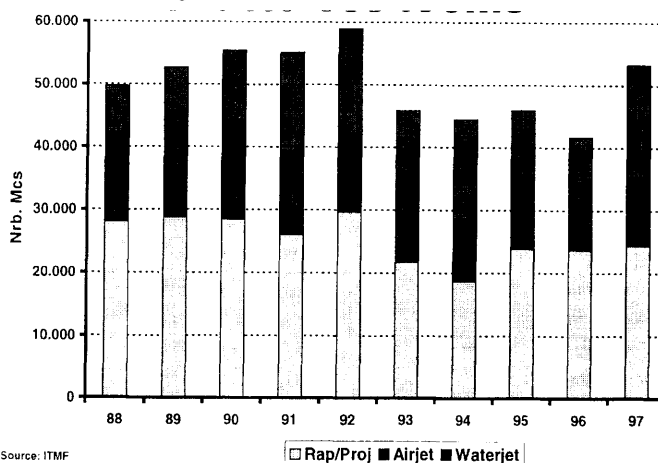
Most of the new rapiers are operating in Europe, followed by Asian countries and the Americas (fig. 4). The machines are installed with 85 customers, who use them to weave styles including fancy denim, shirting, awning, apparel, industrial fabrics, sheeting, ladies' outerwear, upholstery, etc. Significantly, over 15 orders are repeat orders, confirming the confidence of weavers in this new product.

Along with the growing number of applications, we have been able to implement our knowledge in handling new yarns or styles, which have been tested thoroughly in our research and test departments. This transfer of technology is one of the foundations of the GAMMA's success.

The decision to develop and build a new rapier machine, combining a high productivity without committing its flexibility, was a real challenge.

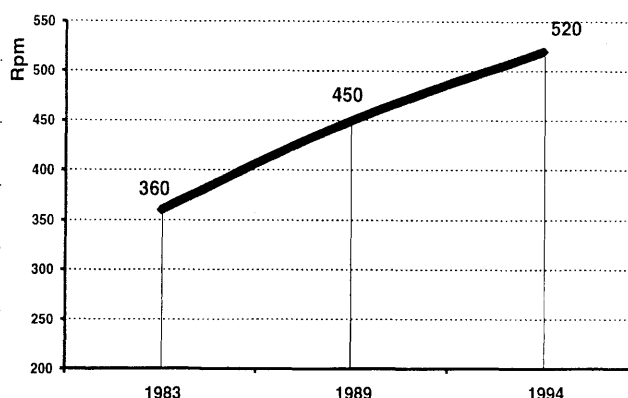
In order to achieve this challenge our engineers completely left the existing ideas and went for a new shed geometry, sley drive with a different law of motion and uncompromised rapier drive mechanism.

Fig. 1 Total Market Shuttless looms



Source: ITMF

Fig. 2 Speed Development Rapier GTM – 190 cm



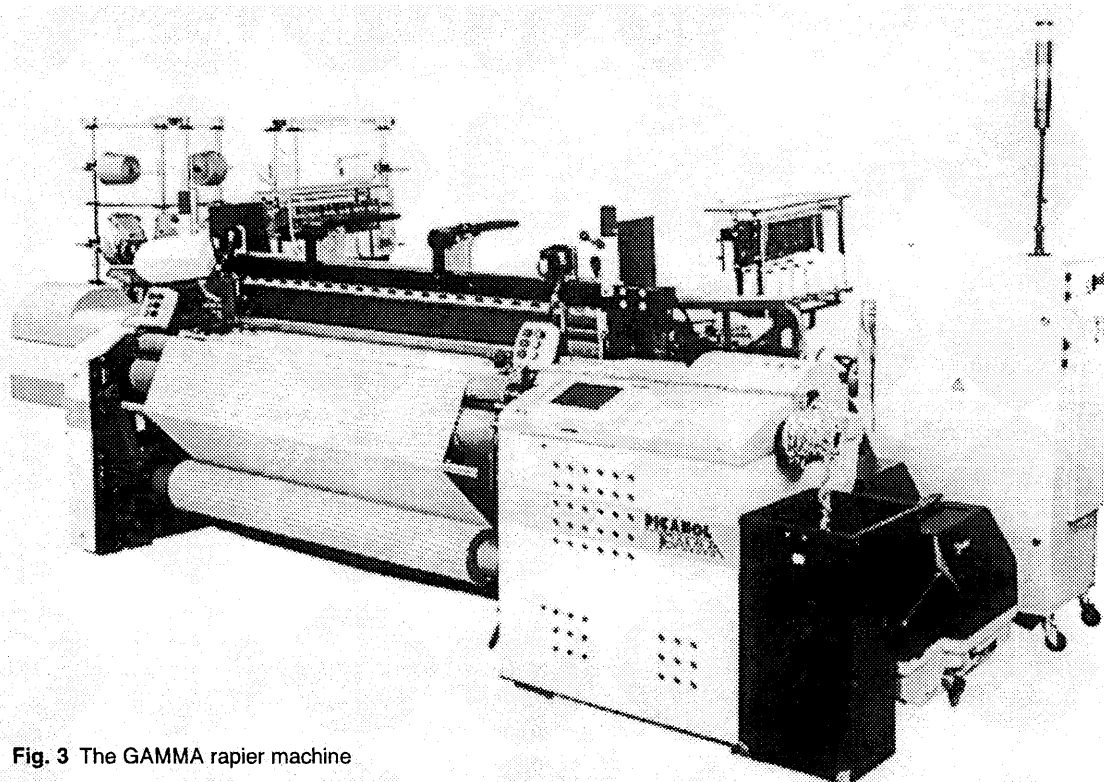
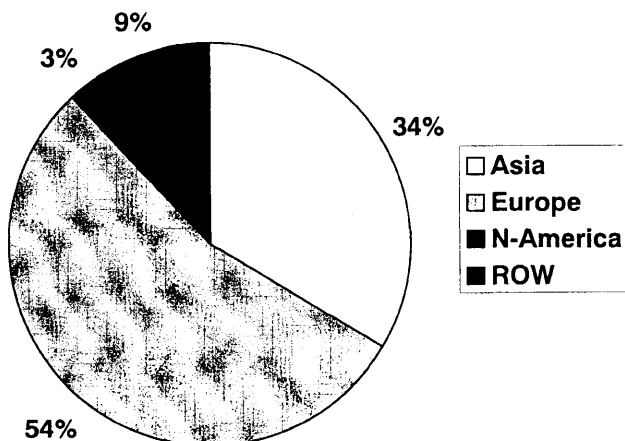


Fig. 3 The GAMMA rapier machine

Fig. 4 Gamma Rapiers Shipments



A completely balanced sley eliminates drastically machine vibrations which has its beneficial effect on the lifetime of machine parts and the stability in fabric quality.

Low vibrations mean reduced dynamic forces which on its turn put less requirements to the floor conditions.

Power consumption

Usually energy requirement increases with performance in an exponential way.

Thanks to the new driving train concept, the position of shedding motion and practically complete absence of outcoming shafts and the reduced weight of grippers

Higher speedpotential

The GAMMA is characterized by high performance level, operating at 600 RPM in 190 cm reedwidth. Compared with the previous generation of rapiers, the new machine reaches a 25% higher insertion rate (fig. 5).

This higher speedpotential is inherent with the machine design: larger bearings, new rapier tape drive, larger cams with cam followers for the sleydrive and a guaranteed continuous oil lubrication of all vital parts.

Also the machinedrive has been rebuilt and a unique drivetrain takes care of a quick and powerful start and a very short stop within one revolution of the sley (fig. 6).

Fig. 5 Comparison Speed Gamma/GTX

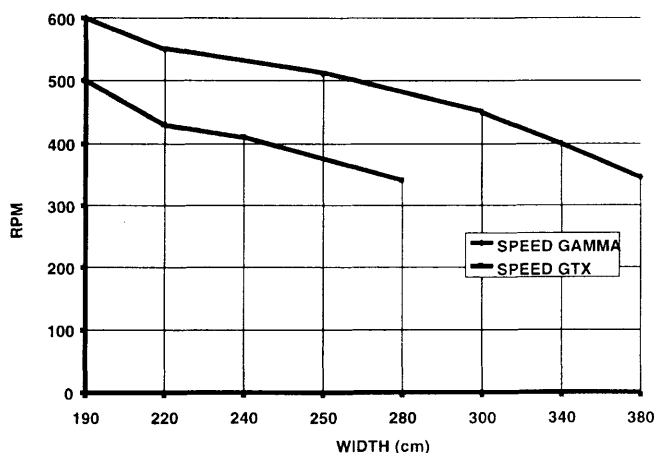
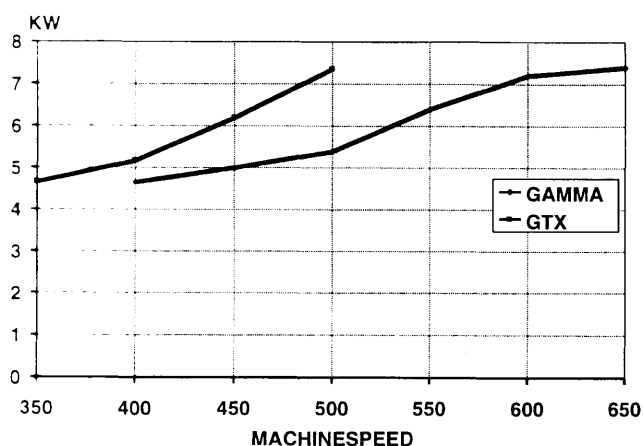


Fig. 7 Total Absorbed Power



and tape, our engineers were able to realize considerable energy savings (fig. 7).

Compared to the most of today's rapiers we may conclude that a 25% performance hike still requires less energy.

Noise level

Fig. 8

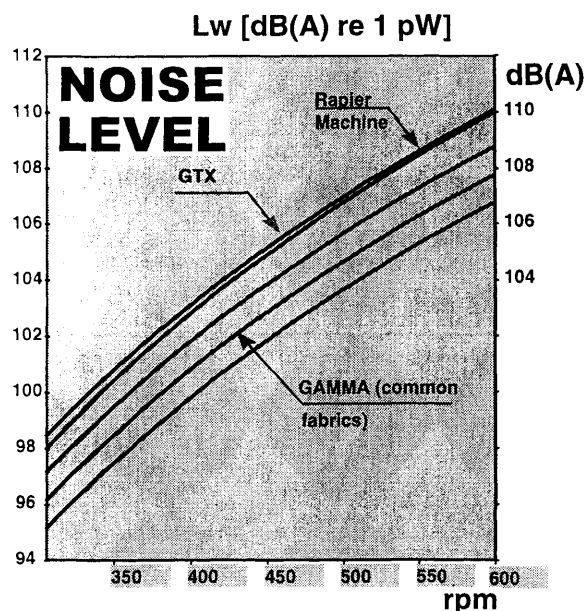
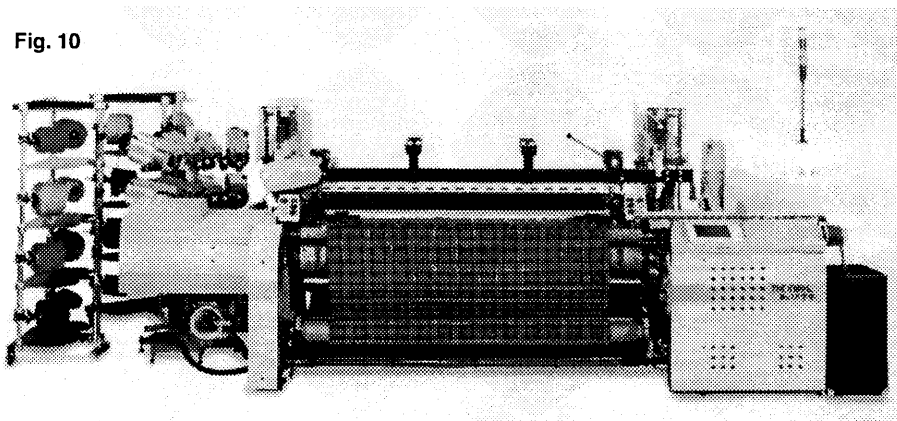


Fig. 10

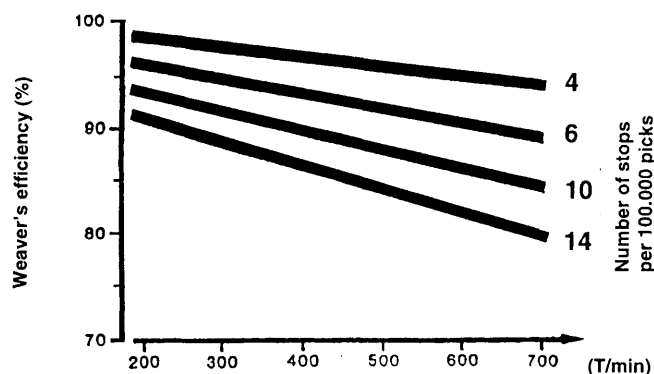


Filling insertion

Different steps were taken to reduce the yarn tension and consequently the stoplevel on the machine (fig. 10).

When we consider the filling insertion, the gentle filling yarn treatment starts at the position of the packages and the creel. Contrary to other rapier machines, the creel is not positioned on top of any heat

Fig. 9 Weaver's Efficiency Depending on Speed and Stop Frequency



We also would expect an upsurge in noise when speed is higher. Measurement of noise levels on GAMMA learned us that we can expect an appreciable lower level at the same speed, compared to our previous rapier and even compared to another machine, well introduced on the market (fig. 8).

Stoplevel

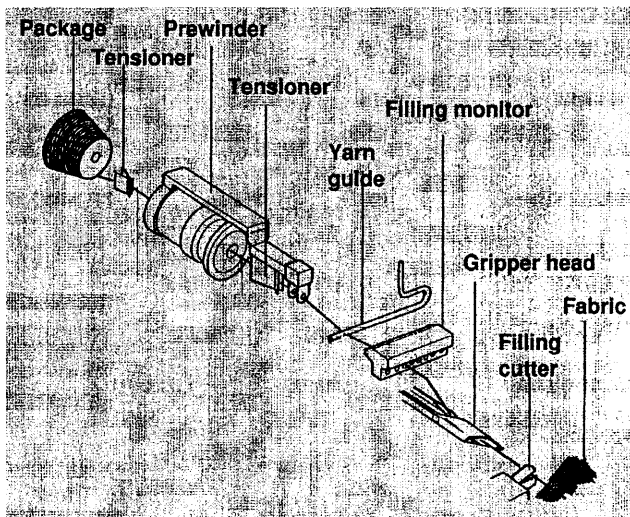
Productivity and efficiency of a machine is determined by its performance on one side and stoplevel on the other side (fig. 9). Stoplevels can be yarn related or linked to the machine stoppage. Yarn related stops can sometimes call for better yarn or preparation.

When we consider a weaving shed with 60 rapier machines producing between 21000 and 22000 m. per day, depending on the efficiency resp. 88 and 92%.

If operating at 88% there is an irrevocable loss of 942 m. per day, at a cost of 1 US\$ per m. of non-produced fabric (loss in sales, raw material cost) means US\$ 343.830 per year. This means that with this money yarn quality can be improved in spinning and or preparation, or better yarn can be purchased, or weaving conditions can be optimised.

On top of this loss is the cost of 1% efficiency loss equivalent to US\$ 1300 per machine and year (according to Prof. Dr. Egbers).

Fig. 11 Filling Tension Build-up



The initial filling yarn tension is very low and no additional friction is build up during insertion.

The automatic pickfinder moves only the harnesses into open shed position so that the weaver only has to remove the broken filling yarn and push the start button, which means time savings.

Programmable filling tensioners reduce peak tensions by as much as 50%, drastically reducing the risk of a pick breakage.

Warp let-off

The let-off motion is driven by a servomotor, the only type of motor that allows accurate tension settings and warp feeding. The warp tension sensor is built into the whip roll bracket, so as to exclude any distortion from additional play in bearings or connections (fig.13).

The initial warp tension is set on the microprocessor (fig.14), and the very accurate detection system enables it to be kept constant from full to empty beam.

Constant warp tension over the full clothwidth and for the complete beam is essential for a reduction in warp breakages which on its turn increases productivity.

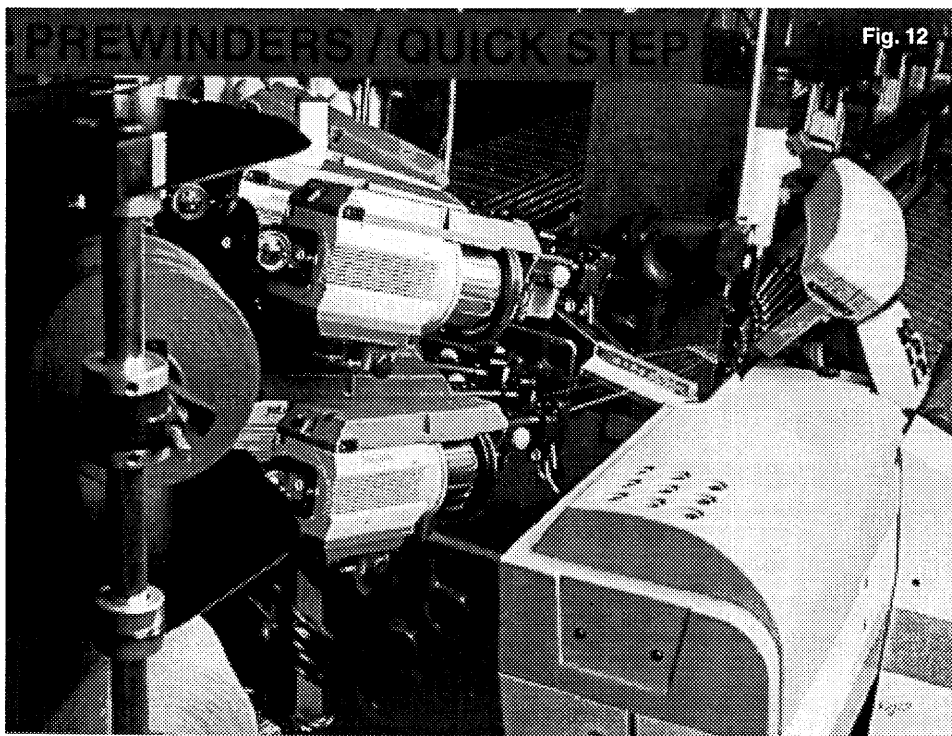
With increasing speed one can expect a slightly higher warp tension (fig.15).

Picanol successfully pioneered electronics on weaving machines, and its electronic communication between let-off and take-up is a major contribution towards the elimination of fabric marks.

Different programs are available for the weaver for correction of starting or stop marks (fig.16).

Factors influencing the performance of the warp in the weaving machine

The shed geometry in front of the reed is inherent in the machine construction, as designed by the machine builder. The weaver has to follow the proper setting instructions when setting the back shed and harness stroke, and when determining the warp tension. These settings have a very significant impact on the performance of the machine. It is therefore essential for them to be optimised. Sometimes the importance of setting

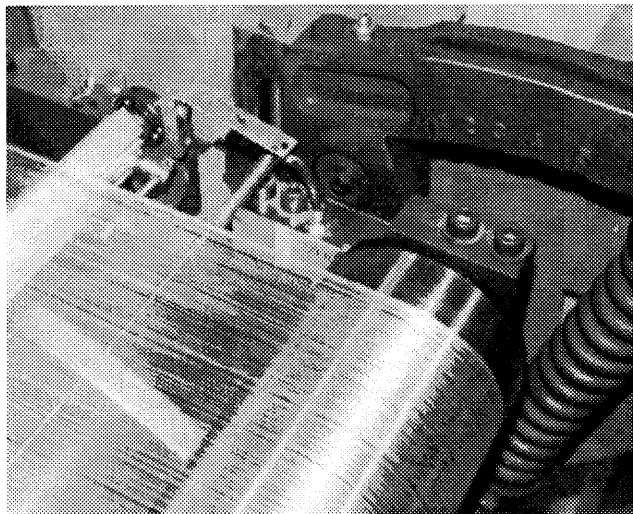


source such as drive motor or shedding motion; consequently, no changes are to be expected on the retained yarn humidity (fig. 11).

It is possible to equip prewinders with an automatic prewinder switch-off system (PSO) whereby at a filling breakage on the package or prewinder the machine continues to work on one instead of two prewinders. This system not only reduces the workload of the weaver but also nihilates possibilities of fabric marks and increases the efficiency.

The Quick Step filling presenter is controlled by a microprocessor. At a filling breakage, the presenter needle is positioned in an ideal position for rethreading, reducing also the intervention time (fig.12).

Fig. 13 Sensor Wrap Tension Roller



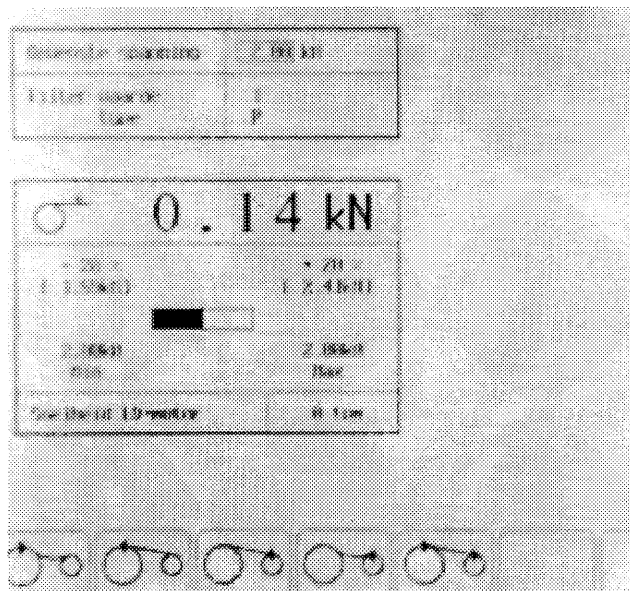
the warp stop motion is underestimated. However, its position has a direct influence on the backshed and thus on the yarn traction forces in the top and bottom sheds. The vertical position of the warp stop motion should therefore be set precisely since it may change the asymmetry of the shed (fig.17).

Setting of selvage and shed crossing

The GAMMA is equipped with a device known as Elsy – an electrically driven, electronically monitored leno selvage unit which is described as “unique on weaving looms” (fig.18).

The selvage motion crossing can be set on the microprocessor keyboard during weaving, independently of the shed crossing and with different timing on each side. The unit moves into the optimum rethreading position at the touch of a button.

Fig. 14 Wrap Tension μP



After rethreading, the machine is started and the Elsy unit automatically returns to its previous position. At style changes Elsy can be removed or repositioned very quickly.

Important settings such as selvage crossing time or shed crossing, which are normally done by the fixer under difficult conditions and which are time consuming, can be done by simply typing the required values into the microprocessor. The settings are very accurate and are easy to reproduce on other machines (fig.19).

Weaving of short runs – flexibility

Market pressure are forcing weaving mills to take on orders for even shorter production runs. These are inevitable linked with frequent warp or style changes which do require more operators and enhance a loss in efficiency. The worshipped “maximum machine speeds” are only a dream, as long as there is no definite solution for cutting longer machine downtimes.

The textile manufacturer who manages to switch from one article to another faster than its competitors has a real advantage over them. Shorter runs not only reduce the amount of capital tied up in production, but they also diminish the risk of piling up old stocks of raw materials or finished textiles.

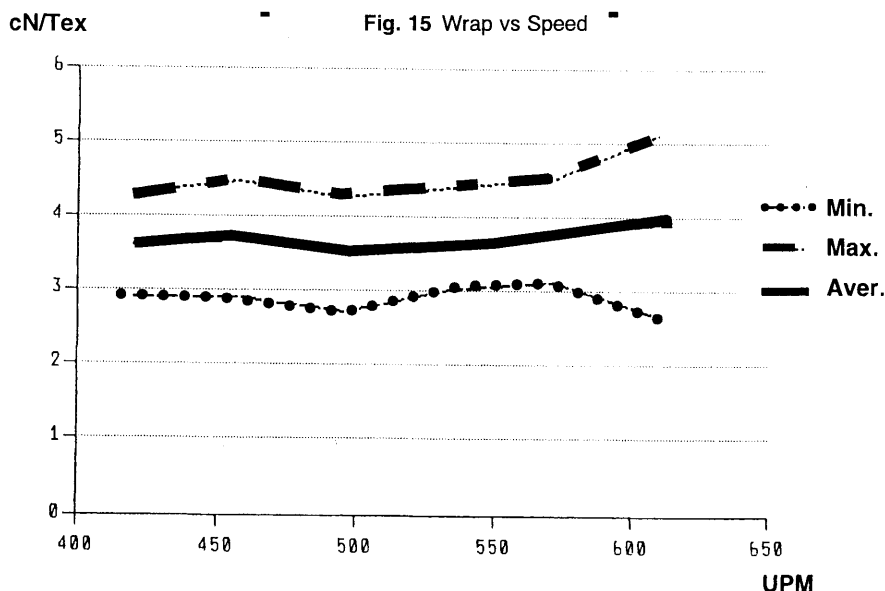


Fig. 16 Take up Corection (Tuco)

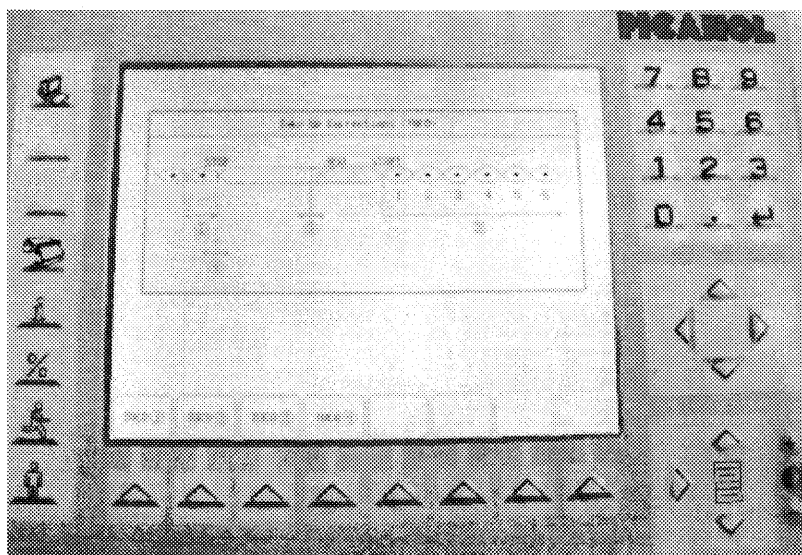


Fig. 17 Filling Yarn tension vs Position of Warpstopmotion

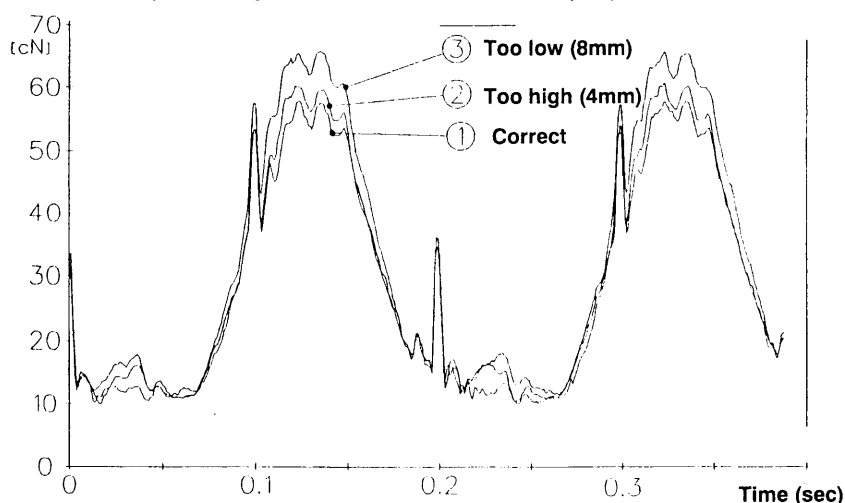
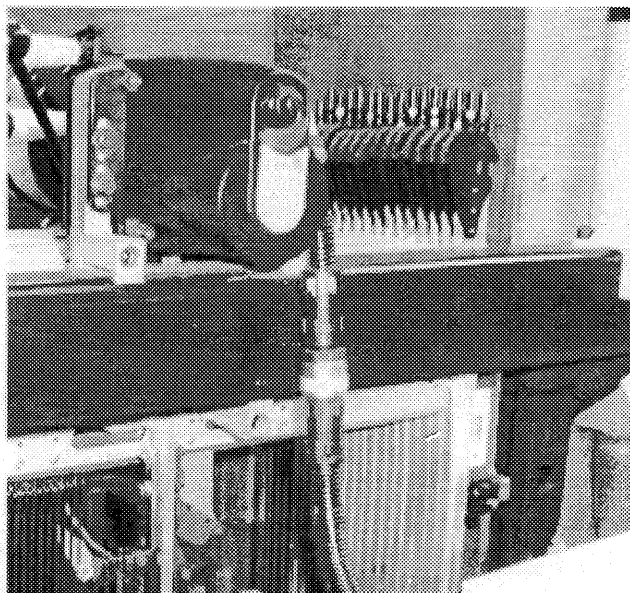


Fig. 18 ELSY



Quick style changes

In many weaving mills there is a significant loss in productivity of style changes and warp beams running out, even with warp beams of 110 cm (43") (fig. 20).

Picanol has made a considerable contribution to reducing machine downtime due to style or warp changes. All Picanol machines can be equipped with a genuine Quick Style Change system, in which the back part or style change module of the loom can be swapped very quickly (in less than 30 minutes) (fig. 21). The principle was introduced some five year ago, and Picanol is now the only manufacturer that can show references of over 3000 machines working with such a Quick Style Change system (fig. 22).

Thanks to the removable style change module, the machine is more accessible for the thorough cleaning required in denim plants. Furthermore, since the style preparation is carried out outside the weaverroom, the planning of all supporting activities can be managed more efficiently. The flexibility afforded by this system becomes a key advantage in terms of delivery time, with smaller stocks of preparation materials and finished products, as well as reduced order sizes (fig. 23).

Conclusion

Highest productivity is a primary objective when operating modern machines. Every machinestop is really cutting down efficiency drastically. In-depth research at Picanol and application of new technologies at different levels helped to reduce machine downtime of the latest GAMMA rapier machine.

Fig. 22

O.S.C.

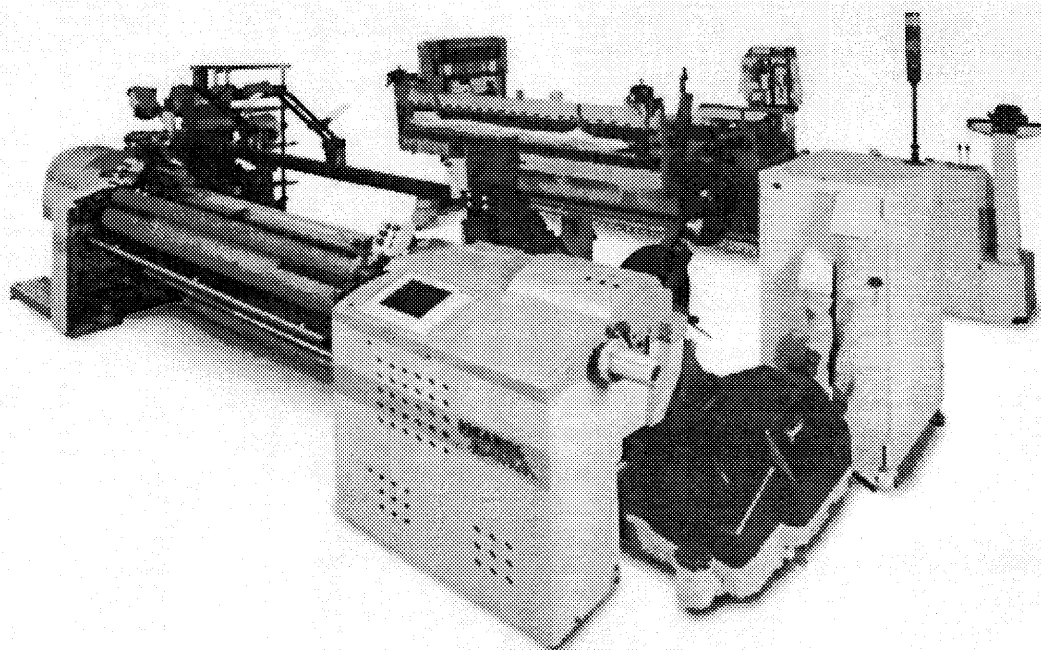


Fig. 23



Theoretical aspects of back rest roller rotation on weaving machines

Dr. ir. L. Vangheluwe and ir. D. Dewaele

*Department of Textiles (Universiteit Gent),
Technologiepark 9, 9052 Zwijnaarde, Belgium
email: Lieven.Vangheluwe@rug.ac.be*

The direction of rotation of back rest rollers can be important for weaving some type of fabrics. The paper considers a theoretical model with which the direction of rotation can be calculated. A model is used that describes the motion of the roller due to the friction exerted by the warp yarns on the surface of the back rest roller. The differential equation obtained in this way is solved with the Runge-Kutta method for numerical integration. The model is used here for a parameter study towards the effect of parameters influencing the rotational speed and direction of the back rest roller.

INTRODUCTION

The back rest plays an important role in weaving. The warp yarns are bent over the roller(s) of the back rest. The back rest roller is used to compensate tension fluctuations due to shedding and beat-up operations in weaving. Active (by means of a cam type mechanism) or passive tension compensation (the back rest is mounted on an elastic medium) are being used. Figure 1 shows an overview of a weaving machine.

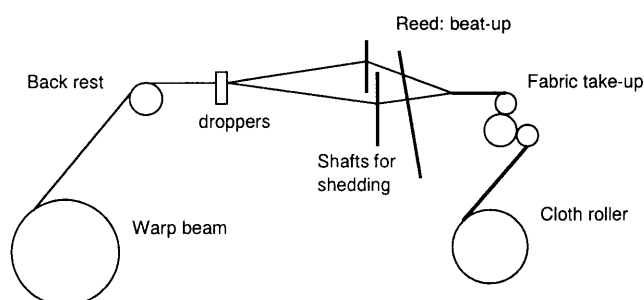


Fig. 1. Overview of a weaving machine

The warp yarn moves over the back rest towards the fabric forming zone. If the back rest roller is not clamped, it rotates. The movement of the yarn over the back rest roller can be with or without slippage over the roller. The motion of the yarns relative to the rollers will depend on a number of parameters. Normally, the roller should rotate in the production direction. In some cases however, it has been observed that the roller rotates in inverse direction. A possible solution is to put a clamp on the roller so that it cannot rotate or to clamp it partially so that the direction and speed of rotation are modified.

It is considered beneficial for high quality weaving if the roller rotates in the correct direction and if slippage between warp yarns and the surface of the roller is

minimised. Weaving practice and the simulations described in the paper show that the direction of rotation of the roller is not always correct.

The problem of back rest roller rotation is not well understood. Only some papers dealing with the problem have been published [1, 2, 3].

Model for back rest roller rotation

The warp yarns undergo dynamic tensions during the weaving process. As the yarns are bent over the back rest, friction will be present resulting in difference in forces in front of and behind the back rest. Furthermore, the frictional force imposes a moment around the axis of the back rest roller. As a consequent of this moment, the back rest roller will rotate against opposing moments originating from friction in the bearings of the back rest roller and the inertia of the roller itself. Figure 2 shows the situation of the back rest roller with respect to its rotation.

The law of motion of the rotation of the back rest motion can be described by a second order differential equation given in formula 1.

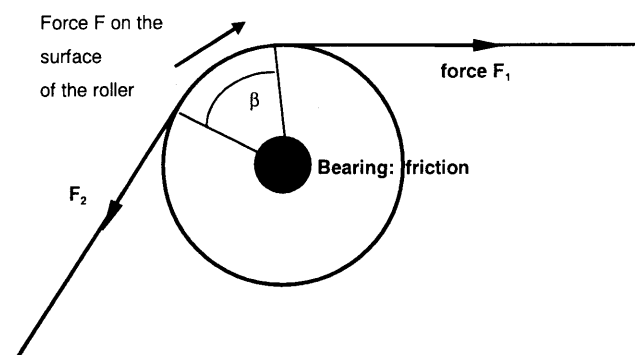


Fig. 2. Back rest roller: forces and rotation

$$I\ddot{\alpha} = M(\alpha, \dot{\alpha}) + nRF \quad (1)$$

I : moment of inertia of the back rest roller for a rotation around its axis, α : angle of rotation of the back rest roller around its axis, M : moment of the forces on the back rest roller (except those from the warp yarns), R : diameter of the roller, n : number of warp yarns, F : force exerted by one warp yarn on the surface of the back rest roller

All parameters and values occurring in the formula must be calculated now for the specific conditions of weaving. The moment of inertia of the back rest roller can be calculated from the geometry and mass of the back rest roller. The moment M comprises frictional restraining forces which basically exist of the friction in the bearings. Appropriate formulas for this aspect have been included in the model for the roller bearings used in the back rest support [4].

The moment exerted by the warp tension (nRF) is more complicated because of the different situations that can occur. The force F is the frictional force between one warp yarn and the roller. Different situations exist:

- due to the dynamic nature of the warp tension, the frictional force will also be dynamic and its direction will also change due to the cyclic tension differences during weaving
- two situations exist concerning the speed of the yarn relative to the surface of the back rest roller. The first situation is that no slippage exists between yarn and roller. The relative speed is zero then. If slippage occurs, the warp yarn slides over the back rest roller. The force exerted on the roller surface still is the friction force. However the relative speed of the yarn must be taken into account for the calculation of the extension of the yarn leading to values for the yarn tension. For the frictional force, the capstan friction law is used.

Table 1 gives an overview of the four possible situations.

Tab. 1. Different conditions concerning frictional force on the roller

	no slippage	slippage
$F_1 > F_2$	$F = F_1 - F_2$	$F = F_2 * (e^{\mu\beta} - 1)$
$F_2 > F_1$	$F = F_1 - F_2$	$F = F_1 * (1 - e^{\mu\beta})$

Yarn tension is calculated accounting for the following dynamic loom operations: warp delivery, cloth take-up, shedding and beating. In the calculation of the tension values in front of and behind the back rest the motion of the warp yarns over the back rest is also taken into account. The value for the relative speed of the yarn to the roller is needed for this if slippage occurs between the warp yarns and the back rest

roller. This is obtained via solving Newton's law for the relative movement of the yarn (see equation 2).

$$m a = F_1 - F_2 - F \quad (2)$$

m : mass of the yarn; a : acceleration of the yarn for the motion relative to the back rest surface; forces F_1 and F_2 as explained in figure 2; F : frictional force of a warp yarn on the roller

If no slippage occurs, the right hand side of equation 2 is zero so that the relative speed between warp yarn and back rest roller surface is zero.

The complete model describing the rotation of the roller as described here can be solved using a Runge-Kutta method for numerical integration [4]. The Runge-Kutta methods give fast and reliable algorithms for numerical integration. The model was programmed in standard C language and implemented on a personal computer. Numerical simulations start from stand still of the loom and are continued until the loom reaches steady state weaving conditions.

RESULTS AND DISCUSSION

Example

A typical example of the curve showing the rotation of the roller during weaving is given in figure 3. From the figure, it is clear that it takes a number of revolutions before the steady state operation is reached. By convention, a rotation in the production direction is represented by an increasing angle. In this example (figure 3), the roller has a resulting forward movement and superimposed is a dynamic movement caused by the dynamic nature of the warp tension. Figure 4 show that a resulting backward rotation is also possible. Some situations have even been observed in which, after start-up phenomena, the mean angle was constant for increasing numbers of loom cycles.

The following differences can be observed between different parameter selections for the model:

- direction of rotation and net change of the angle of rotation per loom cycle

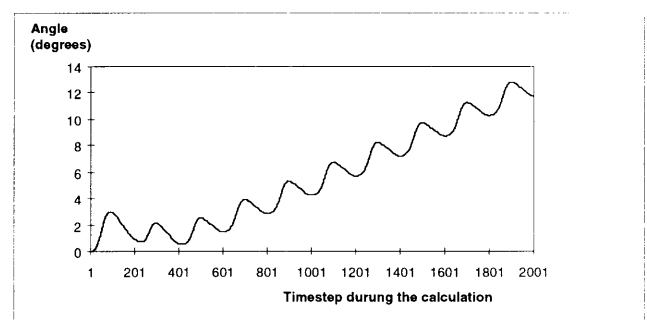


Fig. 3. Example of the calculation of the angle of rotation of the back rest roller: forward rotation

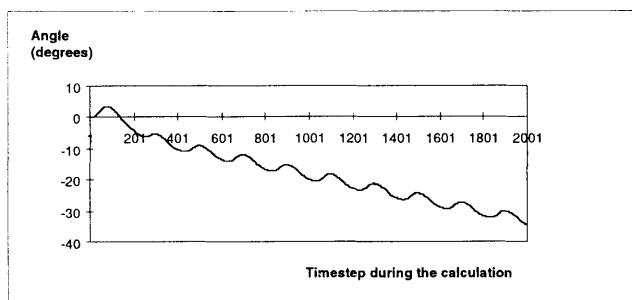


Fig. 4. Example of the calculation of the angle of rotation of the back rest roller: backward rotation

- the dynamic part of the rotational angle (change within a loom cycle)
- the number of loom cycles it takes to attain the steady state situation

In the paper, the first topic will be highlighted. The third characteristic (number of cycles before steady state) is expected to influence the occurrence of set marks as different situations of warp yarn supply over the back rest to the fabric forming zone exist and the warp tension is also affected.

Parameter study

The influence of a selected number of parameters in the model for the angle of rotation of the back rest roller will be studied now.

Loom speed

Figure 5 reflects the influence of the loom speed on the rotation of the back rest roller during weaving. It can be seen that the loom speed has an important effect on the rotation. This can be understood as the model is a second order differential equation. It should be mentioned that the model is more complex than a simple second order differential equation because of the possible occurrence of slippage of the yarn on the back rest roller, slippage which can occur in one or both directions of motion.

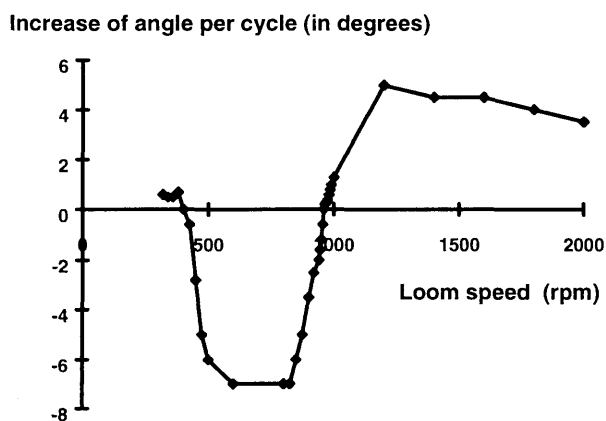


Fig. 5. Effect of the loom speed on the rotation of the back rest

Moment of inertia of the back rest roller

The importance of the moment of inertia of the roller can already be assumed from the differential equation describing the model and is confirmed by the numerical simulations. The higher the moment of inertia of the back rest roller, the longer it takes before the steady state situation is reached. A high moment of inertia does not allow the back rest to follow the tension applied, a large amount of slippage occurs. At lower inertia values, the back rest attains the steady state situation much faster and less or no slippage occurs. For lower values, the tension cycle (shedding and beat-up) can be distinguished in the rotation angle curve, which is not the case for high moments of inertia.

Mean warp tension

The mean warp tension is the average force in a warp end during weaving. Superimposed on this mean force is the dynamic force due to shedding and beat-up. It can be seen from figure 6 that the mean force affects the rotation of the roller in a clear way.

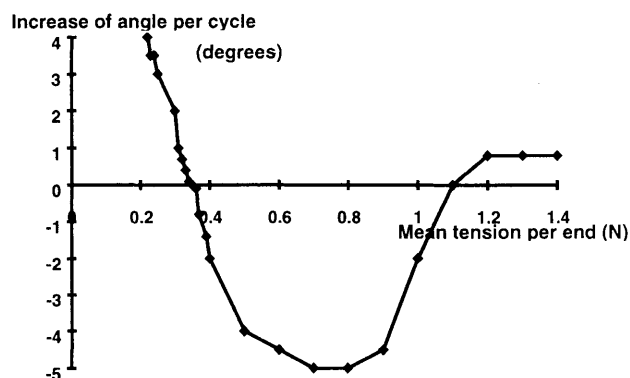


Fig. 6. Effect of mean warp tension on the rotation of the back rest roller

Warp tension amplitude

The effect of the amplitude of the warp tension has also been studied. Results of the calculation showed that an increase in amplitude of the tension due to shedding resulted in an increase of the angle of rotation. At low dynamic tension amplitude values, the direction of rotation was inverse, which changed at somewhat higher values of the tension amplitude.

Coefficient of friction

The coefficient of friction between the warp yarn and the back rest roller is also expected to influence the rotation of the back rest roller as the coefficient of friction will influence the relative values of the warp tension in front of and behind the back rest roller and hence also the frictional force on the roller. As the value of the coefficient will also influence the occurrence of slippage, the situation is expected to be rather complex. Figure 7 shows that the effect of the

coefficient of friction is rather low. The coefficient of friction is even of less importance for the problem studied here than the parameters cited before.

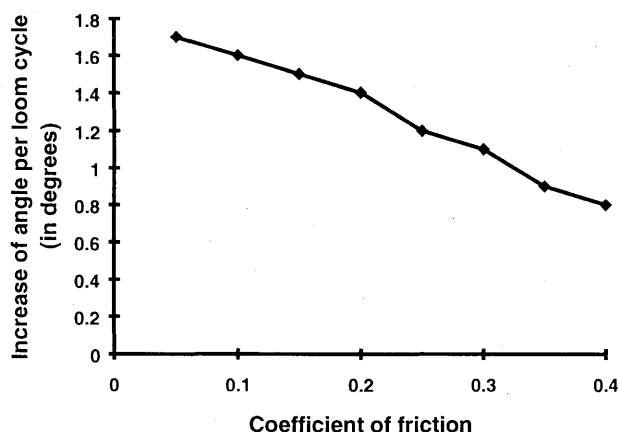


Fig. 7. Effect of the coefficient of friction between warp yarns and roller surface

Another friction effect important for the rotation of the back rest is the friction in the bearings. From simulations performed, it could be seen that a difference in increase of angle per loom cycle of about 1.5 degrees exists between a bearing almost free of friction and one with high friction (e.g. a worn bearing or a soiled one). The effect is such that at higher friction levels in the bearings, the angle of rotation is reduced.

Clamp on the roller

In order to change the characteristics of the rotation of the roller, a clamp can be put on the roller. The

clamp can be set so that no rotation of the roller is possible or via a clamp force to be specified so that the rotation becomes restricted via frictional forces on the roller. The action is the same as an increase of the friction in the bearings but is more severe. Simulations with different clamping forces showed that the angle of rotation was reduced at increasing values of the clamping force. It should be mentioned that in the starting situation without clamp the rotation of the back rest was already in the correct direction.

CONCLUSIONS

The paper describes a theoretical model to investigate the speed and direction of motion of the back rest roller in weaving. The differential equation obtained can be solved via numerical integration. The Runge-Kutta method is used to this end. The model implemented in a C programme allowed to study the influence of parameters on the rotation of the back rest roller theoretically. Results of the simulations indicate the complex influences existing in the problem studied.

REFERENCES

1. Masajtis, J., Dynamic disturbances of warp tension in weaving and behaviour of the let-off motion on the loom, Monograph, to be published
2. Nosek, S., Peculiar Behaviour of the Loom's Back Rest Roller, *Fibres & Textiles in East. Eur.* 5 (4), 87-91 (1997)
3. Hanzl, J., Measuring of the Behaviour of the Back-Rest on the Air-Loom PN-170, *Fibres & Textiles in East. Eur.* 5 (4), 92-94 (1997)
4. Dewaele, D., Mathematical simulation of back rest motion (in Dutch), thesis, Universiteit Gent (1998)

Multifunctional system for controlling and analysis of processes and images in weaving

Dr. Eng. Georgi Popov¹ and Eng. Econ. Gosho Petrov²

¹Technical University, Sofia

²AD Sunitex, Mezdra

INTRODUCTION

A measuring system for controlling weaving processes is supposed to be easy transported to different plants, workshops and labs.

Until recently used measuring system had a big and heavy PC and monitor which was causing problems when moving to various places. On the other hand the fast improvement of Notebooks has made them just right for that purpose. So we have decided to replace our PC with a Notebook. We chose LEO Notebook for its good characteristics and competitive price. It has Pentium processor and all the range of input / output ports including PCMCIA. Choosing a Notebook we had to change DACard, for it was not compatible with it. So after a long research we chose a card made by National Instruments – USA. Due to its fast delivery, high performance and sophisticated software we managed to install the card fast and to put the system into usage.

For that purpose two new and improved transducers have been elaborated. The analogue amplifier, power supplier of the transducers, have been improved too. Its higher filtration frequency was increased, so that high speed processes were able to be registered. Such processes are the peak loading of the yarn when beat-up. After all this has been done, we have decided to use the new DAC capabilities and installed a digital video camera. First we chose a small Internet conference camera which has good characteristics and low price.

We intend to include other transducers too, in order to control the temperature and moisture and to install digital breakers for distinguishing the cycles and for a simultaneous data processing of a couple of sources.

General scheme of the measuring system and module description

Measuring systems structure includes the following elements (Fig. 1):

Transducers (strain gauge installed on a small beam, breakers for synchronizing the signals in time); Improved analogue amplifier for the transducers measuring the yarn stretching; Video camera for displaying images; DACard for data gathering and

transformation of the analogue signals in digital; Notebook with a relevant periphery.

Transducers

Two new transducers have been elaborated.

The first one is for measuring the tensions in a group of yarns – 60 to 100 yarns are measured out of the average 200 threads per dm. This guarantees a good representation of the results. [1]

The second one is for measuring the tension of a single yarn or a couple of yarns from one and the same heald shaft which have the same law of motion. A concept for a construction measuring the stretching of a group of yarns has been used in it. At the same time the transducer is lighter and able to work in accordance to the necessary high speed. A novelty is that it is no longer necessary to hold manually the measuring head which causes additional measuring errors.

The transducers are freely placed over the warp yarns in the zone, between the back rest and drop wire. The small weight of the transducers and the small resistance they exercise over the yarn movement, (secured by the precise bearing locations of the three deviation beams), on one side, and the high sensitive sensors we used, on the other side, allowed us to obtain the necessary representation of the real dynamic tensions in the yarns.

One of the two newly elaborated transducers are shown on Fig. 2. They are high-sensitive semi conductor sensors, which are glued to the beam made by a hardened spring steel. After being applied the high quality glue has been baked at a certain temperature. That guarantees the sensor's long life and prevents from creepage in the glue zone, which could bring to discrepancy in the calculations. Using sensors with higher sensitivity has allowed us to make the beams thicker and this has brought to increasing their natural frequency. By a calculation method the beams were designed for a natural frequency of over 600 Hz. This could make it possible to use them for measuring in the modern high rotation speed weaving machines. Experimental verifications of their characteristics, made by excitation of different frequencies have confirmed

this results. Even more, higher natural frequencies were reached as a result of reserves in the measurements used by us.

A novelty in the transducers is the module design concept, which allows easy replacing of some of details, later on when they have to be improved. The basic part in that case is the beam with the sensors glued on it. The three pins and the six bushes on them are installed on the beam with screws. They could rotate around their pins, but the middle pin is locked, so that some errors due to a deviation from the cylindrical form of bushes could be eliminated. Such deviations appear on some of the bushes, especially on the non metal ones like ceramic or glass made.

Amplifier

We use a Hungarian made ELTENS FY – 23 amplifier from our previous system, due to its good characteristics. It has an input for the transducers, situated in a Whetstone bridge, also has a wide range of adjustments, good sensitivity and amplification. The amplifier is independently power supplied by batteries and has an output to the record unit which we use for connection with the computer. We have rebuilt the amplifier filters for different frequency and have increased its higher frequency limit from 100 Hz up to 1000 Hz, when at the same time we kept the stage restriction capabilities for lower frequencies. That leads to improving the work of the analogue-to-digital converter in the general conversion of the yarn tension curve when weave machine is working.

Data acquisition card (DACard)

When a Notebook is used, due to its different slots arrangement, it is not possible to use an DAC installed on circuits for insertion in desk top PC's. There are output devices meant to be switched to some of the inputs, like for example the parallel one. These devices however are not very compact and are also not too fast. We chose a PCMCIA input, as it is specially adopted for portable PC's and has no speed limitation according to the computer it is working with.

Some of the main characteristics are:

DACard 516:

50 KHz Multifunctional PCMCIA Card, 16-Bit converter, 8 single ended and 4 differential inputs, 8 digitale I/O, 2 Counter/timer

Notebook

Processor Intel Pentium 133 MHz, On board memory 24 MB, Hard Drive 1.4 GB, Diskette drive 3.5 inch, 1.44 MB, PCMCIA socket Type III, Interfaces- serial

port, parallel port, IR port ect, Power system rechargeable battery, AC adapter.

Video camera

The video camera is small desktop camera, adapted for notebook. The camera is equipped with a variable focus lens that can be adjusted from a distance of 0 cm to infinity. It has 512 × 582 active pixels (H × V). Lens mount integrated, 3.8 mm F2.0, Horizontal resolution (TVL) 330 and minimal illumination <10 lux.

Short theoretical description of the signal processing

A high quality measuring system requires that all of its configuration units are compatible in quality. The heavy – current measuring systems have two main parameters: short response time and a small measuring error. These two characteristics have to be on an adequate level with each and everyone of the configuration units. Starting with the transducers, amplifier, through DAC, input ports, the computer itself and its software.

The yarn dynamic tension in the up to date high speed weaving machines is a very fast changing parameter. For example in a middle speed weaving machine, working with 300 rpm, the duration of a cycle creation in the material is around 0,2 sec. If we accept that the beat up has normal measurements and the beat up duration is not higher than 20 degrees per revolution including the back and forth moving of the reed, than the yarn beat-up time is 0,01 sec. (equal to 100 Hz). In order such a curve to be properly described, we need to have a sufficient number of measuring points. This process could be described in detail as follows:

The Nyquist sampling theorem [2] tells us, that we must sample at more than twice the rate of the maximum frequency component we want to detect-the beat-up. Sampling rate – this means how often conversions can take place. So we need a system with a sampling rate greater than 200 S/s (200 Hz).

Further rising up doesn't lead to improvement of the average results.

The natural frequency of the transducer beam has to be 5–10 times higher than the highest frequency of the studied process.[3] Therefore with 300 revolution/min it has to be no smaller than 500 Hz. According to Shlichter, if we like to record every peak in the tension for every 1 degree from the main shaft in 700 revolution/min, is 4000 Hz. This frequency could be made lower – to 1000 Hz. The situation is similar in the measuring of processes that are not periodical or in processes caused by accidental factories, as well as in the separate measuring – the signal sampling rate has

to be heightened several times on account of wished precision.

Excitation frequency of the amplifier influences on the the limit working frequency also. In the most cases it is 5–10 times higher than working frequency. The excitation frequency used by our amplifier for the moment is 4800 Hz. Therefore this condition has been accomplished also. Other characteristics in the process of converting of analogical signals to digital ones are Resolution, Relative Accuracy, Noise and etc. They, according to the characteristic of DACard 516, are in a high level for this type load measuring. This conclusions show that the new measuring system will be suitable for using in future for more high speed weaving machines.

Software

Usually DAQ applications use driver software. Its purpose is to program the DAQ hardware. In this manner driver software hides the low level complicated details of hardware programming. We have chosen NI-DAQ driver software written in full 32-bit code for Windows 95. This driver provides acquisition rates up to 1 Ms/s that is more than our requirement for the measurements of yarn load.

Having in mind our experience with Excel and the good program's statistical functions and design, we used it in new version also. So an additional software has been elaborated for connection of a NI-DAQ driver to Excel. It is possible to use other programs like LabView, Visual Basic also.

The measuring system in practice

One of the main aims of this paper for us is to show the improvements of the measuring system, which has been done. The following two illustrations show part of our achievements in the field of measuring of dynamical tension loads in yarns and registering of yarn's images.

Fig. 3 shows tables, used by Excel, one of the functions for statistical treatment of the measured and

converted signals and a graphic. Here is shown the tension of group of 50 neighboring yarns for plane weave. Well vied is the difference in the top and bottom shed because of its non symmetricality. The used loom is Nuovo Pignone – TP 500. Now we work on the establishment of On-line graphic introduction and statistical treatment. The new appearing versions of program Excel give us additional possibilities for treatment of data registering.

Fig. 4 shows the image of yarns, made by the small video camera and a microscope with polarization. Here we have several images of broken cotton yarns 28 tex, used for investigation of the reasons of the breaks. Yarn's ends are collected from the regular production of "Sunitex" – Mezdra. The good image gives us a hope for the further successful usage of the camera in the observing of the placement of the yarns in fabric and the appearing yarn deformations, and for other purposes also.

CONCLUSIONS

1. The used principle for the establishment of the virtual measuring instrument by modules is suitable for further improvements.
2. The small size of the system, based on Notebook, make itself to be more accessible for work and different purposes- Measuring of dynamical tension loads registering, analyses of images etc.
3. With the high speed working transducers, DACard, Amplificator, Notebook and Software we are able to make more precise results and more easy and quick treatment and analysis.

LITERATURE

1. S. Schlichter. Problems of warp yarn tensile strength measurement in weaving. *Melliand Textilberichte* 68 (1987), 181–184.
2. National Instruments. Catalog 1997, 3–14.
3. R. Makarov and col. *Tensometria v machinostroinii. Spravotchnoe posobie*. Moscow, Machinostroenie, 1975.

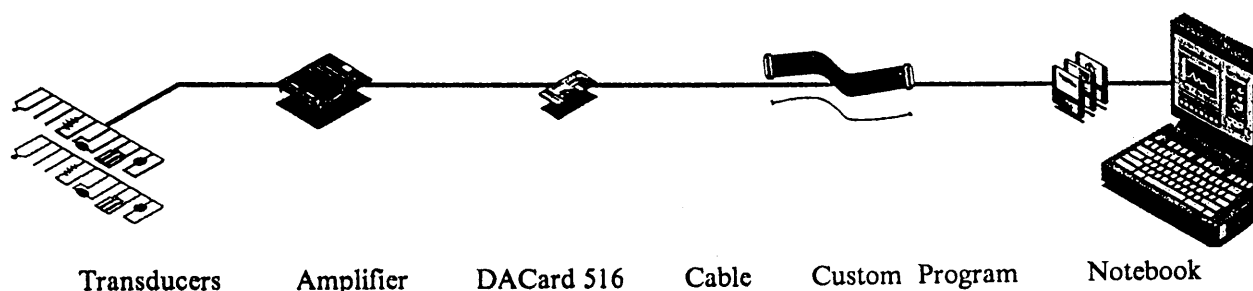


Fig. 1. Portable Measurement System

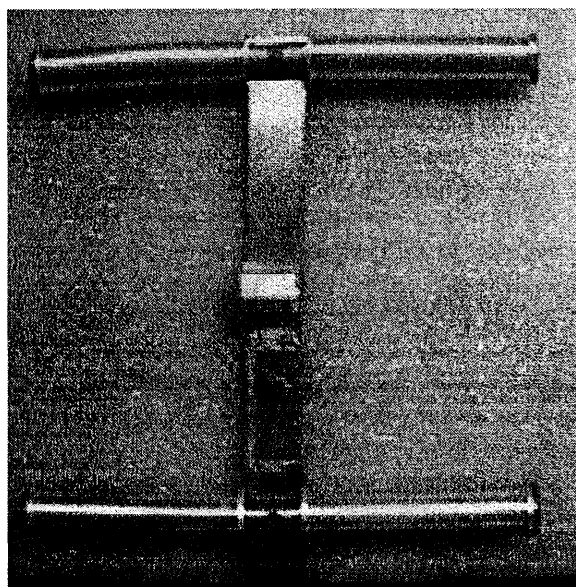


Fig. 2. Transducer for measuring the load of yarns.

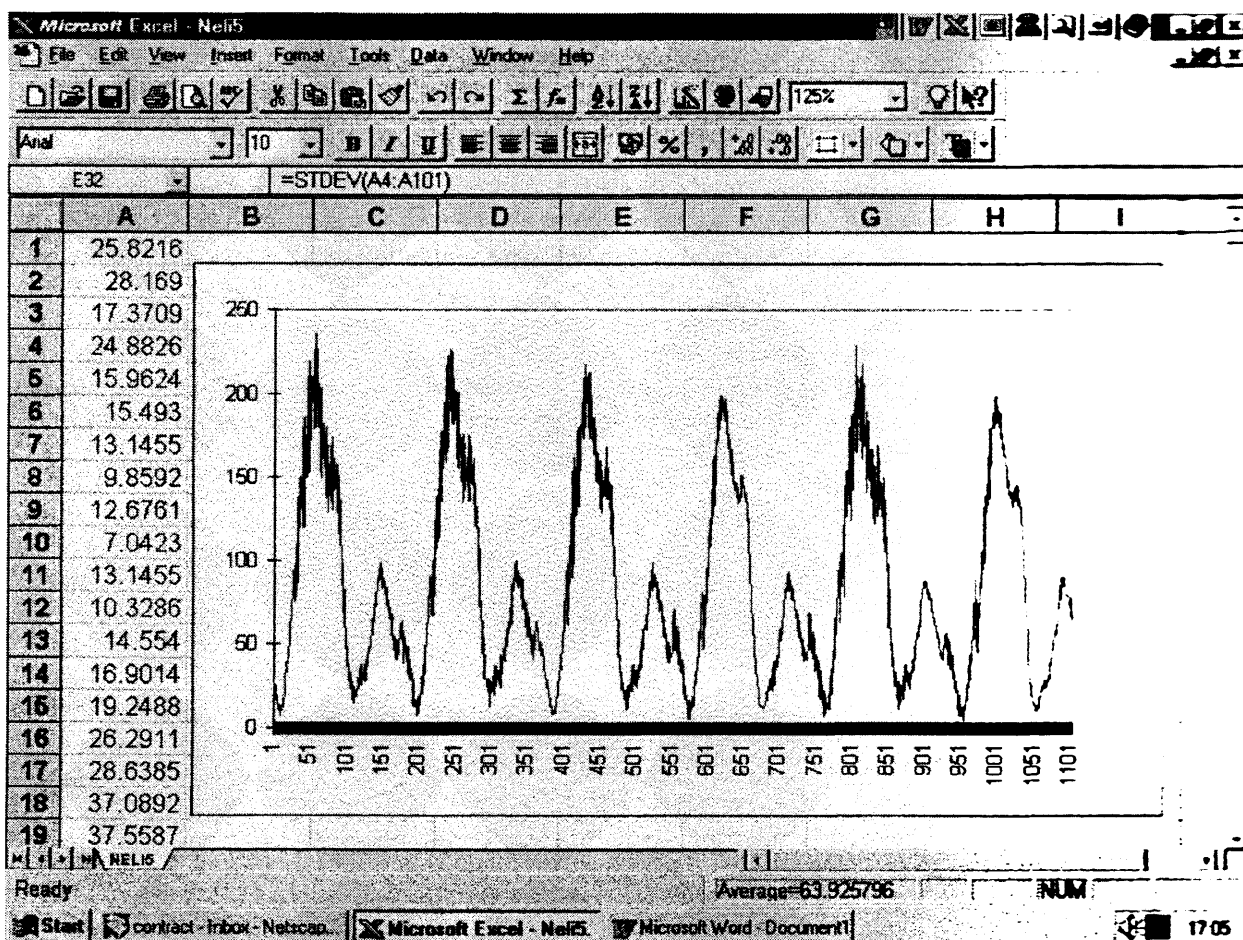


Fig. 3. Datas and graphics of yarns load treated by means of Excel.

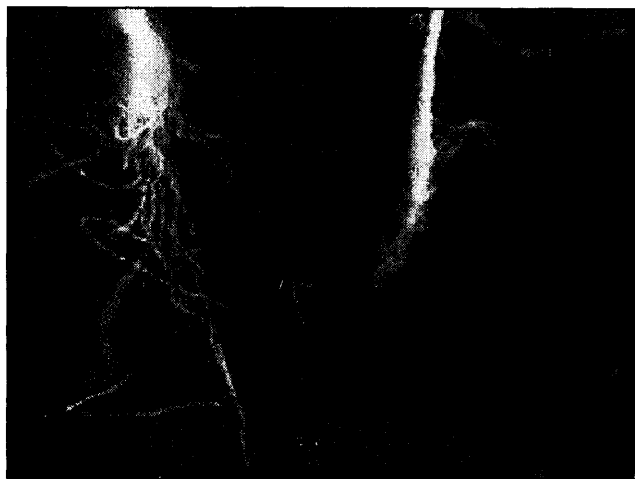


Fig. 4.1. Image of two broken yarns. The left – because of bad cohesion between fibres. The right – because of thin place.

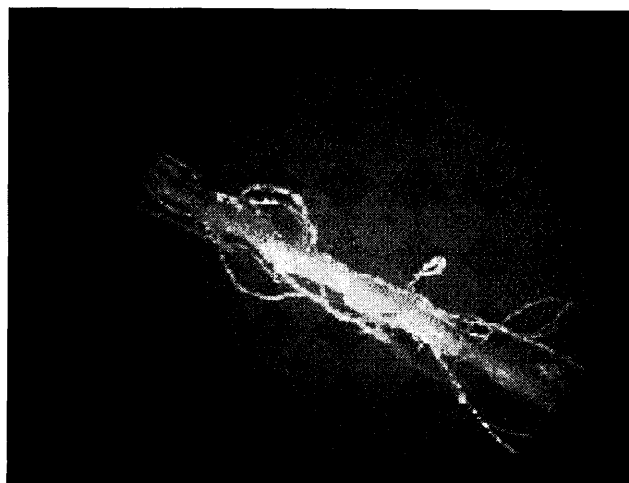


Fig. 4.2. The same yarn – 28 tex.



Fig. 4.3. Broken yarn at thin place.

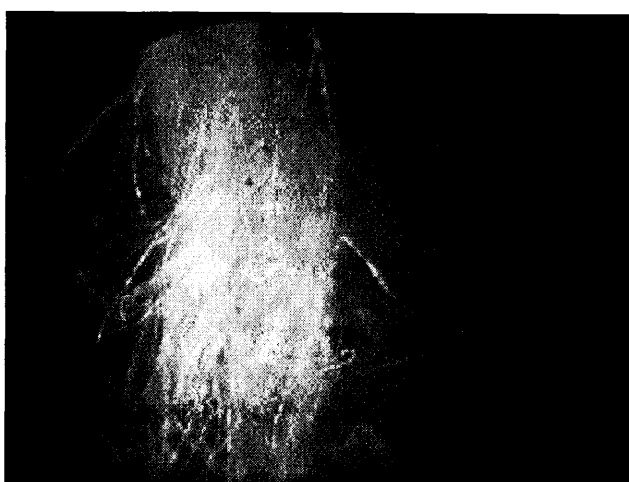


Fig. 4.4. Broken yarn at place without torsion.



Fig. 4.5. Intentionally broken yarn – fibres also are broken.



Fig. 4.6. Broken yarn at the place of bad connection on spinning machine.

Influence of Yarn Deformation on Weaving Process

Radko Kovář and Jana Drašarová

Department of Textile Structures, Faculty of Textile Engineering
Technical University of Liberec

Note: the work was supported by the grant of GACR (Grants Agency of the Czech Republic) no. 106/97/0372.

INTRODUCTION

It is natural that various technologies for flat textiles production are very similar one another. All of them usually use a yarn (thread) as an input material, nevertheless the stress uses to be put on rather different properties of this yarn very often. For both knitting technology and mechanical properties of knitted fabrics, the yarn bend and cross-section deformation belong to the most important ones. The strength of the warp yarn seems to be more important, but we should mind that this yarn must slip over the heald eye, reed dent etc. and that the changes of the yarn tension increase thus very much. Some results, aimed at knitting yarn evaluation, can be probably useful for the weaving technology as well.

The Forms and Importance of Yarn Deformation

The usual yarn break test could not be sufficient for the thread characterisation, even if it is done very thoroughly and includes, for example, investigation of influence of the test length on the strength and elongation at break [1]. Complex yarn evaluation should include other forms of deformation such as yarn bend (never mind that the break caused by yarn bend is unusual), cross-section deformation (that is connected with radial forces and with the bend as well) and yarn torsion. Experiments have shown that under the conditions, usual in the knitting process and in the knitted fabric elongation, the influence of yarn deformation is more important than the surface friction itself [2]. We shall call this phenomenon "inner friction", because it is connected with the change of mechanical into thermal energy in the yarn and fibers.

The example of the experiments is shown in the Fig. 1. About 40 different knitting yarns were investigated by two types of experiments, each experiment was at least 10-times repeated:

a) Tensile force F , necessary to overcome the frictional resistance, is measured. Input force F_0 is received by the weight G_0 , the angle of the contact of the yarn 1 with the hooks of two knitting needles 2 was π . "Apparent" coefficient of friction was calculated using the Euler formula $F = F_0 e^{af_a}$. The attribute "apparent"

means that f_a includes both surface and inner friction and is also dependent on the yarn bending rigidity and the like.

b) The angle φ is slowly enlarged and its value is measured when the yarn 1 starts to move. In this case the angle φ corresponds to surface friction only, the coefficient of friction is f_s and approximately can be counted by the equation $f_s \cong \sin \varphi$.

The graph in Fig. 1 shows that the inner friction, represented by the difference $f_a - f_s$, is greater than the surface friction coefficient f_s . The smaller is the input yarn tension, the greater is the share of inner friction. It is natural, because the relative influence of the yarn bending rigidity etc. is higher. Let us imagine the situation with $F_0 = 0$; the output yarn tension must be of some value ($F > 0$) and the Euler formula would not be useful.

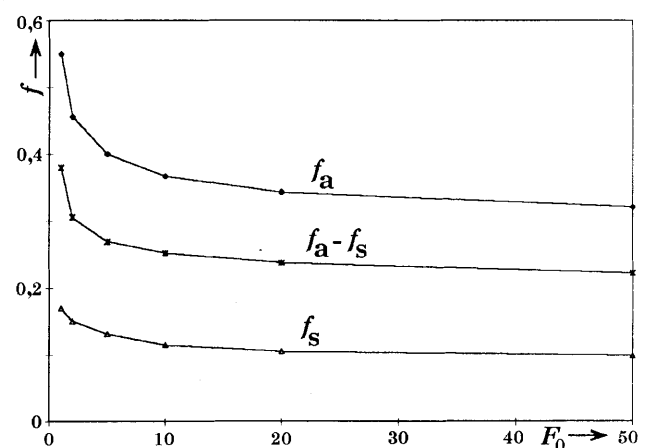
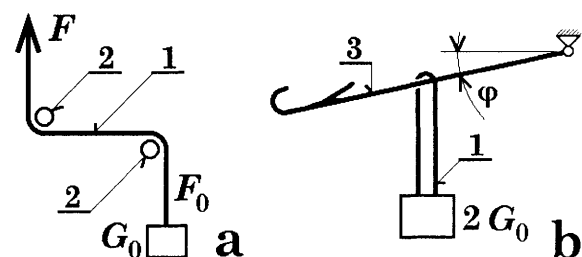


Fig. 1. The measuring of friction with and without yarn deformation

Inner friction and the change of mechanical into thermal energy is caused namely by:

a) The change of the mutual position (slip) of lower structure components. For flat textiles it means the change of the mutual position of yarns and fibres, because there are always some contact forces between fibres and yarns.

b) Non-elastic (viscous and plastic) components of fibre deformation.

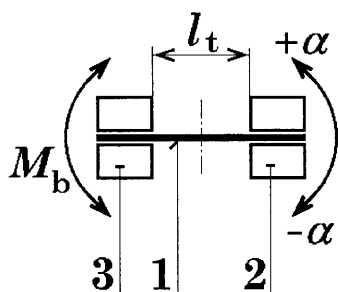


Fig. 2. The measuring of the yarn bend properties.

The experiment in Fig. 1 evaluates simultaneously the influence of the yarn bend and cross-section deformation on the increase of the yarn tensile forces. To separate and to measure only **bend deformation** is difficult, as it is shown in the Fig. 2. Here, the part of the yarn 2 is clamped by two pairs of jaws. The jaws 2 ensure the yarn deformation by turn by the angle $\pm\alpha$ and the jaws 3 measure the bending moment M_b .

If we want to reach the yarn curvature of the same level as it is in the binding point etc., the neutral axes of the yarn should have the radius of $R = 2d$ (d is yarn diameter). As we can turn the jaws 2 not more than by ± 180 ($|\alpha| \leq \pi$), the maximum test length could be $l_t = 2\pi d$, which is only about six yarn diameters. The result of the experiment would be influenced and changed very much by this fact, because the jaws deform the yarn cross-section and alter yarn properties as well (by fixation of fibre position).

The yarn cross-section change is one of the underestimated yarn properties. The assumption that the cross-section is circular in shape and constant in diameter is wrong and leads to great errors of results. The Fig. 3. demonstrates the profile of the weft yarn in the relaxed fabric with the plain weave. The yarn cross-section is changed namely by the yarn bend and by outer forces or a normal tension. For both production and structure of the flat textiles, the places of contact between crossing yarns (binding points) are the most important. For the modelling of the flat textiles it is useful to define the term "effective yarn diameter" d_{ef} that can be described as the minimal distance of yarn neutral axes in binding points. It is the variable, depending on the yarn deformation. The term is not correct (the real meaning is not diameter).

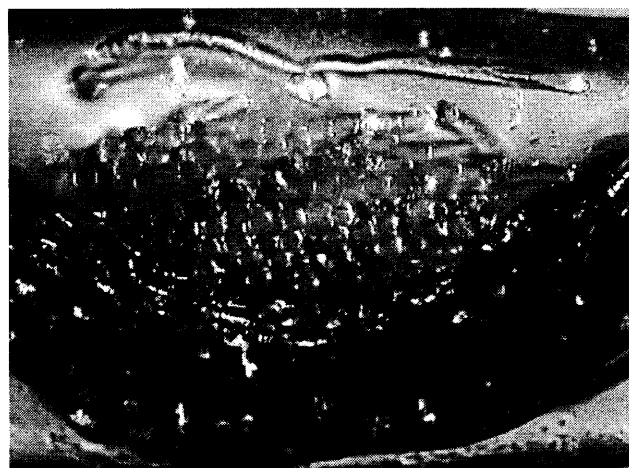


Fig. 3. The example of the yarn crosssection in the woven structure

The torsion deformation is important in some special cases only. The twisting moment in the yarn can change the structure of the knitted as well as the woven fabric, can cause looping of the yarn etc. We could easily find other yarn properties with strong impact on the weaving process which could not be described in this paper, such as cohesion between warp yarns which have to be separated.

Energy Changes, Connected with Yarn Deformation

If the yarn slips over some friction surface, the necessary input energy W corresponds to the product of the yarn displacement (length of path) s and the difference between input and output yarn tension

$dW = (F - F_0)ds$, or under stable (time independent) conditions

$$W = (F - F_0)s \quad (1)$$

The power (energy derivation) $P = dW/dt$ will have s replaced by $v = ds/dt$ and so

$$P = (F - F_0)v \quad (2)$$

All the mechanical energy calculated like this is being changed into thermal one (irreversible act). More complicated situation is from the point of view of yarn deformation itself, as there is a share of the accumulated reversible deformation. There are fibres, almost fully elastic in a certain range of the deformation. More of such fibres in the spun yarn, filament yarn etc. mean that the yarn deformation is connected with the change of the points of the contact between the position of fibres and due to it with the inner friction and energy changes. If we take into account the flat textile product, the deformation is moreover connected with the change of the position of yarns in the binding points.

The example of energy changes in the cyclic yarn and woven fabric deformation can be seen in the Fig. 4.

The fabric twill 1/2 Z, warp and weft yarn Viscose/Polyamid 65/35, $T = 48$ tex, square sett of 3120 yarns per meter. The load was recounted on one warp or weft yarn to compare the curves.

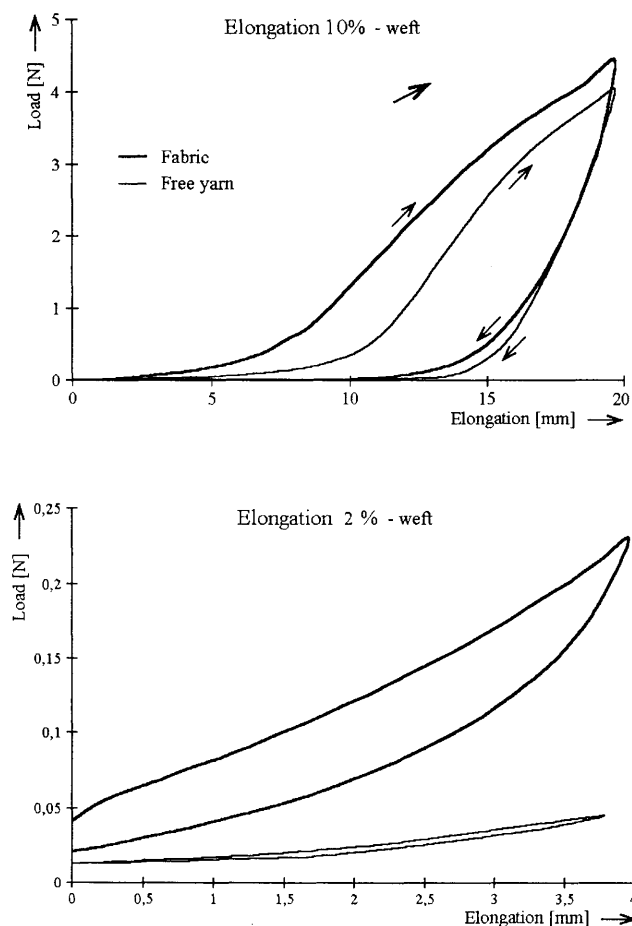


Fig. 4. One cycle of woven fabric and yarn deformation

The values of the woven fabric and yarn hysteresis, connected with one cycle of deformation, are given in the table. As supposed, the lost energy is much higher in the fabric than in the yarn (greater share of inner friction). 66.6 % of weft yarn hysteresis in a cycle of 10 % deformation can be explained by the fact that the elongation was near to the break point and that a certain share of irreversible energy was caused by the plastic yarn prolongation due to slip between the fibres.

	Hysteresis at elongation [%]		
	2 %	5 %	10 %
Fabric – warp	32.6	46.3	64.1
Fabric – weft	33.8	49.2	70.1
Yarn – warp	7.0	12.9	22.1
Yarn – weft	9.0	25.2	66.6

An extremely large hysteresis space is also connected with the covered rubber yarn deformation as well (see

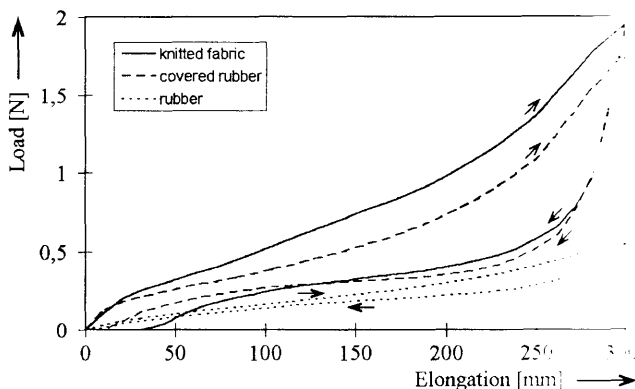


Fig. 5. One cycle of knitted fabric and elastic yarn deformation

Fig. 5, [3]). Speed of deformation was 200 mm min^{-1} . The share of lost energy of the uncovered rubber is much lower than that of double covered one, because of friction between winds of the covering yarn.

Mechanical energy, changed in the course of textile deformation into the thermal one, is necessarily connected with the yarn and fibre damage (abrasion etc.) and with the change of textile properties. The described inner friction mechanics has an important impact on the warp and weft breaks, it can change the sett of the fabric which can be reached, the forces, necessary to keep the fabric in the reed width by the temple, fabric shortening etc. Let us compare two extremes – one plain weave made of monofilament yarn and the other, made of micro-fibres. The possibility to change the cross-section of the second case enables to fill the pores of the structure and to design the fabric that does not let the smallest drops of water penetrate but the vapour (sweat) can pass through.

DISCUSSION

The problem of the influence of the yarn properties on weaving and knitting technologies has not been completely solved up to date. The theory of the yarn structure does not allow yet to predict the change of the yarn bending and cross-section properties and there is a lack of suitable experimental methods as well. At the Department of Textile Structures some other results are available and any co-operation on the topic is welcome.

REFERENCES

1. Neckář, B.: Pevnost a upínací délka příže (Strength and test length of yarn). Seminar STRUTEX, TU of Liberec 1996
2. Kovář, R.: Chosen Properties of Knitting Yarns. In: 34. congress IFKT, Brno 1992
3. Kovář, R., Drašarová, J., Roček, V.: Non-Elasticity of Elastic Fabric. Textile Science, Liberec 1998

Determining of yarn bending deformation module

Dr. Georgi Stoyanov Popov,
Eng. Kalin Georgiev Gjoshkov, and Eng. Violeta Georgieva Peeva

Department of "Textile Technique" at the Technical University, Sofia

A method for determination of yarn bending deformation module is described. For that purpose a durable curvilinear form has been assigned to the yarns by a sample weaving and relaxation. After separating the yarns from the sample they are loaded by a dynamometer. All registered measurement data are being used by calculating of the yarn bending deformation module.

INTRODUCTION

The good knowledge of the mechanical properties of the yarns would allow an application of modern scientific methods for determining of parameters and behavior of the products- knitted and woven textiles with various structures. Despite of the numerous theoretical and experimental works we still don't dispose of sufficient information for the complete determining of the mechanical properties of the yarns.

For determining of the mechanical properties of the yarns a special apparatus is required, of which dispose only a limited number of small scientific labs. The widely used apparatuses as dynamometers allow an universal application of the test and comparison of different results. From this point of view is essential not only to elaborate new apparatuses, but also to establish new tests for dynamometer.

One of the methods for determining of the mechanical characteristics of the yarns [1] consists of a sample weaving in advance. Then the yarns which already have acquired a durable wavy line form are taken out of the sample. While loading of such a yarn by dynamometer simultaneously with the extension of its axial line the yarn gets straight. The arising deformations in the yarn depend directly on its bending deformation module B (bending rigidity). The simultaneous registration of the strength and extension of the curvilinear yarn by its stretching makes it possible to calculate B .

Aim and tasks

Our aim was to develop an accessible and precise method for determining of the yarn bending deformation module. All methods for determining of B were well examined. A method was selected which consists of loading of weaved yarns by dynamometer.

Short description of the method

The determining of the bending deformation module of yarns by their separation is carried out as follows: A

certain number of yarns are being taken out from a selected sample. The sample should be sufficiently relaxed, in order the yarns to gain a durable wavyline form. Parameters of this form and the cross section form are being taken off by microscope and photography and noted down. The yarns are being put into dynamometer and loaded up to the grade of coming in the range of linear deformations, which already have been determined by previous tests. The curvilinear extension – loading is noted down.

The linear elasticity module E is being determined by testing of straight, not used for weaving yarns. The yarns are being loaded by dynamometer, afterward the applied strength and extension are being registered.

After taking off of the described dynamometric yarn properties the tasks about deformation of the tensile – stressed curvilinear yarn is being completed.

A structure-mechanical method for analysis of curvilinear yarns is applied which has been described in details in [3]. Its main point is that the task for the change in curvature of the power stressed plane bent beam is solved. The solution is traditional for construction materials. It is also applicable for textile yarns [1, 2]. Though in that case it is essential to consider their elasticity which can not be neglected.

The following hypothesis has been applied: the yarns are linearly elastic in bending and small deformations.

For the calculations are being used the experimental values gained by the curve extension – loading of the weaved yarn.

The equation system is solved by a digital integration for which a calculation program has been designed.

For determining of the yarn bending deformation module we proceed as follows: A starting curvature is set to the yarn. Its data is obtained from the experimentally taken yarn form. From this data we get also:

- the projection of the wave length of the yarn;
- the wave length.

First we assign some value for B . After that we put in one measured value of the strength applied and calculate the deformation caused by it.

We compare the calculated deformation value with the result from the dynamometer. If both values differ, we change the assigned yarn value of B and repeat the calculations until both values completely coincide.

EXPERIMENTAL RESULTS

A polyfilament polyamid yarn 94 tex without a twist and a polyfilament polyester twisted yarn 94 tex have been tested. Samples with a weft number (PA) 115 threads/dm and a warp number (PES) 140 threads/dm were elaborated. 25 samples were separated from each sample; after that the yarns were loaded by dynamometer TIRA TEST. The loading speed was constant. Each test was done in 20 s, and the distance between jaws = 200 mm. The starting tension of the yarns was 1 cN.

At the beginning a preliminary testing has been completed with straight non deformed yarns in order to establish the validity limits for the Hook's law and for determination of the linear elasticity module. In the area of the small deformations an E was found equal to 400 N for the polyamid yarns and $E = 570$ for the polyester yarns.

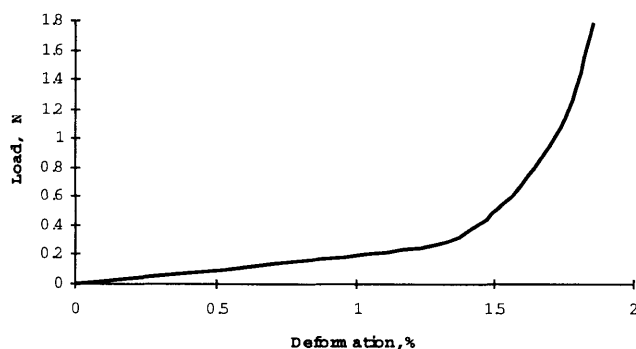


Fig. 1. Connection between load and deformation by unfolding of a wave linear yarn

On Fig. 1 is shown part of the experimental data from the unfolding of the wave linear yarns. As you can see on the graphics are clearly distinguished 2 zones. At the beginning there is a considerable deformation by application of minimum load in this zone the deformation is mainly caused by the unfolding itself and partly – by a pure linear extension of the yarn. Then is following a zone of a linear dependence between the load and the deformation where the load is considerably higher. In this zone the unfolding is already completed by normal hardness and deformation is mostly caused by a pure linear extension of the yarn.

Bending deformation module was determined by the way already shown through the data of the curves written down. So were obtained the following values:

PA $B = 0.3\text{--}0.35 \text{ mN mm}^2/\text{tex}$

PES $B = 0.22 \text{ mN mm}^2/\text{tex}$

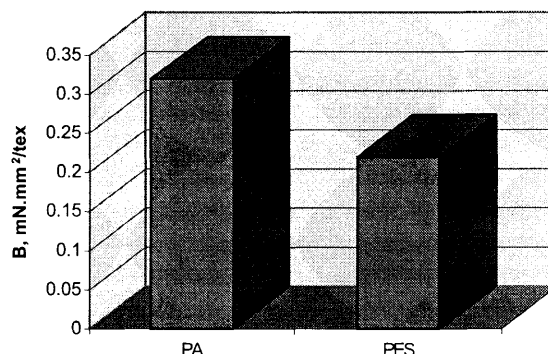


Fig. 2. Yarn bending deformation module PA and PES 94 tex

From the obtained results for B of PA and PES is getting clear, that it is not neglectable small and should be considered in technical calculations when it is required.

CONCLUSIONS

The yarn bending deformation module can be determined by loading of waved yarns by dynamometer and also by application of the structure- mechanical method.

The deformation bending module of the tested yarns from polyfilament PA with linear thickness 94 tex is in the range of $0.3\text{--}0.35 \text{ mN mm}^2/\text{tex}$. The deformation bending module of the tested yarns from polyfilament PES with linear density 94 tex is in the range of $0.22 \text{ mN mm}^2/\text{tex}$.

For a more detailed examination of the process of yarn deformation is essential to observe during a loading also the form and the dimensions of their cross-sections.

LITERATURE

1. B. Olofsson: J. Text Inst., 1964, 55, T541–57.
2. R. Postle, G. A. Carnaby, S. de Jong: The Mechanics of Wool Structures, 1988, Ellis Horwood Limited, 195–224, 307– 338.
3. G. S. Popov: Structure-mechanical method for calculation of deformations and tensions inside yarns and fabrics. It has been given for printing in the yearly edition of the Technical University, 1998.

Frictional model of yarns running against objects

Dang Vu Hung, L. Vangheluwe and P. Kiekens.

Universiteit Gent, Department of Textiles, Technologiepark 9, 9052 Zwijnaarde, Belgium

This paper presents a new approach for evaluating yarn-object frictional behavior. It is clear that the statistical distribution of the yarn tension is more important than its mean value alone. The theory, which is proposed based on the above-mentioned fact, is used to deduce the relationship between the incoming and outgoing tension in a yarn as it laps an object. The validity of the relationship has been verified in terms of the experimental findings. The findings show that the outgoing yarn tension is a function of the contact angle between the yarn and the object, incoming yarn tension and yarn velocity. The theoretical model corresponds well with the experimental values.

Key words: *yarns, friction, statistical distribution, model.*

INTRODUCTION

Friction on yarns is present in almost all textile processes. On modern automatic looms, the warp yarn is in contact with machine elements at several points during the passage from the warp beam to the cloth fell. During shedding, the warp yarns move fast up and down. Some loom parts such as rapier hooks or relay nozzles attached firmly on the sley take much higher speed. The relative speed, therefore, between the warp yarns and these loom parts in contact is high. The interaction taking place between the warp yarns and the loom parts as mentioned above produces friction, which must be overcome during the weaving process. A high friction may enhance tension, leading to a higher risk of having a yarn break. It can also give rise to faster wear of yarn surfaces. The handle of a resulting fabric is obviously dependent on the surface friction of its component yarns [2].

Previous works [1, 3, 5, 6, 7, 8] have shown that when friction is present the value of the outgoing yarn tension depends on several factors, namely on the contact angle between the warp yarn and an object, incoming yarn tension, yarn relative velocity, contact area, roughness of contact surface, temperature at contact point etc.

This study is an attempt to develop a new model to describe the relationship between the incoming and outgoing tension in the yarn-object interaction as far as friction is concerned. The model uses a statistical approach: the statistical distribution of the incoming and outgoing tension is used rather than mean values alone.

The measurement of the friction of yarn against an object

Any assessment of the efficiency of the weaving process should take into account the existence of frictional forces, which are calculated as a difference between the incoming and outgoing tension, produced by contact of yarns with the relevant objects.

A well-known method for the measurement of friction of running yarns is illustrated in figure 1. The experiments described in the paper have been performed on a Rothschild friction meter that uses this principle. The friction meter gives values of input and output yarn tension, which can be read off on a tensiometer. The analogue output of the tensiometer is fed to a computer to obtain a digital value of the recorded tension. In the method, the contact angle of the yarn on the object and the yarn velocity can be set at specific values. In order to enable lap angles less than 180° to be used an auxiliary pulley is added. Because of the friction of this pulley, it is necessary to apply a correction to the measured values of input and output tensions and this has been done when lap angles less than 180° have been used.

Operation principle

The test method for the tension measurement of yarns is dynamic loading in the sense that the yarn is at a relatively high speed. The yarn runs continuously through the instrument with given settings which are specified by yarn input tension, yarn contact angle and yarn velocity. The values of the yarn input tension and output tension are measured alternatively every 5 seconds and the total measurement time is

45 seconds. The values of the input and output tensions are stored in files.

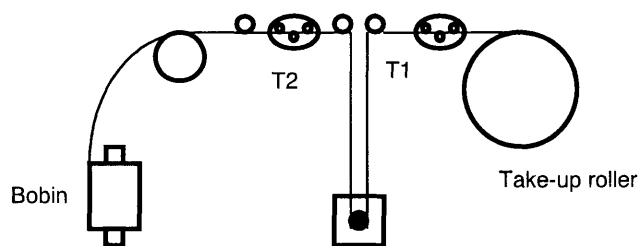


Fig. 1. Test instrument
 T_2 – input tension, T_1 – output tension

EXPERIMENTAL

Ranges of the values of the relevant parameters chosen were as follows:

- Lap angle (α): (15–90°) modified in steps of 15° (this range of contact angle is sufficient as it represents the range of angles occurring in weaving, namely contact of warp yarns with loom elements).
- Yarn speed (V): (50–300 m/min) adapted in steps of 50 m/min (the warp yarn has a high relative velocity against some loom parts. Due to the limitation of the instrument, only this range of velocity could be used).
- Also, different input tensions have been set via an input tensioner. The input tensioner is a type of disk brake allowing to set tension in a rough way.

Experiments were done under standard climate conditions (temperature: 20 ± 2 °C and humidity: 65 ± 2 %). The yarns used were made to pass over a stainless steel object with circular cross-section.

Experimental results given later on were those obtained with a ring-spun cotton yarn.

Theoretical background

A model describing the relationship between the incoming tension (T_2) and outgoing tension (T_1) in dynamic loading can be developed when the statistical distributions of the tensions are known. If Φ represents the cumulative distribution of the tension over a certain range of values and time for a specific yarn and particular test conditions, the relationship between matching tensions T_2 (input tension) and T_1 (output tension) follows the equation given below [9]:

$$\Phi_{in}(T_2) = \Phi_{out}(T_1) \quad (1)$$

Therefore, the outgoing tension T_1 can be calculated out of the input tension T_2 if both statistical distributions are known:

$$T_1 = \Phi_{out}^{-1}(\Phi_{in}(T_2)) \quad (2)$$

RESULTS AND DISCUSSION

Dynamic frictional tests have been executed with all test parameter combinations specified. With the use of the χ^2 -test it was verified that the input as well as output tension follow a normal distribution. The results obtained after using equation 2 in which the normal distribution has been used for both input and output tension showed that a linear relationship between output and input tension exists (see figures 2, 3, 4). For these figures it can be stated that the length of each curve demonstrates the variation range of the data.

The method used expresses the statistical deviation in values measured. Deviations in input tension and also deviations in output tension occur. The deviations in output tension are generated by changes in output tension but also by local differences in yarn properties. The linear curve relating input and output tensions measured for specific conditions (input tensioner setting, angle, velocity, contact object and yarn) exhibits the deviation in properties being present.

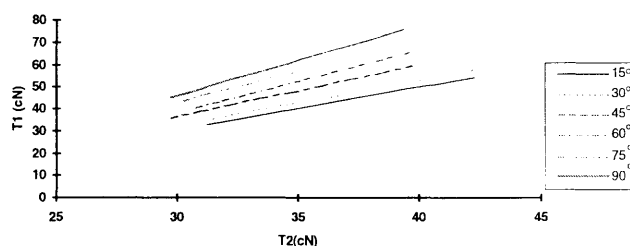


Fig. 2. Output tension T_1 vs input tension T_2 as angle changes in the range of (15° ÷ 90°) and $V = 100$ m/min.

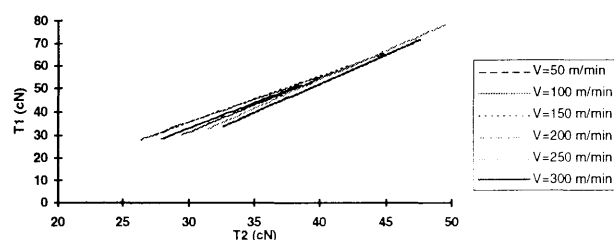


Fig. 3. Output tension T_1 vs input tension T_2 as velocity changes in the range of (50 ÷ 300 m/min) and $\alpha = 30^\circ$.

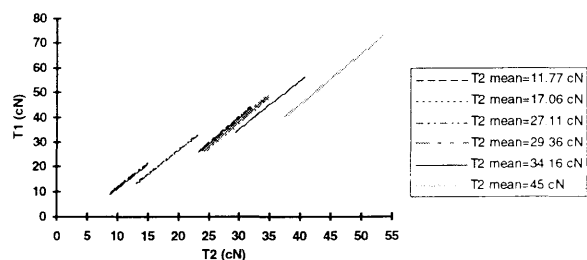


Fig. 4. Output tension T_1 vs input tension T_2 with $\alpha = 30^\circ$ and $V = 100$ m/min for different input tension settings.

The increase in output tension and hence frictional force with the angle can be ascribed to the increase in the area of contact between the yarn and object through an increase in wrap angle as in the capstan equation [4]. We found such an effect when dealing with a yarn running against the high-speed object, shown in the figure 2.

The effect of the yarn relative velocity V on frictional behavior with the object has been investigated in the past [1, 3, 5, 6, 7, 8]. However, there are differences in the results obtained. In this investigation, where the yarn velocity was changed in the range of 50 to 300 m/min, the result in figure 3 shows that at 100 m/min the curve presents lowest gradient and the gradient increases as the yarn velocity is higher than 100 m/min. It can also be seen that the tension ratio (T_1/T_2) increases with an increase of the yarn velocity.

Figure 4 shows the relationship for different settings of the input tensioner. The lines are characterized by the mean input tension. The influence of input tension can be explained by yarn pressure on the object, which increases when the input tension increases.

A new frictional model approach

As both incoming and outgoing tensions follow a normal distribution, a linear relationship as expressed in equation 3 exists.

$$T_1 = AT_2 + B \quad (3)$$

In this equation T_2 , T_1 are actual input tension and output tension respectively.

A and B are parameters depending on yarn type and test parameters.

As three parameters (α , V , \bar{T}_2) have been selected for the experiments and for the model to be developed, it is, therefore, expected that:

$$A = F_1(\alpha, V) \quad (4)$$

$$B = F_2(\alpha, V, \bar{T}_2) \quad (5)$$

with α : contact angle between yarn and object.

V : yarn speed.

\bar{T}_2 : mean input tension determined by the setting of the input tensioner.

The values for A and B of equation 3 can be calculated for specific conditions out of the statistical distribution for T_1 and T_2 . From characteristics of the linear trend, it is generally known that:

$$\sigma_1 = A\sigma_2 \quad (6)$$

$$\mu_1 = A\mu_2 + B \quad (7)$$

σ_1 , μ_1 , σ_2 , μ_2 : standard deviation (σ) and mean value (μ) of output tension T_1 and input tension T_2 respectively.

The task is simple to calculate A and B out of the set of equations given in equations 6 and 7.

The following figures illustrate A as a function of V and B as a function of V for the experiments performed:

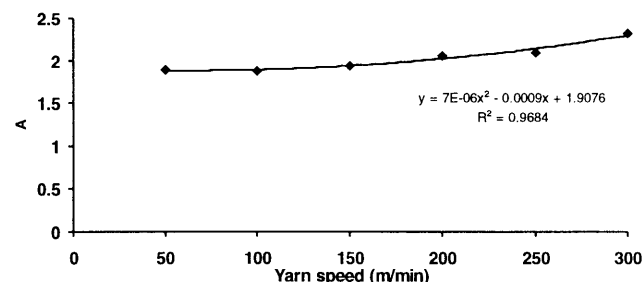


Fig. 5. Effect of velocity on A at the contact angle of 30° and input tension = 31 cN

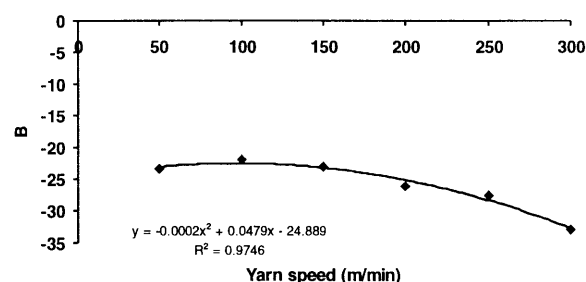


Fig. 6. Effect of velocity on B at the contact angle of 30° and input tension of 31 cN

Based on the experimental values obtained, the least square method was used to perform regression calculations in order to find relations between the values of A and B and the experimental parameters represented by contact angle (α), yarn speed (V) and input tensioner setting (expressed by \bar{T}_2). The equations found are given in formulas 8 and 9. These equations specify the relationship put forward in formula 4 and 5:

$$A = (k_1 + k_2V + k_3V^2)e^{K_4\alpha} \quad (8)$$

$$B = (k_5 + k_6V + k_7V^2)\bar{T}_2 \quad (9)$$

with a coefficient of correlation of 0.99 for equation 8 and 0.98 for equation 9.

Consequently, the relationship between outgoing tension and incoming tension could be described as follows:

$$T_1 = (k_1 + k_2V + k_3V^2)e^{K_4\alpha}T_2 + (k_5 + k_6V + k_7V^2)\bar{T}_2 \quad (10)$$

The values of k_1 ... k_7 are constants, all being dependent on yarn raw material and surface characteristics of object.

The goodness of fit between the predicted values of the output tension calculated from equation 10 and experimental values obtained during the experiments is illustrated in the regression plot in figure 7.

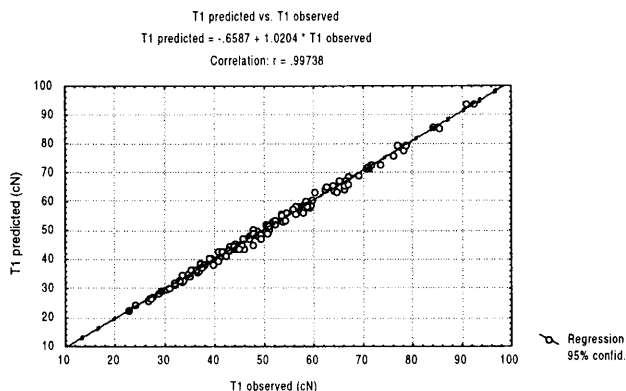


Fig. 7. Relationship between predicted and experimental output tension values

CONCLUSION

The results indicated that factors as contact angle, mean input tension and yarn velocity have an important effect on the frictional behavior between yarn and a metal object. Any increase in contact angle and preset input tension leads to an increase in the values of output tension, and hence friction. The effect of the velocity is more complicated and expressed in terms of a quadratic equation.

The new model we have developed agrees well with the experimental results. The equation showed good fit with a coefficient of correlation of 0.99738. The values of the constants all depended on yarn raw material and surface characteristics of the object.

ACKNOWLEDGEMENTS

The authors would like to thank Mrs. Marian Ledoux of the Department of Textiles, Universiteit Gent, for her help with the experimental set-up.

LITERATURE

1. Baird M. E.: Friction Properties of Nylon Yarn and Their Relation to the Function of Textile Objects, *J. Textile Inst.*, **46**, 101–111 (1955)
2. Chattopadhyay R.: The Friction Behaviour of Ring-, Rotor- and Friction Spun Yarn, *J. Textile Inst.*, **87**, 59–66 (1996)
3. Galuszynski S.: Frictional Forces in the Heald Eye, *Textile Res. J.*, **53**, 462–468 (1983)
4. Howell, H. G. and Mazur, J.: Amontons Law and Fibre Friction, *J. Textile Inst.*, **44**, 41–58 (1955)
5. Lyne D. G.: The Dynamic Friction Between Cellulose Acetate and a Cylindrical Metal Surface, *J. Textile Inst.*, **46**, 112–118 (1955)
6. Olsen, J. S.: Frictional Behaviour of Textile Yarns, *Textile Res. J.*, **39**, 31–37 (1969)
7. Rubenstein C.: The Friction of a Yarn Lapping a Cylinder, *J. Textile Inst.*, **49**, 181–191 (1958)
8. Schick, M. J.: Friction and Lubrication of Synthetic Fibres, Part 1, 2, 3, *Textile Res. J.*, **43**, 103–109 (1973)
9. Thomasian, A. J.: The Structure of Probability Theory with Applications, McGraw-Hill, 320–446 (1969)

Forecasting the technical properties of woven fabrics with the aid of Finite-Element-Analysis

Dipl. Ing. Andreas Müllen and Prof. Dr. Ing. Burkhard Wulforth

Institut für Textiltechnik der Rheinisch-Westfälischen Technischen Hochschule Aachen

INTRODUCTION

The market share of technical fabrics in total fabric production has increased substantially in the recent years. This market segment is of major importance to European weaving mills in particular, as it offers an opportunity to take up a leading position on the international market by means of a lead in know-how and modern machine technology. This results in growing demands on the industry concerning quality, time, human power and cost.

In the area of technical fabrics, such as filter fabrics, coatings, strip or supporting fabrics, specific mechanical properties are of special interest. One of the most fundamental properties are the mechanical characteristics of the strength and ductility. At present the construction of technical woven fabrics is usually carried out manually, based on personal experience and trial and error.

Although the predicting of tensile properties for a woven fabric has received attention from many scientists around the world, no computer-aided instruments have been available to the designer for predicting these technical properties. This outlines the need of advanced simulation and calculation techniques to design and develop quality products in a simple and easy-to-use way. This is also important with regard to the development of new fabrics and the optimisation of existing fabrics. These requirements are met by the development of inexpensive and powerful computer technology during the last couple of years.

In a research project at ITA, the theoretical basis for calculating the properties of technical fabrics with the aid of the Finite-Element-Method has been developed [1]. In a follow-up project, a simulation program for industrial use is currently being developed for the purpose of forecasting and optimising the stress/strain characteristics of fabrics subjected to tensile loads [2]. This program is intended to help systematise and simplify the design of technical fabrics. The number of labour-intensive and time-consuming weaving tests and trials can be minimised. The designing of fabrics in accordance with the loads encountered during processing enables reductions in input materials and the opening-up of new applications.

State of the art and literature review

Over the years, many different forms of woven fabric simulations have been developed. Some of them have been used in determining geometrical and tactile properties like cloth setting, maximum weavability and fabric tightness [3–6] and some attempts have been made to predict mechanical properties like load-elongation behaviour, fabric bending and shear or fabric drape [7–11].

Such a simulation program can be a means of describing, representing, forecasting and optimising the characteristics of the physical system "woven fabric".

The first step of any form of simulation always involves mapping the real system in a model. This model must describe the real system and its characteristic physical parameters with sufficient accuracy to attain the desired results. In order to minimise the scope of work relating to description and calculation, the model description should always be as simple and as accurate as possible. For this purpose, simplifying assumptions are to be drawn up and their applicability has to be tested by appropriate means.

The classical description of woven fabric geometry was developed by Peirce [3] in 1937. In this model the cross-section of the warp and weft yarns are assumed to be circular and always remained undeformed. Peirce established a flexible thread model for a plain weave, in which he assumed, that the yarns are perfectly flexible and incompressible.

Another structural model for plain weaves has been introduced by Kawabata et al. [10]. In this model, the warp and weft yarn axes are assumed to be straight lines between the crossover points. The warp and weft yarns are assumed to be perfectly flexible and although due to this, forces caused by yarn bending are ignored, the sawtooth model takes yarn compressibility at the crossover points into account.

These model descriptions are most commonly used as a starting point for theoretical investigations of the mechanical deformation of woven fabrics.

The next step of the simulation process involves transforming the model into an analytical or numerical description. Over the years various processes and methods were established in the area of woven fabric

simulation. These approaches range from e.g. geometrical description of plain weave, load-elongation models based on flexible thread geometry or on elastica theory, nonlinear analysis, boundary-value problems and various energy principles and the principles of virtual work. Up to date only two papers are known to be dealing with the Finite-Element-Methods for the prediction of uniaxial load-elongation behaviour of woven fabrics [1, 2, 12]. In the area of yarn and fibre assemblies, fabric drape and the simulation of composite materials some more applications of the FEM are found [9, 13–15].

Transformation of the model into a form of analytical or numerical description suitable for computer calculations is acquiring ever-increasing importance as the possibilities of computer technology continue to expand. The numerical processes in particular, such as the calculation of non-linear systems, often require the resolution of very large equationsystems, which impose the very highest performance requirements on computer technology with regard to speed and memory capacity. As a result of the development of low-cost and effective PC-based computer systems, these methods are now in widespread use.

The Finite-Element-Method serves as an example here. Until a few years ago, the effective application of this method was only possible on a small number of very expensive large-scale computer systems. Due to the ever more widespread use of high-performance PCs, the Finite-Element-Method has now become an effective design instrument in many branches of industry.

Transformation of the model into a computable program enables calculation and evaluation of the desired variables within the simulation system. One of the advantages of this method is the ability to vary the input parameters quickly and to examine the effects of this variation on the target variables.

The aim of this research work is the development of an easy-to-use FEM simulation program for the prediction of the load-elongation behaviour of technical woven fabrics, because this is the most interesting parameter for the designer of technical fabrics.

Finite-element-method for woven fabric calculation

The basic requirements for each FEM-Calculation are the description of the real system as a computermodel in terms of the physical and geometrical boundaries of the system.

In a research project at ITA, the theoretical basis for calculating technical fabrics with the aid of the Finite-Element-Method has been developed. For this basic evaluation we have used the FEM programme MARC and the interactive graphical pre- and postprocessor MENTAT. Especially in the field of nonlinear FEA, this

program yields very good capabilities. In the fabric simulation all of the three major types of nonlinearities occur: The geometric nonlinearity due to the de-crimping of the fabric in the low load region of the load-elongation curve, the large deformations and the large strains during the loading. The material nonlinearity of all kinds of textile materials are well known. The boundary nonlinearity takes place in the crossing points due to contact and friction.

For the purpose of the model description in the finite element analysis process, the fabric structure is approximated by straight bar elements between the crossing points. Each of these elements contains two nodes located in the crossing points and the deformation of the elements is described by six degrees of freedom in each of this nodes. The coordinates of the element-nodes are describing the fabric geometry. These coordinates depend on the yarn parameters like count, twist and density, the weave crimp, weave pattern, the number of threads in the weave repeat and the deformation of the threads in the crossing points. The bending characteristic of the yarns can be derived from the description of the cross-section or via experimental data.

With the geometric and material descriptions, these elements contain all the relevant characteristics of the real warp and weft yarns. Especially the nonlinear material behaviour of the yarns was taken into account. The description of the nonlinear elastic-plastic material behaviour is based on the flow theory [16]. For this description we need a yield condition, that separates the elastic and inelastic behaviour of the material. Since the yield stress is generally measured from uniaxial tests, and the stresses in real structures are usually multiaxial, the yield condition of a multiaxial stress state must be considered. We chose the von Mises yield condition, which states that yield occurs when the effective stress equals the yield stress as measured in a uniaxial test. The conditions of the subsequent yield, the work hardening rules, must also be applied. The work hardening rule relates the incremental stress to incremental plastic strain in the inelastic region and dictates the conditions of subsequent yielding. An isotropic work hardening rule was chosen, assuming that the centre of the yield surface remains stationary in the stress space, but that the size of the yield surface expands, due to work hardening.

The comparison between the theoretical calculations and the experimental results of an uniaxial yarn load-extension test shows very good correspondance (Fig. 1). This confirms the accuracy of the material description chosen.

The description of the linking conditions at the crossing points requires special attention. The advantages of the FEM method in the calculation of non-linear systems become apparent both in this connection and in the highly non-linear material descriptions. The compres-

sional behaviour of the warp and the weft yarns can be modeled in every required accuracy, using experimental data or an analytical description of the compressional behaviour of the used yarns.

Due to the nonlinear nature of woven fabric simulation, an incremental method must be used to solve the equilibrium equations. In large deformation analysis the relationship between incremental load and displacement is called the tangent stiffness, described by the material behaviour. When solving this type of problem the load is increased in small increments, the incremental displacement is found, and the next value of the tangent stiffness is calculated, before the next increment starts. There are different approaches available to solve this kind of problems. We chose an updated Lagrangian method, where the node coordinates are updated after each increment and which refers everything to the original undeformed geometry. Due to this, the flattening of the yarn cross-section during the loading of the fabric is taken into account.

Under these assumptions, all necessary data are established for the FEM simulation of the uniaxial load-extension behaviour of woven fabrics.

EXPERIMENTAL VALIDATION

In order to verify the results of the FEM model, measurements were made on a plain woven fabric made from multifilament PES yarns (warp 22 picks/cm PES 280 dtex f48 z60) and PA yarns (weft 12 picks/cm PA 480 dtex f72 z30).

Figure 2 show the comparison between the theoretical calculation and the experimental results of an uniaxial load-extension test. Both tests in warp and weft direction show a very good correlation between the simulation and the measurement. In the high load area of the weft direction appear differences between measurement and simulation results. This deviation appears due to the insufficient model description of the crossing points and the high crimp magnitude of 11 % of the weft yarn. After the initial crimp interchange in the low load region of the load-elongation curve, stick-slip effects occur. These effects are not fully simulated by the chosen model description of the crossing points.

The current material description of warp and weft yarns did not include the maximum force and the elongation at break. In the following, the material description must be extended to this parameters.

The FEM results obtained in this research are not complete but show sufficient accuracy for calculating the load-elongation behaviour of woven fabrics. The next step will be the extension of this work to an applicable easy-to-use program as a tool for designing fabrics.

Outlook

In order to minimise computing time and computer capacity requirements, a new FEM program is being developed which fulfils the special requirements of fabric calculations. The known yarn characteristics and the desired weave structure serve as input parameters. Also the process variables during processing are taken into account. These variables have a strong influence on the geometric parameters of the resulting fabric, such as shrinkage of the cloth and end spacing and crimp. In turn, the geometry of the fabric has a strong influence on strength and elongation characteristics.

The new model description should be extended due to the deformation and friction behaviour in the crossing points and the material description in the high load area of the tensile curves. Special attention will be given to the accurate calculation of the warp and weft crimp, as an important factor of tensile behaviour and costs of the fabric. The new program contains a database with all necessary values to estimate the fabric forming costs due to the geometric parameters of the weave. The program is designed for the use of mono- and multifilament yarns first. An extension to all other yarns is planned. Based on this new model, the uniaxial load-deformation behaviour of the fabric is calculated by means of especially defined Finite-Element-Algorithmen.

This programme is intended to help systematise and simplify the design of technical woven fabrics and to reduce the labour-intensive and time-consuming weaving tests and trials.

ACKNOWLEDGEMENTS

This work AIF-No. 11094 was supported via the Forschungskuratorium Gesamttextil by the funds of the Federal Ministry of Economy with a contribution of the Arbeitsgemeinschaft Industrieller Forschungsvereinigungen (AiF)

The authors also like to thank the German Research Association (Deutsche Forschungsgemeinschaft, DFG) for the financial assistance which they have given to the DFG project WU 159/2-2 "Analyse des Kraft- und Spannungsverlaufs in Geweben".

LITERATURE

1. Wulforth, B., Müllen, A.: Analyse des Kraft- und Spannungsverlaufs in Geweben, Abschlußbericht zum Forschungsvorhaben DFG Wu 159/2-2 am Institut für Textiltechnik der RWTH Aachen, Aachen 1995
2. Wulforth, B., Müllen, A.: Entwicklung eines Simulationsprogramms zur Vorhersage und Optimierung des Kraft/Dehnungsverhaltens zugbelasteter Gewebe, laufendes Forschungsvorhaben AiF 11094, Institut für Textiltechnik der RWTH Aachen, Aachen 1998
3. Peirce, T. F.: The geometry of cloth structure, Journal of the Textile Institute 28 (1937), T45-T59

4. Kienbaum, M.: Gewebegeometrie und Produktentwicklung, *Melliand Textilberichte*, 71 (1990), 737–742
5. Newton, A.: The Comparison of Woven Fabrics by Reference to Their Tightness, *Journal of the Textile Institute* 86 (1995), 232–240
6. Ajayi, J. O., Elder, H. M.: Tactile and Instrumental Evaluation of Surface Contour of Fabrics, *Journal of the Textile Machinery Society of Japan*, 43 (1997), 25–37
7. Dastoor, P. H., Hersh, S. P., Batra, S. K., Rasdorf, W. J.: Computer-assisted Structural Design of Industrial Woven Fabrics, Part I: Need, Scope, Background, and System Architecture; Part II: System Operation, Heuristic Design; Part III: Modelling of Fabric Uniaxial/Biaxial Load-Deformation, *Journal of the Textile Institute*, 85 (1994), 89–157
8. Asvadi, S., Postle, R.: An Analysis of Fabric Large Strain Shear Behaviour Using Linear Viscoelasticity Theory, *Textile Research Journal* 64 (1994), 208–214
9. Ascough, J., Bez, H. E., Bricis, A. M.: A simple finite element model for cloth drape simulation, *International Journal of Clothing Science and Technology*, 8 (1996), 59–74
10. Kawabata, S.: The Finite-Deformation Theory of Plain-Weave Fabrics, Part I: The Biaxial-Deformation Theory; Part II: The Uniaxial-Deformation Theory; Part III: The Shear-Deformation Theory, *Journal of the Textile Institute*, 64 (1973), 21–85
11. Kawabata, S.: A Finite-Deformation Theory of the 2/2-Twill Weave Under Biaxial Extension, *Journal of the Textile Institute*, 70 (1979), 417–426
12. Offermann, P., Floß, A., Rösel, B.: Erarbeitung der Zusammenhänge zwischen speziellen Gewebeparametern und der Festigkeit und Dehnbarkeit eines Gewebes, *Abschlußbericht zum Forschungsvorhaben DFG Of 17/3-3 am Institut für Textil und Bekleidungstechnik der Technischen Universität Dresden*, Dresden 1995
13. Chen, B., Govindaraj, M.: A Physically Based Model of Fabric Drape Using Flexible Shell Theory, *Textile Research Journal* 65 (1995), 324–330
14. Ganesh, V. K., Naik, N. K.: Failure Behaviour of Plain Weave Fabric Laminates under On-Axis Uniaxial Tensile Loading: I-Laminate Geometry, *Journal of Composite Materials*, 30 (1996), 1748–1778
15. Munro, W. A., Carnaby, G. A., Carr, A. J., Moss, P. J.: Some Textile Applications of Finite-element Analysis. Part I: Finite Elements for Aligned Fibre Assemblies; Part II: Finite Elements for Yarn Mechanics, *Journal of the Textile Institute*, 88 (1997), Part I, No. 4, 325–351
16. MARC-Manual

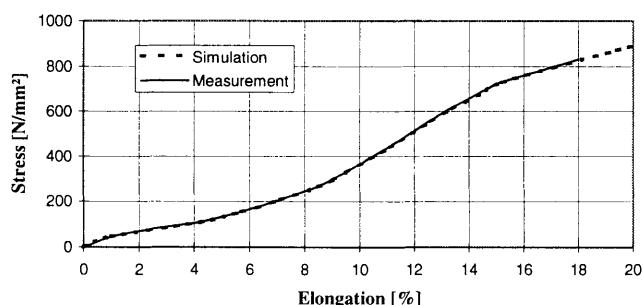


Fig. 1. Comparison of simulation and measurement PA 480 dtex f72 z30

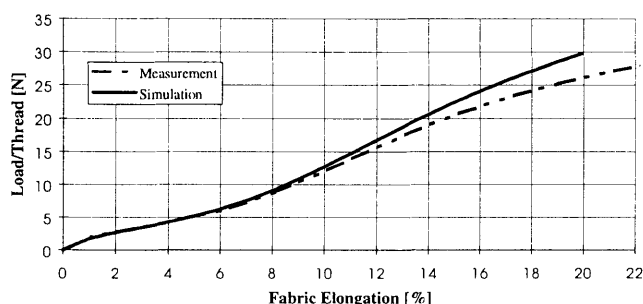


Fig. 2. Comparison of simulation and measurement plain weave weft direction

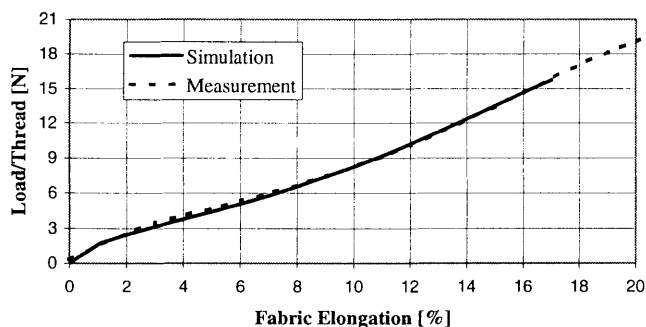


Fig. 3. Comparison of simulation and measurement plain weave warp direction

Methods for Reduction of Manufacturing Costs in Production of Fine Woollen Fabrics

Zoran Stjepanovič¹, Milena Žiberna-Šujica¹, Zoran Grobelšek²,
Danica Voglar-Štic² and Polona Dobnik Dubrovski¹

¹University of Maribor, Faculty of Mechanical Engineering, Maribor, Slovenia

²Merinka-Tkanina d.o.o., Maribor, Slovenia

Influence of composition of woollen fibre mixture on weaving efficiency and production costs when manufacturing fine worsted woollen fabrics will be presented within this contribution. The aim of the research work was to improve the productivity parameters and to reduce the production costs. Fabric quality was carefully observed in order to establish the influence of measures applied on textile products. Two methods to reach the above goals have been investigated. The number of yarn breaks during the weaving process was reduced in both cases. The experiments were carried out in a real production environment using the Dornier weaving machines.

1. INTRODUCTION

The reduction of manufacturing costs is a trend that can be observed constantly also in production of fine woollen fabrics. Wool fibre is relatively expensive raw material, which price is determined by world's market. The market with woollen fibres is controlled by leading producers and distributors, therefore one can not influence the raw material price. On the other hand, we can discover new possibilities regarding better productivity and reduction of costs, caused by low fabric quality. With the aim to reduce the manufacturing costs and quantity of weaving faults, and therefore to contribute to improved economy of production, we have decided to investigate the influence composition of woollen fibre mixtures on weaving efficiency. Two methods to reach the above goals have been investigated. The essence of the first method was the addition of the three percents of PA fibres to a regular woollen mixture. The tensile properties of produced woollen yarns were improved which was reflected in higher efficiency of the weaving process. The second method consists of the substitution of a part of regular woollen fibres with fineness of 20.5 μm in a mixture with finer woollen fibres (19.5 μm). Three parallel analysis were made where we varied the share of finer fibres and observed the resulted effects. This measure increased the number of fibres in a yarn cross-section and consequently improved the yarn's tensile properties. Our goal was to determine which of the above two methods is more suitable considering the quantity of a fabric to be woven, as well as to solve all the technological difficulties that could occur in conquering the new technology. Analysis of results of the research work and achieved effects will be shown in this contribution.

2. THEORETICAL PART

The world market is more and more oriented towards lighter and finer woollen fabrics having low mass and high degree of porosity and air permeability. Such fabrics require fine woollen yarns with linear density between 20 and 10 tex. The production of fine woollen yarns is conditioned with numerous technological difficulties which are reflected as yarn faults and increased number of yarn breaks. The weaving machine efficiency depends on yarn quality and its mechanical properties. Above all the warp is exposed to high dynamic loading during the weaving process. Therefore, the yarn should be engineered in such a manner that it will be strong enough to bear those loading. Knowing the fact that yarn tensile properties can be improved with the right selection of raw material, we decided to add a certain share of stronger, respectively finer fabrics into fibre mixture.

The theoretical part of the research involved:

- Theoretical principles of influential parameters regarding the tensile properties of yarns, produced from different fibres and fibre mixtures,
- A model for prediction of breaking strength of yarns, spun from woollen fibres and mixtures of woollen and polyamide fibres.

2.1 Influence of raw material and yarn structure on breaking strength of spun yarns

The strength of material (fibres, yarns) is determined as a resistance of its inner forces against the action of outer forces (tensile, bending, torsional, etc.), which are trying to destroy material's cohesion and break it. During the technological process, the yarn, and therefore

also fibres, are above all exposed to tensile loading. The yarn breaking strength depends on numerous parameters which can be subdivided into two main groups: fibrous material properties and yarn structure.

2.1.1 Properties of raw material

Generally, the fibre breaking strength depends on number of joining molecules in fibre cross-section, their rigidity and linkage in lamellate crystallites. The breaking strength of idealised pure crystallised fibre can be calculated from the energy of chemical joints between the atoms of functional groups and can be as high as 1000–1200 cN tex⁻¹ [1]. Minimal breaking strength of fibre, required to enable its processing, is approximately 6 cNtex⁻¹. The majority of new spinning techniques do not enable the complete usage of fibre strength which has therefore even higher importance [2]. It has been proved that, considering the same fineness, use of longer fibres results in slight improvement of breaking strength and breaking elongation [3]. More important is the influence of homogeneity and length uniformity of applied fibres. Breaking strength of yarns, spun from fibre blends, is as a rule lower than in yarns, spun out of stronger component. The result depends on a kind of applied fibres and their share in the fibre blend [4].

2.1.2 Yarn structure

Appropriate fibre arrangement in yarn is needed to achieve the optimal exploitation of fibre strength and required yarn appearance and touch. Therefore, the following preliminary conditions must be fulfilled: high degree of straighten and paralleled fibres, right mutual position of fibre ends, appropriate fibre length diagram and wrapping of the whole fibre into the yarn structure [2]. Fibre fineness influences directly the number of fibres in yarn cross-section. Increased number of fibres in yarn cross-section results in better tensile properties of a yarn.

2.2 Model for prediction of breaking tenacity of spun yarns, produced from woollen fibres and wool/polyamide fibres

From a technological point of view, the prediction of spun yarn breaking strength has a great importance. Experimental equations which give solid results are based on simplifications regarding the yarn geometrical structure. Furthermore, this approach presumes that fibre properties remain the same during the whole spinning process. Taking into account the above facts, the breaking tenacity of yarn produced from the blend of wool and polyamide fibres, can be expressed as follows:

$$S = \frac{X_{W_0}}{100} S_{W_0} + \frac{X_{PA}}{100} S_{PA} \frac{\varepsilon_{W_0}}{\varepsilon_{PA}} \quad (1)$$

where:

S – breaking tenacity of yarn spun from Wo/PA blend (cN tex⁻¹)

S_{W_0}, S_{PA} – breaking tenacity of yarns, spun from woollen and polyamide fibres, calculated by Berezina's and Usenko's formulae (cN tex⁻¹)

X_{W_0}, X_{PA} – share of a certain fibre component in a fibre blend (%)

$\varepsilon_{W_0}, \varepsilon_{PA}$ – breaking elongation of a single component yarn after Uster statistics (%)

Berezina's formula for calculation of breaking tenacity of woollen yarn component [5]:

$$S_{W_0} = S_f R \left(0.018 - 0.062 \sqrt{\frac{T_f}{T_y}} \right) K_\alpha \eta \quad (2)$$

where:

S_{W_0} – breaking tenacity of yarn (cN tex⁻¹)

S_f – breaking tenacity of fibre (cN tex⁻¹)

R – fibre quality number

T_f – linear density of fibres (tex)

T_y – linear density of yarn (tex)

K_α – correction factor for twist

η – correction factor for processing techniques.

Breaking tenacity of polyamide yarn component can be calculated by Usenko's formula:

$$S_{PA} = S_f \left(1 - 0.0375 H_0 - \frac{2.8}{\sqrt{\frac{T_y}{T_f}}} \right) z K \beta \quad (3)$$

where:

S_{PA} – breaking tenacity of yarn (cN tex⁻¹)

S_f – breaking tenacity of fibre (cN tex⁻¹)

H_0 – coefficient of processing techniques

T_f – linear density of fibres (tex)

T_y – linear density of yarn (tex)

z – correction factor of fibre length

K – coefficient for effects of yarn twist

β – coefficient for effects of the irregularity of fibre length

Values of correction factors can be found in [5].

3. EXPERIMENTAL PART

With the aim to increase the yarn's breaking strength, improve the productivity parameters and therefore to reduce the production costs, it has been decided

to carry out the research which comprehended two methods [6]:

- Composition of fibre blend made up of 97 % of woollen fibres and 3 % of polyamide fibres.
- Set up of fibre blend of pure woollen fibres with different fineness. A certain share of regular fibres (20.5 μm) was substituted by finer woollen fibres (19.5 μm). Three parallel analysis were made where we varied the share of finer fibres.

The theoretical values of breaking strength, which were calculated using the mathematical expressions worked out in pt. 2.2, were compared with results of analyses of real yarn's breaking strength.

3.1 Composition of fibre blend with up to 3 % of polyamide fibres

The main idea of this method was to replace a small share of woollen fibres with stronger polyamide fibres. It is allowed, namely, to replace up to 3 % of woollen fibres with other fibrous material, and still to declare the produced fabric as 100 % woollen fabric. Using this method we expected the yarn with improved tensile properties which would lead to lower number of yarn breaks during weaving. On the other hand, one must consider also higher costs of dyeing of polyamide fibres in a fibre blend. Woollen fabric in twill weave having surface mass 225 g m⁻² (340 g/running meter) was produced in order to confirm the above statement. Constructional parameters of the fabric are listed in Table 1.

Tab. 1. Constructional parameters of sample woven fabrics

Fibre content	100 % wool
Linear density and twists of warp yarns	17 x 2 tex 700 S (720 z)
Linear density and twists of weft yarns	17 x 2 tex 700 S (720 z)
Warp sett (yarns · 10 cm ⁻¹)	255
Weft sett (yarns · 10 cm ⁻¹)	220
Fabric reed width (cm)	176

3.1.1 Materials

The yarns have been produced and two parallel trials have been observed:

- Regular yarn spun of 100 % merino wool with fineness 20.5 μm and staple length 68 mm
- Yarn spun of fibre blend composed of 97 % of same merino wool as stated above and 3 % of polyamide fibres PA 6, having the fineness 3.3 dtex and staple length 88 mm.

In both cases the technological process was disposed in such a way that all the applied fibres were dyed in a form of worsted tops. Spinning of yarn with

linear density 17 tex and 720 "z" twists followed. This stage of production process was concluded with twisting. Ply yarn 17 x 2 with 700 "S" threads was produced. Dornier weaving machine was used for weaving in both observed cases. Insertion speed was 360 picks per minute.

3.1.2 Registered efficiency parameters

The following results, given in Table 2, have been obtained in practical application of both yarn types [6]:

Tab. 2. End breakage rate and weaving efficiency

Yarn breaks in 8 hours (Break type)	Fabric 1 (100 % wool)	Fabric 2 (97 % wool, 3 % PA)
Break between slay and harnesses	23	14
Break between harnesses and yarn rider	10	8
Break between yarn rider and warp beam	6	1
Total No. of ends down	39	23
Length of fabric (meters per 8 hours)	59	65
Loom efficiency (%)	87	96

3.1.3 Comparison of results

It is a fact that dyeing of polyamide fibres in fibre blend presents additional production cost. However, the savings due to lower number of yarn breaks and improved productivity, enabled up to 3 % reduction of fabric own price. The saving could be even greater taking into account larger fabric orders. Table 3 presents the comparison between indexed costs for particular production stages [6]. Costs of those processes that remained same were treated as constants.

Tab. 3. Comparison of indexed production costs

Cost Type	Price Index	
	Fabric 1 (100 % wool)	Fabric 2 (97 % wool, 3 % PA)
Raw material	100	98,3
Dyeing	100	100,5
Weaving	100	90,8
Together	100	97,8

3.2 Fibre blends of pure woollen fibres with different fineness

From expression (2) it can be seen that use of finer wool fibres leads to increased yarn breaking strength which is reflected in lower number of yarn breaks during weaving and improved weaving machine efficiency. On the other hand it is necessary to

consider higher price of fibre blend due to more expensive finer wool. Therefore, it was our objective to find the optimal balance between the costs and savings. The experiment was based on three parallel fibre blends:

- a)
 - 80 % woollen fibres 20.5 μm
 - 20 % woollen fibres 19.5 μm
- b)
 - 70 % woollen fibres 20.5 μm
 - 30 % woollen fibres 19.5 μm
- c)
 - 60 % woollen fibres 20.5 μm
 - 40 % woollen fibres 19.5 μm

As a reference served the yarn spun from 100 % regular wool fibre 20.5 μm . Fibre length was in all cases constant – 68 mm. Woollen fabric in twill weave having the surface mass 185 g m⁻² (280 g per running meter) was produced next. Constructional parameters of the fabric are listed in Table 4.

Tab. 4. Constructional parameters of sample fabrics

Linear density and twists of warp yarns	17 x 2 tex 450 Z (720 z)
Linear density and twists of weft yarns	28 x 1 tex (540 z)
Warp sett (yarns · 10 cm ⁻¹)	240
Weft sett (yarns · 10 cm ⁻¹)	230

Dornier weaving machines were used for weaving in both observed cases. Insertion speed was 360 picks per minute. One worker served eight weaving machines.

Tab. 5. End breakage rate and weaving efficiency

Yarn breaks (in 8 hours) (Break type)	40 % 19.5 μm 60 % 20.5 μm	30 % 19.5 μm 70 % 20.5 μm	20 % 19.5 μm 80 % 20.5 μm	100 % 20.5 μm
Break between slay and harnesses	22	24	27	31
Break between harnesses and yarn rider	11	12	14	16
Break between yarn rider and warp beam	3	4	5	10
Total No. of ends down	36	40	46	57
Length of fabric (meters per 8 hours)	56.8	54.5	51.6	47.2
Loom efficiency (%)	75.6	72.5	68.6	62.8

Tab. 6. Yarn quality parameters

Raw material	No. of fibres in yarn cross-section	Breaking tenacity predicted (cN tex ⁻¹)	Breaking tenacity measured (cN tex ⁻¹)	Measured breaking elongation (%)
100 % Wo 20.5 μm	37	6.19	5.13	3.91
97 % Wo 20.5 μm 3 % PA 3.3 dtex	39	6.25	6.09	4.60
80 % Wo 20.5 μm 20 % Wo 19.5 μm	39	6.26	5.65	4.12
70 % Wo 20.5 μm 30 % Wo 19.5 μm	39.5	6.30	5.88	4.74
60 % Wo 20.5 μm 40 % Wo 19.5 μm	40	6.34	5.95	4.82

3.2.1 Registered efficiency parameters

The following values, presented in Table 5, have been registered during the production process:

4. DISCUSSION AND CONCLUSIONS

The analyses of results of experimental work have shown the importance of parameters that influence the tensile properties of woollen yarns.

Table 6 presents some predicted and measured properties of yarns involved into experimental part of this research. Confirmed were the assumptions involved into the model for prediction of breaking strength of spun yarns, produced from pure woollen fibres and wool/polyamide fibres. Slight differences, above all regarding the values of predicted and measured breaking tenacity of pure woollen yarns spun out of fibres with fineness of 20.5 μm , can be explained by the impact of spinning process peculiarity. End breakage rate was decreased with application of a certain part of both stronger and finer fibres in fibre blend. With addition of the 3 percents of polyamide fibres the weaving efficiency was improved for 8 percents regarding pure woollen yarns. Also the second method investigated resulted in improved yarn properties and has shown increased weaving efficiency. Although the best results were obtained with fibre blend described as c) in pt. 3.2, the fibre blend with 30 % of finer woollen fibres can be regarded as optimal regarding both weaving efficiency and raw material costs. Loom efficiency was improved for nearly 10 % in this case.

Analyses of raw material costs shown that the application of finer woollen fibre presents considerable increase of a product own price. Therefore, it can be stated that this method to increase the weaving efficiency and therefore to reduce the manufacturing costs can be used in connection with smaller work orders up to 300 meters and lighter, pastel fabric colours. Namely, the application of polyamide fibres in fibre blend sets in these cases major problems from the point of view of dyeing uniformity.

Also the quality and tensile properties of produced woollen fabrics have been improved significantly. The breaking strength of woollen fabric, described in pt. 3.1, was increased for 1.37 % in warp direction and for 11.06 % in weft direction. At the same time the breaking elongation was increased for 4.71 % in warp direction and for 7.97 % in weft direction. It is a fact that those values, together with better fabric quality because of lower number of faults caused by yarn breaks and set marks, contribute to producer's self-confidence and better placement of fabrics on demanding world's markets.

ACKNOWLEDGEMENT

Thanks are due to the European Commission for subsidising the INCO-COPERNICUS Network for Studying the Warp related Weaving Problems, to which belongs the work, described within this contribution.

LITERATURE

1. Bukošek V. et al.: Application of New Raw Materials. Report on Research Work (in Slovenian). Faculty of Natural Sciences and Technology. Department of Textiles, Ljubljana. 1985
2. Klein W.: The Technology of Short-staple Spinning. The Textile Institute, Manchester, 1987
3. Perič P., Oreškovič V.: Physical Properties of Yarn (in Croatian). Tekstil 32(4), 1983, pp. 209–224
4. Seshradi S., Balasubramanian P.: Control of Yarn Strength and Its Variability. The Indian Textile Journal, April 1988, pp. 74–76
5. Žurek W.: The Structure of Yarn. US Department of Agriculture and the National Science Foundation, Washington, D.C., 1975
6. Internal research reports of Merinka Tkanina (in Slovenian), 1996–1998

Mechanics of threads systems (warps, fabrics)

Conception of Plane Elasticity of Fabrics

Prof. RNDr. B. Stříž, DrSc.

TU Liberec

INTRODUCTION

Mechanics of textiles can be based on the application of the equation of continuum mechanics. Every material has its structure, it is not homogeneous, but some materials are closer to the idea of environment continuity than others. That goes for textile materials as well. The model of the continuum is natural for non-woven textiles, and we consider fabrics of various weaves as the continuum. Knitted fabrics are furthest to the idea of continuum. In spite of that we can introduce, even for such a textile, and thus for every material, the substitute continuum of the same mechanical properties. The equations of mechanics and physics go for this substitute continuum. The problem is to determine the deformational properties of the textile and assign them to the substitute continuum.

The textile is such a special formation that it is necessary to describe its mechanical properties for each specific state of stress and reformation. Unlike the solid bodies, the uniaxial state of stress of the textile does not capture its mechanical properties. That is why the strength hypotheses are of no use for them. It is fundamental to determine for the textile stressed by biaxial state of stress and reciprocally perpendicular directions whether these directions are principal even for deformations. If so, the textile behaves as the transversal isotropic continuum. In the opposite case it behaves as a flat anisotropic material. It concerns, especially, non-wovens, multilayer fabrics, knitted fabrics, textile composites, and the like.

For the determination of mechanical properties of textiles, it is fundamental to carry out the experiment

when the given outer biaxial stress of textile (Fig.1) and the shifts are measured by means of the "picture analysis Lucie". The non-dimensional shifts u_{ij} are calculated on the basis of the relations between the coordinates in Lagrangian and Euler description of motion of particles of the continuum. Even small forces, acting at the level of the textile, can cause big reformations. That leads to the necessity to apply non-linear mechanics of the continuum, namely for geometric and physical reasons. Due to the fact that with the change of geometry of the starting element also the inner forces, which affect them, are changed, it is necessary to determine the Cauchy tensor of real tensions (of relative forces) and the energy conjugated Almansi tensor of deformation corresponding to it.

Relations for the deformation tensor and the tensor of real relative forces

The Almansi tensor of deformation is determined by the dependence corresponding to the Euler description of the continuum motion (so called spatial coordinates) [1]:

$$\varepsilon_{ij} = \frac{1}{2} \left[\frac{\partial u_i}{\partial x_j} + \frac{\partial u_j}{\partial x_i} - \frac{\partial u_k}{\partial x_i} \frac{\partial u_k}{\partial x_j} \right] \quad (1)$$

Assuming the equivalence of the deformation of the textile and the deformation of the substitute homogeneous plane medium, it is possible to determine the process of calculation of tensor deformation for the final small area of the textile. The position of the general point A of the plane continuum

is determined in the Lagrangian (material) coordinate system by its projections x_1^0, x_2^0 . Due to the continuum reformation it shifts to the position A' by the value u , with the components u_1, u_2 (Fig. 2). The Euler coordinates of the shifted point are.

$$x_i = x_i^0 + u_i, \quad i = 1, 2 \quad (2)$$

The near point B , with coordinates $x_i^0 + dx_i^0$, is shifted to the position B' with coordinates $x_i + dx_i$. The differential of the equation (2) depending on material coordinates x_i^0 is of the form.

$$dx_i = dx_i^0 + u_{ij} dx_j^0, \quad u_{ij} = \frac{\partial u_i}{\partial x_j^0} \quad (3)$$

For the determination of four non-dimensional shifts u_{ij} of the small textile element, we will approximately express the equation (3) in the differential form

$$\Delta x_i = dx_i^0 + u_{ij} \Delta x_j^0$$

and the differences will be determined as the differences of coordinates of peaks of the element in the diagonal direction (Fig. 1) that means: up to the deformation and after the deformation. We will get (the second index [superscript] of the coordinate denoting the point number)

$$\begin{aligned} (1 + u_{11})(x_{11}^0 - x_{13}^0) + u_{12}(x_{21}^0 - x_{23}^0) &= x_{11} - x_{13} \\ (1 + u_{11})(x_{12}^0 - x_{14}^0) + u_{12}(x_{22}^0 - x_{24}^0) &= x_{12} - x_{14} \\ u_{21}(x_{11}^0 - x_{13}^0) + (1 + u_{22})(x_{21}^0 - x_{23}^0) &= x_{21} - x_{23} \\ u_{21}(x_{12}^0 - x_{14}^0) + (1 + u_{22})(x_{22}^0 - x_{24}^0) &= x_{22} - x_{24} \end{aligned} \quad (4)$$

We will express the shift derivation in the equation (1). It holds true

$$\frac{\partial u_i}{\partial x_k} = u_{ij} \frac{\partial x_j^0}{\partial x_k}, \quad i, j, k = 1, 2 \quad (5)$$

The spatial deformation gradient $(\partial x_j^0 / \partial x_k)$ will be determined in the differential form by inverting a matrix (4). We will get where

$$\begin{aligned} \frac{\Delta x_j^0}{\Delta x_k} &= \frac{A_{kj}}{J}, \quad A_{11} = 1 + u_{22}, \quad A_{22} = 1 + u_{11} \\ A_{12} &= -u_{21}, \quad A_{21} = -u_{12}, \quad J = A_{11}A_{22} - A_{12}A_{21} \end{aligned} \quad (6)$$

The deformation tensor (1) in the non-dimensional shifts u_{ij} is expressed in the form

$$\begin{aligned} \varepsilon_{ij} &= (2J^2)^{-1} \{ J(u_{i1}A_{j1} + u_{i2}A_{j2} + u_{j1}A_{i1} + u_{j2}A_{i2}) - \\ &\quad - (u_{11}A_{i1} + u_{12}A_{i2})(u_{11}A_{j1} + u_{12}A_{j2}) - \\ &\quad - (u_{21}A_{i1} + u_{22}A_{i2})(u_{21}A_{j1} + u_{22}A_{j2}) \} \end{aligned} \quad (7)$$

For expressing the Cauchy tensor of real relative forces n_{ij} of the deformed textile, we will apply the symmetric second tensor Piola-Kirchhoffa of relative forces n_{mk}^0 [1], which is the well-known loading of the

cross pattern bends of the textile sample in preparation:

$$n_{ij} = \frac{1}{J} \frac{\partial x_i}{\partial x_m^0} n_{mk}^0 \frac{\partial x_j}{\partial x_k^0} \quad (8)$$

If we replace material deformation gradients by differences, then on the basis of the equations (4), (6) we will get:

$$\frac{\Delta x_1}{\Delta x_1^0} = A_{22}, \quad \frac{\Delta x_2}{\Delta x_2^0} = A_{11}, \quad \frac{\Delta x_1}{\Delta x_2^0} = -A_{21}, \quad \frac{\Delta x_2}{\Delta x_1^0} = -A_{12} \quad (9)$$

Using the symmetry of both tensors, we will get the components of the Cauchy tensor of real relative forces acting at the element of the textile by dependencies:

$$\begin{aligned} n_{11} &= J^{-1} [A_{22}^2 n_{11}^0 - 2A_{21}A_{22} n_{12}^0 + A_{21}^2 n_{22}^0] \\ n_{12} &= J^{-1} [-A_{12}A_{22} n_{11}^0 + (A_{11}A_{22} + A_{12}A_{21}) n_{12}^0 - \\ &\quad - A_{21}A_{11} n_{22}^0] \\ n_{22} &= J^{-1} [A_{12}^2 n_{11}^0 - 2A_{11}A_{12} n_{12}^0 + A_{11}^2 n_{22}^0] \end{aligned} \quad (10)$$

GENERAL PHYSICAL DEPENDENCIES IN A LEVEL ANISOTROPIC MEDIUM

We will assume that the directions 11, 22 are not principal for deformation tensors and relative forces. For the deformation tensor (7) we will determine the main directions 1, 2.

(Fig. 1) and we will calculate the main deformation components $\varepsilon_1, \varepsilon_2$ and the components of the tension tensor n_1, n_2, n_τ . If both tensors are coaxial, it will be $n_\tau = 0$, where we assume a small error in calculation. Let be $n_\tau \neq 0$, that means: the fabric is anisotropic. In its case, it is impossible to expect the orthotropy, because the symmetric structure of the textile up to the deformation can change into non-symmetric due to non-symmetric loading.

For the small interval of validity the equations [2] will be fulfilled:

In the directions 11, 22:

$$\begin{aligned} n_{11} &= E_{11}\varepsilon_{11} + A_{12}\varepsilon_{22} + 2A_{14}\varepsilon_{12} \\ n_{22} &= A_{12}\varepsilon_{11} + E_{22}\varepsilon_{22} + 2A_{24}\varepsilon_{12} \\ n_{12} &= A_{14}\varepsilon_{11} + A_{24}\varepsilon_{22} + 2E_{4}\varepsilon_{12} \end{aligned} \quad (11)$$

In the directions 1, 2:

$$\begin{aligned} n_1 &= E_1\varepsilon_1 + B_{12}\varepsilon_2 \\ n_2 &= B_{12}\varepsilon_1 + E_2\varepsilon_2 \\ n_\tau &= B_{14}\varepsilon_1 + B_{24}\varepsilon_2 \end{aligned} \quad (11)$$

Among mechanical parameters the relations resulting from dependencies of the continuum mechanics hold true:

$$\begin{aligned}
E_1 &= E_{11}b_1^4 + E_{22}a_1^4 + E_4a_2^2 + 0.5A_{12}a_2^2 + \\
&\quad + 4A_{14}a_1b_1^3 + 4A_{24}a_1^3b_1 \\
E_2 &= E_{11}a_1^4 + E_{22}b_1^4 + E_4a_2^2 + 0.5A_{12}a_2^2 - \\
&\quad - 4A_{14}a_1^3b_1 - 4A_{24}a_1b_1^3 \\
B_{12} &= (E_{11} + E_{22})a_1^2b_1^2 + A_{12}(a_1^4 + b_1^4) - E_4a_2^2 + \\
&\quad + 4A_{14}(a_1^3b_1 - a_1b_1^3) + 2A_{24}(a_1b_1^3 - a_1^3b_1) \\
B_{14} &= -E_{11}a_1b_1^3 + E_{22}a_1^3b_1 + 2E_4(a_1b_1^3 - a_1^3b_1) + \\
&\quad + A_{12}(a_1b_1^3 - a_1^3b_1) + A_{14}b_1^2(b_1^2 - 3a_1^2) + \\
&\quad + A_{24}a_1^2(3b_1^2 - a_1^2) \\
B_{24} &= -E_{11}a_1^3b_1 + E_{22}a_1b_1^3 + 2E_4(a_1^3b_1 - a_1b_1^3) + \\
&\quad + A_{12}(a_1^3b_1 - a_1b_1^3) + A_{14}a_1^2(3b_1^2 - a_1^2) + \\
&\quad + A_{24}b_1^2(b_1^2 - 3a_1^2)
\end{aligned} \quad (12)$$

$a_1 = \sin\varphi$, $b_1 = \cos\varphi$, $a_2 = \sin 2\varphi$, $b_2 = \cos 2\varphi$ (Fig 1.)

By solving the system of equations (11), (12), and (13) we will determine the mechanical parameters of the textile: the modules of elasticity E_{11} , E_{22} , the module of slide elasticity E_4 and the Poisson numbers.

$$v_{12} = \frac{A_{12}}{\sqrt{E_{11}E_{22}}}, \quad v_{14} = \frac{A_{14}}{\sqrt{E_{11}E_4}}, \quad v_{24} = \frac{A_{24}}{\sqrt{E_{22}E_4}} \quad (14)$$

TRANSVERSAL ISOTROPY OF FABRICS

If the principal axes of the deformation tensor and the Cauchy tensor of relative forces are approximately coaxial, the system of equations (11–13) is badly conditional. The determinant of the system of equations is near to zero. In that case it is convenient to look for an approximate solution. Regarding the fact that for the orthotropic materials (axes alignment of both tensors) is $v_{14} = v_{24} = 0$, are $A_{14} = A_{24} = 0$ and from the equation of the continuum mechanics

$$G = (E_{11} + E_{22} - 2A_{12})a_1^2b_1^2 + E_4b_2^2 + 2A_{14}(a_1^3b_1 - a_1b_1^3) + 2A_{24}(a_1b_1^3 - a_1^3b_1) \quad (15)$$

and the approximate equality $G \cong E_4$ we will determine [3]

$$A_{12} = \frac{1}{2}(E_{11} + E_{22}) - 2E_4 \quad (16)$$

Then from the systems (11) and (13) it will follow

$$\begin{aligned}
E_4 &= \frac{n_{12}}{2\varepsilon_{12}} \\
E_{11} &= \frac{\varepsilon_{12}(n_{11}(\varepsilon_{11} + 2\varepsilon_{22}) - n_{22}\varepsilon_{22}) + 2n_{12}\varepsilon_{22}^2}{\varepsilon_{12}(\varepsilon_{11} + \varepsilon_{22})^2} \\
E_{22} &= \frac{\varepsilon_{12}(n_{22}(2\varepsilon_{11} + \varepsilon_{22}) - n_{11}\varepsilon_{11}) + 2n_{12}\varepsilon_{11}^2}{\varepsilon_{12}(\varepsilon_{11} + \varepsilon_{22})^2} \\
v_{12} &= \frac{\frac{1}{2}(E_{11} + E_{22}) - 2E_4}{\sqrt{E_{11}E_{22}}}
\end{aligned} \quad (17)$$

In limit for $\varepsilon_{12} \rightarrow 0$ and $n_{12} \rightarrow 0$ we will get

$$\begin{aligned}
E_1 &= E_2 = \frac{n_1\varepsilon_1 - n_2\varepsilon_2}{\varepsilon_1^2 - \varepsilon_2^2} \\
E_4 &= \frac{n_1 - n_2}{2(\varepsilon_1 - \varepsilon_2)} \\
v_{12} &= \frac{n_1\varepsilon_2 - n_2\varepsilon_1}{n_1\varepsilon_1 - n_2\varepsilon_2}
\end{aligned} \quad (18)$$

CONCLUSION

As a rule, fabrics have different mechanical properties in various directions at uniaxial stress. Under the stress by biaxial tension in mutually perpendicular directions at biaxial structure (warp – weft) they become, so called, transversally isotropic. Mechanical properties are determined by five parameters: by two in the surface of textile (e.g. E_1 , v_{12}) and by three in the direction of the normal to the textile surface (E_3 , v_{13} , v_{23}). The last three cannot be determined experimentally and they are even not necessary. Then, from the practical point of view, the fabric behaves as an isotropic material whose mechanical properties are dependent on the instant state of stress, and its deformations. In the narrow interval of the validity of the equations (11), the so called “secant” modules can express relations (17) in the physically non-linear area.

The work was developed thanks to the grant of the agency GACR (Grant Agency of the Czech Republic) 106/97/0372.

LITERATURE

1. Chandrasekharaian, D. S., Lokenath Debnath: Continuum Mechanics, Academic Press, 1994
2. Cernych, K. F.: Vvedēnīe v anizotropnuju uprugost', Moskva, 1988.
3. Stříž, B.: Identifikace mechanických vlastností plošných textilií, In: Engineering Mechanics 1998, Svratka, 11–14 May 1998

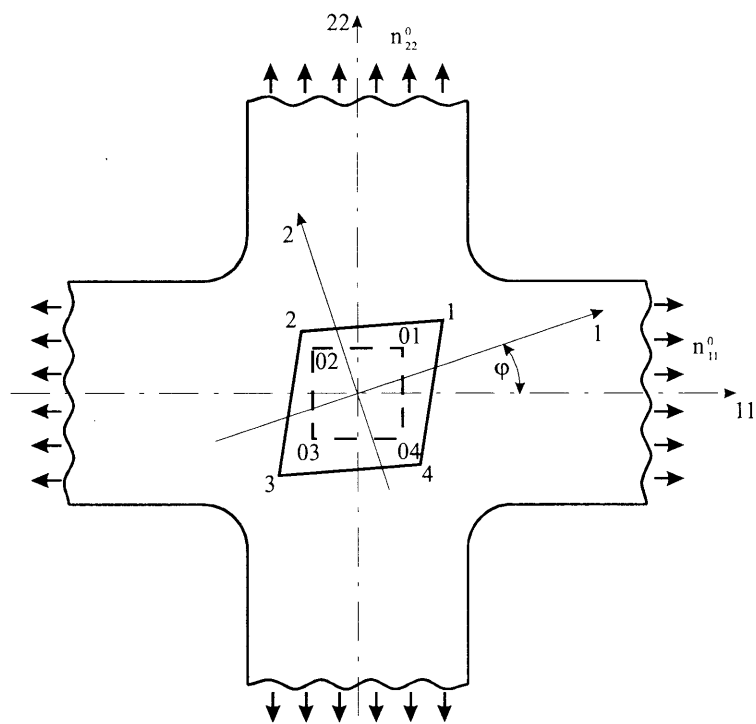


Fig. 1.

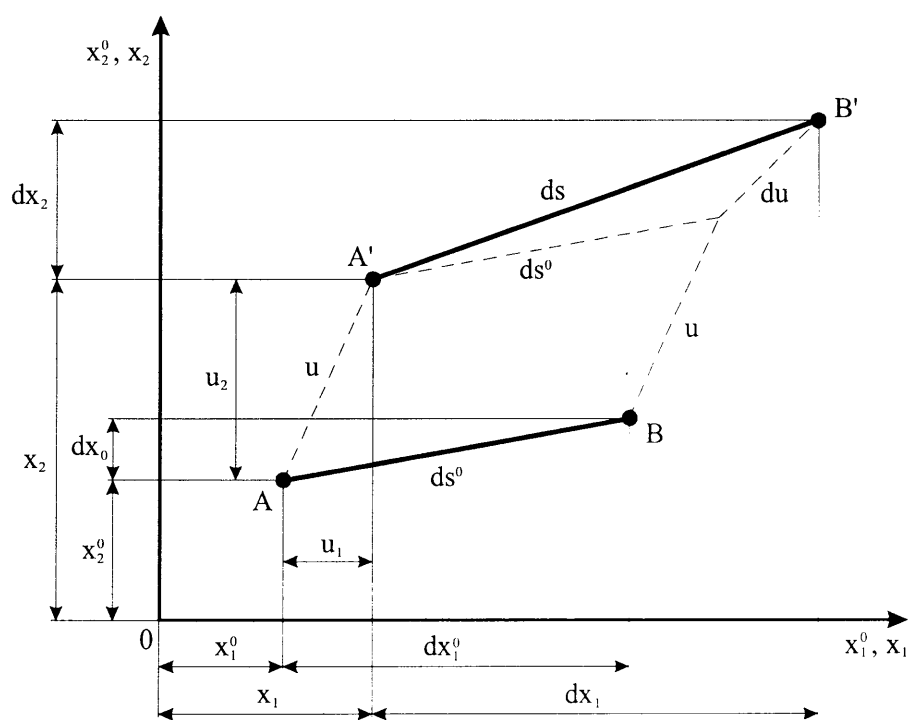


Fig. 2.

The tension pulses generated in the textile linear products

Janusz Szosland and Zbigniew Stempień

The Technical University of Lodz

SOURCES OF TENSION PULSES GENERATED IN VISCO-ELASTIC LINEAR TEXTILE PRODUCTS

In the present century the operating speed of a greater part of the textile machinery has been on average increased about tenfold. On the other hand, more and more textiles, whether as self-contained products or important parts of textile structures, are exposed to substantial impact loads of which their capability to carry is often important for the safety of man and equipment. The new high kinematic and dynamic values have generated new qualitative and quantitative phenomena among which the tension pulses in linear textiles are of particular importance.

METHODS OF INVESTIGATION OF THE PROPAGATION OF TENSION PULSES IN LINEAR TEXTILES

Methods employed hitherto

Already in the 1960's the propagation of tension pulses was studied by hitting a thread with a projectile shot from a miniature cannon. This produced first a transverse wave and then a longitudinal wave. Then came the work of M. Czołczyński [1]. The advantages of Czołczyński's method are that it preserves continuity of the test object and permits repeated analysis of pulse propagation and of the part played in it by the friction barriers.

There is need for analysis of the propagation of longitudinal tension pulses as there is incomplete understanding of a number of phenomena such as, for instance, the rebounding of a pulse from an insurmountable barrier, collision of pulses, occurrence of resonance, distribution of momentary elongation and momentary distribution of tension loads, as well as changes in the structure and physical properties of the test object caused by the passage of a tension pulse.

Guidelines for a method of assessment of the propagation of a longitudinal tension pulse

In this situation important are becoming the experimental methods. What makes it even more difficult is that the high accuracy must be attained in absence of electrical conductivity, as the tested object

is usually non-conductive, at a rate of propagation of the longitudinal tension pulse between 500 and 5000 m/s, without the pulse energy being absorbed by the tension gauge, and when the duration of the phenomenon is often no more than 100 μ s.

All effective methods used in the investigating of the propagation of tension pulses in linear textile products were essentially confined to recording the displacements of the selected cross-sections of the tested threads. The measurement is based on a non-contact observation of a selected length of the test thread, while recording the effects in real time (Fig. 1).

Known are three methods which are based on the principle as presented in Fig. 1:

a) *The method based on electrical capacitance*: – the advantages of the method consist in the direct measurement of a displacement and simple test circuit. Its disadvantages include the necessity to calibrate each converter, disturbance of thread structure around the moving electrode, low repeatability of the measurements, and susceptibility to transverse vibration.

b) *The method based on emf induction*: – the advantages of the method include direct measurement of the rate of displacement and simple test circuit, whereas the disadvantages are non-linear conversion, difficult calibration, susceptibility to transverse vibration, and no possibility to measure the constant component.

c) *The cinematographic method*: – The observer in this method is a high-speed movie camera. The response is recorded by filming the mark placed on the test object and entering the data in the memory of a video camera or recording it on film. Preliminary tests [4] have shown that it is the only method which ensures a true mapping of the displacements of the cross-sections of a thread. Its disadvantage, however, is the need to use an expensive cinematographic apparatus (capable of recording up to 10000 frames per second) and analyse hundreds of metres of film. To offset this disadvantage a modification of the cinematographic method was developed.

The method used for determining the kinematics of cross-sections of linear textiles

The device which records responses of the thread to singular tension loads is an optical oscilloscope consisting of an optical microscope and a rotating camera (Fig. 2).

The microscopic picture of the observed segment of the thread is projected on the peripheral surface of the rotary drum with a taut photographic film. The camera is located in a dark room.

The flash lights (5) are triggered one after another by the control unit (9) upon sensing by the detector (3) of a passing tension pulse. The correct timing of pulse location and triggering of the flash lights is controlled through the oscilloscope (8) and light detector (6). The duration of a flash is selected so as not to exceed the time of a single revolution of the drum in order to avoid a repeated exposition of the film.

Test results

The test object was a 5.25 m long elastomer in a wrap. The tension pulse was generated as in Czołczyński's method [1]. The tension was fixed at 2,000 cN and loading of the auxiliary tension member at 500 cN. The tests were programmed so as to enable investigation into the kinematics of the tension pulse itself and the kinematics of the cross-section located half way along the length of the test object and cross-sections located in the area of pulse rebound from an insurmountable barrier (Fig. 3).

Kinematics of the cross-section of a thread in response to a tension pulse

For numerical analysis all photograms are processed in a computer. The exposed streak which represents the travelling segment of the thread is described, by the computer program, along its contour by Bezier four-control-point parametric functions:

$$x(u) = P_{0x}(1-u)^3 + P_{1x}3u(1-u)^2 + P_{2x}3u^2(1-u) + P_{3x}u^3$$

$$t(u) = P_{0t}(1-u)^3 + P_{1t}3u(1-u)^2 + P_{2t}3u^2(1-u) + P_{3t}u^3$$

$$0 \leq u \leq 1$$

$P_0 \dots P_3$ – co-ordinates of control points on plane $x-t$ (travel-time).

The rate is determined by dividing the derivatives of the parametric functions.

In Fig. 4 represented is the response of a cross-section at distance of 3 m from the source of the tension pulse. The vibration period is 8.3 ms, which means that for the test object the average rate of travel of the tension pulse, at the pre-set initial tension, is about 630 m/s. At the moment the pulse arrives at the observed cross-section the latter continues to travel until all pulse has passed through. In that time, the rate of travel of the cross-section attains a maximum value of about 5 m/s. Upon passage of all impulse, the cross-section remains relatively static until the arrival of the rebounded wave, whereupon the cross-section reverses at a rate reduced to about 3 m/s. This is

caused by changes in the pulse front geometry which are due to damping by the test object itself and attenuation associated with the rebounding from the insurmountable barrier.

The effect of disturbances in the structure of a thread on the propagation of a tension pulse

With the test conditions being as in Fig. 4 external disturbances in the form of knots were introduced to the structure of the test thread: a) without an external disturbance of structure; b) structure disturbed by 1 knot; c) structure disturbed by 6 knots.

The obtained photograms show that the introduced disturbances have no significant effect on the kinematics of the observed cross-section.

Analysis of the changes in the very shape of the marks

Also analysis of the changes in the very shape of the marks of the selected cross-sections is very helpful in the evaluation of the destruction of the threads due to the dynamic longitudinal loading:

– in the case of a monofilament (Fig. 5a) – here is only deformation of the thread material.

– in the case of a spun yarn (Fig. 5b) – the response represents a deformation of the thread material but not always of all the component fibres alike. A simplified model is shown in Fig. 6.

The observation is very important for evaluation of the destruction of the thread and particularly important for identification of the breaking of the thread.

The role of friction barriers in the propagation of impact tension pulses (impact load waves)

It is known that in the propagation of an impact tension pulse or impact load wave an important part is played by various friction barriers each of which can present an obstacle which is either surmountable, at least in part, or completely insurmountable. In the latter case all of the dynamic load wave rebounds from the barrier with possibly a very destructive effect on its carrier, i.e. the thread which is transmitting it.

Of all the friction barriers special attention should be paid by researchers to the edge-type barriers. Examples of such barriers are the healds and reed dents. To assess the degree of destruction which a thread of yarn undergoes when passing through a friction barrier, used was an impact pulsator provided with various types of friction barriers (Fig. 7) selected so as to simulate the conditions existing on a weaving loom.

Evaluated were:

- changes in length of zones $L I$ and $L II$ marked on the test threads;
- breakage of the threads.

For the purposes of the test selected were the two types of friction barriers: barriers with an edge-like surface of friction and barriers with a rounded surface of friction. One of the rounded-surface barriers satisfied the condition of offering the same resistance to the passage of a thread as an edge-type barrier ($\Delta F_b = \Delta F_0$) and another the condition of having the same wrap angle ($< \alpha_b = < \alpha_0$).

The number of cyclic longitudinal impact loads (n) was varied between 1000 and 15000.

It was found that with the adopted test conditions:

- Where there was no friction barrier the values of elongation were negligibly small, $\Delta L I = \Delta L II$;
- Where a friction barrier was present:

Elongation of the threads in the zones was varied, but always $\Delta L I > \Delta L II$;

For all types of friction barriers elongation in zone $L I$ was greater than in the case with no barrier;

For barriers with rounded friction surfaces elongation in zone $L II$ was lower than in the case with no barrier;

With impact tension pulses in excess of 10000 the number of breaks on the edge-type barriers was so great as to prevent further testing.

These results seem to indicate that the impact tension pulses generated by the moving clamp of the pulsator do not surmount the friction barrier, but instead they rebound from it many hundreds of times, travelling backwards and forwards between the clamp and the barrier until decay. It is manifested by an increased length of zone $L I$ and means greater destruction of the

thread. In the test, it was also reflected by a clearly increased breakage of the threads.

It can be seen that the edge-type friction barrier had the most destructive effect. The comparing of the destructive action of different types of friction barriers, based on the same values of their frictional resistance and wrap angle of the thread, proved ineffective, and it points up the need of a different approach to the edge-type barriers, as the phenomena they generate are qualitatively and quantitatively different. The results of the investigation of which only a small part is presented seem to indicate that friction barriers, especially the edge-type barriers, play an important role in the propagation of impact tension pulses or impact load waves.

LITERATURE

1. Czołczyński M.: Rozchodzenie się impulsu napięciowego w nitkach oraz przechodzenie jego przez bariery cierne i masowe (*Propagation of a tension pulse in a linear textile and its passage through frictional and massive barriers*). Doctoral thesis, Technical University of Łódź, 1972
2. Szosland J.: Znacznikowa metoda oceny nierównomierności dynamicznych napięć nitki osnowy podczas tkania (*A method using marks for assessment of variation in the dynamic tension of warp ends in weaving*). Przegląd Włókienniczy 1990, 5, 145
3. Stępień Z.: Opracowanie metody pomiaru propagacji impulsów napięciowych w lepko-sprężystych liniowych wyrobach włókienniczych (*Developing a method for measurement of tension pulse propagation in visco-elastic linear textiles*). Research project financed by KBN, 1995–96

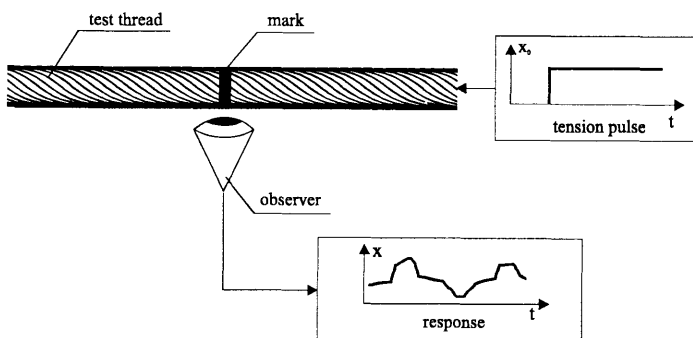
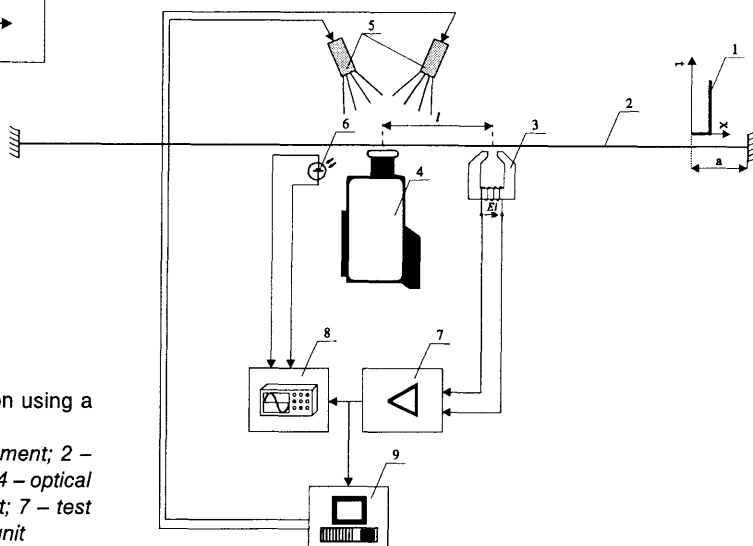


Fig. 1. Schematic diagram of non-contact observation of a selected length of thread

Fig. 2. Test rig for analysis of tension pulse propagation using a high-speed camera:

- 1 – tension pulse represented as a unit displacement; 2 – test object; 3 – detector of tension pulse passage; 4 – optical oscilloscope; 5 – flash lights; 6 – detector of light; 7 – test amplifier; 8 – recording oscilloscope; 9 – control unit



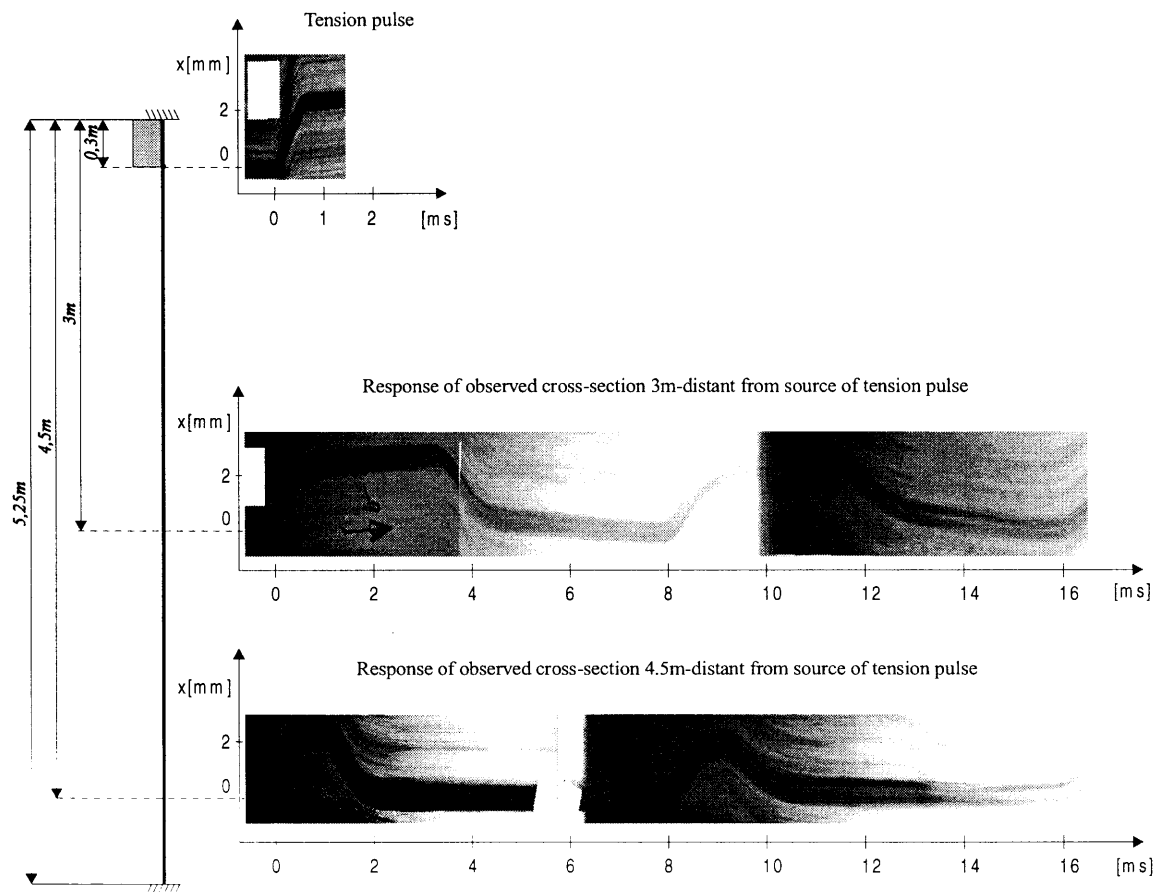


Fig. 3. Photographs of displacements of selected cross-sections

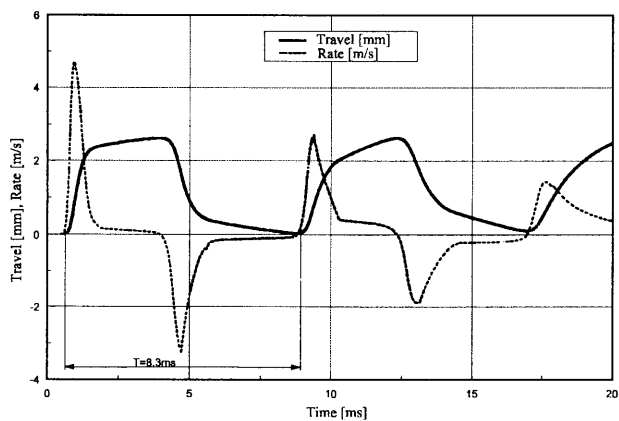


Fig. 4. Response of cross-section to tension pulse

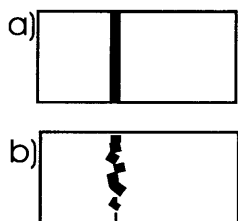


Fig. 5. Views of cross-section marks; a) monofilament, b) spun yarn

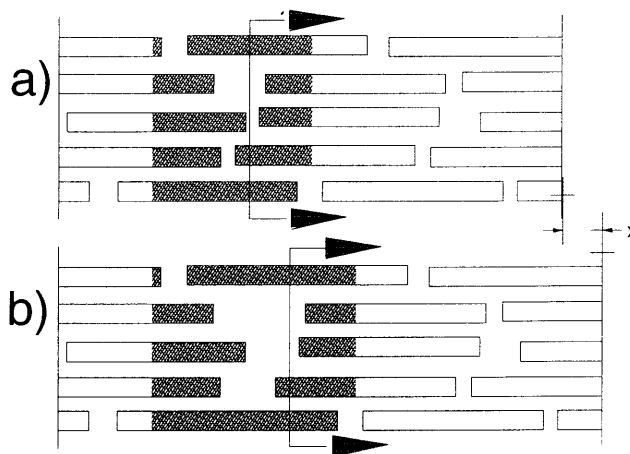


Fig. 6. A simplified model of the behaviour of a spun yarn subjected to longitudinal loading

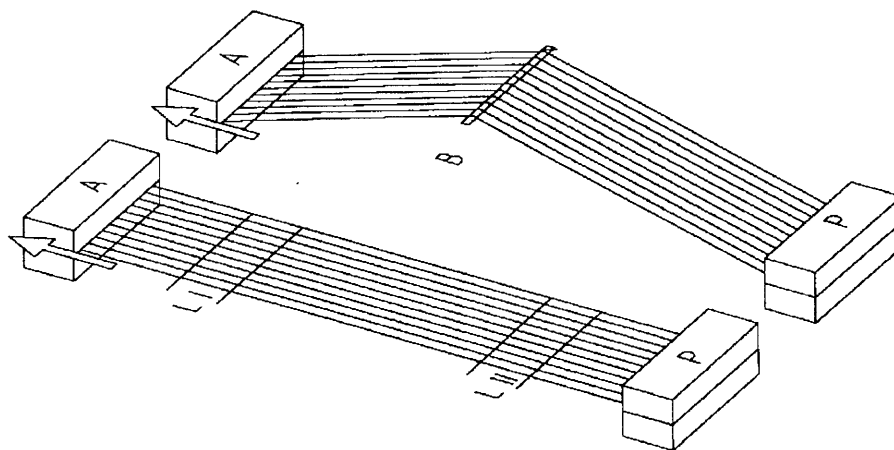


Fig. 7. A schematic diagram of impact pulsator with friction barriers and with test zones L I and L II marked on the test threads

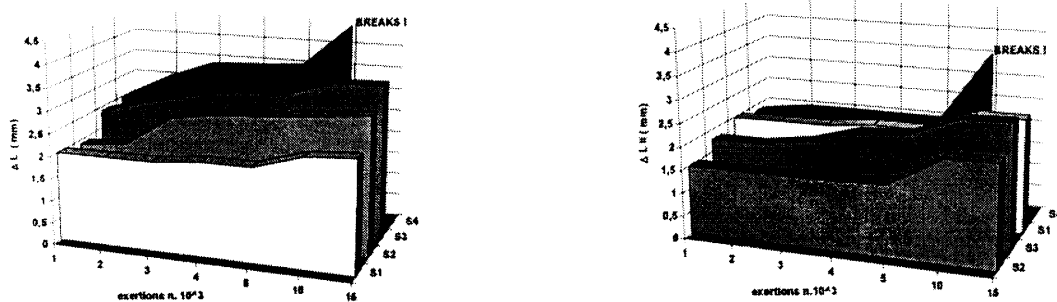


Fig. 8. Values of elongation in zones L I and L II for varied number of impact tension pulses (n) and conditions of friction: S_1 – without a friction barrier; S_2 , S_3 – with rounded-surface barriers, respectively with wrap angle same as S_4 , and with friction resistance same as S_4 ; and S_4 – with an edge-type barrier

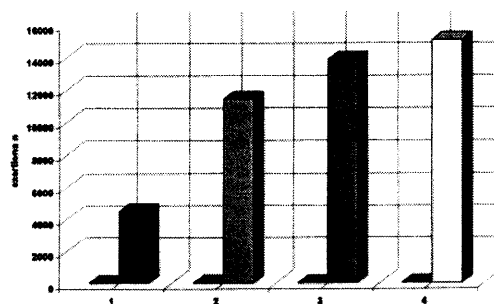


Fig. 9. Number of impact pulses (n) till break of thread on pulsator: 1 – edge-type barrier; 2, 3 – rounded-surface barriers (with friction resistance and thread wrap angle same as on edge-type barrier); 4 – without friction barrier

Tension Pulse Propagation through the Warp (numerical solution)

J. Mevald and J. Nosek

INTRODUCTION

Dynamic phenomena in the linear elastic continuum, described by partial differential equations, can be investigated by analytic methods in many technical applications. For example, the longitudinal vibration, or the impact in non-damped, thin, elastic bars, was already mentioned by Timošenko in his textbook on vibration in 1928. Wave phenomena, tension pulse propagation and impact actions in the elastic continuum with inner damping, or with dispersion, are described, for example, by Brepta [1].

The analysis of tension pulse propagation through warp modeled as the visco-elastic continuum, is complicated due to warp pre-stress, to non-linearities in dynamic behaviour of warp threads, to marginal conditions, including interactions with the environment, and so on. It is possible to suppose that a more fitting description of real dynamic actions leads to non-linear differential partial equations whose analytic solution is impossible. If we substitute the continuum by the discrete system of elements n of the chain, which the system n – of ordinary second-order differential equations (in general non-linear) corresponds to, we can usually solve the problem by a suitable numerical method. If there is a sufficient number of elements n of the discrete model (with regards to the velocity of tension pulse propagation, i.e. regarding the tension wave length), the dynamic response of the model is approaching the response of the real continuum. The error of the numerical solution depends not only on the fitting of the chosen model, and on the accuracy and reliability of the determination of the input parameters, but mainly on the character of the short-time pulse or impact.

The aim of this work is to point out some possibilities of the description of the warp discrete model regarding the investigation of dynamic actions occurring in warp during weaving.

Numerical values of input parameters are chosen; they can be understood only as values of orientation for qualitative assessment of the model. It is obvious that for a more exact description of the real system, it is necessary to come out from the measured values and to compare the results of numerical simulated solutions with the results of the experiment.

Solitary pulse propagation – method of physical discretisation

The warp thread is considered as a chain composed of identical elements – links which substitute the visco-elastic properties of the homogeneous continuum in the dynamic regime. The simple linear type of the link composed of parallel tied-up spring of rigidity k [N/m], with a cataract having the damping coefficient b [N s/m], in connection with the element mass m [kg], as shown in Figure 1a: the so-called Kelvin-Voigt model. In Figure 1b, there is the chain link with linear visco-elastic members, considered as the standard model. An example of a link with a non-linear dissipated member, with the character of the Coulomb friction force r [N], is shown in Figure 1c. It is evident that with a suitable arrangement (parallel or serial) of different groups of springs, cataracts, or non-linear members, it is possible to create a model with the required visco-elastic properties, including inertial effects. A specific problem is to determine the input parameter values of the chosen model on the basis of suitable experiments.

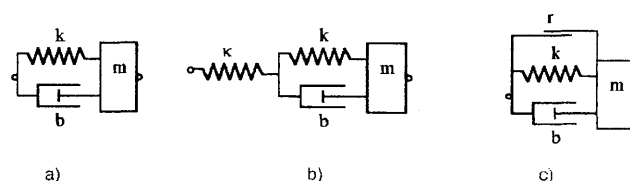


Fig. 1. Examples of link types for dynamic analysis of homogeneous chain

Amplitudes of shifts and forces from periodical pulses – method of transfer matrixes

Let us consider the constant artificial vibration in the axial direction caused by periodical pulses transferred into the tight warp. We again replace the warp by the chain composed of elements n , containing springs and cataracts, with linear characteristics. If we investigate the constant state (after fading away the transient process after the start), the amplitudes of shifts and forces, at excitation by periodical pulses, can be investigated by the method of transfer matrixes [3]. In the case of the linear system, it is possible to

approximate the periodical function by the Fourier series and to superimpose the individual response components into the resulting amplitudes. The transfer relation between the state vectors z_{i-1} and z_i in the form of $A_i \cdot z_{i-1} = z_i$ holds for the linear elements according to Figure 1a. After distribution it has the following form

$$\begin{bmatrix} 1 & \frac{1}{k_i + j\omega b_i} \\ -m_i \omega^2 & 1 - \frac{m_i \omega^2}{k_i + j\omega b_i} \end{bmatrix} \begin{pmatrix} u_{i-1} \\ N_{i-1} \end{pmatrix} = \begin{pmatrix} u_i \\ N_i \end{pmatrix} \quad (5)$$

or for the chain element i according to Figure 1b the following transfer relation holds

$$\begin{bmatrix} 1 & \frac{\kappa_i + j\omega b_i}{k_i \kappa_i + j\omega b_i (k_i + \kappa_i)} \\ -m_i \omega^2 & 1 - \frac{m_i \omega^2 (\kappa_i + j\omega b_i)}{k_i \kappa_i + j\omega b_i (k_i + \kappa_i)} \end{bmatrix} \begin{pmatrix} u_{i-1} \\ N_{i-1} \end{pmatrix} = \begin{pmatrix} u_i \\ N_i \end{pmatrix} \quad (6)$$

In the preceding relations j stands for an imaginary unit. In the case of the homogeneous chain, the transfer matrix of the element i is obviously $A_i = A$, for $i = 1, 2, 3 \dots n$. At the kinematic periodical excitation in the form of the harmonic row on the left end of the chain (like the action of the solitary pulse in Figure 2), it is possible to record the transfer relation through the non-homogeneous chain in the form of

$$A_n \cdot A_{n-1} \cdot A_{n-2} \dots A_i \dots A_2 \cdot A_1 \cdot z_0 = z_n$$

resp. $Cz_0 = z_n$, where $C = \prod_{i=1}^n A_i$ (7)

In the case of the homogeneous chain the total transfer matrix, in the preceding transfer relation, is $C = A^n$. Regarding the marginal conditions, we know $u_0 = a_{0v}$, $U_v = 0$, $\omega = \omega_v = v\omega$ and we will calculate N_{0v} from the relation (7) which, after distribution, contains the condition for the calculation $N_{0v} = -a_{0v} C_{11}/C_{12}$, where a_{0v} means v -th amplitude of the exciting function with the frequency ω_v as v -th member of the Fourier row, $v = 1, 2 \dots s$. From the known starting state vector $z_{0v} = \{a_{0v}, N_{0v}\}^T$, it is easy to calculate the state vector $z_{iv} = \{a_{iv}, N_{iv}\}^T$ in the i -th place, $i = 1, 2 \dots n$, for the v -th exciting frequency $v = 1, 2 \dots s$, using the transfer relations

$$z_{i,v} = \left[\sum_{p=1}^s A_{p,v} \right] z_{0,v} \quad (8)$$

Summing up the individual components of the complex amplitude in the i -th place from all $v = 1$ to

s -members of the Fourier series, we will get the resulting amplitudes of the axial shifts U_i and normal forces N_i as the absolute values of the sum of the complex numbers. Let us remark that to values calculated like this, the force and deformation static effects from thread pre-tension, are superimposed which, in the case of the described linear chain at the calculation of dynamic effects, are not taken into consideration.

Let us suppose that the investigated model of warp thread of total length L and of total mass M is on both sides fixed in a solid side. The thread has the static pre-tension P to which time varying, dynamic strength effects are superimposed from the pulse. We consider the pulse as the shift $u(t)_0$ of the left end of the thread in the axial direction to the left in the sense of tensile increase of the axial force according to Fig. 2.

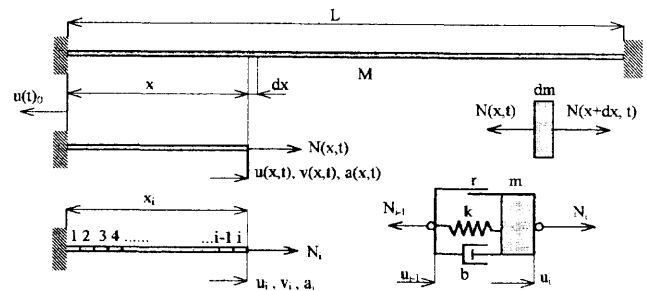


Fig. 2. Model of warp thread. Discretisation of visco-elastic mass continuum

In any place remote by x from the left end ($0 < x < L$) kinematic and force effects at the continuum are functions of remoteness x and time t , so we denote the cross-section shift $u = u(x, t)$, velocity $v = v(x, t)$, and acceleration $a = a(x, t)$. Let us remark that the axial (normal) force $N = N(x, t)$ including pre-tension can gain only positive values in the case of threads. If we divide the continuum into the chain of elements n , the remoteness x will correspond to the position of the i -th element, $i = 1, 2 \dots n$. Individual variables at this discretisation are functions of place $x_i = i \cdot L/n$ and time t . In the following text in accordance with Fig. 2 we denote the variables in the i -th place briefly u_i, v_i, a_i, N_i . The equation of motion of the i -th element with the mass $m = M/n$ in Fig. 2 has a simple form

$$ma_i = N_i - N_{i-1} \quad (1)$$

where forces

$$N_{i-1} = (P + r \cdot \text{sgn}(\Delta v_i) + b \Delta v_i + k \Delta x_i) \geq 0, \quad i = 1, 2 \dots n \quad (2)$$

are the functions of pre-tension P , of differences of velocities $\Delta v_i = v_i - v_{i-1}$, or differences of shifts $\Delta x_i = u_i - u_{i-1}$. The boundary conditions correspond to

the type of excitation on the left end, or to fixing on the right end of the considered chain. In the traced model according to Fig. 2 it holds

for $i = 1$

$$u_{i-1} = u(t)_0 = \frac{U_0}{2} \left(1 - \cos\left(\frac{2\pi}{t_0} t\right) \right)$$

for $0 < t < t_0$, resp. $u(t)_0 = 0$ for $t_0 < t < t_k$

$$v_{i-1} = v(t)_0 = U_0 \frac{\pi}{t_0} \sin\left(\frac{2\pi}{t_0} t\right)$$

for $0 < t < t_0$, resp. $v(t)_0 = 0$ for $t_0 < t < t_k$ (3)

or for $i = n$

$$u_n = 0 \text{ and } v_n = 0 \text{ for } 0 < t < t_k$$

In the preceding relations t_0 denotes the time of pulse duration, which is supposed to be in the form of the cosine curve with the amplitude of U_0 ; the end of the time interval of the traced response is denoted t_k .

As $a_i = dv_i/dt$ and $v_i = du_i/dt$, it is possible, instead of the equation (1), to write down the equivalent system of the $2n$ first-order differential equations in the form

$$\frac{du_i}{dt} = v_i, \quad \frac{dv_i}{dt} = \frac{1}{m} (N_i - N_{i-1}) \quad (4)$$

where we calculate the forces from the relations (2) and (3). It is evident that at numerical simulation we can easily, in relation (2), also consider non-linearities in elastic, or viscous characteristics.

Fig. 3 is a sample of the record of the simulation of tension pulse propagation through warp according to relations from (2) to (4). The course of the traced quantities along the chain corresponds to time $t = 0.000269$ s, where the starting (chosen) parameters are $m_d = 1.75 \cdot 10^{-5}$ kg/m, $L = 3$ m, $U_0 = 0.003$ m, $t_0 = 0.0002$ s, $\zeta = 0.02$, $K = 1000$ N/m, $r = 0$, $P = 2$ N with the time step of integration $\Delta t = 2 \cdot 10^{-8}$ s. Before the simulation itself we will calculate $m = m_d L/n$, $k = Kn$; $b = \zeta \cdot 2 \cdot (k \cdot m)^{0.5}$; the number of chain elements was $n = 100$. Fig. 4 is showing the record of the same simulation in time $t = 0.000833$ s, corresponding, approximately, to return of the reflected wave.

In Fig. 5 you can see the example of the amplitude solution of fixed axial shifts and forces from periodical tensile pulses acting on the left end with the amplitude of $U_0 = 0.003$ m which we replaced by $s = 20$ – members of the Fourier series. This replacement, at time of period $T = 0.1$ s (i.e. 600 pulses per minute), at time of pulse $t_0 = T/20 = 0.005$ s, approximates the

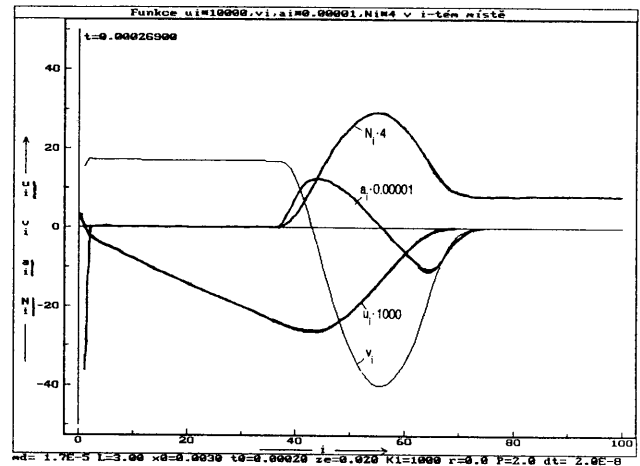


Fig. 3. Course of shifts $u_i(t)$, 1000, velocities $v_i(t)$, acceleration $a_i(t)$, 0.00001, forces $N_i(t)$, 4 for $t = 0.000269$ s

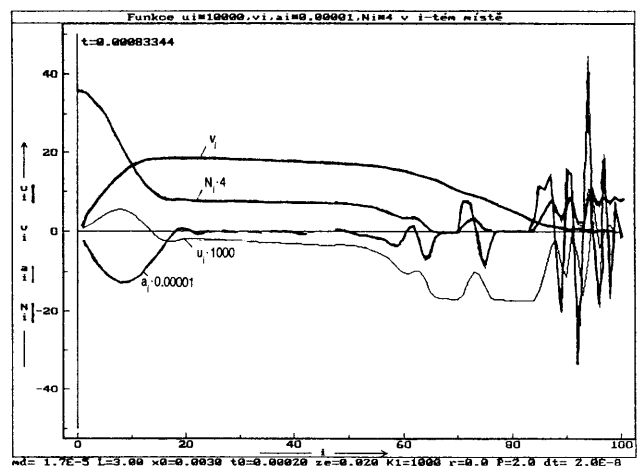


Fig. 4. Course of shifts $u_i(t)$, 1000, velocities $v_i(t)$, acceleration $a_i(t)$, 0.00001, forces $N_i(t)$, 4 for $t = 0.000833$ s

course in the form of shifted cosine curve (3) with convenient accuracy. Analogously, as in the case of numerical simulation in paragraph 2, we chose numerical values of parameters $m_d = 1.7 \cdot 10^{-5}$ kg/m, $L = 3$ m, $K = 50$ N/m and, moreover, for the standard model $K_0 = 100$ N/m. The number of chain elements was $n = 500$. In Fig. 5 above, there are the courses of fixed amplitudes of axial shifts $U(x)$ along warp thread for various values $\zeta = 0.001$ to $\zeta = 1$, and coefficients of damping $b = \zeta \cdot 2 \cdot (KM)^{0.5}$ which were calculated from them beforehand. It is evident that damping has no essential influence on the course of amplitudes of shifts, while its influence on the course of fixed amplitudes of axial forces $N(x)$ can be seen in the lower part of Fig. 5; at the same time we can see that the fixed amplitudes of forces are going up with the increasing remoteness of x from the place of acting of pulses on the left end.

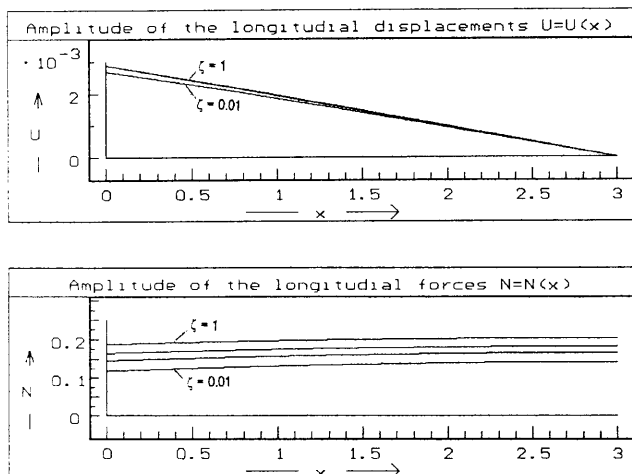


Fig. 5. Amplitudes of fixed axial shifts and forces from periodical pulses

CONCLUSION

Tension pulse propagation in warp threads can be solved numerically, with a certain care, by using suitable discrete models of the continua. It is necessary to mention that such models have rather different properties than the continuum and namely at stress by short-time pulses or impacts.

At physical discreteness and numerical integration of ordinary differential equation system it is possible to consider even non-linear characteristics of chain elements. The application of this method is limited to shorter time intervals corresponding to the return of the reflected tension wave.

Investigation of the distribution of fixed amplitudes of axial shifts and forces along warp thread at excitation by periodical pulses in the case of linear chain enables to utilise the principle of superposition. Periodical pulses can be approximated by a suitable number of members of the Fourier series. For numerical solution the method of transfer matrixes has proved successful in the complex field.

By a similar procedure it is possible to investigate dynamic effects on more precise models with an apter description of excitation and marginal conditions. But for further theoretical analysis co-operation with experimental research is essential.

LITERATURE

1. Brepta, R., Půst, L., Turek, F.: Mechanické kmitání. Tp. sv. 71. Sobotáles, Praha 1994
2. Brepta, R.: Modifikace metody konečných prvků pro nestacionární problémy dynamiky. Studie ČSAV č. 13. Academia, Praha 1982
3. Pestel, E. C., Leckie, F. A.: Matrix Methods in Elastomechanics. McGraw-Hill. B.C.I., N.Y.-S.F.-T.-L. 1963

Theoretical aspects regarding the behaviour of the warp yarns submitted to dynamic tensile stresses

Dorin AVRAM, Mihai CIOCOIU, Dumitru MIHAESCU, and Nicolae IRIMICIUC

INTRODUCTION

The behaviour of the warp yarns on the weaving loom is determined by the nature of the loading they are submitted to during the weaving process.

The present paper deals with theoretical aspects regarding dynamic tensile loading of the warp yarns, establishing a theoretical model for the tension in these yarns during weaving.

On the basis of this model it is determined the tension variation in the warp yarns during shedding and beat-up function of the initial tension and of the weaving conditions (specific to a weaving loom).

WORKING HYPOTHESES

The elaboration of the new mathematical model for the tension variation in the warp yarns is based on the following hypotheses:

H1. The main shaft has a uniform rotation movement and the driving device (mechanism) of the reed revolves with angular speed:

$$\omega = d\varphi/dt = \omega_0 \quad (1.1)$$

not affected by other devices of the weaving loom.

The rotation angle of the reed's driving mechanism

$$\varphi = \omega_0 t \quad (1.2)$$

will be chosen as independent variable in the study on the evolution of warp yarns dynamic tensioning process.

This process is considered periodical with the period P and pulsation p :

$$P = 4\pi \quad (1.3)$$

$$p = 2\pi/P = 0.5 \quad (1.4)$$

H2. The dependence of the φ_v angle upon the reed's to and for movement in respect to it's vertical position (Figure 1.1) and the rotation angle φ of the reed's driving mechanism is determined experimentally by measuring the horizontal distance

$$S_A = A_0 A \quad (1.5)$$

for different φ_i angles within the domain $[0, 4\pi]$, thus obtaining by calculus the reed's deviation (movement) angle

$$\varphi_{vi} = \arctg \frac{a - S_{Ai}}{H}, i = 1, 2, \dots \quad (1.6)$$

where

a – the distance between the vertical position of the reed and the weft insertion zone, S_{Ai} – the distance between the reed's arbitrary "i" position and the weft insertion zone, H – the distance between the oscillation point of the reed and the horizontal position of the warp yarns (levelling position) (Figure 1.1).

The φ_{vi} values depend upon the constructive parameters of the weaving loom.

H3. The law of dependence of the heddles' shafts movement function of the rotation angle of the reed's driving device $h = h(\varphi)$ is determined experimentally and depends on the fabric's weave type and the shafts' driving.

H4. The beat-up of the weft yarns takes place during the reed's forwarding phase towards the weft insertion zone ($\varphi_v > 0$), beginning from the moment when the point A of the reed reaches the position A_1 placed at the distance $e = A_0 A_1$ from the extreme position A_0 and ending when the point a reached A_0 .

Thus, to this value of e corresponds a variation φ_v of the reed's oscillation angle, satisfying the condition

$$\tg \varphi_v = (a - e)/H \quad (1.7)$$

Because the value of the reed's oscillation angle at the beat-up end corresponds exactly to the maximum value of this angle, φ_{vm} , it results that the beat-up process takes place in the following interval of variation of the oscillation angle:

$$\varphi_v \in (\varphi_{vb}, \varphi_{vm}) \quad (1.8)$$

From the reed's rotation angle variation function of it's driving device rotation angle it can be observed that the beat-up process takes place at the end of the 2π period.

The displacement S during weft beat-up (according to Figure 1.1) can be determined by the use of the relation

$$S = \frac{H(\varphi_v - \varphi_{vb})}{\cos \varphi_{vm} \cos \varphi_{vb}} \quad (1.8)$$

where φ_{vb} represents the angle of the reed in the moment when beat-up begins.

Because $\varphi_v = f(\varphi)$, the expression (1.8) becomes

$$S = \frac{H(f(\varphi) - \varphi_{vb})}{\cos \varphi_{vm} \cos \varphi_{vb}} \quad (1.9)$$

Representing graphically the evolution of S function of the rotation angle of the reed's driving device it can be observed the periodical variation and that the maximum value was reached at the moment of beat-up end.

H5. During one running cycle of the weaving loom, the warp yarn tension has two components:

a) A static component, T_{st} , caused by the initial static strain, ΔL_{st} , of the yarn segment A_1B ; the unstrained length is

$$L_0 = l_1 + l_2 - e - \Delta L_{st} \quad (1.10)$$

The static tension, which is permanent, becomes:

$$T_{st} = AE \Delta L_{st} / L_0 \quad (1.11)$$

where A represents the area of the yarn's cross section and E the tensile modulus.

b) A dynamic component caused by the dynamic strain of the yarn due to shafts movement and beat-up process; it is admitted that in the lapse of the weft yarn, the extremity of the warp yarn from the weft insertion zone remains in the position A_1 .

In such conditions, the length of the warp yarn in the considered position A has the value:

$$L = AC + CB \quad (1.12)$$

Considering the notations from the figure 1, it is obtained:

$$L = (l_1 + l_2) - e + S + \frac{1}{2} \left(\frac{1}{l_1 - e + S} + \frac{1}{l_2} \right) h^2 \quad (1.13)$$

approximated by

$$L \approx (l_1 + l_2) - e + \frac{1}{2} \frac{l_1 + l_2}{l_1 l_2} h^2 \quad (1.14)$$

The total elongation of the warp yarn, in the considered moment, will be given by the expression:

$$\Delta L = L - L_0 = \Delta L_{st} + S + \frac{1}{2} \frac{l_1 + l_2}{l_1 l_2} h^2 \quad (1.15)$$

and the corresponding tension will be:

$$T = \frac{AE}{L_0} \Delta L = \frac{AE}{L_0} \Delta L_{st} + \frac{AE}{L_0} S + \frac{1}{2} \frac{AE}{L_0} \frac{l_1 + l_2}{l_1 l_2} h^2 \quad (1.16)$$

or

$$T = T_{st} + \frac{AE}{L_0} S + \frac{1}{2} \frac{AE}{L_0} \frac{l_1 + l_2}{l_1 l_2} h^2 \quad (1.17)$$

The direct use of this expression is not possible because the functions $S(\varphi)$ and $h(\varphi)$ are defined on intervals, during one period of the loom's working. Even there are discontinuities between them, in order to make the relation (1.17) operable there will be firstly established two additional mathematical models to permit the expressing of the function $T(\varphi)$ as a continuous function of φ variable.

THE ADDITIONAL MATHEMATICAL MODELS

The mathematical model for the heddles' movement

The shafts' law of motion is determined by the fabric's weave and it is expressed by $f_i(\varphi)$, $i = 1, 2, \dots$, which must represent, as correct as possible, the function $h(\varphi)$ for one period, under the form of:

$$h(\varphi) = \begin{cases} f_1(\varphi), & \varphi \in [\varphi_{(0)}; \varphi_{(1)}] \\ \dots & \\ f_i(\varphi), & \varphi \in [\varphi_{(i-1)}; \varphi_{(i)}] \\ \dots & \\ f_n(\varphi), & \varphi \in [\varphi_{(n-1)}; \varphi_{(n)}] \end{cases} \quad (3.1)$$

The periodicity of the function $h(\varphi)$ with the period P and the pulsation p permits it's expressing by means of Fourier series:

$$h(\varphi) = \frac{a_0}{2} \sum_{n=1}^{\infty} [a_n \cos(np\varphi) + b_n \sin(np\varphi)] \quad (3.2)$$

with the coefficients

$$\begin{cases} a_n = \frac{1}{2\pi} \sum_{j=0}^n \int_{\varphi_{j-1}}^{\varphi_j} f_j(\varphi) \cos(np\varphi) d\varphi \\ b_n = \frac{1}{2\pi} \sum_{j=0}^n \int_{\varphi_{j-1}}^{\varphi_j} f_j(\varphi) \sin(np\varphi) d\varphi \end{cases} \quad (3.3)$$

Generally, these series are rapidly convergent and they can be expressed under the form of a N degree trigonometric polinom:

$$h(\varphi) = \frac{a_0}{2} + \sum_{n=1}^N [a_n \cos(np\varphi) + b_n \sin(np\varphi)] \quad (3.4)$$

The mathematical model of the displacements during weft beat-up

The function $S(\varphi)$ is specific to the weaving loom's type and might be expressed for one period of work of the loom by the equations:

$$S(\varphi) = \begin{cases} f_1(\varphi) = 0, & \varphi \in [\varphi_{(0)}; \varphi_{(1)}] \\ f_1(\varphi) = k_1\varphi + k_2, & \varphi \in [\varphi_{(i-1)}; \varphi_{(i)}] \\ f_j(\varphi), & \varphi \in [\varphi_{(j-1)}; \varphi_{(j)}] \\ f_n(\varphi) = k_3\varphi + k_4, & \varphi \in [\varphi_{(n-1)}; \varphi_{(n)}] \end{cases} \quad (3.5)$$

Due to its 4π periodicity, $S(\varphi)$ can be expressed by means of Fourier series as follows:

$$S(\varphi) = \frac{A_0}{2} + \sum_{n=1}^{\infty} [A_n \cos(np\varphi) + B_n \sin(np\varphi)] \quad (3.6)$$

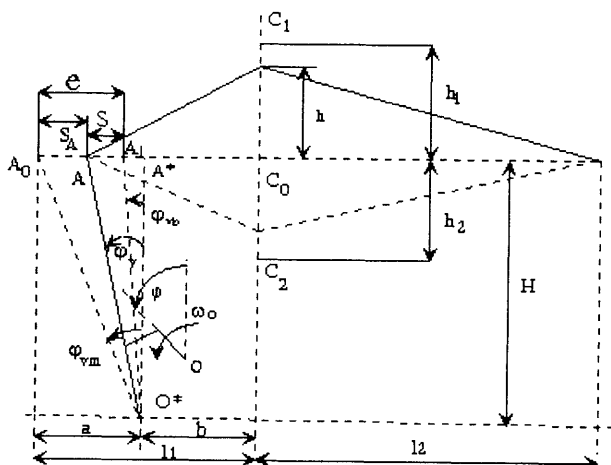
with the corresponding coefficients:

$$\begin{cases} A_n = \frac{1}{2\pi} \sum_{j=0}^n \int_{\varphi_{j-1}}^{\varphi_j} f_j(\varphi) \cos(np\varphi) d\varphi \\ B_n = \frac{1}{2\pi} \sum_{j=0}^n \int_{\varphi_{j-1}}^{\varphi_j} f_j(\varphi) \sin(np\varphi) d\varphi \end{cases} \quad (3.7)$$

The mathematical model for warp yarns tension variation

Introducing the relation (1.17) in the relations (3.4) and (3.6) it can be obtained the following expression for the warp yarn tension:

$$\begin{aligned} T = T_{st} + \frac{AE}{L_0} & \left[\frac{A_0}{2} + \sum_{n=1}^N [A_n \cos(np\varphi) + B_n \sin(np\varphi)] + \dots \right. \\ & + \frac{1}{2} \frac{AE}{L_0} \frac{l_1 + l_2}{l_1 l_2} \left[\frac{a_0}{2} + \sum_{n=1}^N [a_n \cos(np\varphi) + b_n \sin(np\varphi)] \right] \end{aligned} \quad (3.8)$$



The calculus of the warp yarns tension by means of the relation (3.8) it is possible after determining the elements presented in Figure 4.1 establishing experimentally the motion law of the reed, the shed's height evolution (Figure 4.2) and the variation of the distance between the reed and the weft insertion zone (Figure 4.3), for a certain type of weaving loom. An example is presented in Table 1.

EXPERIMENTAL WORK

The testing conditions were:

- 15 tex polypropylene yarn
- yarn diameter: 0.015 [cm]
- tensile modulus, E : $0.283 \cdot 10^8$ [cN/cm²]
- initial tension, T_{st} : 30; 60; 90 [cN]
- initial length, L_0 : 81.5 [cm]
- number of considered terms in the Fourier approximation, N : 8
- the coefficients of the Fourier series and the variation of the total tension in the warp yarns are presented in Table 1.

CONCLUSIONS

The new mathematical model for the warp yarns tension shows the tension dependence of the yarn's characteristics, weaving loom type (driving devices for the heddle shafts and the reed), fabric weave, law of movement for the shafts and of the technological weaving conditions.

By the use of this mathematical model it can be realised a computer program to permit quick and accurate evaluation of the warp yarns tension function of the technological conditions and of the weaving loom type.

Fig. 1.1.

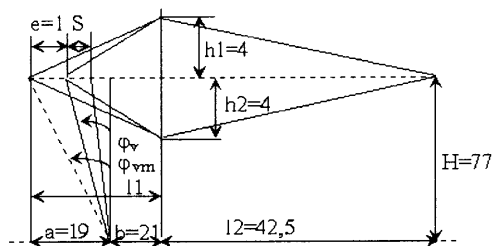


Fig. 4.1. Geometrical elements needed for calculus

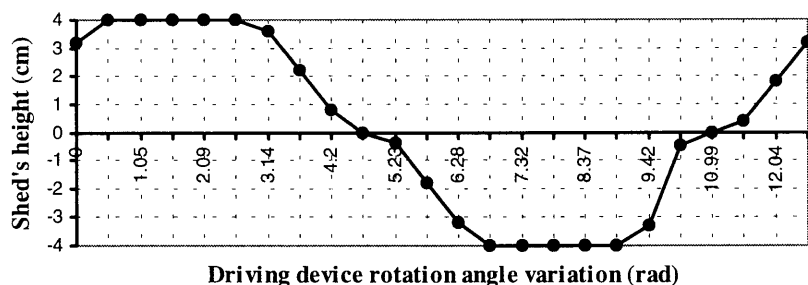


Fig. 4.2. Shed's height dependence upon the rotation angle of it's driving device

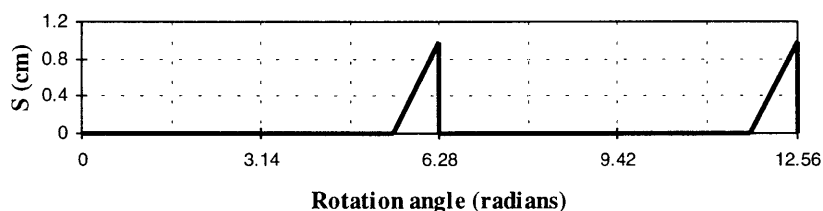
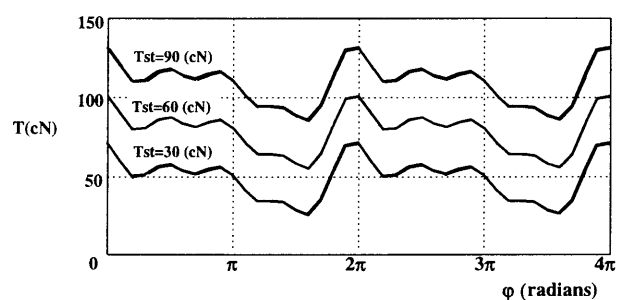


Fig. 4.3. The variation of the distance between the reed and the weft insertion zone (S) during one period (P)

Tab. 4.1.

a_n	a_0	a_1	a_2	a_3	a_4	a_5	a_6	a_7	a_8
	-0.001	2.901	0.002	$4.331 \cdot 10^{-4}$	$4.711 \cdot 10^{-4}$	0.23	$7.425 \cdot 10^{-4}$	0.11	$8.603 \cdot 10^{-4}$
b_n	b_0	b_1	b_2	b_3	b_4	b_5	b_6	b_7	b_8
	0	3.171	0.002	0.001	$-2.86 \cdot 10^{-4}$	0.365	0.002	-0.055	$9.174 \cdot 10^{-4}$
A_n	A_0	A_1	A_2	A_3	A_4	A_5	A_6	A_7	A_8
	0.127	$-7.319 \cdot 10^{-5}$	0.119	$-6.372 \cdot 10^{-5}$	0.1	$-4.386 \cdot 10^{-5}$	0.073	$-3.268 \cdot 10^{-5}$	0.046
B_n	B_0	B_1	B_2	B_3	B_4	B_5	B_6	B_7	B_8
	0	$9.322 \cdot 10^{-6}$	-0.034	$2.498 \cdot 10^{-5}$	-0.061	$3.294 \cdot 10^{-5}$	-0.077	$3.169 \cdot 10^{-5}$	-0.08



Possibility of Adjusting the Optimum Tensile Properties of Yarns to Processing Conditions Thereof

Jerzy Słodowy

Department of Weaving Technology and Structure of Fabrics, Technical University of Łódź

The aim of the procedure described herein was to determine the effect of the fatigue strength of a yarn on its performance in weaving. The tests involved in the procedure are comparative in nature and their coverage is confined to the relationship between the operation of the loom and behaviour and performance of the warp.

For the purposes of the study selected were two cotton yarns, one ring-spun and one rotor-spun, having the same linear density 1×40 tex and made from the same supply lot of raw material. Each of the two yarns was subjected to a series of dynamic impact loads being a simulation of the action the loom on the warp in weaving which were applied to the yarn on a specially designed test station incorporating a generator of dynamic tension pulses described as a dynamic pulsator (Fig. 1).

The two yarns were tested at the same settings of the pulsator, as follows. In every test a group of 20 threads of yarn were applied to an initial static load F_s to impart to each thread a tension equal to 15 % of its value of breaking load. The values of mean breaking load F_{ro} and mean elongation at break λ_{ro} had been in each case determined for either yarn in its condition as spun on a tensile tester.

Every test on the pulsator was carried out in two stages. In stage 1 both yarns were subjected to a series of fatiguing actions of the pulsator, with the number of impact tension pulses being suitably varied. The frequency of the pulsation was constant at 200 cpm. (cycles per minute). For each test group of threads determined was the mean breaking load F_r and mean elongation at break λ_r . For every next test group mounted on the pulsator the number of fatigue pulses was increased by 1,000, starting from 1,000 pulses. For the ring-spun yarn the test was terminated after 13,000 cycles of pulsation due to increased breakage. Test of the rotor-spun yarn was arbitrarily terminated after 100,000 cycles despite there being no breaks even after that amount of fatigue.

In the first stage of pulsation, the tested group of threads were exposed to a constant tensile load F_s and tensile load F_{dyn} applied impactwise in a constant amount by equipping the pulsator with compensation for elongation of the threads. Following the test on the pulsator, each thread of the test group was tested on a tensile tester to determine its F_r and λ_r the values of which were adopted as a measure of fatigue strength of the yarn.

In the second stage, both yarns were subjected to a series of fatiguing actions of the pulsator at varied frequency of pulsation with the maximum number of pulsation cycles being 1,000 for all test groups of threads. Testing was started at 50 cpm and terminated at 590 cpm.

The test results are shown in Figs. 2 and 3 in which the mean values of breaking load (bars) and elongation at break (dots) are represented for the two yarns as a function of the number of fatigue cycles (k) and pulsation frequency (n). On the graphs marked as reference are the values of F_{ro} and λ_{ro} for the yarns before fatigue.

It is seen from the results that in the condition before fatigue the ring-spun yarn is stronger by about 35 % than the rotor-spun yarn, while the latter has a slightly higher elongation at break.

When comparing the two yarns with regard to the number of fatigue cycles which they can withstand the rotor-spun yarn stands out very superior as it shows an extremely low susceptibility to long-term fatigue. The values of breaking strength of the test threads subjected to thousands or even tens of thousands of fatigue cycles are little different from those of the same yarn in unfatigued condition. Even after 100,000 fatigue cycles the breaking strength of the yarn remains unimpaired. However, elongation at break is in all cases lower than in the unfatigued condition.

Also for the ring-spun yarn the elongation at break is at all levels of fatigue lower than unfatigued. But there is a distinct drop in the breaking strength of the ring-spun yarn at all levels of fatigue except after 11,000 cycles when the yarn reaches a maximum value of breaking strength due to its having undergone sort of mechanical conditioning. At first the breaking strength of the yarn is decreasing till about 7,000 cycles to reach a local minimum, whereupon its breaking strength is increasing till a maximum when it exceeds the initial value and then it drops rapidly with increasing breakage on the pulsator. In the case of the ring-spun yarn the curves of variation of breaking strength and elongation at break manifest an interesting parallelism consisting in that the value of elongation is decreasing and then increasing till a maximum (11,000 cycles) coinciding with the maximum for breaking strength to drop equally rapidly in the end.

Analysis of pulsation frequency shows that after a full range of testing on the pulsator the values of breaking strength for both the ring-spun and rotor-spun yarns do not descend below the level of strength shown by either

yarn before being fatigued. This would suggest that while being tested on the pulsator the yarns receive some mechanical conditioning. Also here the ring-spun yarn has its tensile maximum coinciding with about 420 cpm at which also its elongation at break is the highest.

Similarly as in the tests for resistance to fatigue the rotor-spun yarn shows a very low susceptibility to changes of the manner it is fatigued, i.e. in this case to changes in pulsation frequency, and maintains a more or less constant level of breaking strength. Its elongation at break shows some variability and oscillates close to λ_{r0} .

The above results are an encouragement to seek an explanation of the mechanism leading to the fatigue of a yarn resulting in its disruption, although in some cases the yarn may retain its strength to fatigue loads.

The decreasing elongation at break of the test threads as their fatiguing is continued suggests that the threads are stiffening up. Confirmation of the stiffening process was sought by measuring the free vibration frequency of the threads.

The free vibration frequency ν of a cut length of a test thread was measured on a test device as shown in Fig. 4. Free vibration frequency was determined for both the ring-spun and rotor-spun yarn by first mounting, on the test device, a sample of unfatigued yarn to determine the ν_0 and then the yarn was given a suitable number of fatigue cycles. The results are presented in Fig. 5.

An increasing effect of fatigue on free vibration frequency could be seen for both yarns. The ring-spun yarn, however, differed in its changes of ν from the rotor-spun yarn. In the ring yarn, ν increased rapidly during the first short phase of fatiguing to assume a decreasing tendency as fatiguing was being continued, while in the rotor-spun yarn free vibration frequency increased incrementally as fatiguing was continued, which seems to suggest that each of the two yarns takes up fatigue according to a different mechanism.

CONCLUSIONS

The results of the tests show that the yarns differ in their load-carrying capacity which may be increasing or decreasing as a function of the number and frequency of applied pulsation cycles, this being systematically observed in the case of the ring-spun yarn. Worthy of noting is the parallelism of changes in breaking strength and elongation in the case of the ring yarn, which may be interpreted that the two parameters are inter-related in indicating the degree of degradation of the yarn. The optimums of the curves allow to postulate that it possible to select yarns with optimum fatigue strength, tested on the pulsator, for the intended further processing. According to this supposition a given ring-spun yarn would have to be assigned, for instance, the function of warp on a loom operating with a frequency acceptable for the yarn and optimum number of the tension imparting cycles.

The tests of strength to both fatigue and pulsation frequency revealed that the rotor-spun yarn (These yarns in their unfatigued condition are, according to the conventional tensile tests, weaker than ring yarns) was much less affected by fatigue and was, therefore, more suitable for further processing. In the discussed tests the behaviour of the rotor yarn was very stable and it was quite resistant to fatigue. This was confirmed by experimental tests on the loom.

LITERATURE

1. J. Szosland et al., Destruction and Degradation of Linear Textile Processes, *ZESZYTY NAUKOWE Politechniki Łódzkiej* No. 736, Łódź, 1996
2. J. Słodowy, M. Snyckerski, A comparative Study of Yarns Subjected to Multicyclic Impact Tensile Loading of Varied Parameters, *COPERNICUS - PROJECT: New Advanced Yarn Test Methods for High Quality Weaving*, Łódź, 1997

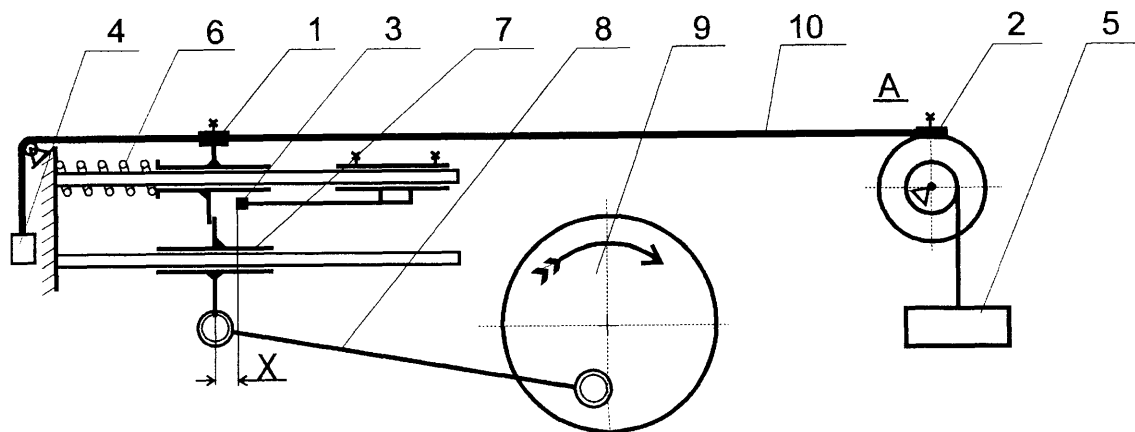


Fig. 1. The dynamic pulsator: 1 – active clamp; 2 – passive clamp; 3 – travel limiter of active clamp; 4 – weight to even up tension in test threads; 5 – weight to produce initial tension in test threads; 6 – active clamp return spring; 7 – slide; 8 – connecting rod; 9 – drive eccentric; 10 – test sample

Cotton yarn 40 tex

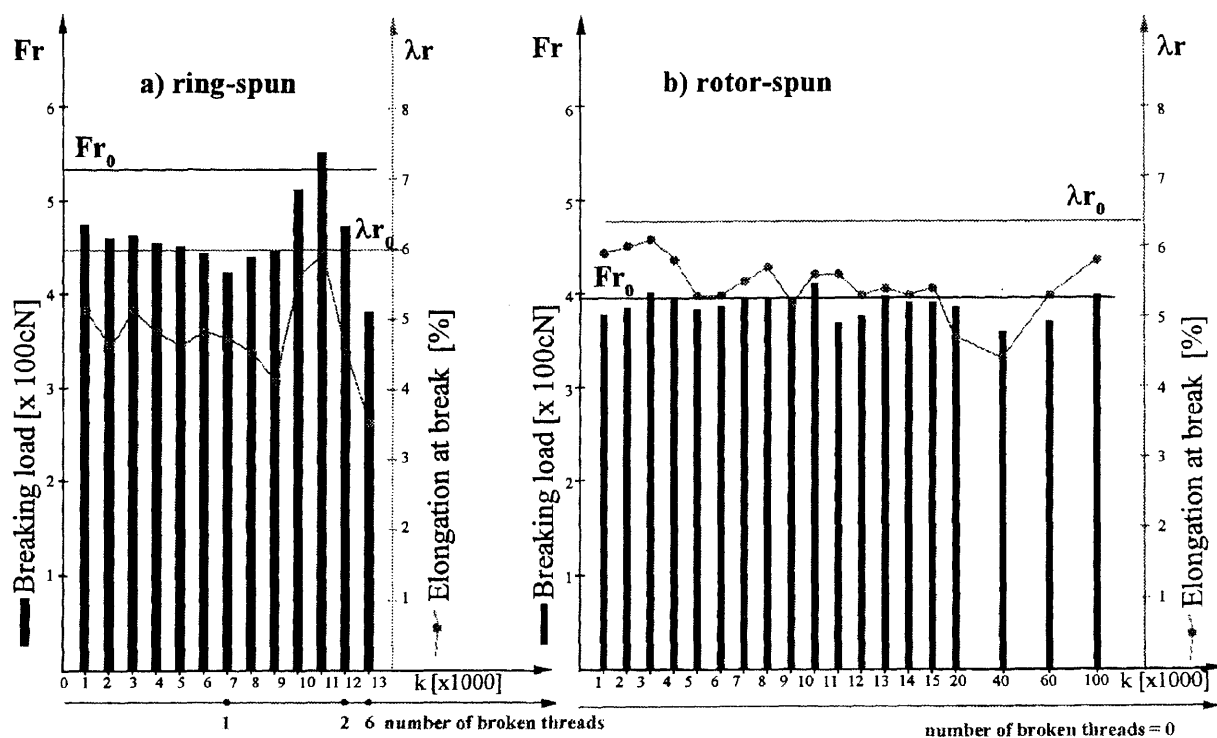


Fig. 2. Effect of fatigue on strength of yarn

Cotton yarn 40 tex

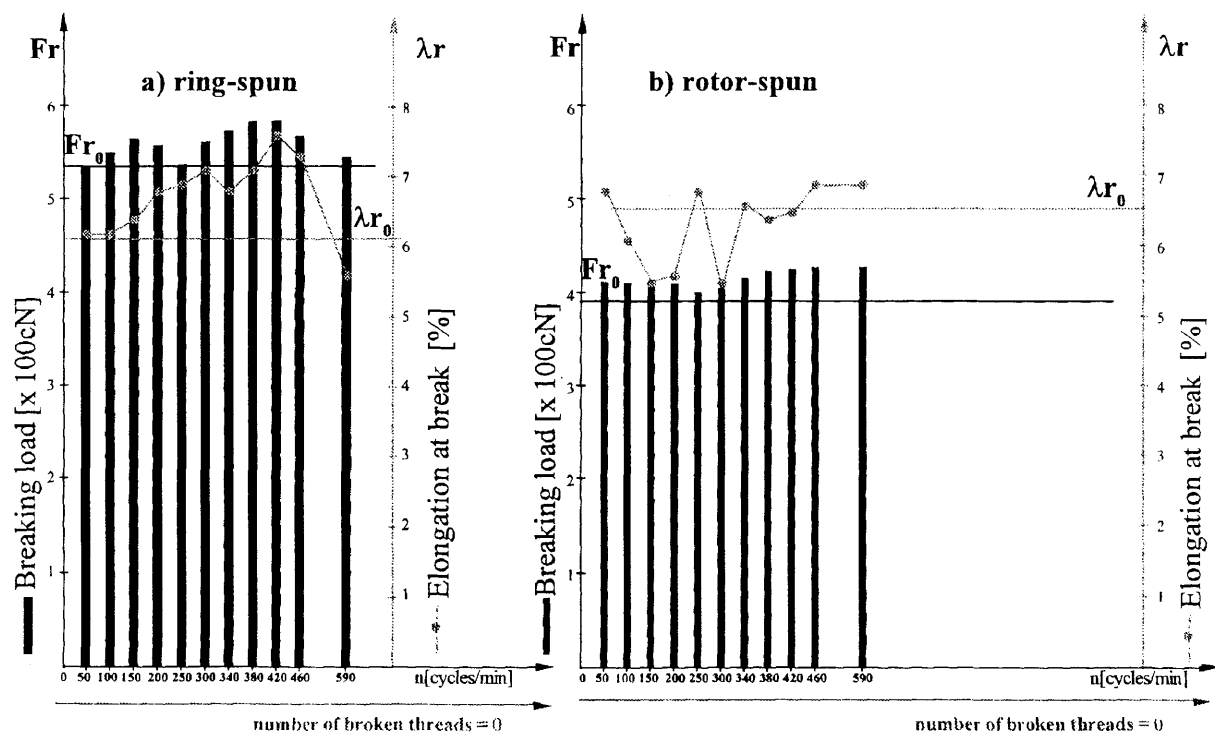


Fig. 3. Effect of pulsation frequency on strength of yarn

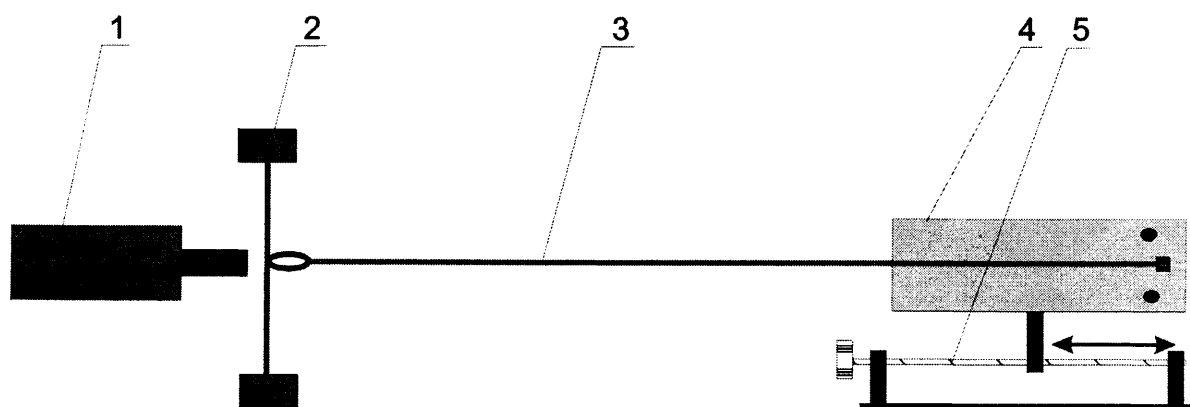
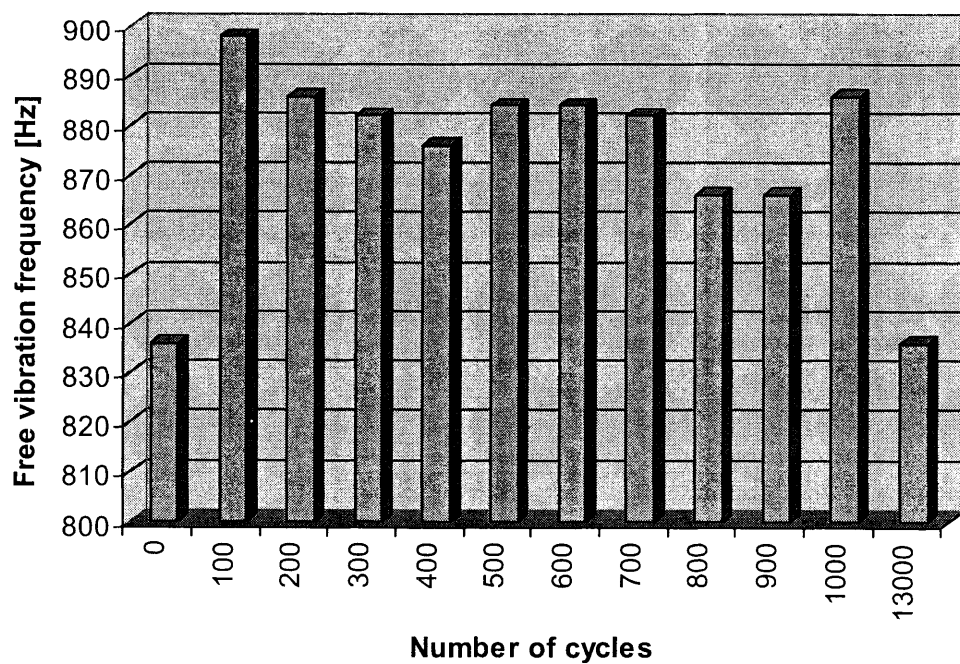


Fig. 4. Test device for measuring free vibration of yarn: 1 – programmable generator of vibration; 2 – vibration transmitter; 3 – tested yarn; 4 – vibration receiver; 5 – tension imparting system

Ring-spun yarn



Rotor-spun yarn

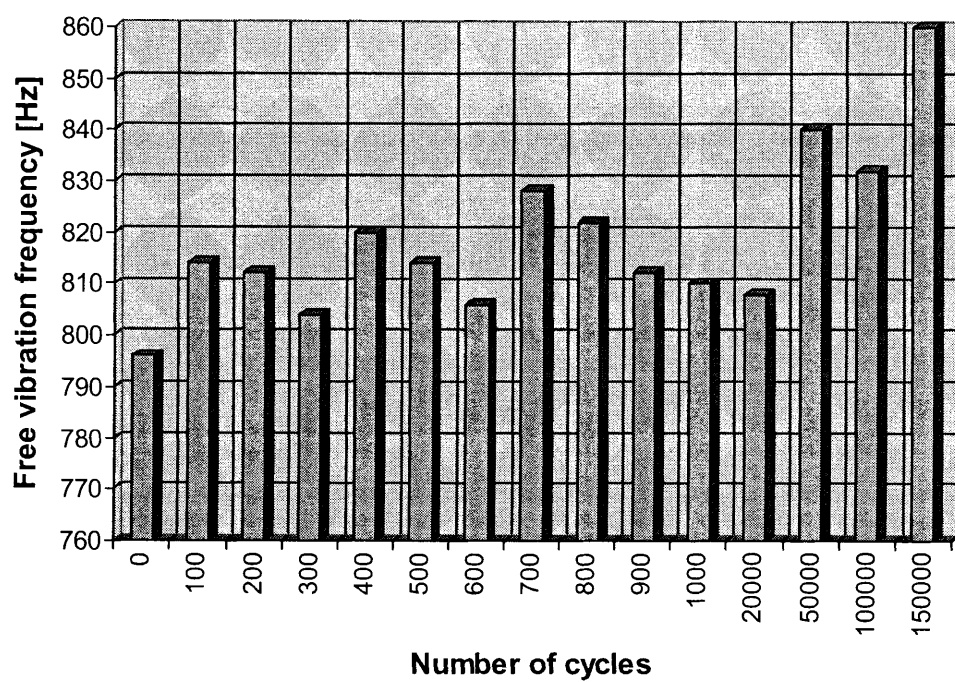


Fig. 5. Effect of fatigue on free vibration frequency of yarn

New Concept of Formating of Properties of the Weft Package

Marek Snyckerski

Department of Weaving Technology and Structure of Fabrics, Technical University of Łódź

So far the structure and, therefore, also the properties of the commonly used filters, including textile multilayered filters, are stochastic, since for a filter to be fully definable it is necessary that its structure is determinable and determinable are also the dimensions and shapes of the filtering spaces and their patency. Such conditions can be satisfied only by structures that are both porous and channelled. The question is if a precision-wound single-thread package can be made to have such a determinable structure.

As it is, the literature devoted to analysis and formation of the structure of a precision-wound package is rather scanty and so the structure of the common package is unavoidably random. Important contribution to the understanding of the structure of a package was made in the late 1960's by Leopold Górecki who was the first to make an analysis of structure of a package network, based on known winding ratio expressed as $i = L/M$. (Fig. 1) The expansions of the three package networks wound at ratios 39/19, 44/19, and 50/19, which are presented in Fig. 1, are seemingly identical. Górecki introduced the following concepts: angular coil gauge φ ; winding cycle M ; and package network rank R . The angular coil gauge φ of a package is the angle of rotation of the package between its adjacent coils. Winding cycle M is the number of cycles of the guide after which the order in which the coils are laid in the package is repeated. Winding cycle is an indirect measure of the density of coils in a package. Package network rank R is the number of different values of coil gauge within a winding cycle. Thus, a package network formed at winding ratio 39/19 is a rank-one network, 44/19 gives a rank-two network, and 50/19 a rank-three network. All of the presented networks have the same winding cycle $M = 19$ and the same coil gauge $\varphi = 2\pi/19$. Although Górecki's findings are important they do not provide a sufficient basis on which to program the structure of a package network.

In my doctoral thesis I demonstrated evidence that decisive for the structure of the network of a precision-wound package is the fraction of winding ratio expressed as $i = A + a/M$, and decisive for the stability of the coil network (and, therefore, for durability and unwindability of the package) is the spacing of the spans formed by the crossing coils. I introduced the concept of spacing number 'k' and demonstrated that package network structure can be programmed by selecting the

appropriate values of the spacing number 'k'. On the basis of 'k' the required winding ratio can be determined.

So far, despite of the great advances in the winding technology, programming of structure of package networks permits only to optimise the stability of a precision-wound package and thereby to improve the winding/unwinding conditions. However, it is reasonable to suggest that of all types of packages the precision-wound type has the greatest potential for rational shaping of its structure.

The present description of the structure of a precision-wound package is insufficient to solve problems associated with dyeing and filtration of packages which are generally difficult to dye evenly or are undyeable.

The thesis can be put forward that a single-thread precision-wound package is a porous and channelled structure which, owing to the layout of its coils being fully definable, meets the condition of definability of the dimensions of the filter spaces and, therefore, their shapes and patency are programmable.

The coil network (Fig. 2) of a precision-wound package is built up of inter-crossing coils laid out on a cylindrical surface. The repeating element in this network is an eye. As the networks are superimposed in the successive winding cycles a network of straight, radially oriented channels is formed. (Fig. 3). The dimensions of the diagonals of the eyes and, therefore, dimensions of the channel cross-sections can be found from the parameters of the package l , D , yarn d and winding ratio i . Depending on the technological assignment of the package it can be designed to have the wanted coil spacing 'b' or eye area 'S'. Then the corresponding winding cycle is:

$$M = \frac{\pi D}{2 \left(b + \frac{d}{\sin 2\alpha} \right) \cos \alpha}$$

$$M = \frac{-a + \sqrt{a^2 + 4(S \sin 2\alpha - d^2)(\pi D h \sin \alpha \cos \alpha)}}{2S \sin 2\alpha - d^2}$$

$$a = \pi D d \sin \alpha + d h \cos \alpha$$

where: M – winding cycle, D – diameter of package, d – diameter of thread, α – winding angle, S – eye area, b – coil spacing.

The spatial structure of package networks was analysed on models. In Fig. 4 a view of a flat model of a package network formed with a fraction of winding ratio 29/70 is presented. In the next figures photograms of the same model made by placing the camera at different heights and in a direction concurrent with and opposite to the real direction of formation of the network are presented. Although the photograms represent the same object, what is viewed looks different. An analysis of the distribution of the coil crossings in a plane normal to the package axis, (Fig. 5), reveals characteristic void spaces in the package which are described as inclined channels. Of these, the channels inclined in the direction of package rotation are described as concurrent channels and those inclined in the opposite direction as counter-current channels. Channels of opposite orientations inter-cross to form a network which permits access of dyebath to every part of the package. A generalisation of the conclusions of the analysis led to the formulation of mathematical relations by which the number and type of the inclined channels can be determined, depending on the rank of the coil network of the package.

The number of channels of each type can be found from the following relations:

Number of straight channels: $K_{pr} = M^2 i$

where: M – winding cycle; i – winding ratio;

Number of inclined channels built on i -rank coil gauge: $O(\varphi) = i k_1^2 k_2^2 \dots k_n^2, k_n^2$

where: k_1, \dots, k_n are corresponding coil spacing numbers.

To verify a flat model of a package network a cylindrical model of a real package was made using a copper wire wrapped with rayon. Cross-sections were obtained after setting the model with chemically cured resin. The view of a cross-section of a real package model presented in Fig. 6 and 3.20 shows that the model is consistent with the flat models except that the inclined channels are curved and therefore difficult to observe in the real packages. The continuity of the channels in a package is preserved owing to the fact that they continue through the borderlines between the layers wound in the successive winding cycles and as it can be seen from Fig. 7 the corresponding inclined channels are shifted in relation to one another.

Therefore, (Fig. 8) if the coils of yarn are laid out in a controlled manner, a precision-wound package can be obtained with programmed layout of channels having defined dimensions and continuity. This would be the first case of it being possible to create a programmed non-stochastic porous structure.

The objective of the experimental verification of the designed packages with a porous and channelled structure was to assess if there were conditions in the packages for migration of a liquid to every part of the package. The methods by which the verification was carried out included photogrammetry, tomography, and direct dyeing.

The effect of migration in the surface layer was recorded by photogrammetry (Fig. 9) and the direct process of migration by tomography. The method of direct dyeing consisted in dyeing packages under industrial conditions. Used were packages of polyamide filament yarn of a hardness 55° Sh and specific density 680 kg/m³ and packages of textured polyester yarn of a hardness 40° Sh and specific density 510 kg/m³. In industrial practice package dyeing is usually confined to packages of a specific density about 200 kg/m³.

The dyeing experiments showed that the rate of migration grows with increasing cross-sectional area of the channels, giving a greater amount of migration per unit time.

Analysis of the tomograms presented in Fig. 10 reveals differences in the character of migration between individual package structures. They show that migration was the best in the package of which the structure is marked 4, while in the remaining packages migration varied with size of the channels.

Since the aim was to assess the improvement of dyebath migration in the packages, the experiments included dyeing under normal conditions and dyeing with reduced heating and dyeing times. The results of dyeing with normal dyeing time are presented in Table 1. Impaired migration of the dyebath due to hydrothermal shrink manifested itself in packages 1 and 2 as poorly dyed edges of the packages where the cross-sectional area of the channels was not large enough. The package used in industry for dyeing textured polyester yarn is not suitable for dyeing polyamide filament yarn because it gives an under-dyed central part of the package and fully non-dyed top and base of the package. In packages 1, 2, and 3 (Table 2) which were dyed with dyeing time reduced by half and heating time reduced by a quarter impaired migration was observed due to insufficient size of the channels.

Final remarks

The structure of a precision-wound single-thread package is programmable.

The parameters of package structure which can be programmed are:

1. For the purposes of handling and storage of yarn:
 - density of coils in package;
 - layout of coils in package;
2. For the purposes of dyeing and filtration:
 - number and type of channels;
 - cross-sectional area of channels;
 - layout of channels.

LITERATURE

1. M. Snyckerski: Multidimensional single thread structures. Scientific Bulletin of Łódź Technical University No 747, Łódź 1995

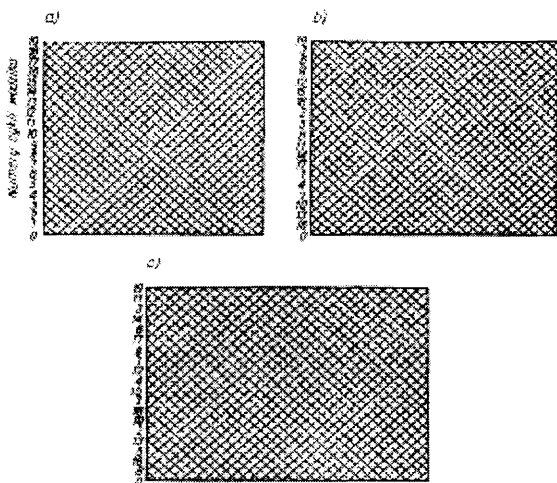


Fig. 1. The expansions of the package networks wound at ratio: a) 39/19, b) 44/19, c) 50/19

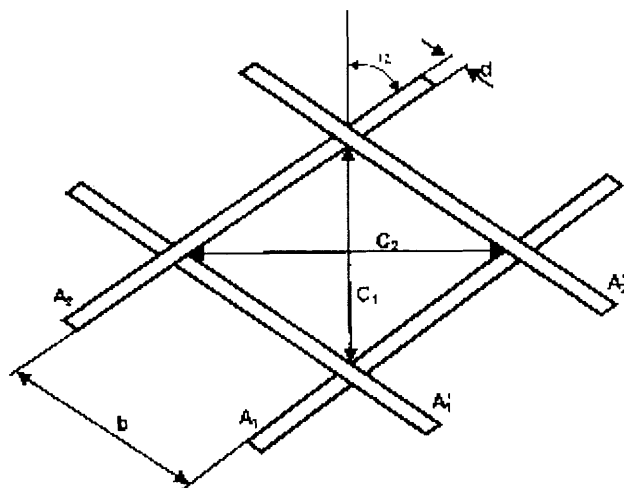


Fig. 2. Scheme of the network's eye

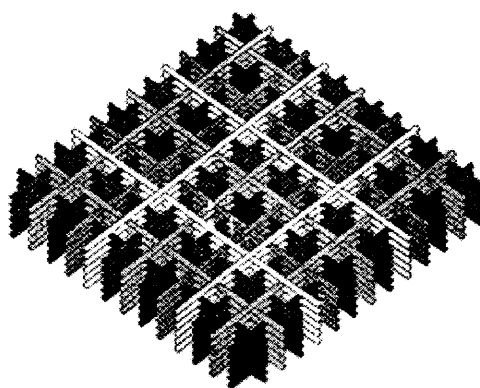


Fig. 3. The repeting elements in the network

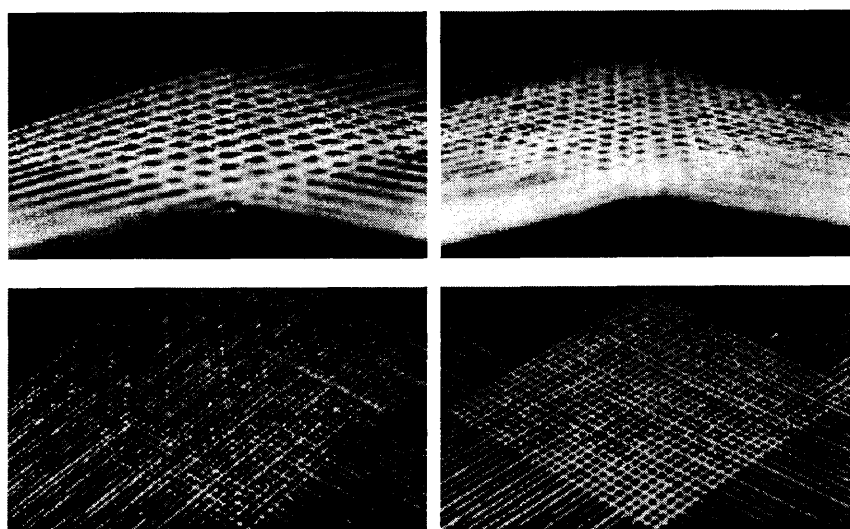


Fig. 4. View of a flat model of network formed with a winding ratio 29/70

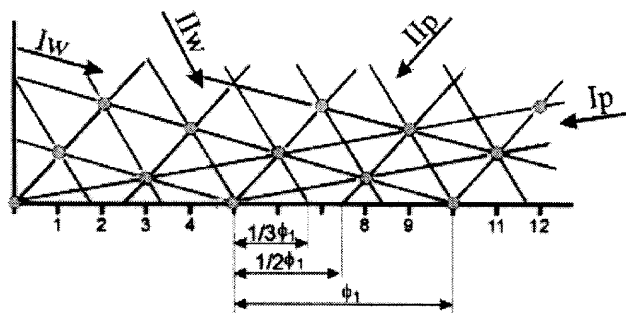


Fig. 5. Example of distribution of the coil crossings in a plane normal to the package axis

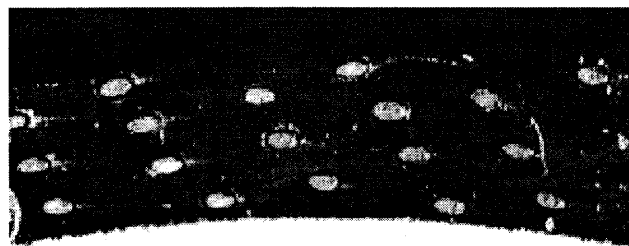


Fig. 6. View of a cross-section of a real package model

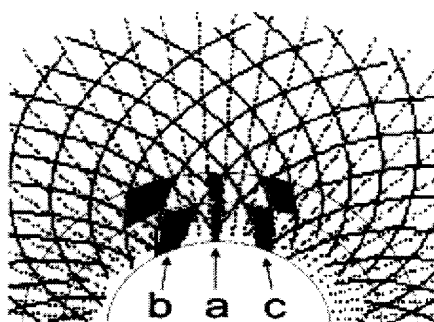


Fig. 7. The continuity of the channels in a package

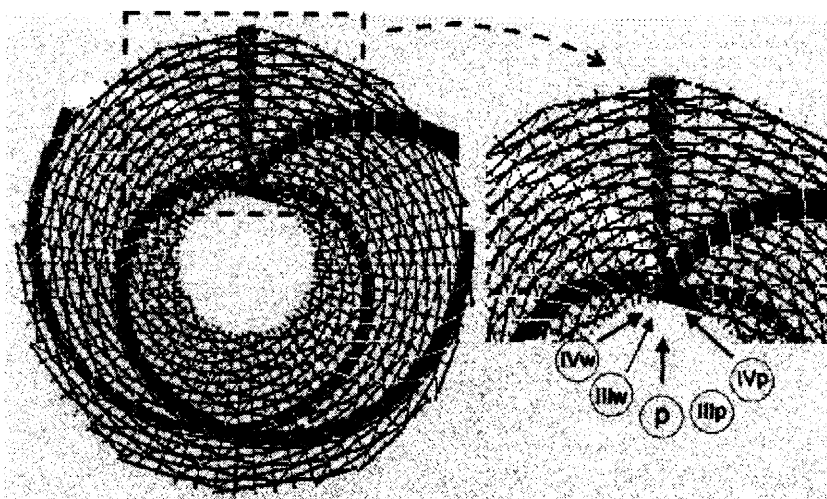
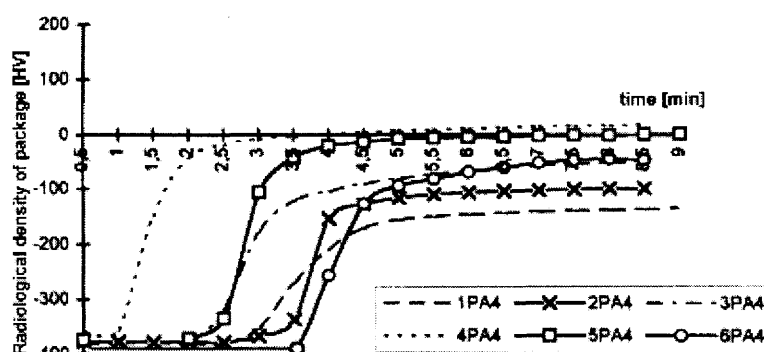
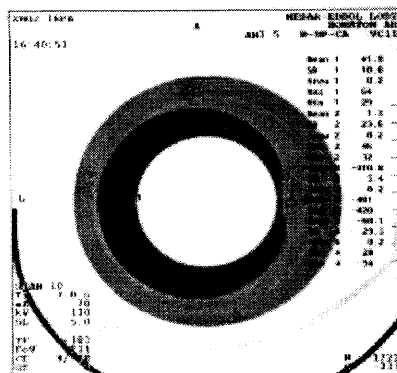


Fig. 8. The package with a programmed non-stochastic porous structure



Tab. 1.

Package	The results of dyeing with normal dyeing time			
	Intensity of dyeing on medium of package		Intensity of dyeing on border of package	
	Equability [%]	Tone	Equability [%]	Tone
1	100	5.0	90	5.0
2	100	5.0	95	5.0
3	100	5.0	100	5.0
4	100	5.0	100	5.0
5	100	5.0	90	5.0
6	90	5.0	20	5.0

Tab. 2.

Package	The results of dyeing with 0,5 time of dyeing			
	Intensity of dyeing on medium of package		Intensity of dyeing on border of package	
	Equability [%]	Tone	Equability [%]	Tone
1	90	4.0	90	2–3
2	90	4.3	90	3.0
3	80	4.5	90	3.5
4	100	5.0	100	5.0
5	100	5.0	50	2–4
6	80	4.0	90	1.0

Straining Of Various Linear Textile Bodies (LTBs) In Generalized Drawing Fields, Mainly In Warps On Looms

Stanislav Nosek

The Textile Faculty, Technical University of Liberec

Problem of steadiness of warp tension during weaving as the impulse for studying stress-strain states of linear textile bodies (LTBs) during tensioning in textile processes

The impulse for studying the stress state of LTBs in various extension or drawing fields in textile machines originally arose in connection with arising of a theoretic problem in weaving of leno fabrics. These fabrics consist of two warps of standing and crossing threads. Yet both warps are taken-up from one single warp beam simultaneously and in the same lengths, but they are tensioned during weaving quite differently. Each of the two warps is lead through a different path with different length and frictional resistance (see Fig. 1a), and also each warp is consumed differently in the produced fabric due to different bindings of the two warps. The question was whether, in the group of crossing threads with permanently higher consumption and with higher resistance against their run through the loom, the warp tension wouldn't increase gradually in the course of longer time of weaving until the threads would break completely.

Later it appeared that some considerations used in the solution of the leno weaving problem have a common validity also for other textile processes. Such a consideration dealt e.g. with the problem of distribution of local velocities $v(x)$ and local deformations $\varepsilon(x)$ along a LTB (linear textile body) between the feeding and taking-up rollers or other feeding places (Fig. 2). This problem comprises 1. the case of straining of an elastic warp between the warp beam and raw beam on the loom, 2. the case of a running elastoplastic fibre between the rollers during stretching, 3. the draft of a bundle of fibres (of a sliver) in the drawing field, etc. Due to the numerous practical occurrences of extension of LTBs between the feeding and take-up places in textile processes under various conditions, the problem has been watched both for purely elastic as well as for elastoplastic material, without- and with own masses dispersed in the LTB, and also the effect of inner friction between elements (between individual fibers) of the LTB has been taken in consideration.

THE BEHAVIOUR OF PURELY ELASTIC LTB'S IN A GENERALIZED DRAWING FIELD

Stretching of chemical fibres, drawing of slivers or rovings, tensioning of yarns on the looms etc. represent special cases of *the general situation of lengthening of linear textile bodies (LTB) in an extension (drawing) field* between the feeding and taking-up spots. These spots can be realized as rollers, jets, warp- and raw beams on the loom, pressuring drums etc. The areas between the spots can be called *the generalized drawing or extension field*.

In many textile processes, stretching, drawing or extension of textile materials is of basic importance. It causes elongation or yielding of material or sliding of molecules or fibres or threads on each other, aiming to reach a certain equilibrium position of particles in the material.

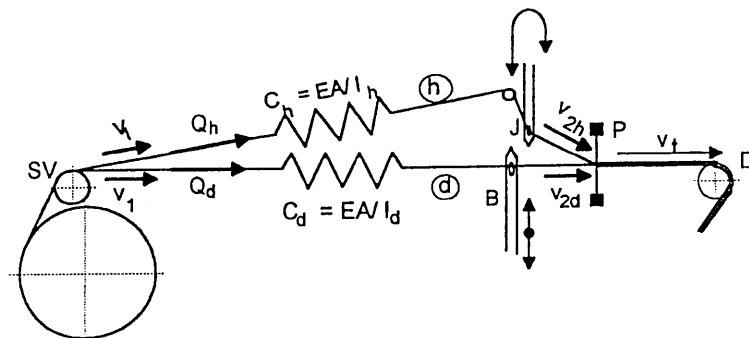
At the beginning of this paper it will be first supposed that the processes of extension or drawing of textile materials in the machines are relatively only so slow that it is not necessary to take in account the inertia masses of materials or the propagation of tension waves in them.

The "principle of relativity" in drawing of textile materials.

Studying of behaviour even of the simple elastic LTBs without own masses needs some correctness. Let us consider an example of an elastic LTB tensioned between two pairs of rollers with different velocities. Due to the difference between the taken-

up and delivered lengths of material $\int_0^t v_2 dt, \int_0^t v_1 dt$ during the time t , the tension varies according to the

Hook law: $Q(t) = \frac{EA}{l} \left(\int_0^t v_2 dt - \int_0^t v_1 dt \right)$ (E – the elasticity modulus, A – the cross section area). At first sight, the distance L between the input and output rollers is



Weaving of leno fabric – the original problem leading to the study of deformation problems of linear textile bodies (LTB) in textile processes

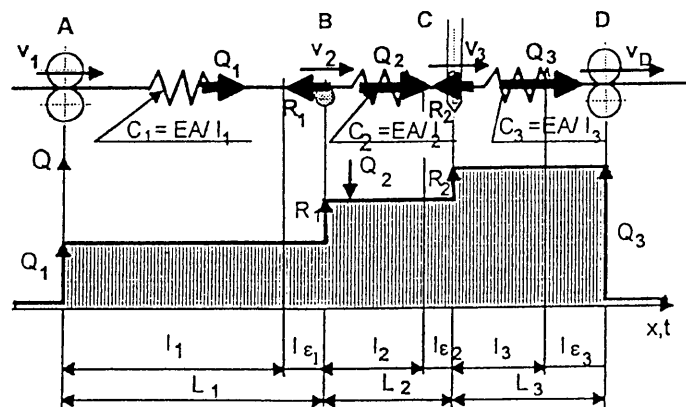


Fig. 1a, 1b. Stress state and thread consumption in the upper branch of warp

GENERAL STRAINING OF LTBs IN TEXTILE TECHNOLOGIES
(LTB = LINEAR TEXTILE BODY – FIBRE, BUNDLE OF FIBRES,
SLIVER, THREAD, WARP...)

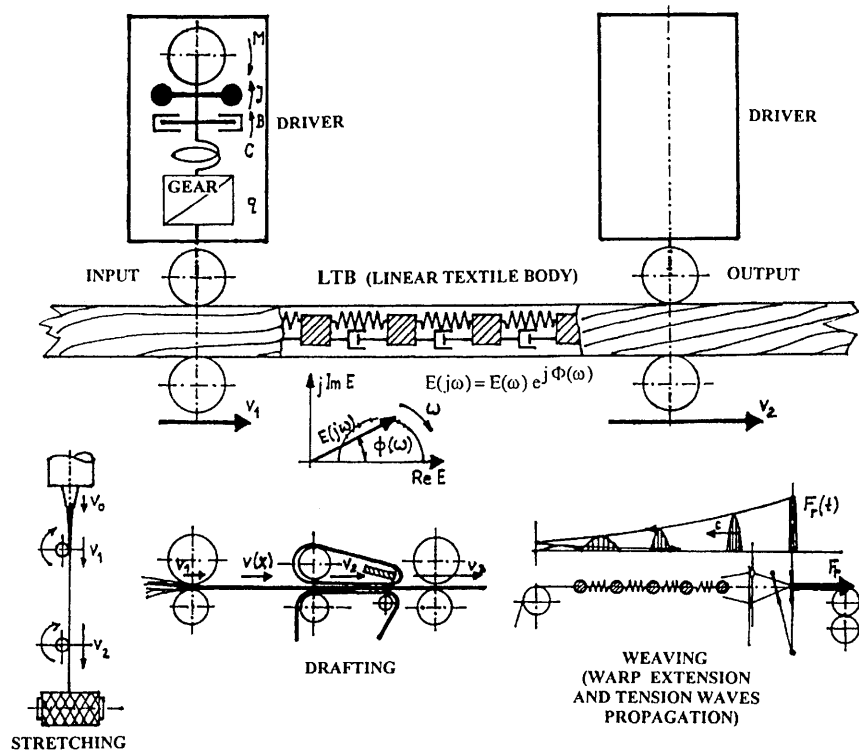


Fig. 2. Stress-strain states in linear textile bodies in various drawing fields...

often simply taken as the length l of material to be deformed. For steady velocities the tension is then $Q(t) = (EA/L)(v_2 - v_1)t$. We see from this result that the tension *would increase* until the breakage of material.

Yet this does not usually occur in practice. The substantial inaccuracy of the above mentioned consideration lies in the fact that the relevant length of the LTB which is deformed, is not L , but, in fact, only a shorter relative length $l = L/(1 + \varepsilon) = L/(1 + Q/EF)$; it is the original length of material *before elongation* to L . The relative output velocity $v_{2\text{relat}}$ of the *taken-up material* is therefore lower than the peripheral absolute velocity v_2 of the rollers, $v_{2\text{relat}} = v_2/(1 + \varepsilon)$. That leads to a certain „principle of relativity of material drawing“: the relative velocity $v_{2\text{relat}}$ of yarn or other LTBs in the clamping line of the rollers depends on the absolute take-up velocity v_2 of rollers so that it relatively decreases with increase of v_2 due to the increase of elongation ε of the LTB.

The distribution of “drawing” rate $v(x)$ in an elastic LTB (warp) at low extension speed

According to the preceding paragraph the tension in a LTB between two pairs of feeding rollers does not permanently increase with time but steadies on a constant value. Consequently also the distribution of the drawing rate $v(x)$ steadies on a certain profile between the rollers. Yet the form of the distribution is not evident at first sight: 1. does $v(x)$ according to Fig. 3 increase from the starting value v_1 to the limiting value v_2 *immediately after passing the input rollers*? 2. or does it increase *from v_1 to v_2 linearly* in connection with the successive elongation of threads in the drawing field? 3. or does it increase *exponentially* in result of a certain feedback effect between the velocity and elongation? 4. or at last, does it not change *jumpwise to the value of v_2 only at the end* of the drawing field when entering the take-up rollers?

Let us prove it: Suppose that an initial point X on the thread reached in the time t_x a position x in the “drawing field” by the average velocity $v_{\text{aver}}(x)$. In this position and time the thread is stretched by a relative elongation $\varepsilon(x)$. Its free (unstretched) length equals to the rolling-up of the surface of input rollers, $x_1 = v_1 t_x$. The relative elongation of threads is then

$$\varepsilon = \frac{x - x_1}{x_1} = \frac{v_{\text{average}}(x)t_x - v_1 t_x}{v_1 t_x} = \frac{v_2 - v_1}{v_1} \quad (1)$$

But everywhere between the rollers the drawing force is equal, $Q(x) = \text{const}$, and so the elongation ε of a purely elastic body must be equal, too. In the eq. (1), to this condition corresponds the only possible value of the average translation velocity $v_{\text{aver}} = \text{const} = v_2$. Consequently, in the drawing field containing elastic material, *the velocity $v(x)$ jumps to the terminal velocity*

v_2 immediately after passing the input rollers. The drawing force in the threads is everywhere

$$Q = EA\varepsilon = EA \frac{v_2 - v_1}{v_1} \quad (2)$$

The force Q represents the basic tension of warp on the loom (i.e. the tension not affected by the influence of shed opening and beat-up pulses). It is obvious that *the values of the tension tend to copy the variations of consumption rate of warp*, $v_2 = v_f(t)$.

In the course of weaving process the rate of consumption $v_2(t) = v_f(t)$ can vary randomly or by a prescribed law, e.g. at the weaving of transversal binding stripes with different warp consumption or at the set of the machine in motion. Due to this the warp tension would also vary and leave structural bars in the fabric. Therefore, the warp tension must be controlled on the loom by means of a regulator which changes properly the input velocity v_1 . The input velocity of warp v_1 (equals to the peripheral velocity of the warp beam) is controlled by the let-off motion of the loom, and the warp tension Q is held approximately on a standard value [3].

The transition process in the elastic LTB (in warp on loom) after the start of “drawing”

The theoretical linear increase of tension $Q(t)$ in a LTB after the start of its elongation, described earlier in this paper (eq. (1)) and declared as being wrong, due to the incorrect length taken in account for elongation, nevertheless, occurs for a short while after the start of weaving. But later the tension steadies asymptotically on a standard level according to eq. (2).

Let us observe Fig. 4 above. At the beginning of drawing or extension the input rollers start to deliver a nonstretched material with the standard velocity v_1 . The delivered length $d\xi_2$ in the time dt equals to the rolled-up periphery of the rollers $dx_1 = v_1 dt$. Yet after entering the drawing field the threads extend themselves jumpwise by the relative value ε . Therefore, the length $dx_2 = v_2 dt$ taken-up by the output rollers is a length of *already extended* material. The really taken-up length is shorter by the elongation, $d\xi_2 = dx_2/(1 + \varepsilon)$, and *the real take-up velocity $v_{2\text{relat}}$ of the free unstretched thread is lower than the speed v_2 of output rollers*.

The total set of equations describing the time course of elongation of the LTB is:

$$\begin{aligned} dQ &= EA \frac{d\xi_2 - d\xi_1}{l} = EA \frac{d\xi_2 - d\xi_1}{L/(1 + \varepsilon)}; \quad d\xi_1 = dx_1 = v_1 dt \\ d\xi_2 &= \frac{dx_2}{1 + \varepsilon} = \frac{1}{1 + \varepsilon} v_2 dt; \quad \varepsilon = 1/EA \end{aligned} \quad (3)$$

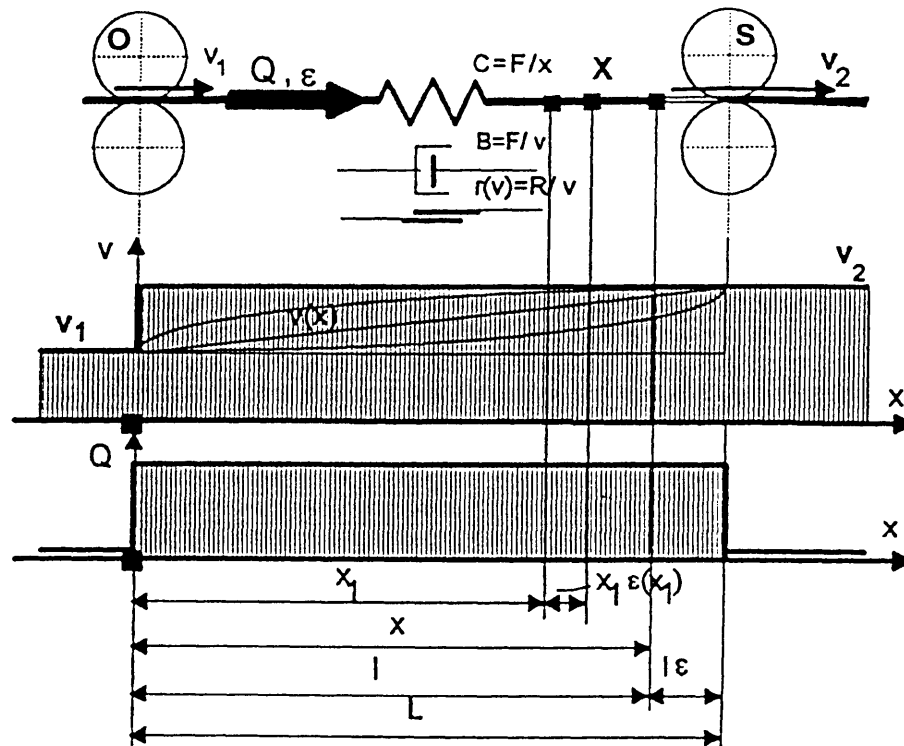


Fig. 3. The problem of distribution of the drawing (elongation) velocity $v(x)$ along a stretched elastic linear textile body (LTB)

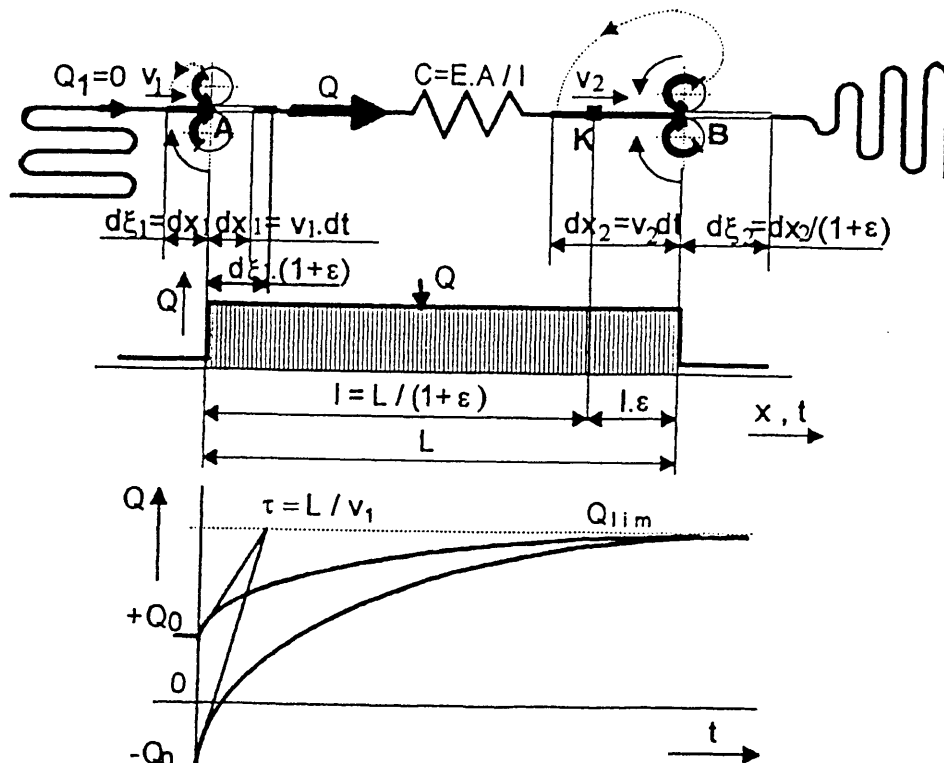


Fig. 4. Below: The results are exponential transition curves aiming at a steady value of Q according to the equation above. Above: The steadied process of extension of a LTB between two pairs of rollers with different feeding – and take-off velocities v_1 , v_2 . The tension Q is constant and depends on the input and output velocities.

From here results a differential equation and the corresponding solution of $Q(t)$

$$\frac{dQ}{dt} + \frac{v_1}{L} Q = \frac{EA}{L} (v_2 - v_1) \Rightarrow$$

$$\Rightarrow Q(t) = Q_0 e^{-t/L} + EA \frac{v_2 - v_1}{v_1} \left(1 - e^{-t/L} \right) \quad (4)$$

The resulting equation of tension in the LTB during a transition process after the machine start consists of a transition part beginning with the initial value of warp tension Q_0 at the loom start (Fig. 4 below), and of a part reacting to the changes in the rate of delivery and consumption of warp. Clearly, the first part can react also to "negative" initial tension. For example, on a loom the warp reacts to the surplus of length at the machine start. The second part reacts to jumps in taking-up velocities during the machine run with a certain exponential starting process; it may cause transition bars in the fabric density (stop-set bars).

Weaving of warps containing groups of threads with different consumption in comparison with the average value (e.g. weaving of leno fabric) from one single beam

During the weaving of fabric with leno binding, or of fabric with longitudinal stripes (e.g. with satin binding) as a result of uneven weaving-in of individual warp ends in the bindings the consumption of all warp threads is not equal. The feeding speed of the warp beam v_1 is common for both systems of threads, all threads being controlled at once by the let-off motion. The take-up velocities of standing or crossing threads, or of threads in satin stripes and in the fabric bottom (let's call them v_{2d} and v_{2h}), are different from the feeding speed v_1 ; e.g. $v_{2h} > v_{2d} > v_1$.

For weaving a leno fabric the warp ends are drawn into the harnesses, e.g. like in Fig. 1a. The system of standing threads (the lower branch "d" of warp) is drawn into the shaft practically directly in a length L_d . The system of crossing threads (upper branch "h") is drawn into a needle shaft in a broken line across a leading rod in a bigger length L_h . Beside that, on the leading rod and in the eyes of the needles a considerable friction resistance arises thanks to the bending of threads round the total angle of almost 180° . That leads now to several questions:

– The upper path of threads is longer than the lower one. Does the surplus of the upper length mean a certain abundance of material during weaving?

– It is probable that at the moment of drawing-in of warp or setting the loom in motion the desired tensions of both systems of warp ends will be not secured. It

can be expected that the tension of the upper branch of warp will be higher. Where does the surplus of tension vanish?

– In the upper branch of warp arises a significant friction resistance. Does it affect the weaving tension and the weaving-in (consumption) of yarns in the fabric?

From practical experience we know that these questions do not mean any serious problems for weaving, and that the stress state of warps and the values of threads consumption settle themselves automatically on equilibrium levels corresponding to the desired weaving process. According to the relation (4) the tensions in the threads settle themselves after some time t on two different values which will be really reached in practice:

$$Q_h = EA \frac{v_{2h} - v_1}{v_1}; \quad Q_d = EA \frac{v_{2d} - v_1}{v_1} \quad (5)$$

The warp lengths L_h , L_d play no role; the velocities of consumption v_{2d} , v_{2h} play the only role.

Concerning the influence of frictional resistances in the path of upper warp (Fig. 1b) on tension and elongation in yarns, for the sections between frictional spots the following equations hold:

$$Q_3 = Q_2 e^{f\alpha_1} = Q_1 e^{f(\alpha_1 + \alpha_2)} = Q_1 e^{f\alpha} \quad (6)$$

To judge the tendency of warp to steady itself, let us scope the transition processes in warp tension after the start of the machine with some initial tension deviations from standard values in sections Q_{10} , Q_{20} , Q_{30} . During the transition process at each increment dt of time the warp tension increases by dQ . The elongation ε and real velocities of sliding have to be related again to the free – nonstretched lengths of warp in each section. It will then hold (for relatively negligible length L_2 and its elongation)

$$dQ_1 = EA \frac{d\xi_3 - d\xi_1}{l_1} = \frac{EA \left[\frac{v_3}{1 + \varepsilon_1} - v_1 \right] dt}{\frac{L_1}{1 + \varepsilon_1}} =$$

$$= \frac{EA}{L_1} [v_3 - v_1 (1 + \varepsilon_1)] dt$$

$$dQ_3 = EA \frac{d\xi_D - d\xi_3}{l_3} = \frac{EA \left[\frac{v_D}{1 + \varepsilon_3} - \frac{v_3}{1 + \varepsilon_1} \right] dt}{\frac{L_3}{1 + \varepsilon_3}} =$$

$$= \frac{EA}{L_3} \left[v_D - v_3 \frac{1 + \varepsilon_3}{1 + \varepsilon_1} \right] dt \quad (7)$$

By putting approximately $(1 + \varepsilon_3)/(1 + \varepsilon_1) \cong 1 + \varepsilon_3 - \varepsilon_1$, from here results a set of (nonlinear) equations

$$\begin{aligned} L_1 \frac{dQ_1}{dt} + Q_1 v_1 + 0 &+ 0 - EAv_3 = -EAv_1 \\ 0 - Q_1 v_3 + L_3 \frac{dQ_3}{dt} + Q_3 v_3 + EAv_3 &= +EAv_D \\ 0 - Q_1 e^{f\alpha} + 0 + Q_3 + 0 &= 0 \end{aligned} \quad (8)$$

For the steady state it holds that $\lim_{t \rightarrow \infty} \frac{dQ_1}{dt} = 0$. If we introduce $EA/L_{1,3} = \varepsilon_{1,3}$, we obtain for the tensions $Q_{1,3}$ and elongations $\varepsilon_{1,3}$ in the upper warp the following steadied values (here in a simplified linear form)

$$\begin{aligned} \varepsilon_1 &= \frac{Q_1}{EA} = \frac{v_D - v_1}{v_1} \frac{1}{e^{f\alpha}}; \\ \varepsilon_3 &= \frac{Q_3}{EA} = \frac{v_D - v_1}{v_1} = \varepsilon_1 e^{f\alpha}; \\ v_3 &= \frac{v_D + v_1(e^{f\alpha} - 1)}{e^{f\alpha}} \end{aligned} \quad (9)$$

It is clear that also the crossing ends in all sections of drawing into the needle shaft reach a steady distribution of tensions or elongations, as well as of sliding velocities. The abundant or missing lengths will be absorbed in the fabric by that the delivered warp will be temporarily elongated less or more than normally. That will also temporarily affect the fabric structure – the waveness of threads will be different from the standard. The deviation of waveness can be then visible as a glossy or dark bar.

THE BEHAVIOUR OF VISCOELASTIC LTBS

First, let us neglect the effect of dynamic properties of the drafted or stretched medium. That means that we do not take into account continuous masses distribution in the medium, supposing that still today the propagation of tension and deformation waves in the LTBS (e.g. in the warp) is significantly faster than today's highest processing rates. Kinematic scheme of the motion of medium in the drawing field (of warp on the loom, of fibre during stretching or of an *idealized sliver* in a drafting device etc.) is in Fig. 5.

The course of motion velocity of a LTB and the distribution of deformations during stretching of a viscoelastic medium in a drawing field

The following considerations deal with a viscoelastic LTB – in fact with a sliver with *inner time-dependent friction* between the fibers modelled as a Newton element and a spring.

Thanks to the speed dependent resistance of the medium against elongation, its sections Δx will be not elongated to the finite state by a jump, but by a certain transition process. The resulting advancing velocity $v(x, t) = v_1(t) + d\xi(t)/dt$ inside of the drawing field in this case does not also change immediately to the take-up speed $v_2(t)$, as it would theoretically do with the elastic medium. The velocity $v(x, t)$ increases as shown in the figure.

The motion of particles of the medium in the drawing field in the case of material with rheologic behaviour is described by a system of equations, leading to a resulting partial differential equation of additional shifting ξ of the particle

$$BA \frac{\partial^2 \xi(x, t)}{\partial x \partial t} + EA \frac{\partial \xi(x, t)}{\partial x} = Q(t) \quad (10)$$

and to the *differential equation of elongation* in a viscoelastic LTB...

$$BA v_1(t) \frac{\partial^2 \xi(x, t)}{\partial x^2} + EA \frac{\partial \xi(x, t)}{\partial x} = Q(t) \quad (11)$$

From its solution results:

a) **the distribution of the elongation (particles displacement) in the drawing zone**

$$\xi(x, t) = \frac{Q(t)}{EA} x - \beta v_1(t) \left[\frac{Q(t)}{EA} - \varepsilon(0) \right] \left[1 - e^{-x/[\beta v_1(t)]} \right] \quad (12)$$

(see the course in Fig. 6a). $\beta v_1 = (BA/EA)v_1$ is a constant of the exponential increase of elongation in x direction, $Q/EA = \varepsilon = (v_2 - v_1)/v_1$ is the starting elongation of the LTB, and $\varepsilon(0)$ is the elongation in $t = 0$.

b) On the base of known displacement $\xi(x)$ of the particle Δx in the point x of the free (nonstretched) medium, it is possible to calculate **the real position of this particle in the extended medium** $X = x + \xi(x)$. Especially a **relation between the whole non-stretched length l of the medium and the length L of the drawing field** can be written. The unstretched length l of the LTB between the rollers is from here

$$l \cong \frac{L + \beta v_1(t) \left[\frac{Q(t)}{EA} - \varepsilon(0) \right]}{1 + \frac{Q(t)}{EA}} \quad (13).$$

c) Differentiating the shift ξ of medium particles along x we obtain the **distribution of relative medium elongation** in the drawing zone

$$\varepsilon(x, t) = \frac{d\xi(x, t)}{dx} = \frac{Q(t)}{EA} \left(1 + e^{-x/[\beta v_1(t)]} \right) \quad (14)$$

(See graph 6b). The full draft approaches the steady

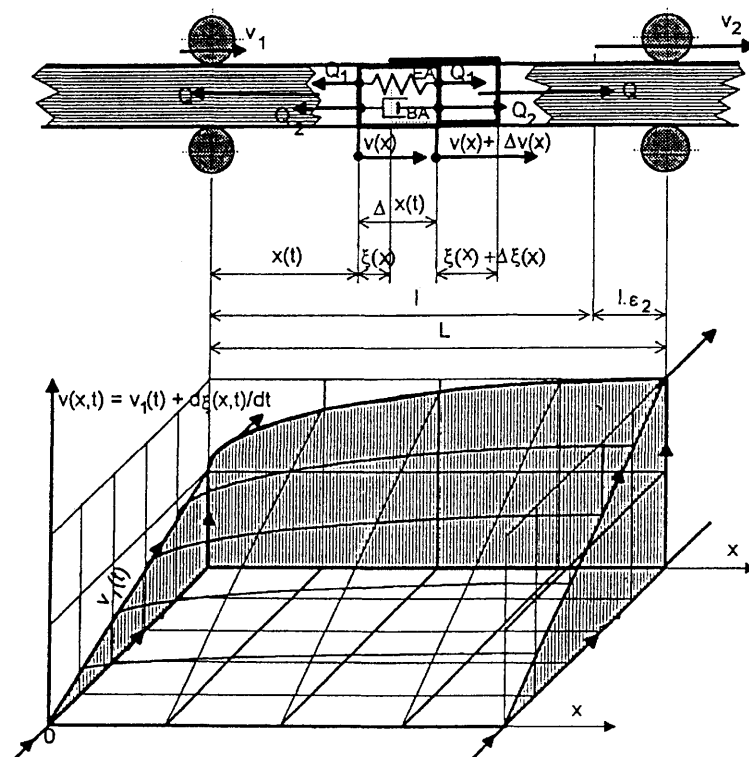


Fig. 5. Distribution of drawing (stretching) velocity $v(x, t)$ along the drawing (extension) field in a LTB with *elastoplastic properties*. The velocity increases exponentially from the input velocity v_1 up to the output velocity v_2

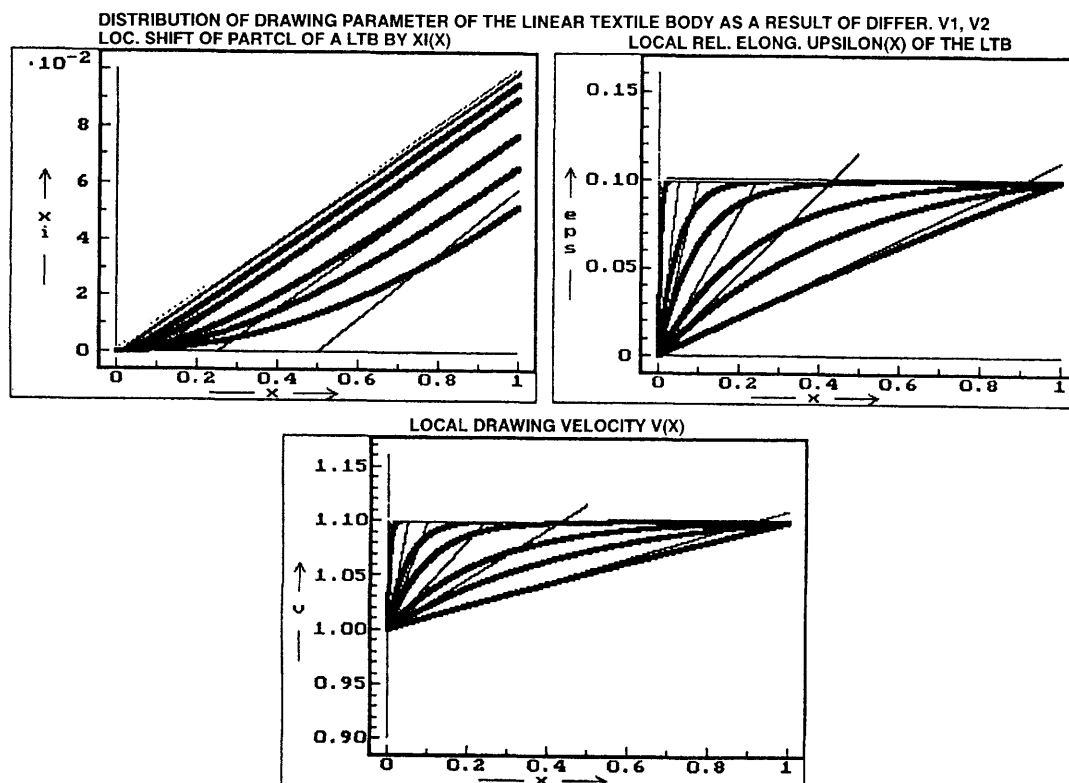


Fig. 6a–6c. Distribution of stretching (drawing) parameters of a LTB (fibre, sliver, warp...) in the drawing field in result of different input and output feeding velocities v_1 , v_2 . $\xi(x)$ – local displacement of a particle Δx of the LTB, $\epsilon(x)$ – local relative elongation of the medium, $v(x)$ – local stretching (drawing) velocity.

value with a transition process with the "time" constant $X = \beta v_1(t)$. In a sliver, at higher drawing velocities the *maximum drawing speed arises almost near the end of the drawing field*, yet not jumpwise as often supposed. d) by differentiation of the displacement (shift) ξ by time t we obtain **the motion velocity of medium particles $v(x)$ in individual places x**

$$v(x) = v_1 + \frac{\partial \xi(x, t)}{\partial t} = v_1 + \frac{\partial \xi(x, t)}{\partial x} \frac{dx}{dt} = v_1[1 + \varepsilon(x)] \quad (15)$$

(see Fig. 6c).

DYNAMIC TENSIONING OF LTBs WITH EVENLY DISPERSED MASSES

In textile machines not only steady extension of textile materials between the feeding and take-up places can appear. Often the deformations are periodic or impulse-type or random processes with a complete spectrum of harmonics. Such straining in LTBs we can name

- the motion of long warp ends between the creel and warping machine (cca 5 m) with excitation caused by unwinding threads from bobbins and by vibrating thread tensioners;
- warp motion after the impulse-type, beat-up or after the shed opening on very fast looms;
- the weft insertion on the loom, etc.

In these cases *the distribution of own masses and rheologic properties* in the linear textile bodies (LTBs) have to be respected. In looms, designed at present, (more than 1000 up to 2000 rpm) the distributed masses and the propagation of tension waves in the long LTBs start to play an important role. The solution in such cases leads to analysis of propagation of pulses and deformation waves in yarns. A model of a LTB – e.g. of a thread or warp end – with distributed differential masses connected by three-element models of elasticity was shown already in Fig. 7a.

The system can be described by a set of equations in the operator form

$$\frac{\partial^2 \xi(p, x)}{\partial x^2} - \frac{\rho}{|E|} p^2 \xi(p, x) - b_1 p \xi(p, x) = 0;$$

$$F(p) - E(p) \frac{\partial \xi(p, x)}{\partial x} dx = 0 \quad (16)$$

Here $E(p) = |E| (1 + pT)/(1 + p\tau)$ is the elasticity modulus; $\tau = b_1/C_1$, $T = b_1/C_1 + b_1/C_0$.

From here results the operator elasticity constant of a massive body with the total length l

$$C(p, l) = \frac{F(p, l)}{x(p)} = \rho A c \frac{p}{G(p)} \frac{e^{+pG(p)\frac{l}{c}} + e^{-pG(p)\frac{l}{c}}}{e^{+pG(p)\frac{l}{c}} - e^{-pG(p)\frac{l}{c}}} \quad (17)$$

where

$$G(p) = p \sqrt{\frac{1+pT}{1+p\tau}}; \quad c = \sqrt{\frac{|E|}{\rho}}$$

is the velocity of tension waves propagation.

The operator elasticity constant $C(p, l)$ can be transformed into the complex constant $C(j\omega, l)$ for periodic straining by formal substituting $p \rightarrow j\omega$. The frequency characteristics of the elasticity constant of a thread (of a LTB) of the length l is plotted in Fig. 7b. The characteristics show that the LTBs get "harder" with higher frequencies of deformation. At very high frequencies on the characteristics in several places alternately high peaks and low amplitudes arise, where the material is very hard or, on the contrary, very compliant. These resonance places mean that with the excitation on the corresponding frequencies $\Omega_1, \Omega_2, \dots$ the threads are coming into resonance vibration or "antiresonance" damping. On the loom the excitation is brought mainly on the weaving frequency $\omega_k = 2\pi n/60$, on the frequency of the beat-up pulses which is higher in order and also on a row of higher harmonic components of the warp straining. The effect of dynamic constants of elasticity of LTBs manifests itself in a row of textile processes, mostly rather negatively, but sometimes even positively.

THE INFLUENCE OF DYNAMIC ELASTICITY OF WARP ON WEAVING

Effect of varying dynamic elasticity (rigidity) of warp on weaving processes in the future

We can see on the characteristics of the elasticity constant of LTBs (e.g. of a warp) that the elasticity constant or the thread rigidity $C(\omega)$ on average grows with increasing frequency ω of straining. As the outputs of machines permanently increase due to the work of designers and inventors, the weaving rates and deformation frequencies of warp and weft will grow, too. The materials of warp and weft become quasi more rigid as if became gradually shorter than they really are on the loom. Weaving becomes more difficult. Higher beat-up forces and, of course, more end downs have to be expected. The fabric will be more sensitive to low stability of the weaving system. It starts to be necessary to search for new ways of solution of these future effects.

The shedding and the beat-up

1. Let the excitation function $x(t)$ acting on the warp on the loom represent a step in elongation (e.g. approximately a *very steep opening of almost "rectangular" shed* on the weaving loom, or some sort

of the beat-up pulse): $x(t) = X \cdot 1(t) \equiv x(p) = Xp^{-1}$. The response on such a step-shaped deformation of warp with elasticity modelled by a three-element member will be a step in tension, yet starting with a higher peak of force:

$$F(p) = C(p)x(p) = C_0X \frac{1+pT}{p(1+p\tau)} \equiv \\ \equiv F(t) = C_0X \left(1 + \frac{T-\tau}{\tau} e^{-t/\tau} \right) \quad (18)$$

The underlined expression represents here the peak of tension as if the material of warp was temporarily harder in the very moment of the start of the coming deformation signal. The peak of tension means a harder straining of warp. In the case of rectangular beat-up pulse it would mean a significantly higher beat-up force.

2. If the excitation function $x(t)$ acting on warp and fabric is specially harmonic, $x(t) = x \sin \omega t \equiv x(p) = x\omega/(p^2 + \omega^2)$ the operator constant of elasticity $C(p)$ can be transformed by substituting $p \rightarrow j\omega$ into the s.c. complex constant of elasticity. That is a complex number with the amplitude and phase angle depending on the excitation frequency ω

$$C(j\omega) = C_0 \frac{1+j\omega T}{1+j\omega\tau} = \\ = C_0 \frac{\sqrt{1+\omega^2 T^2}}{\sqrt{1+\omega^2 \tau^2}} e^{-j(\arctg \omega T - \arctg \omega \tau)} = |C(\omega)| e^{-j\Phi(\omega)} \quad (19)$$

It is evident that, as $T \geq \tau$, the absolute value (the amplitude) of the complex constant of elasticity $|C(\omega)|$ increases (hardens) with increasing excitation frequency ω . That must be taken in account in today's looms working in practice round 500 revs min^{-1} or a little higher. At periodic straining with medium frequency the warp is seemingly more rigid than it corresponds to results gained on a slow working standard laboratory dynamometer used for measuring of warp elasticity.

3. The beat-up force $F_p(t)$ can be expressed as the equivalence of the reaction $R(t)$ of warp and fabric on the deformation of the cloth fell $x(t)$ at the beat-up pulse. In the complex form (in Fourier transform) it sounds

$$F_p(j\omega) \equiv R(j\omega) = [C_1(j\omega) + C_2(j\omega)]x(j\omega) = \\ = C_{ef}(j\omega)x(j\omega) \quad (20)$$

Clearly with heightening the beat-up frequency the dynamic elasticity constant of warp and fabric $C_{ef}(j\omega)$ grows and the resulting beat-up force increases, too.

Other examples of influences of dynamic elasticity of threads

4. Besides the warp on the loom there are other cases in textiles, where the mass distribution and inner elasticity and damping of motions play their role. One of them is the tensioning and straining of threads between the creel and winding stand on a warping machine (see Fig. 8). Firstly, the tension in the threads is excited jumpwise by the fact that the threads get from stillstand immediately into a very fast motion. Secondly, the tension is excited randomly as a result of unwinding of threads from the bobbins, and also as a result of unsteady tensioning of threads by mechanic tensioners with pressuring masses which often tend to jumping in the friction places. In the threads vibrations with a wide spectrum of frequencies arise which propagate themselves with exponential damping along the thread length between the bobbin and the guiding roller of the winding stand.

5. Another example is the insertion of weft on a weaving loom (Fig. 9). Between the inserting nozzle and the storage (which is here presented as a bundle of threads – without resistance of unwinding from a bobbin) the weft is tensioned. At the time of insertion a wave of motion with a velocity $v_i(x, t)$ runs from the nozzle backwards to the storage, varying its form in the direction of the weft and also increasing and later decreasing in the course of time. Due to high velocity of insertion, no vibration can arise. Yet the starting peak of tension may be rather high and may even break the weft.

LITERATURE

1. Kolskij, H.: Investigation of the Mechanical Properties of Materials at Very High Rates of Loading. Proc. Phys. Soc., London 1949, A-197
2. Eyring, H., Halsey, G.: The Mech. Properties of Textiles. The Textile Foundation, Princeton Univ. Press 1948
3. Kolskij, H.: Stress waves in Solids. Oxford Univ. Press 1953.
4. Kožešník, J.: Dynamika strojů. (The Dynamics of Machines) SNTL, Praha 1958
5. Brepta, R., Prokopec, M.: Šíření napětových vln a rázy v tělesech. (The Propagation of Tension Waves and the Impacts in the Bodies). Academia Praha 1972
6. Nosek, S.: Některé aspekty ovlivňující výkon tkacích strojů... (Some aspects influencing the output of weaving looms – a study of dynam. of the weft insertion.) Conf. IFTOM Liberec 1984
7. Nosek, S.: Příspěvek k průměrové adaptivitě osnovních regulátorů (A contribution to the diameter adaptivity of let-off motions). Int. Conf. on Mechanisms and Textile machines, Liberec 1979
8. Nosek, S.: The Dynamics of Fabric Forming on the Loom at High Weaving Rates. J. of Fibre and Textile Research. 19 (1994), p. 125–138

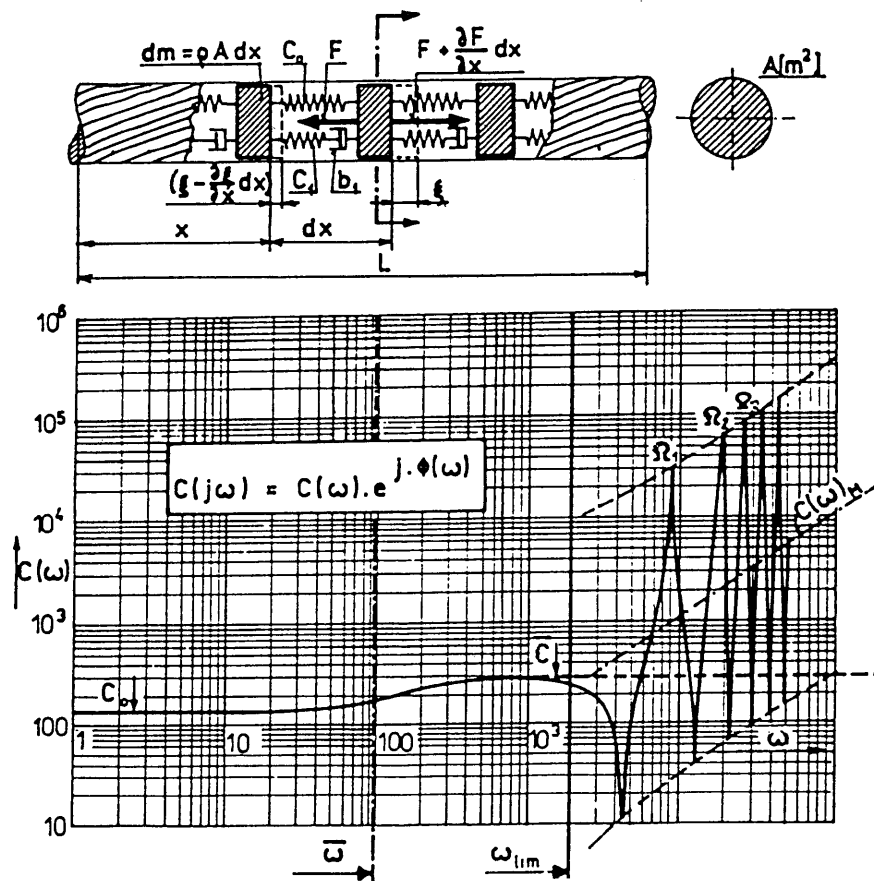


Fig. 7. The elasticity constant of a massive yarn at the given length l .

- a) The distribution of masses dm , of elasticities $C = EF/dx$, and damping (energy dispersions) $b dx/dt = BF/dt$
b) The frequency characteristics of the elasticity constant $C(j\omega)$; for $\omega < \omega_{lim}$ viscoelastic, for $\omega > \omega_{lim}$ dynamic with distributed mass

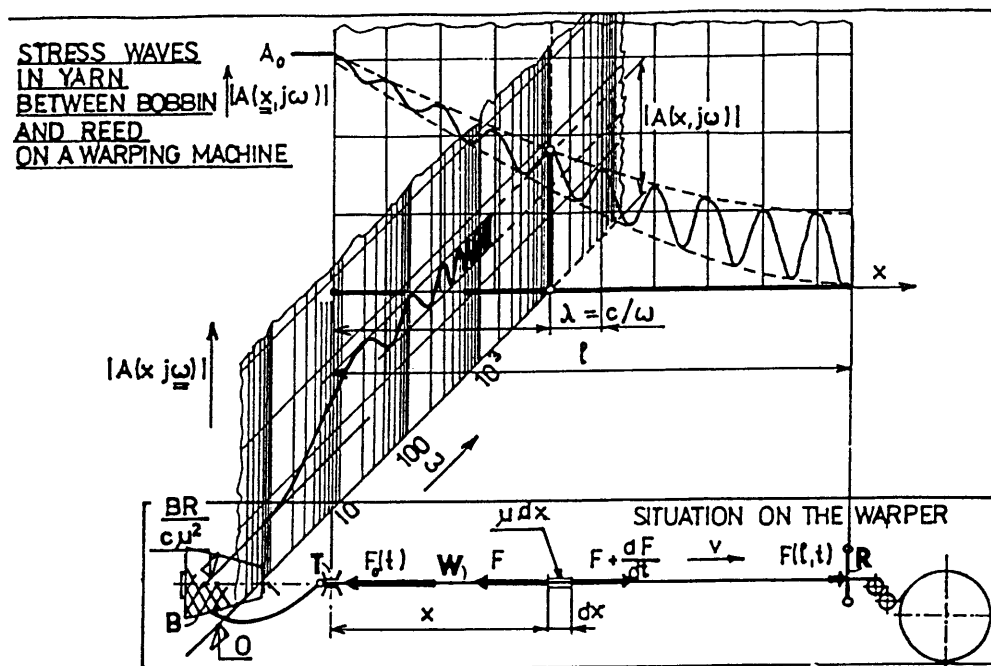


Fig. 8. Stress waves in threads between the bobbin on the creel and reed or guiding roller of a warping machine

DEFORMATION WAVE PROPAGATION IN THE INSERTED WEFT (W) ON A LOOM
BETWEEN STORAGE (S) AND NOZZLE (N)

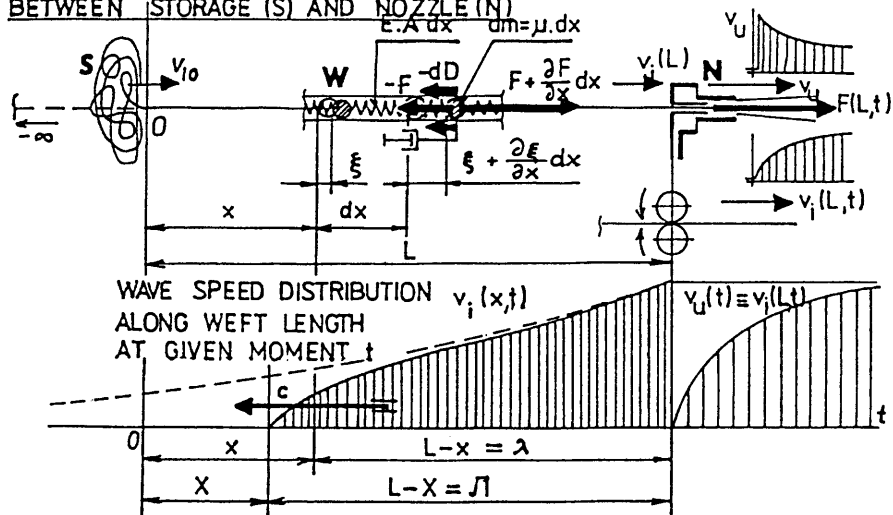


Fig. 9. Propagation of the deformation wave in the inserted weft on an air jet loom in the section from the nozzle back to the weft storage